The

Exploring the Surface of Titan

by

R. D. Lorenz

A thesis submitted in partial fulfilment of the requirements of the degree of Doctor of Philosophy at the University of Kent at Canterbury

University of Kent at Canterbury
United Kingdom

July 1994

To planetary explorers everywhere :

labouring in the laboratory and workshop; perched cold and clouded-out on mountaintop observatories; seated, frustrated, in front of uncooperative computers; and above all fidgeting in the many interminable meetings that characterise this business,

Despite the frustrations, would we rather be doing anything else ?

EXPLORING THE SURFACE OF TITAN

R. D. Lorenz

The exploration of Saturn's giant satellite Titan is considered, with particular reference to its surface which is hidden beneath a thick atmosphere. Groundbased observations, in which great progress has been made recently, and the measurements made by the Pioneer and Voyager spacecraft, are reviewed. Concepts for spacecraft to perform in-situ measurements on Titan are reviewed, as is the development of the NASA/ESA Cassini mission, how the mission constrains scientific investigations, and in turn how the mission has been constrained by funding pressures. The capabilities of the Cassini payload for investigating Titan's surface are critically assessed, and the ability of the Surface Science Package (SSP) on the Huygens probe to determine the composition of surface liquids is examined. Some thoughts on payload selection and the value of individual measurements are presented.

The development of an impact penetrometer, and the interpretation of penetrometer and accelerometer data to measure surface mechanical properties , is described. It should be noted that Huygens is not a vehicle expressly designed as a lander, so the impact dynamics are complex. Additionally, the examination of the prospects offered by acoustic instrumentation are investigated.

Modelling of a number of Titan surface processes is presented, including rainfall, photochemical and meteoric deposition, tidal dissipation in the interior, regolith processes such as volatile heat transport, annealing and aeolian transportation and the effects of tidal and crustal processes on lakes.

A key subtopic of the thesis addresses the theme of planetary exploration as a whole, with the interaction between and the limitations of the exploration 'triad' of observations, in-situ measurements and theory. Note is made of the remarkably significant role played by individuals and their perceptions.

Acknowledgements

I owe much to the many individuals who have encouraged me along the path which has ultimately led to the submission of this thesis.

Working with the Huygens project team in ESTEC, a talented and colourful group of individuals, was a great experience from which I learned much. I thank 'mon chef', Michel Verdant, who encouraged some investigations and patiently tolerated others. I had the good fortune to be the 'sidekick' of Don McCoy whose quiet diplomacy has saved experimenters much grief. Some special mentions are also appropriate for Peter Caseley (for his 'ageing space pioneer' act), Paul Morgan (some cracking squash games), Kai Clausen (wit and technical excellence), Hamid Hassan (getting the job done), Jean-Pierre Lebreton (defending science against the predations of the project) and Anne C. (for maternal concern and many cups of tea).

It has been a great pleasure to work with (and to continue to work with) the Huygens Science Working Team, and the various industrial teams working on Huygens and the Cassini project as a whole. Additionally, Bruce Battrick (ESA publications division) and Lilian Valentin (ESTEC library) have helped much.

At University of Kent, my thanks go to my supervisor John Zarnecki, whose 'hands-off' style has allowed us both to get on with what we want to do. I acknowledge his resourcefulness in putting SSP together, and in funding my activities. Simon Green offered valuable scientific help in preparing proposals (alas unaccepted) for observing Titan.

Mark Leese and Malcolm Wright are thanked for handling most of the tiresome documentation, PA and procurement details of the penetrometer. Richard 'ground systems' Miller saved me much effort in setting up suitable datalogging equipment, and the mechanical workshops did a splendid job of all my various widgets. Trevor Reece's efforts in the electronics workshops are also acknowledged. The other members of the Unit for Space Sciences are thanked for their assistance with procedures, forms, computers, equipment and for their amiable companionship, especially the gang in 164; Mark, Paul, Niel, Nick and Jon.

Various co-workers have given encouragement to particular avenues of research which have proven fruitful: Drs Athena Coustenis, Jonathan Lunine and Jean-Pierre Lebreton are thanked particularly in this respect.

I have had the pleasure of working closely with a number of colleagues on work which I would have been unable to accomplish alone: Luisa Lara (IAA, Spain), Mark English (UKC), Paul Ratcliff (UKC), Frank Sohl (Universitat Kiel, Germany), William Sears (University of Arizona, USA), Marek Banasciewicz and Konrad Kossacki (Space Research Centre, Warsaw, Poland).

Lynn, Neil, Chen, Helen and especially Jerry at STA Travel helped me to weave my way around the world quickly and cheaply. During the various travels associated (directly or indirectly) with the work reported in this thesis, I have been supported by a number of organisations to whom I offer my thanks:

Science and Engineering Research Council (SERC); British National Space Centre (BNSC); European Geophysical Society (EGS); British Association for the Advancement of Science (BAAS); Unit for Space Sciences, University of Kent; Huygens Project Division, European Space Agency; Mrs Margaret Lorenz; The Institute of Physics (IOP); Micro Sci Tech Limited (MST); Commercial Space Technologies Limited (CST); Irvin (GB) Limited; Centre Nationale de Recherches Scientifiques (CNRS); Lunar and Planetary Laboratory, University of Arizona; Space Research Centre, Polish Academy of Sciences; Astronomiska Observatoriet, Uppsala.

Additionally, many friends have kindly given me a place to rest my head during my wanderings: Edwin Van Dijk (Delft, The Netherlands), Susan Hornung (Rheims and Paris, France and Sandbach, England), Frank Martin Seifert (Munich, Germany), Dr. Luisa Lara (Granada, Spain and Paris, France), Erwin Mooij (Delft, The Netherlands), Bruno Muller (Dusseldorf, Germany), Dr. Athena Coustenis (Paris, France), Patrick North (Kobe, Japan), Marie-Claire Delprat (Paris, France), Stephan Ott (Leiden, The Netherlands), Dhugal Bedford (Oxford, England), Kirsty Lorenz (London, England and Edinburgh, Scotland), Veronique Lemaire (Lille, France), Dr. Don Niblett (Canterbury, England), Andrew Nairn (Namur, Belgium), Mark English & Neil McKay (Whitstable, England), Dr. Graham Dorrington (Southampton, England), Prof. Chris Talbot (Uppsala, Sweden).

A comfortable and quiet home is a key to productive research: I have enjoyed sharing 20 Willows Court with Susan, Marie-Claire, Dave and Dan, and 4 Remston Mews with Mike, Christine, Ann and Eugene.

Last, but by no means least, I thank my parents Margaret and Detlef and my sister Kirsty, who have helped in so many ways.

Exploring the Surface of Titan

Appendices

List of Figures

List of Tables

List of Acronyms

A/D	Analogue to Digital
ADC	Analogue to Digital Converter
AAT	AngloAustralian Telescope
ACC	Accelerometer
ACC-E	Accelerometer - external (SSP)
ACC-I	Accelerometer - internal (SSP)
ACP	Aerosol Collector Pyrolyser
AGC	Automatic Gain Control
AIT	Assembly, Integration and Test
AIV	Assembly, Integration and Verification
API	Acoustic Properties Instrument (SSP subsystem)
API-S	Acoustic Properties Instrument - Sounder
API-V	Acoustic Properties Instrument - Velocity
ASTRA	Altimetry and Sounding of Titan by Radar Altimeter
AU	Astronomical Unit
BBC	British Broadcasting Corporation
BDR	Battery Discharge Regulator
C3	Launch Energy
CAPS	Cassini Plasma Spectrometer
CCD	Charge Coupled Device
CDA	Cosmic Dust Analyser
CDMS	Command and Data Management System
CFH	Canada France Hawaii (Telescope)
CG	Centre of Gravity
CGS4	Cooled Grating Spectrometer 4 (UKIRT)
CIRS	Composite Infrared Spectrometer (Cassini)
Co-I	Co-Investigator
ConDR	Conceptual Design Review
CRAF	Comet Rendezvous/Asteroid Flyby
DC	Direct Current
DEN	Density (SSP subsystem)
DISR	Descent Imager and Spectral Radiometer
DSN	Deep Space Network (NASA)
DSP	Digital Signal Processing
DWE	Doppler Wind Experiment
EGSE	Electrical Ground Support Equipment
EID	Experiment Interface Document
EJGA	Earth-Jupiter Gravity Assist
EM	Engineering Model
EMC	Electromagnetic Compatibility
EPDR	Experiment Preliminary Design Review
ESA	European Space Agency
ESD	Electrostatic Discharge
ESO	European Southern Observatory
ESOC	European Space Operations Centre
ESTEC	European Space Research and Technology Centre
FIFO	First In First Out
FM	Flight Model
FMCW	Frequency Modulation Continuous Wave
FWHM	Full Width Half Maximum
FOV	Field of View
FS	Flight Spare
FUSSR	Former Union of Soviet Socialist Republics
GC	Gas Chromatography
GCMS	Gas Chromatograph Mass Spectrometer
GEC	General Electric Company

GEE	Greatest Eastern Elongation
GFRP	Glass Fibre Reinforced Plastic
GSFC	Goddard Space Flight Center
GWE	Greatest Western Elongation
HASI	Huygens Atmospheric Structure Instrument
HGA	High Gain Antenna
HST	Hubble Space Telescope
HSWT	Huygens Science Working Team
I/O	Input/Output
IBM	International Business Machines
IDS	Interdisciplinary Scientist
INMS	Ion and Neutral Mass Spectrometer (Cassini)
IOS	Institute of Oceanographic Sciences
IRU	Inertial Reference Unit
IPA	Iso Propyl Alcohol
IR	Infrared
IRAM	Institut de RadioAstronomie Millimetrique
IRIS	Infrared Spectrometer (Voyager, AAT)
IRTF	Infrared Telescope Facility (NASA)
ISS	Imaging Science Subsystem
I/SS	Impact/Surface Science
IUE	International Ultraviolet Explorer
JGA	Jupiter Gravity Assist
JPL	Jet Propulsion Laboratory
JWG	Joint Working Group
LECP	Low Energy Charged Particle detector (Voyager)
LED	Light Emitting Diode
LGA	Low Gain Antenna
MGSE	Mechanical Ground Support Equipment
MIMI	Magnetospheric Imaging Instrument
MLI	MultiLayer Insulation
MM2	Mariner Mark 2
MOI	Moment Of Inertia
MoU	Memorandum of Understanding
MS	Mass Spectrometry
N/A	Not Applicable
NASA	National Aeronautics and Space Administration
NIMS	Near-Infrared Mapping Spectrometer (Galileo)
NPL	National Physical Laboratory
OAO	Orbiting Astronomical Observatory
ODM	Orbiter Delay Manoeuvre
ODT	Orbiter Delay Time
PA	Product Assurance
PAA	Probe Aspect Angle
PATT	Panel for the Allocation of Telescope Time
PC	Personal Computer
PCB	Printed Circuit Board
PCDU	Power Control and Distribution Unit
PER	Permittivity (SSP subsystem)
PI	Principal Investigator
PIRLS	Probe InfraRed Laser Spectrometer
POC	Probe Operations Centre
PRA	Planetary Radio Astronomy (Voyager)
PRA	Probe Relay Antenna
PROM	Programmable Read-Only Memory
PSG	Project Science Group
PWA	Plasma Wave Analyser (HASI)
PWS	Plasma Wave System (Voyager)
PZT	Lead-Zirconate Titanate

RAL	Rutherford Appleton Laboratory
REF	Refractometer (SSP subsystem)
RF	Radio Frequency
RHU	Radioisotope Heater Unit
RITO	Refractive Index of Titan's Ocean
RO	Radio Occultation
ROM	Read Only Memory
RPWS	Radio and Plasma Wave Spectrometer
RSS	Radio Science Subsystem (Cassini, Voyager)
RTG	RadioIsotope Thermoelectric Generator
SAR	Synthetic Aperture Radar
SERC	Science and Engineering Research Council
SEU	Single Event Upset
SMU	Stimuli Monitoring Unit
SO2P	Saturn Orbiter with 2 Probes
SOI	Saturn Orbit Insertion
SOI	Saturn Orbit Insertion
SOS	Silicon on Sapphire
SOTP	Saturn Orbiter/Titan Probe
SRC	Science Research Centre (Poland)
SRM	Solid Rocket Motor
SRMU	Solid Rocket Motor Unit
SSD	Space Science Department (ESTEC)
SSP	Surface Science Package
SSPE	Surface Science Package Electronics (box)
STPM	Structural Thermal and Pyrotechnic Model
TBC	To Be Confirmed
TBD	To Be Determined
THP	Thermal properties (SSP subsystem)
TIL	Tilt (SSP subsystem)
TIR	Total Internal Reflection
TM	Telemetry
UK	United Kingdom
UKC	University of Kent at Canterbury
UKIRT	UK Infrared Telescope
UMIST	University of Manchester Institute of Science and Technology
US	United States
USO	Ultrastable Oscillator
UVS	Ultraviolet Spectrometer (Voyager)
V1	Voyager 1
VIMS	Visual and Infrared Mapping Spectrometer (Cassini)
VLA	Very Large Array
VSTOL	Vertical/Short Take-Off and Landing
VVEJGA	Venus-Venus-Earth-Jupiter Gravity Assist

Chapter 1

Introduction

Titan is a lovely, baffling and instructive world,
which we suddenly realise is accessible for exploration

Carl Sagan, Broca's Brain, 1975

Exploration is an activity which does not confine itself to a single discipline. This thesis is perhaps unusual in the number and breadth of scientific and technical issues it touches upon. Rather than investigate in depth a single scientific question, such as 'What is the possible range of compositions of an ocean on Titan?', or 'How may radar observations be used to identify the composition and topography of Titan's surface?', it attempts to address a number of such issues, in order to understand how a variety of theoretical, observational and in-situ measurement techniques can be used to elucidate the nature of the surface of Titan.

Thus, the thesis attempts to investigate how Titan has been explored, how it may be explored, and what we may hope to learn from measurements made by spacecraft near and on Titan's surface. The question 'How should Titan be explored' is largely avoided, since this depends, as will be shown, on many factors - most particularly on the discipline of whomever is asking the question.

Titan is a large moon of the planet Saturn; at 5150km diameter it is larger than the planet Mercury, but somewhat smaller than Mars. Its size, then, is unremarkable, although it is the second-largest satellite in the solar system. However, what makes Titan so unique and wonderfully mysterious is that it finds itself with a thick atmosphere, unlike any other satellite.

Further, this atmosphere is dominated by nitrogen; the only similar atmosphere in the solar system is that of the Earth. Yet more intriguing, photochemistry of the ~2% of methane in Titan's atmosphere yields complex organic molecules (of which around 20 have already been detected): it is exciting to question whether the organic molecules which led to the origin of life on Earth 3.5 billion years ago may have formed by processes similar to those occurring in Titan's atmosphere today.

Thus Titan and its atmosphere are the subject of intense scientific interest: closer study may help understand how solar system bodies (including the Earth) and their atmospheres formed and evolved. While Titan's atmosphere has been the subject of close scientific attention, particularly since the Voyager 1 encounter in 1980, its surface and interior have remained essentially unknown. This is because the thick atmosphere is laden with opaque orange layers of organic haze, which until recently have hidden the surface from attempts at observation.

However, the prospect of making observations from a probe descending beneath the haze layers down to the surface and mapping the surface from orbit has renewed interest in Titan's surface, and has prompted recent advances in observation techniques which are giving us our first tantalising glimpses of this exotic world. This thesis documents these new observations, and describes the instrumentation that will be carried to Titan by the Cassini mission, on both the orbiter spacecraft and the ESA Huygens probe.

The observations and spacecraft measurements form two elements of the exploration triad. The third element, which is also addressed in this thesis, may be broadly called planetology, the study of worlds. Application of universal physical principles, and intercomparison of features and processes occurring elsewhere in the solar system, give insight into what we may expect on Titan. Comparative planetary studies and theoretical modelling of physical processes allows us to place constraints on the processes that shape the surface of Titan: we can make educated guesses at the face of Titan, before spacecraft allow us to lift her orange veil.

Planetology should not be regarded solely as a means to anticipate direct observation, for which there will never be a replacement. Rather, its principal use is to interpret what information we have; worlds are systems, and complex ones at that. Individual observations or measurements are of little use by themselves; they must be integrated with other data, and a theoretical framework in order to understand what is happening: as Poincare pointed out

'Science is facts. Just as houses are made of stones, so is science made of facts. But a pile of stones is not a house, and a collection of facts is not necessarily science'.

With any multidisciplinary work, it is difficult to develop a coherent one-dimensional structure, such as a list of contents. After a brief comparison with the exploration of Venus, I therefore begin where, chronologically, Titan's exploration begins, namely with a review of groundbased observations of Titan. Astronomy from the ground is being increasingly supplemented by astronomy from space: the chapter therefore goes on to discuss recent and imminent contributions from space-based observatories.

The following chapter continues in the spaceward direction, describing the great (but finite) advance in our knowledge of Titan from the encounters with the Voyager spacecraft, and Pioneer 11 before it. The relevant parts of the Voyager and Pioneer payloads are briefly discussed, to put the Cassini instrumentation in context.

The fourth chapter discusses concepts for the in-situ exploration of Titan by spacecraft, and explains how the joint NASA/ESA Cassini mission evolved. Chapter 5 goes on to discuss the details of the Cassini mission and the engineering design of the NASA Saturn Orbiter spacecraft and the ESA Huygens probe: although current descriptions may be found elsewhere,

this section describes in detail how the mission has evolved and how investigation of Titan's surface is limited by engineering constraints. As a thought experiment, consideration is given as to how a probe should look if Titan surface investigation was its only mission.

Chapter 6 investigates critically the capabilities of the formidable array of instrumentation to be carried to Titan on the Cassini mission, addressing the studies to be made by the orbiter, by the probe during descent and, if it survives, after impact on Titan's surface. The payload selection process, and the evolution of some payload elements are also described. The capability of the Surface Science Package (the Huygens experiment devoted most directly to Titan's surface, and that in which I have been most closely involved) to determine Titan ocean composition is investigated. Additionally, some thoughts on the 'value' of individual measurements are presented.

Chapters 7 and 8 investigate in detail what we may learn from two payload elements, in the development of which I have played a significant role. These are, respectively, measurement of the mechanical properties of Titan's surface by accelerometry and penetrometry, and acoustic measurements and sounding of the surface. These are described in some detail, first because they are in themselves novel developments in planetary exploration, and secondly they serve to demonstrate the interaction of science, technology and perception, an interaction which forms a key subtopic of this thesis.

Chapter 9 summarises theoretical work on Titan in a planetological context, describing some models of Titan's origin and evolution, and predictions for what processes and features may be found on Titan's surface.

Chapter 10 summarises the fundamental conclusions of this work, and is followed by references and appendices, which comprise some thoughts on what might or should happen if Cassini fails, a list of the conferences attended during the studies reported here, and several of the refereed publications generated during the study.

Thus the thesis presents an overview of the current understanding of Titan's surface, in the context of its imminent exploration. Significant items that are novel, where the author believes he has made an original contribution are:

- addressing the theme of planetary exploration as a whole, with the interaction between observations, in-situ measurements and theory.
- noting the remarkably significant role played by individuals and their perceptions.
- a critical examination of the payload of the Cassini mission, and its capabilities for Titan surface investigation.

• the development of an impact penetrometer, and the use of accelerometry to measure surface mechanical properties on a vehicle that is not expressly designed as a lander.
• the examination of the prospects offered by acoustic instrumentation.
• modelling of a number of Titan surface processes; rainfall, photochemical and meteoric deposition, tidal dissipation in the interior, regolith processes such as volatile heat transport, and annealing, and aeolian transportation and the effects of tidal and crustal processes on lakes.

1.1 Comparisons with the Exploration of Venus

In order to put the progress to date of the exploration of Titan into context, it is instructive to compare Titan with another body, whose exploration has reached a more advanced stage. Since Venus is hidden by an optically-thick atmosphere, like Titan, it seems the most appropriate body for comparison. Being so much closer to the Earth, it is both easier to observe telescopically, and is much easier to reach by spacecraft.

Galileo noted that Venus showed phases like the Moon in 1610 (see, e.g. Cruikshank, 1983) while later workers (including Cassini) in the 17th and 18th centuries reported seeing features on the illuminated part. In 1716, Edmond Halley anticipated the 1761 transit of Venus across the face of the Sun and urged astronomers after him (he died in 1742) to observe it. The Russian observer Lomonosov reported that the silhouette of Venus during this event was surrounded by a grey halo and inferred that Venus had an atmosphere. This may be compared with Comas Sola's 1908 observation of Titan (see chapter 2).

At this point, then, progress in Titan's exploration was over a century behind that of Venus.

The next big step, spectroscopic identification of the dominant atmospheric constituent, was achieved by Adams and Dunham in 1932. The corresponding 'milestone' for Titan was only 12 years later, due to Kuiper.

Spectral imaging of Venus was performed by the Galileo spacecraft NIMS instrument, and revealed that the cloud opacity was variable, and that in certain IR atmospheric windows it is possible to see deep into the atmosphere (although cloud-tracking in the UV had been noted long before). In the wake of this observation, groundbased imaging in the IR windows is planned. This level of development is virtually equivalent to imaging of Titan, although the latter requires adaptive- or space-based optics to achieve useful spatial resolution.

UV observation of Titan was first performed in 1972 by the OAO-2 spacecraft (indeed, it was the first spaceborne observation of any planetary satellite - J. Caldwell, personal communication). The corresponding measurement for Venus was made only about 8 years

previously, by the Russian Zond 4 and Venera 5 spacecraft.

Titan's observation at radio wavelengths lagged that of Venus by some 20 years, due to the greater distance and much lower brightness temperature of Titan. It was not clear, however, whether ~600K brightness temperature of Venus was due to high surface temperature, or ionospheric emission (this uncertainty may be compared to the mid-1970's thick/thin ambiguity of Titan's atmosphere). Theoretical arguments, such as the greenhouse model (Sagan, 1962) argued for a high surface temperature, but the truth of this hypothesis was only established after the 1962 flyby of Venus by the spacecraft Mariner 2 which detected microwave limb darkening, incompatible with ionospheric emission. The analogue dilemma for Titan (the rival atmosphere models) was similarly resolved by the Voyager 1 radio-occultation experiment in 1980.

Radar observations of Venus (to measure its rotation, amongst other things) began a little before 1970, in advance of Titan radar studies by some 20 years, due to the extreme distance of Titan (radar signal-to-noise ratio is inversely proportional to the fourth power of range). By the late 1970's groundbased radar mapping of Venus (especially using the Arecibo dish) became fairly detailed, although the coverage was necessarily limited. Groundbased radar studies of Venus has slowed in recent years, however, since they have been superceded by spacecraft radar measurements.

Spacecraft exploration of Venus (see, e.g. Wilson, 1987) began early, with the first flyby in 1962 (Mariner 2). The corresponding events for Titan (Pioneer 11, Voyager 1) occurred ~18 years later. Entry probes (Veneras 4,5 and 6) investigated the Venusian atmosphere in 1967-69, although they all failed at about 27 bar pressure (~30km above the surface). Venera 7 in 1970 suffered a similar failure, but limped to the surface, with its radio transmitter operating at 1% power and its telemetry multiplexer 'stuck' on the temperature measurement. First pictures of the surface were obtained by Venera 9 in 1975.

The 1978/79 Pioneer Venus mission included four descent probes, and coarse radar mapping from orbit. Higher resolution mapping of part of the surface (~1-2km resolution, similar to that achieved by groundbased work, but at higher latitudes) was achieved in 1983 by Veneras 15 & 16. The 1985 Vega mission released balloons into the Venusian atmosphere, as well as landers. The present era of Venus exploration seems set to close with the end of the 1990-1994 high resolution (~100m) radar mapping and gravity field measurement by Magellan.

Because Venus is so much more accessible from Earth, Venus exploration has been rather incremental, at least by FUSSR. The exploration of Titan is necessarily more episodic, although it could be argued that US exploration of Venus has been similarly episodic, with long 'fallow' periods between missions. The Cassini mission will accomplish many of the

incremental steps in exploration (atmospheric descent, surface imaging and radar mapping; milestones which spanned ~17 years) in one go. Again, however, these milestones will occur ~20 years after they were achieved on Venus.

The big remaining questions regarding Venus, now that radar mapping of its geologic features has been performed, regard its internal structure, dynamics and composition. These are being in part addressed by the Magellan extended mission, which is mapping the gravity field to correlate this with topography, but require seismology data and better geochemical data to more fully understand how the interior is coupled to the surface. Thus future Venus missions, which we probably would not expect until after the year 2000 (J W Head, personal communication, 27/4/94) might include landers focussed on geochemistry and equipped with coolers to enable long-term survival on the Venus surface to perform seismometry.

The corresponding mission goals for Titan, although in part addressed in previous mission (e.g. penetrators) or experiment (e.g. XRF) proposals, will have to wait for future missions, which we probably cannot expect to arrive until ~2020 (See Appendix 1), again ~20 years post-Venus.

On the theoretical side, except where theory is constrained by the availability of data, planetological studies are probably at an equivalent stage, which is unsurprising, given the comparative nature of planetology. Also (see above) the state-of-the-art of certain niche observational techniques is broadly equivalent (although the IR window imaging technique could probably have been applied long ago to Venus, it was only the *knowledge that such observations would be useful* that, as on Titan, stimulated the application of the technique).

However, where physical barriers (such as distance, signal-to-noise, trip time etc.) are the limitations on exploration, as with most groundbased observations and spacecraft exploration there seems to be a remarkably consistent delay of ~20 years between Venus and Titan exploration.

Chapter 2

Earth-based Observations of Titan

In her starry shade of Dim and Solitary Loveliness,
I learn the language of another world

Lord Byron, English Poet
She Walks in Beauty

In this chapter, I review Earth-based observations of Titan (Earth-based = groundbased measurements, and those from Earth-orbiting spacecraft) and their contribution to the understanding of surface conditions.

2.1 Historical Overview

Galileo observed Saturn telescopically in 1610, but failed to detect (or at least recognise) Titan, largely due to the poor optical quality of his telescope: for a description of what Galileo probably saw, see Ringwood (1994). Titan was observed and recognized by Christian Huygens (Huygens 1656) in the Netherlands in 1655 (when Huygens was aged 25). It had been seen by Wren and Hevelius previously (Van Helden, 1986), but was not recognised as a satellite of Saturn. Huygens soon also measured its period as 16 days.

Comas Sola in 1908 (Comas Sola, 1908) reported seeing limb-darkening of Titan's disk, suggestive of an atmosphere, although given the difficulty of making this observation with even the best current telescopes, this observation was given little credence, and was never repeated.

James Jeans, in his treatise on Kinetic Theory of Gases (Jeans, 1925) noted that Titan would be able to retain an atmosphere for the age of the solar system, and mentions that an atmosphere had been discovered. He does not identify the observation that suggested an atmosphere, but presumably it was that of Comas Sola.

Undisputed evidence of an atmosphere was obtained in the USA in 1944 by spectroscopic means by Gerard Kuiper (another Dutchman - he began his career aged 22 at the Sterrewacht in Leiden, only 20km from Huygens' birthplace, and 10km from ESTEC). His observations comprise photographs of spectra and show distinctive absorption bands in the spectra of giant planets, which correlate with laboratory measurements of methane absorption bands. Since his spectra of Titan also show these bands (but, for example the Galilean satellites of Jupiter do not) he inferred the presence of gaseous methane on Titan.

Subsequent observations were essentially unable to discriminate between two dominant atmosphere models that evolved, namely the Caldwell (a thin, cold atmosphere consisting

mostly of methane) and Hunten (a warmer, thicker atmosphere, with methane dominated by another constituent, possibly nitrogen) models, although they were able to detect some additional organic compounds. The resolution of the atmospheric structure question awaited the arrival of Voyager (see chapter 3). For a description of the two models mentioned above, and an excellent review of the pre-Voyager understanding of Titan, see Hunten (1992).

Until the late 1980s, there were a few significant observations, which are mentioned briefly in the rest of this section : details of the more significant recent observations form the remainder of this chapter.

In 1988, groundbased infrared observations (from 1982) were used to determine CH_3D (monodeuterated methane) to CH_4 ratio, and hence infer the D/H ratio in Titan's atmosphere (De Bergh et al. 1988: see therein for a mention of an earlier, incorrect determination of this ratio from Voyager spectra by Kim and Caldwell, 1982). Measurement of the D/H ratio is a factor that constrains theories about the formation and evolution of the atmosphere and surface of Titan. Interestingly, this quantity is enriched by a factor of a few with respect to the protosolar cloud (and the giant planets) but is about the same as that of the Earth's oceans, raising the intriguing notion that volatile inventories on Earth and Titan may share a common source, perhaps comets (which also have a similar D/H ratio) - see chapter 9.

In 1990, millimetre-wave measurements (Tanguy et al. 1990) using the 30m IRAM telescope enabled the measurement of a profile (abundance vs. altitude) of CH_3CN which had only been detected by Voyager. While not in itself a crucial step, this represents an impressive observation, and provides important data for the validation of photochemical models, which are in turn used to predict deposition of materials on the surface.

Detection (Lutz et al. 1983) and abundance measurement of CO (at $6x10^{-5}$ mole fraction) has also been significant, first in verifying models, and also in realising the importance of the meteoric delivery of oxygen compounds into the atmosphere.

Theoretical investigation of meteoric deposition, and subsequent oxygen chemistry, is under way (see chapter 9). It may be possible to confirm the predictions of the oxygen chemistry by further millimetre-wave observations, which might be able to detect CH_3OH, CH_2O and other compounds.

2.2 Stellar Occultation Measurements

During 1989, the relatively bright star 28 Sagitarii (magnitude 5.5) was occulted by Titan (magnitude 8.3). This type of event (Hubbard et al. 1990, Sicardy et al. 1990) might be expected to occur every few centuries, so its timing in the early stages of preparation for the Huygens mission is exceptionally fortuitous, as was the fact that it was visible from Europe, thus

allowing a large number of observers to contribute, ranging from amateurs in the UK, to a University of Arizona portable occultation photometer set up in an Israeli kibbutz, to the Vatican Observatory. A comprehensive summary of the observations and their interpretation is given in Hubbard et al. (1993). While the occultation measurements contribute to our understanding of Titan's atmosphere, and not directly to the surface, they are worthy of mention for two reasons:

1. they indicate the occasional value of even (relatively) simple amateur measurements in making genuine contributions to planetary science, and
2. the atmospheric oblateness inferred from the occultation measurements was consistent with an atmospheric super-rotation, which had been until then only suggested by the Flasar et al.(1981) measurement of latitudinal variation of Voyager 1 infrared brightness temperatures. These super-rotating winds are in fact, a strong driver for the telemetry link performance for the Huygens probe at the end of its descent.

The super-rotation also suggests the nature of the general circulation of Titan's atmosphere at low levels, and consequently on wind stress on seas, and possible aeolian transport of surface particulates and hence dune formation (see Chapter 9). Thus there is an indirect link between these observations and Titan's surface.

2.3 Radar Observations

Direct radar sensing of Titan's surface was first achieved in 1989 by Muhlemann et al. (1990), although several other workers attempted the observation earlier, e.g. according to a footnote in Muhleman et al. (1990), Goldstein and others obtained a statistically significant peak in a return signal spectrum, but did not publish their result. Radar reflectivity of the surface, albeit at low signal-to-noise, was successfully measured by Muhleman's team on 3 nights as 0.38, 0.78 and 0.25 - i.e. highly variable, but quite high (much higher than the reflectivity of a global hydrocarbon ocean): Subsequent measurements (Muhlemann et al. 1992) have confirmed the results, noting that there is a 'bright spot' of high radar reflectivity (~0.75), and that the radar reflectivity resembles (although generally somewhat lower than) those of the icy Galilean satellites Europa and Ganymede, although similar to that of Callisto - see table 2.1. These reflectivities, are rather higher than would be expected, for example, from smooth spheres of reflecting material.

Various mechanisms have been proposed to account for the anomalously high radar cross-sections of Titan and the Galilean satellites. One idea (Hagfors et al. 1985) suggests that gradual variations in refractive index with depth slowly bend the incident radar beam around until it leaves the surface again.

A more widely accepted explanation, for Ganymede at least, is that total internal reflection (TIR) occurs at cracks in the ice regolith (Goldstein and Green, 1980) As the absorption of radar

waves in ice is modest, the incident energy can be reflected many times before re-emerging from the regolith. The TIR mechanism also accounts for the polarization of the echoes. A refinement of this idea, which explains the intensity of the echoes rather better, is based on the TIR at a low dielectric layer (e.g. frost, regolith) in buried craters. This reflection generates a phenomenon related to the 'glory' seen sometimes on terrestrial clouds (see Eshleman, 1986; 1987; Gurrola and Eshleman 1990,; see also Hapke, 1990).

As discussed by Muhleman et al (1990), and by Lunine (1992, 1993), this mechanism, and the more general idea of Goldstein and Green (1980), falter if the regolith is 'soaked' in liquid hydrocarbons, since the dielectric contrast (i.e. difference in dielectric constant) between these and the ice is much lower than that between ice and a vacuum, so reflection is relatively inefficient.

The most recent reported observations for Titan (Muhleman et al.,1993) include spatially resolved (albeit poorly) measurement of radar reflectivity: reflectivity in 3 longitudinal strips parallel to the rotation axis was measured (presumably by utilising the doppler effect - see Muhleman et al. 1990) These measurements suggest that Titan is not reflecting the radar energy specularly (i.e. only from the centre of the disk, as would be expected from a smooth ocean) but all over its surface : this appears consistent with some kind of scattering mechanism.

Thus, while plausible explanations of high reflectivity for icy satellites have been offered, and are compatible with the reflectivity noted for Titan, and with the fact that the reflection is not specular, the anomalous (paradoxically, the 'expected') polarization for Titan's echoes cannot be adequately explained at present.

It may be noted that the radar observations are incompatible with a deep global ocean of hydrocarbons on Titan: due to the significant attenuation of the radar signals by the hydrocarbon fluid, an ice or rock surface submerged in a depth of 35-150m of ethane would have an effective reflectivity of only 1% of its 'dry' value (Muhleman et al. 1990)

Note that this last statistic has been sometimes misinterpreted as suggesting that the radar measurements imply a maximum ethane depth of 35-150m (see, e.g. Birchley, 1993; Griffith 1993) This is not the case. Rather, Muhleman et al. simply state that this range of depths would attenuate the effective reflectivity of the underlying surface by about two orders of magnitude : a smooth ice surface covered even by only a few metres of liquid would still have too low a reflectivity. Presumably, therefore, at least some areas must be 'dry' enough that the reflective contrasts in dielectric constant are able to reflect the radar signal efficiently. Further, the above estimates of 'attenuation depths' are perhaps too large : Thompson and Squyres (1990) note that the dissolution of polar molecules (such as CH_3CN, soluble to a mole fraction of up to 6×10^{-5}) would increase the attenuation of the ocean by a factor of at least 2-3.

Attempts have been made to devise scenarios with deep global oceans which are themselves radar-reflective; Masson and Caudal (1991) presented a 'bubbly ocean' model at the 1991 Toulouse conference on Titan, although this idea has not been examined fully (but see Lunine (1993) for a brief discussion. Lunine (1992) suggested that aerosol particles could be suspended in the ocean in sufficient concentrations to make it radar-reflective, due to the long sedimentation times of particles. These exotic models are no longer required, however, since revised photochemical models suggest a lower ethane depth on the surface, and a re-examination of tidal effects (Sohl, Sears and Lorenz, 1994; see also chapter 9) has suggested that shallow ocean and mixed land-sea surfaces should not be excluded. A mixed land-sea surface would be perfectly compatible with the radar observations, as would a global 'dirty ice' surface.

Interestingly, the 'bright spot' mentioned above appears slightly earlier from year to year than would be expected from synchronous rotation (15.945 days) - tracking of this bright spot suggests a rotation period of 15.911 days, 0.82 hours shorter than the orbital period (Muhleman and Grossman, 1992). Alternatively, Titan could be rotating synchronously, but with a significant libration, although this seems less likely than non-synchronous rotation, which might be expected due to the eccentricity of the orbit (Sears et al. 1993). Subsequently, however, IR measurements have indicated that Titan is synchronous after all (Lemmon et al. 1994).

2.4 Microwave Radiometry

A significant problem with measuring (thermal) radio emission from Titan is that high angular resolution is required to eliminate background radiation from Saturn. Thus either very large telescopes are required, or interferometric methods must be employed.

Jaffe et al (1980) reported 6cm measurements of Titan, taken with the newly-commissioned Very Large Array (VLA) of telescopes in New Mexico. These data (which were published shortly after the Voyager encounter, and therefore probably didn't receive the attention they deserved) were able to indicate a surface brightness temperature of 87±9K. This was not accurate enough to discriminate between the 'thick' (Hunten) and 'thin' (Caldwell) models of Titan's atmosphere, but the authors did note - with some prescience - that this temperature was close to the triple point of methane and that part or all of the surface could be covered with liquid methane.

Microwave radiometry has also been used in an attempt to constrain the methane clouds that may exist above Titan's surface (Thompson and Sagan, 1984), although more recently Voyager infrared data has been used in preference.

More recent microwave radiometry, again with the VLA, (Muhleman et al. 1990; Grossman and Muhleman, 1992) measure the surface emission temperature at about 82±3K, suggesting (given

Body	Reflectivity at 3.5cm	Reflectivity at 12.5cm	Brightness Temperature (K)	Surface Temperature (K)	Emissivity
Callisto		0.25±0.05	92±9	115	0.72-0.88
Ganymede	0.4±0.06	0.61±0.15	67±6	107	0.57-0.68
Europa		1.1±0.25	47±10	97	0.38-0.59
Titan	0.33±0.25 0.19±0.11		80.4±0.6	92.5-101	0.81-0.90

Table 2.1 Radar reflectivities and microwave emissivities of icy satellites, after Lunine (1993). Note the similarity of Titan values to those of Callisto. Titan reflectivities are in opposite polarisation sense, Galileans are same sense : higher Titan value includes 'bright spot', lower value does not.

Proposal	U/Y/31	738RDL	A/94A/30
Title	Titan's Surface and Low Atmosphere, by Monitoring Variations in the 1-5 micron Windows	Monitoring Titan's Near-IR Albedo	Titan's Surface and Meteorology by Monitoring Orbital Variations in 1-2 micron Windows
Principal Applicant	A Coustenis	R Lorenz	J Zarnecki
Collaborators	R Lorenz, S Green, J Zarnecki, E Lellouch	A Coustenis, S Green, J Zarnecki	R Lorenz, S Green, A Coustenis
Observation Period	August-October 1993	July 1993-	July-September 1994
Telescope/Instrument	UKIRT/CGS4	UKIRT/CGS4	AAT/IRIS
Reason for Non-Award of Observing Time	CGS4 in wrong configuration (short camera not mounted)	Service observations too scattered to merit effort	Instrument Oversubscribed

Table 2.2: Observation Attempts during the PhD period of the present author

the surface temperature from the Voyager 1 radio-occultation measurement) an emissivity of about 0.8-0.9, consistent with a dirty ice surface , but not with a global ocean.

Such a high emissivity (higher than those of the Galilean satellites Europa and Ganymede, but similar to that of Callisto) is difficult to reconcile with a high reflectivity. It suggests the surface is solid, but is not 'clean' ice : ice contaminated with organic compounds and perhaps silicates too, seems to be the most plausible answer.

Table 2.1, taken from Lunine (1993) summarises the centimetre-wave reflectivities and emissivities of Titan and the icy Galilean satellites.

2.5 Near -Infrared Spectroscopy and Photometry

While the atmosphere is opaque at most optical and infrared wavelengths, due to absorption and scattering by the haze and gases (the haze dominates the opacity at visible wavelengths; gas opacity dominates in the IR), there are some near-infrared 'window' regions (0.94, 1.08, 1.28, 1.58, 2 and 5 microns) between the methane absorption bands, where it may be possible to sense the surface (Grundy et al., 1991; Stammes 1992; Lemmon et al. 1992). Recent observations (Lemmon et al. 1993; Griffith 1993) have noted a variation in albedo at these window wavelengths (see figure 2.1) that is correlated with the orbital period, suggesting that it is possible to sense the surface, or at least the lower troposphere, in these regions.

Observations by Griffith et al. (1991, 1992) at 1.28, 1.68 and 2.0 μm suggested a 'dirty ice' surface - neither completely dark, such as would be expected for a surface covered in organic material, nor a completely bright icy surface - the analogue suggested by Griffith et al. (1991) is "$^1/_3$ Ganymede+$^2/_3$ Phoebe". One scenario is a mixed surface - organics (solid and liquid) with ice, although it is impossible to discriminate with the data currently available whether this is an intimate mixture (dirty ice everywhere), an icy surface with lakes and seas present, or a dark organic/ice surface with some bright regions of ice exposed.

Observations at 5 μm (Noll and Knacke, 1993) also suggest, if the atmosphere is relatively transparent, then the surface albedo is too high for a global hydrocarbon covering, and resembles that of Callisto.

In an attempt to add to the growing body of data in this area, I have generated or been associated with several observation proposals during my PhD study period: all were unsuccessful. These proposals are listed in table 2.2 , together with their reasons for failure, as stated by PATT, the Panel for the Allocation of Telescope Time.

Recently, Lemmon et al. (1994) has produced a lightcurve of Titan, in several of the atmospheric windows, see, for example, figure 2.2. It is found that the lightcurve can be

Figure 2.1 Near-IR spectra of Titan at greatest Eastern and Western elongations, from Lemmon et al (1993). Note the spectrum is constant, except in the window regions at 0.94, 1.08, 1.28 μm where Titan is darker on its trailing face (that seen at GWE).

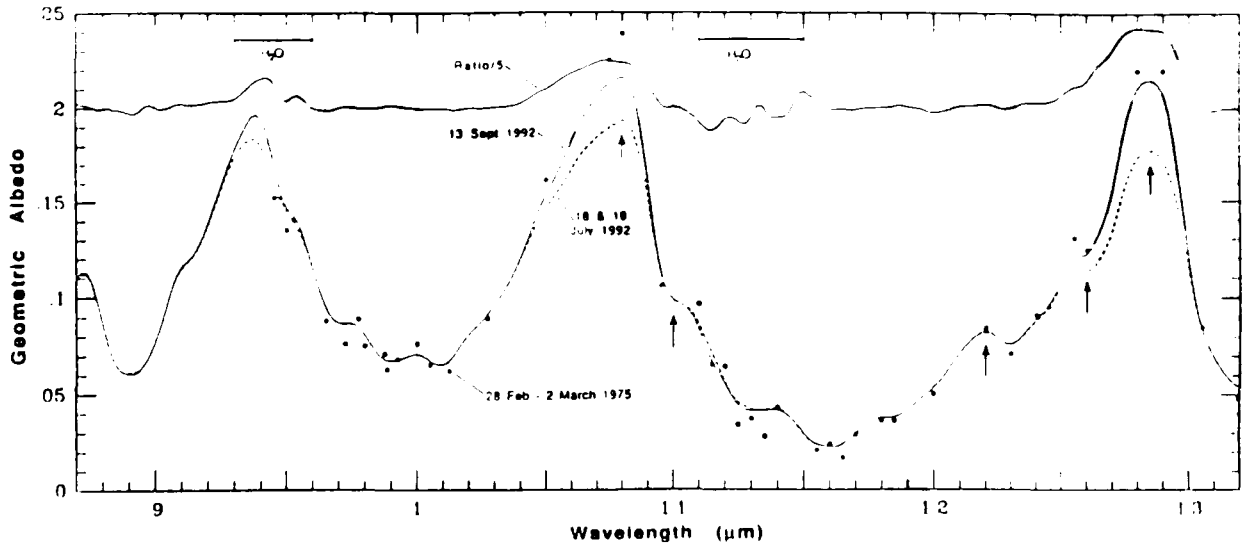

Figure 2.2 Lightcurve of Titan in the 2μm window, from Lemmon et al (1994). A model of Titan with two bright spots appears to reproduce the observed lightcurve.

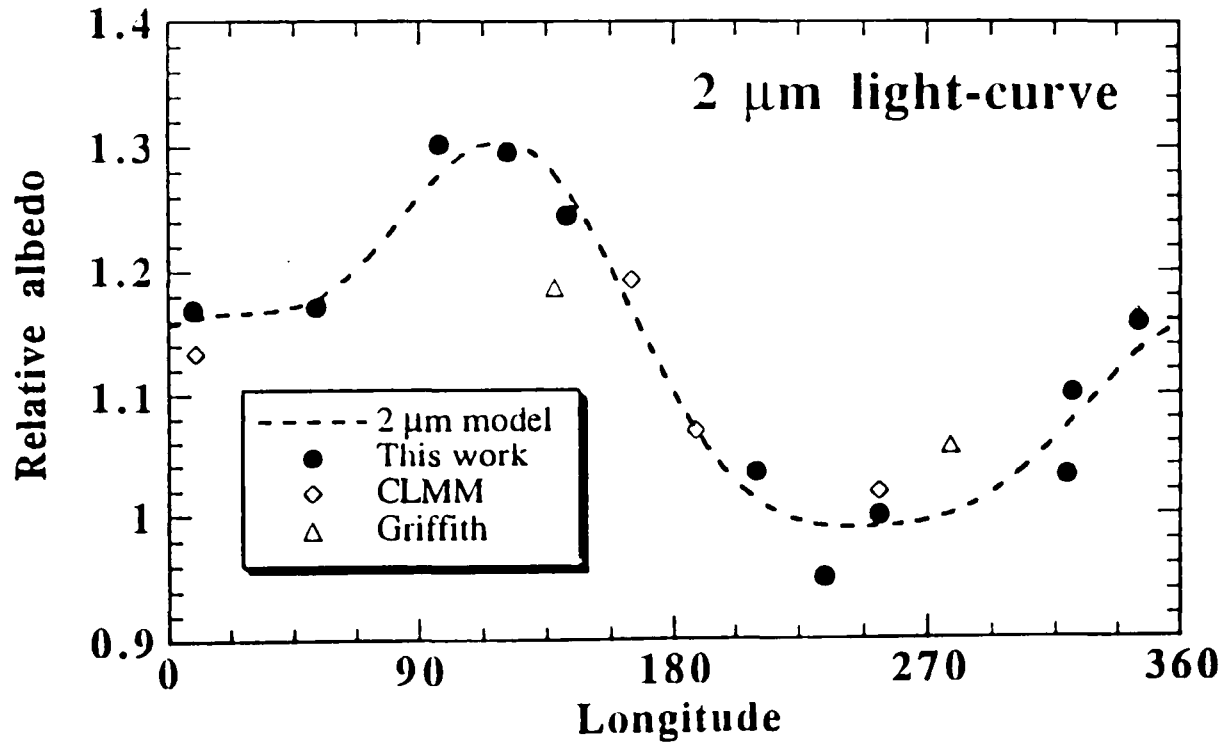

Figure 2.3 Adaptive optics image of Titan at 2μm with PSF for comparison (from Saint-Pe et al, 1993).The image is distinctly noncircular, although other details are difficult to see in this reproduction: see text for details

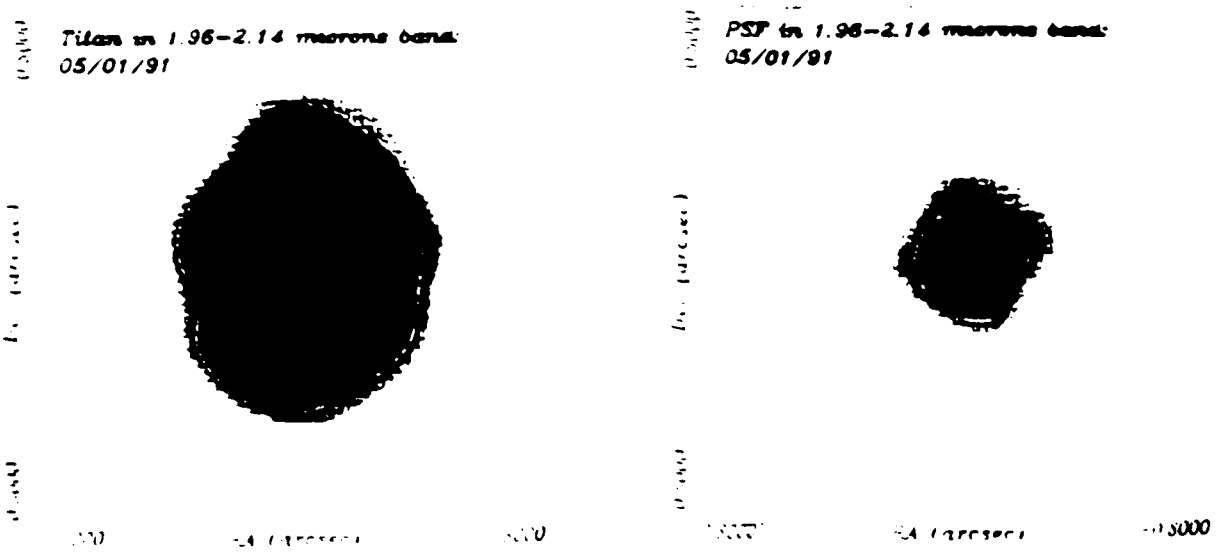

reproduced by a model of Titan with two bright spots, one near the sub-Saturn point, the other on the leading face of Titan, although he notes that many other surface albedo distributions could also generate the observed lightcurve. Additionally, by combining their data with that of earlier workers (Fink and Larson, 1979), Lemmon et al. (1994) have demonstrated that Titan's rotation is very close to synchronous (15.945±0.002 days).

Absolute measurement of the surface albedo is difficult, in part due to atmospheric effects on Titan. However, Coustenis et al. (1994) have derived estimates of the surface albedo in the 0.9-2μ window regions, and have inferred that the dominant surface material may be anhydrous silicates, although the spectrum is consistent with other surface types. I have argued that planetological considerations (see chapter 9) make silicates (especially anhydrous ones) unlikely as the dominant surface constituent. Additionally, Lemmon et al. (1994) have suggested that the calibration of Coustenis et al.'s results may be in error. Thus the issue remains as a 'hot topic' in Titan science.

2.6 Groundbased Adaptive Optics

The resolution of grounbased measurements by the larger telescopes is limited by the quality of atmospheric seeing: while the diffraction-limited resolution of large telescopes is of the order (λ/D, or about 0.1 arcseconds for a 4m telescope at near-IR wavelengths), the practical limit is of the order of 0.4 arcseconds. Titan is typically 0.8 arcseconds in diameter, so resolved measurements are impossible (cf. Comas Sola's observation, mentioned earlier).

However, the blurring and twinkling due to atmospheric turbulence (which causes small changes in the refractivity of the air along the line of sight, thereby disrupting the wavefront of light) can be compensated by modern techniques. In particular, the use of adaptive optics (see, e.g. Wild and Fugate, 1994) allows the diffraction-limited resolution to be recovered. In this technique, the wavefront is sensed using part of the incident light and the mirror shape is distorted in real-time (it is flexible, and its shape can be modified by piezoelectric transducers) to compensate for the atmospheric effects.

This technique has been successfully demonstrated on the ESO 4m telescope in Chile. Saint-Pe et al. (1993) obtained an image of Titan in the 2μm window region, sampled at 0.1 arcsecond/pixel. This image (fig 3.3) shows a distinct departure from circular symmetry. The interpretation of Saint-Pe et al. (1993) is that the polar cloud deck is enhanced in thickness, and that there are surface or deep atmosphere features at mid-latitudes.

In the coming years, we may expect considerable progress in this area.

2.7 Hubble Space Telescope Observations

The other way to avoid atmospheric effects on observations is to move the observatory above the atmosphere. Early assessments of the utility of the Hubble Space Telescope (HST) for Titan studies (Prange, 1985) focussed on UV observations (to detect aurora-like features in the upper atmosphere. Note that the UV albedo of Titan, useful in constraining the UV attenuation by Titan's atmosphere as an input to photochemical models, had been measured by both the IUE spacecraft, and the OAO-2 (Copernicus) satellite many years before). Also, since we are now almost one half a Saturnian year from the Voyager encounter, images in visible light have been used to study seasonal variation in the atmosphere (Caldwell et al. 1992). The HST also has a substantial IR capability, and with the realisation that the surface may be detected in the window regions, the exciting prospect of imaging the surface has emerged.

P Smith (private communication, see also Smith and Lemmon, 1993) has obtained 8 well-exposed images of Titan (~20 pixels across) with the Hubble Space Telescope on August 21, 1992 using the Wide-Field/Planetary Camera (WF/PC). This set of observations is limited, however, because:

1. the filters are not optimal - the 'surface' image is obtained by subtracting an image (showing a substantial hemispherical variation) in the methane absorption band from a broadband image (i.e. to synthesize spectrally an image in the methane window at 0.94 μm.) Naturally, the quality of, and confidence in, such an image is not as good as one using a 'real' filter.

2. the much-publicised error in the shape of the primary mirror of the telescope leads to a much broader point spread function than planned (i.e. spatial resolution of the image is degraded.) It is difficult to be certain that features in the image are real, rather than artifacts of the deconvolution algorithms used to artificially 'sharpen' the image.

Additionally, a single image is difficult to interpret unambiguously. The 'best guess' interpretation of the image is that there is a bright region around the pole, suggestive perhaps of polar clouds, and there are several distinct darker features in mid-latitudes, perhaps seas. However, the contrast of these features depends on the processing, so this interpretation is not conclusive.

(Interestingly, the image has yet to be widely published, in part, perhaps (Smith, personal communication) because Titan looks like a 'smiley face', and the observation might not be taken seriously by a public already fascinated with a 'face on Mars'. This is an interesting example of how politics, mass psychology and the presentation of an observation must be considered in planetary science. As a related point, the images of Halley's comet displayed during the live TV coverage of the Giotto flyby of comet P/Halley used false colour, to enhance contrasts.

However, since the public (and the scientific community) were not prepared what to expect, these multicoloured images were highly confusing, and instant interpretation of the images was impossible, and some of the dramtic impact was lost.)

A much more useful dataset will be obtained in autumn 1994, during Titan's next apparition. A sequence of images will be obtained using WF/PC-2 (the 2nd-generation wide-field/planetary camera): with a number of images (~10) in various filters covering an entire Titan orbit (~16 days) In this dataset, since WF/PC-2 incorporates corrective mirrors in its optical path, the uncertainties in image processing are obviated, and WF/PC-2 is equipped with much better filters for improving contrast in the window regions.

Since a large number of images will be obtained, it should be possible to track individual image features. Features moving at Titan's orbital angular rate may be expected to be either surface features or low-atmosphere features (e.g. orographic cloud) associated with surface topography, while faster moving features are presumably clouds at higher altitudes moving in the zonal wind field. Additional confirmation of the altitude features may be expected from comparison of feature contrasts in different filters, using models of the atmospheric opacity as a function of altitude and wavelength.

As an aside, it is interesting to note that the discrimination of surface and atmospheric features in the outer solar system is not a novel problem. In 'The Celestial Worlds Discover'd' (Huygens 1698, p.26) we find the following debate concerning features on Jupiter

> *'And at the going off of these Clouds, some spots have been taken of notice in him, much brighter than the rest of his Body, which remain'd but a little while., and then were hid from our sight. These Monsieur Cassini thinks are only the reflection from the Snow that covers the tops of the Hills in Jupiter: but I should rather think that it is only the colour of the Earth, which chances to be free from those Clouds that commonly darken it.'*

It is likely that the HST/WF-PC2 dataset will be the best information available on the geographical distribution of features on Titan's surface until the Cassini mission arrives, although if progress in groundbased adaptive optics continues, even HST imagery may be superceded.

2.8 X-Ray Observations

Zarnecki et al. (personal communication) have proposed observing Titan in X-rays. Ordinarily, a body with a thick atmosphere would not be expected to be detectable in X-rays, but if there is significant (~10%) abundance of argon in the atmosphere, fluorescence of argon excited by solar flare activity or magnetospheric electrons might yield a detectable X-ray flux. The proposed

instrument is an X-ray detector on the Japanese ASCA satellite, but to date no observing time has been awarded.

2.9 Timing of Observations

When Galileo first observed Saturn, he noted it had an unusual appearance - he interpreted its curious shape as being due to two large satellites. Huygens, four decades later, was the first to correctly interpret the appearance as being due to flat rings around the planet. He had two advantages - first his optics were of better quality (he made them himself), and second, he was a 'Cartesian' thinker (Van Helden, 1984, notes the probable influence of Descarte's ideas on Huygens: see also Huygens 1698), and having already discovered Titan and knowing the plane of its orbit, was perhaps 'expecting' the rings to lie in the same plane, as indeed they appear to do. When both Galileo and Huygens observed Titan, the ring-plane was nearly edge-on to the Earth.

The tilt of the ring plane is still of importance today. First, the tilt of the ring plane (which is also the plane of Titan's orbit) leads to seasonal variations such as the North-South asymmetry - Huygens himself remarked that the seasons would be tediously long due to the length of the Saturnian year. Secondly, during those times (next occurring in 1996) that the ring plane is edge-on from the Earth, Titan is obscured by Saturn at superior conjunction, and difficult to discriminate from Saturn at inferior conjunction and so can only be observed at eastern and western elongations.

If Titan is in synchronous rotation, then the anti-Saturnward face of Titan (180° longitude - near where the Huygens probe will enter and land) cannot therefore be seen between about 1996 and 2002.

2.10 Conclusions

Groundbased measurements in the last 4 years have been crucial in shaping our understanding of Titan's surface; these measurements have often used the most powerful instruments available (the VLA, the IRAM instrument, and 4m infrared telescopes (UKIRT, Kitt Peak, ESO, CFH, and IRTF). Perhaps the most significant observations have been the Goldstone/VLA radar measurements, which have been instrumental in largely eliminating the 'global ocean' model of the surface.

It is interesting to note that not all of the advances in observations have been due to technological improvements in the instruments themselves. A large part has been played by the refinement of models and the improved interpretation of data - the near-IR window studies rely neither on difficult techniques nor on especially advanced instrumentation; the critical

advance was the realisation itself that such measurements might reveal the surface. Similarly the stellar occultation measurements require only modest equipment, but the achievement of deducing the atmospheric superrotation from various groundbased occultation profiles (including those obtained by amateurs) is remarkable.

We may expect some further modest progress in the next couple of years due to continued radar and IR monitoring, plus the HST WF/PC-2 observations. These will give us - probably - a good idea of the gross distribution of features on the surface (i.e. large continents/seas) and possibly the identification of spectral features of water ice. However, the real revelation of Titan's surface must await the arrival of Cassini.

Chapter 3

Pioneer and Voyager Results

Thy cheeks look red as Titan's face, Blushing to be encounter'd with a cloud
William Shakespeare
Titus Andronicus

In this section I review some pertinent results from the Pioneer and Voyager missions to the Saturnian system, in order to point out the constraints they put on surface conditions on Titan, and to put into perspective the capabilities of the instrumentation on Cassini/Huygens, and how the Cassini results may be used.

3.1 Pioneer 11

The Pioneer 11 spacecraft (see figure 4.1) was only modestly equipped with scientific instruments, by comparison with the much larger and more sophisticated Voyager spacecraft (see table 3.1). However, its payload did provide some information about the Saturnian environment and Titan itself.

3.1.1 Dust Measurements

The Pioneer spacecraft were equipped with a dust impact detector comprising a number of sealed cells. When the metal foils forming the cells were punctured, the gas was lost, the evacuation of the cell being detected by electrical means. Thus, by monitoring the number of cells which retained their gas over time, the flux of meteoric material could be inferred. To date, the Pioneer 10 and 11 observations remain the only direct dust measurements beyond Jupiter. (The Voyager spacecraft did measure dust populations in the Saturnian ring system, but only indirectly - see later.)

The Pioneer 11 measurements, which found an approximately constant number density of meteoroids between 1 and 18 AU from the sun (Humes 1980) have been used to refine the models used in estimating the size and velocity distributions of the meteoric flux incident on Titan (see chapter 9).

3.1.2 Photopolarimetry

Unlike the complex vidicon camera system of the Voyagers, the imaging capability of the Pioneers was based on a very simple device, essentially a telescope with a (non-spatially-resolved) detector at its focus (i.e. a photometer.) Images were obtained by using the spin of the

spacecraft to sweep a 'raster' pattern. While crude, and offering spatial resolutions far poorer than an imaging detector, such a technique does have some advantages, particularly where photometric measurements are concerned . In addition to colour filters, polarising filters could be placed in the optical path, hence the instrument is a photopolarimeter, and obtained better polarisation measurements than was possible with Voyager.

Pioneer 11 passed 360,000 km from Titan (60 times further away than Voyager 1): images from Pioneer had a resolution of ~170 km (Smith, 1980).

These polarisation measurements (Tomasko, 1980) naturally only probed the upper haze layers. However, they were instrumental in pointing to the fractal nature of Titan's aerosols, in that the polarisation data obtained (suggesting small particles, with diameter 0.09 μm) was incompatible with the larger aerosol particles required to fit Voyager infra-red measurements (Toon et al. 1988).

3.1.3 Infrared Measurements

The infrared instrument on Pioneer was relatively simple, measuring flux at only 20 μm and 45 μm. The measurements of Titan (brightness temperature of 56K at 20 μm and 75K at 45 μm) were difficult to make, since at the large encounter distance, Titan did not fill the field of view, and integration times were limited by the spacecraft (Froidevaux and Ingersoll, 1980). The measurements were in good agreement with groundbased observations.

3.2 Voyager

3.2.1 Imaging Science

The Voyager cameras were able to image Saturnian satellites with resolutions down to 1km, three orders of magnitude better than groundbased observations, and two times better than Pioneer 11. For a summary of results in the Saturnian system, see Smith et al. (1981).
While Titan was given close attention during the encounter (50% of the illuminated disk was imaged at resolutions better than 1.3 km per line pair) there was no small-scale contrast detected. Smith et al. thereby inferred, on the basis of albedo ranges 0.35-0.50 (typical for many Saturnian satellites) that the (visible) optical depth of the atmosphere $\tau>5$ (i.e. at least as great as that on Mars at the height of a global dust storm.)

Some large-scale contrasts were noted, in particular a north-south assymmetry, with the northern hemisphere slightly darker and redder than the south, and with a dark polar hood,

these features being due to seasonal effects or perhaps due to periodic variations in the charged particle flux and consequent aerosol chemistry. The seasonal explanation (it was just after northern winter during the Voyager 1 encounter) seems most likely: see Sromovsky et al. (1981) for a fuller discussion. The 'equator' lies (within observational error) in Titan's orbital plane, suggesting that Titan was tidally locked, although see chapter 2.

Contrast enhancement revealed zonal features, implying an atmospheric circulation reminiscent of Jupiter or Saturn. Extreme enhancement suggested trackable cloud features, moving in a prograde direction (Wenkert and Garneau, 1987), but as the features are enhancement-dependent these data have not been considered reliable, and have never been fully published.

Thus, while the images of Voyager were able to prove important in our understanding of Titan's circulation (and probable rotation) and the aerosol structure, they provided no data about the surface itself: the optical limb was estimated at 240km above the solid surface measured by the radio-occultation experiment (hence the view once held that Titan was the largest satellite in the solar system: the 250km depth of the optically-thick atmosphere was the upper limit deduced by Smith (1980) from Pioneer data.)

3.2.2 Ultraviolet Spectrometer

The results (Broadfoot et al., 1981) from the Ultraviolet Spectrometer (UVS) gave the initial confirmation that the 'thick' atmosphere suggested by Hunten (1974) was the correct one, in that nitrogen was present (detectable by its UV emission in the upper atmosphere).

Further, the UVS results pointed that the dominant atmospheric constituent with m=28, which could have been either CO or N_2, was the latter. (This of course raised the subsequent question: where is all the CO that was expected from cosmogonical considerations? The CO question has important implications for the origin and evolution of Titan and its atmosphere: see chapter 9).

Argon, which would be expected from cosmic abundance considerations, might also be present in Titan's atmosphere. The relative molecular mass constraint imposed by the RO data, and the methane abundance allowed by saturation above the tropopause, would allow argon abundances of up to 20%.

However, large amounts of argon, it was realised in Phase B of the Huygens project, would lead to an enhanced radiative heat flux from the shock layer during the entry phase of the probe, requiring a redesign of the thermal protection system. Thus constraining the argon abundance

became a matter of scientific urgency: Strobel et al (1993) re-examined the V1 UVS data, and inferred that the argon abundance in the atmosphere is <10% (although this may be sensitive to the assumed stratospheric methane abundance - see later).

3.2.4 Infrared Measurements

The Infrared Instrument (IRIS) on Voyager 1 used a Michelson interferometer to record spectra between 180 and 2500 cm^{-1} with a resolution of 4.3 cm^{-1} (i.e. 55 μm to 4 μm, with $\lambda/\Delta\lambda$~580.) A spectrum of Titan taken by IRIS is shown in figure 3.1 ; the peak due to C_2H_2 is striking.

Detection of HCN by IRIS confirmed the presence of nitrogen as an atmospheric constituent (as suggested by the UVS), while no oxygen compounds were detected by IRIS, eliminating an atmosphere dominated by CO (although CO was detected later as a trace gas- see chapter 2).

CH_4, C_2H_6, C_2H_2 and C_2H_4 were identified (with tentative identifications of C_3H_4 and C_3H_8) from the data, and estimates made of their abundances (several of these compounds had already been detected by groundbased observations).

Measurements across Titan's disk allowed the variation of radiance with emission angle to be measured. Limb brightening occurs for wave numbers >600 cm^{-1}, implying emission from above the temperature minimum, whereas for 200 to 500 cm^{-1}, limb darkening occurs, suggesting emission from below the minimum. It was inferred from these observations that the atmosphere was transparent (τ<0.1) for 500 to 600 cm^{-1}, where the brightness temperature was 93K (with the consequent implication that the surface temperature was around this value.)

(As an aside, the IRIS PI originally indended to be taking spectra of the polar regions during the closest approach. However, the imaging team preferred to be looking at the centre of Titan's disk, to obtain maximum spatial resolution. As a result, an IRIS dataset was obtained (since the imager and IRIS are mounted coaxially) near the equator with nadir viewing conditions. This proved fortuitous (Samuelson, private communication), since this data could be compared with the limb-viewing data obtained near the radio-occultation measurement site, at a similar latitude. This comparison allowed the detection of molecular hydrogen in Titan's atmosphere much more easily than would otherwise be possible).

Interpretation of the IRIS data for abundance measurements of the various species relies on a good estimate of the temperature profile. Similarly, the range in estimated ocean depth (Dubouloz et al., 1989) is due to the uncertaintly in surface temperature and composition.

Table 3.1 Payloads of Pioneer and Voyager Spacecraft

Pioneer 11 Instrument	Mass	Voyager Instrument	Mass	
Imaging Photopolarimeter	4.3	Imaging Science Subsystem	38.2	
Infrared Radiometer	2.0	Infrared Spectrometer	30.2	
Magnetometer	2.6	Ultraviolet Spectrometer	4.5	
Plasma Analyser	5.5	Photopolarimeter	4.4	
Charged Particle Composition Expt	3.3	Planetary Radio Astronomy	7.7	
UV Photometer	0.68	Magnetometers	5.6	
Cosmic Ray Telescope	3.2	Plasma Particle Experiment	9.9	
Geiger Tube Telescopes	1.6	Low Energy Charged Particles	7.5	
Jovian Trapped-Radiation Detector	1.77	Plasma Wave System	1.4	
Asteroid-Meteoroid Detector	3.3	Cosmic Ray Telescope	3.2	
Meteoroid Detector	1.68	Radio Science Subsystem	1?	
Total	30		114	(kg)

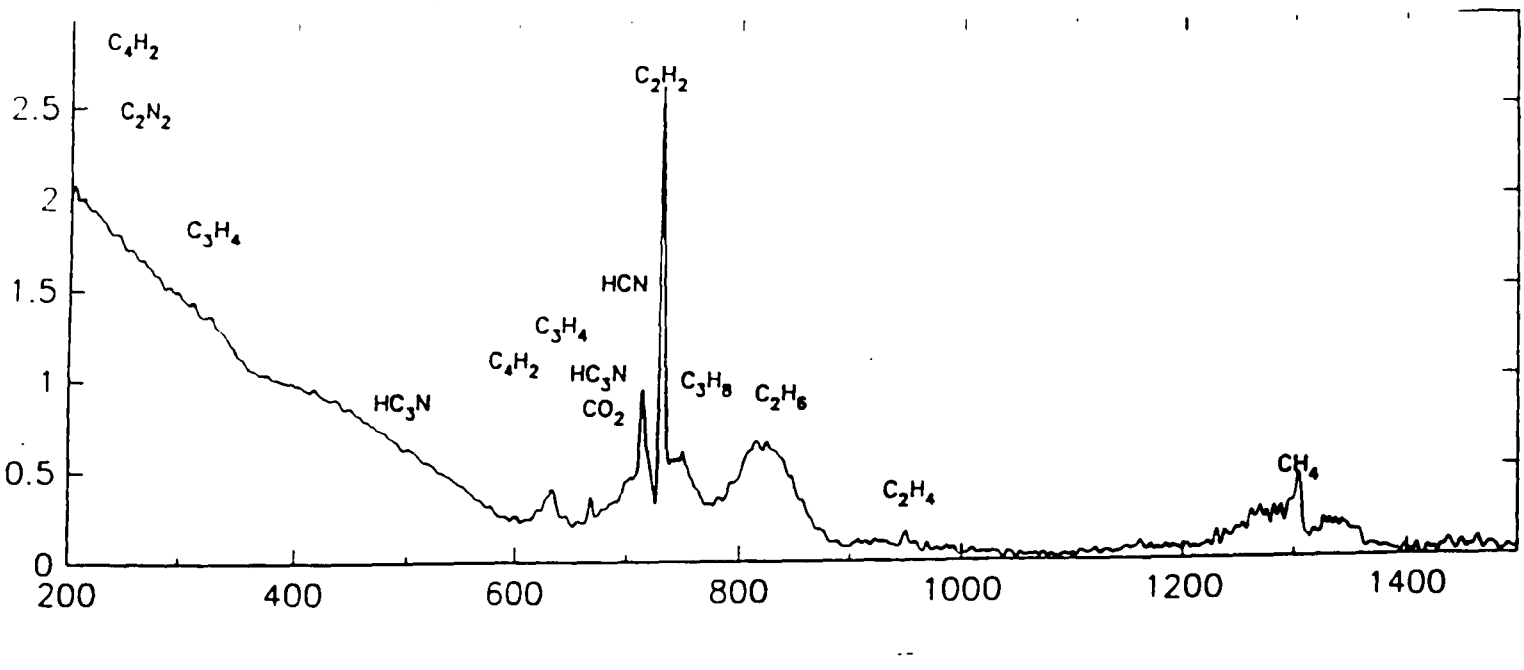

Figure 3.1 Infrared spectrum of Titan's equatorial region. The atmosphere is totally opaque in this spectral region, and the spectrum is dominated by gas emissions: prominent peaks are identified: the acetylene peak is striking. Abscissa is wavenumber in cm^{-1} , ordinate is radiance in erg s^{-1} cm^{-2} sr^{-1}/cm^{-1}

(See, e.g. Hanel et al.(1991), Coustenis et al.(1989) etc.)

Lellouch et al. (1989) made a close analysis of the RO and IRIS data, to improve the model temperature profile. This, and improved laboratory data, enabled Coustenis et al. (1989a,b, 1991) to perform a painstaking and systematic analysis of the V1 IRIS data, most of which had lain untouched in archives since the encounter. As well as measuring spatial variations in composition (connected with the hemispherical assymetry mentioned above) Coustenis (1990) was able to make vastly improved abundance estimates (with error bars : it is noted that the error bars are dominated by uncertainty in the thermal profile) of a number of compounds. These abundance measurements have been instrumental in validating revised photochemical models of Titan's atmosphere (such as that of Lara(1993)), and in turn suggesting the accumulated ethane depth on Titan's surface may be lower than was originally thought.

Flasar et al (1981) used the meridional variation in IRIS brightness temperature to infer an equator-to-pole temperature gradient, that in turn implied a planetary circulation dominated by strong zonal winds (of order 100 ms^{-1} at 200km altitude near the equator). These zonal winds have since been confirmed by the fortuitous occultation by Titan of the star Sgr 28 and by circulation models (see Chapter 2). The direction of the winds (of considerable importance for estimating the landing point of the Huygens probe - see chapter 5) cannot be confidently predicted as prograde, although V1 image data (see above) hinted at prograde rotation, and there is in any case no good reason to suspect counter-rotating winds. The question will probably be resolved soon, thanks to spatially-resolved interferometric doppler measurements of millimeter-wave HCN emissions and the use of HST images in the near-IR windows to track cloud features.

The pole-equator contrast in brightness temperature at 340 cm^{-1} from the IRIS measurements was inferred by Stevenson and Potter (1985) to echo a similar contrast in surface temperatures, and that the lower polar surface temperature was consistent with polar 'caps' of liquid methane (which would float above any ethane-rich seas present, they argue) pinning the polar temperatures to a fixed value throughout the seasonal cycle. This interesting interpretation remains controversial, however (Flasar 1992), since the 340 cm^{-1} radiance may not be sensitive to surface conditions, but rather dominated by stratospheric contributions (Toon et al. 1988), and the retention of polar caps of liquid in the face of a strong tidal potential seems problematic.

A hemispheric assymetry in the brightness temperature of the 1304 cm^{-1} IR emission (due to methane emission in the stratosphere) suggests that this emission lags the solar heating by one season (as, approximately, does the visible assymetry noted above) but at this altitude the radiative time constant is too short to account for this lag. This has been interpreted by Flasar and Conrath (1990) as an effect of dynamic inertia, whereby the response to solar forcing is slowed by the involvement of deeper layers of the atmosphere. During the Voyager encounter,

this would have been an upwelling at northern midlatitudes (where it was spring) and a subsidence at southern midlatitudes. Observations by Cassini, which will cover about half a Titanian season, will help to understand this phenomenon, which may be coupled to photochemical effects (Coustenis, 1990).

Above 250km, where the V1 RO data has too poor a signal-to-noise to be useful, IRIS and UVS data have been used to constrain the thermosphere profile (Lellouch et al. 1989). This region is particularly important, since the Huygens probe experiences its maximum deceleration and heating above 250km.

The IRIS data, 14 years on, is continuing to yield information. Coustenis et al. (1994b) have identified water ice features in the stratosphere in IRIS data. Additionally Samuelson (private communication) has suggested that the best spectral fits to IRIS data are obtained by assuming a supersaturation of methane in the upper troposphere (a phenomenon which carries important implications for the Huygens probe, for both entry heat fluxes and potential icing, and for condensation physics) and that the ortho:para ratio of hydrogen may differ from its equilibrium value, suggesting hydrogen is rapidly transported away from its formation region.

The enormous contribution, in several diverse disciplines, of the IRIS measurements may be noted. The contribution from the Cassini IR instrumentation (VIMS, CIRS and DISR) may be expected to be similarly formidable.

As an aside, it may be mentioned that some IRIS data on Titan was taken by V2, some months later. This data, due to the much greater distance from Titan, has much poorer signal to noise, and was thus left unused. Recently Letourneur and Coustenis (1993) examined the data, and were able to extract composition measurements, in agreement with the data from V1.

3.2.4 Radio Occultation

The close flyby of Titan, and in particular the requirement to perform radio-occultation measurements of its atmosphere, was the prime driver of Voyager 1's trajectory selection through the Saturnian system, a trajectory which caused it to be deflected out of the ecliptic, precluding further planetary encounters. Its sister spacecraft, Voyager 2, free of the Titan encounter constraint, was able to go on to make startling discoveries at Uranus and Neptune. It must be stressed that, the Titan encounter was of such importance that had V1 developed a fault en route to Titan, V2 would have been retargeted to make the Titan encounter instead, and we would be largely ignorant today of the Uranian and Neptunian systems.

The two dominant atmosphere models, that of a thin methane atmosphere, and a much thicker nitrogen-methane one, could only be resolved by Voyager. The presence of nitrogen was detected by the UVS experiment, suggesting the latter (suspected in any case, owing to the high optical depth of the atmosphere) but the only way to discover the surface conditions was by radio-occultation. (Hunten's 1974 graph of his suggested temperature profile has an adiabatic lapse rate below the tropopause, but there was no way to know where it stopped, i.e. at what barometric altitude the 'ground' was : a surface pressure of up to 20 bar was considered.

The radio-occultation technique relies on passing the radio signal from the spacecraft through the atmosphere, and noting the signal strength received on the ground. A priori knowledge of the spacecraft trajectory allows calculation of the planetocentric altitude of the radio beam : the ground signal strength depends on the attenuation along this path, but more importantly on the refraction of the beam (the tiny change in direction of transmission has a detectable effect because of the huge 'optical lever' due to the large Titan-Earth distance). Thus the initial data product is a profile of refractivity against altitude. This is essentially proportional to the ratio of absolute temperature to relative molecular mass. If temperature is known at a given altitude (e.g. from infrared measurements) then the relative molecular mass can be determined, and (assuming this remains constant with altitude) the temperature profile throughout the atmosphere can be computed.

The cut-off altitude of the signal determines the radius of the planet at that point. The ingress and egress occultation points were at 6.2°N, 258°E and 8.5°S, 76°E respectively, with the two profiles being essentially identical.

The initial results of the V1 RO experiment are given in Tyler et al. (1981), where the temperature profile was computed for a nitrogen (m=28) atmosphere: see figure 3.2. A more detailed analysis is found in Lindal et al. (1983). The implications of the RO experiment for surface conditions are given in Flasar (1983) and Eshleman et al. (1983); see also Maguire et al. (1981). These analyses indicate that the near-surface atmosphere at the two occultation points (equatorial, and about 180° apart) had a methane humidity <70°; see figure 3.3. A natural implication is that a pure methane ocean could not exist at these points, although as Flasar (1981) states in a note added in proof, and Lunine et al.(1983) explain in detail, a mixed hydrocarbon ocean is compatible with these data.

A subsequent re-analysis, in conjunction with IRIS data, was performed by Lellouch et al. (1989) to evaluate the error bars associated with this profile, and to generate an engineering model of the atmosphere (Lellouch and Hunten, 1987). An important result was the range of allowable surface conditions, with a temperature from 92.5K to 101K. This 'hot' case allows a high

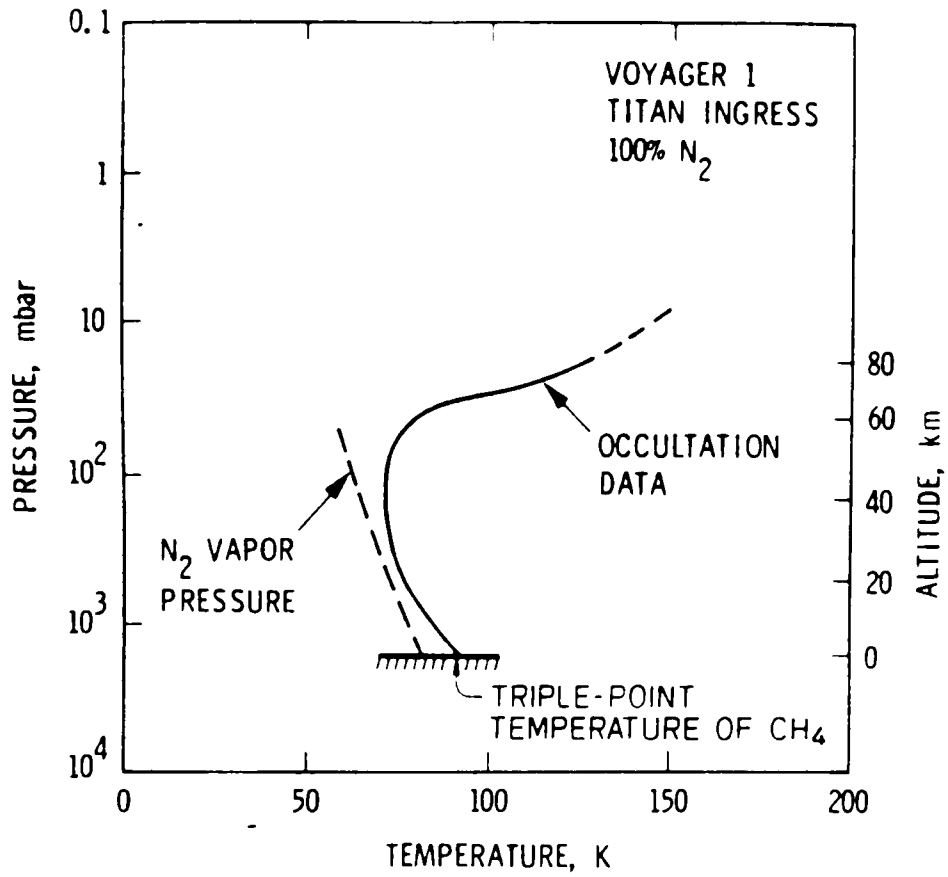

Figure 3.2 Radio-occultation profile from Lindal et al (1981)

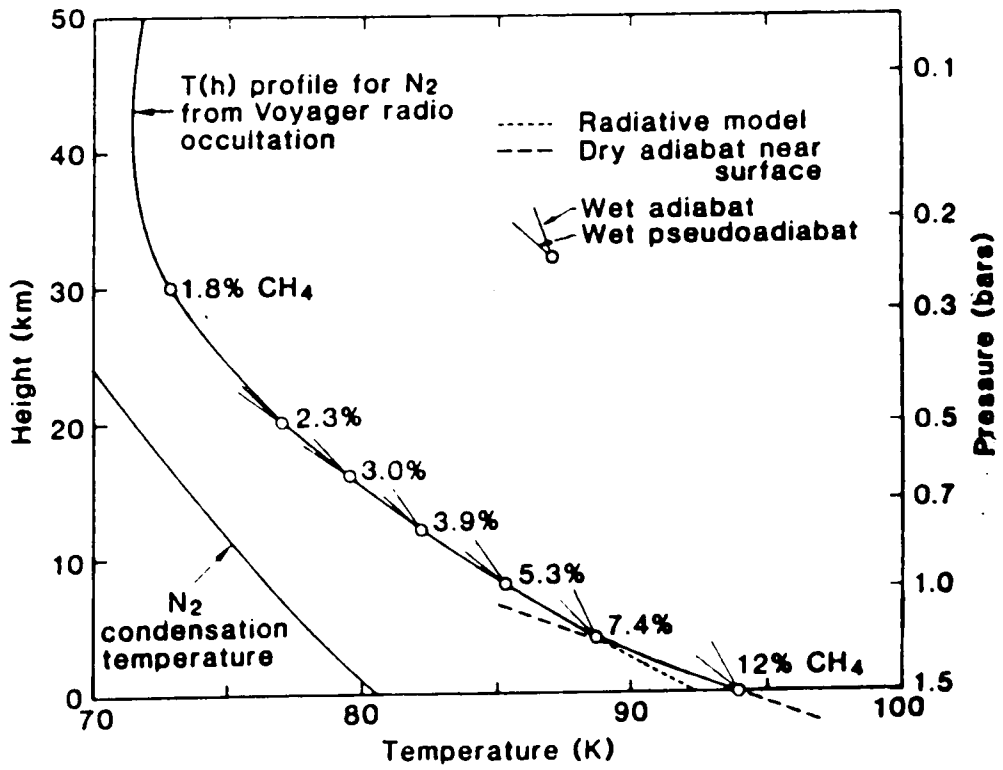

Figure 3.3 Detail of near-surface radio-occultation profile, showing undersaturation of lowest few kilometres. From Eshleman et al. (1983)

methane humidity, coupled to a high methane abundance in the ocean, leading to an upper limit of 9km global depth.

Some additional features of Titan's atmosphere were deduced from analysis of the RO data. For example, short-term variations in the received signal strength have been interpreted as being due to gravity waves in the atmosphere (Hinson and Tyler, 1983): an alternative, but less likely, explanation involves patchy, but thick, clouds (the atmospheric attenuation of the signal, at both S- and X- bands, was less than 2 dB - this argues against, perhaps, extremely high liquid content of clouds/rain). Differential dispersive measurements were used to measure electron density in the upper atmosphere: ionisation levels of less than about $4x10^3$ cm^{-3} were deduced (which are important in assessing the detectability of lightning on Titan).

3.2.5 Planetary Radio Astronomy

The PRA antennae on Voyager were used, without success, to search for emissions due to lightning on Titan. (Lightning would have important implications for the Huygens probe design, and has been invoked to explain the abundance of certain organic species which are difficult to produce photochemically).

The failure to detect emissions placed an upper limit on the level of lightning activity on Titan (Desch and Kaiser, 1990) although Grard (1992) and Grard et al. (1993) have argued that such emissions would have been shielded by a layer produced by meteoric ionisation (Ip, 1990). The failure of the V1 RO experiment to detect this may have been due to spatial and temporal variability in the thickness and density of the layer, Grard argues, although recent work on the meteoric input into Titan (section 9.3, and English et al. 1994 - Appendix 10) suggest that meteoric ionisation is small. Further, I (with others) have argued on the basis of PRA results and theoretical considerations that no lightning should occur (Lorenz, Coustenis and Zarka, unpublished).

3.2.5 Plasma Instrumentation

A variety of 'fields and particles' experiments were carried on Voyager, for example the Plasma Wave System (PWS) which used the PRA antennae to search for varying electric fields. While such classic 'space physics' measurements are not directly associated with the study of planetary surfaces, the PWS is relevant in that it detected impulsive 'shot noise' as the Voyager spacecraft crossed the ring plane. This noise is believed to be due to the impact of dust particles with the spacecraft (Gurnett et al., 1983).

These data have been used, in conjunction with Voyager photometry data, to constrain the number density of particles in the Saturn environment (clearly dust impact is a potential danger to the Cassini mission - see chapter 5). Dust in the Saturnian system is also of relevance for assessing the input of meteoric material to the atmosphere of Titan.

Other plasma instrumentation (Low Energy Charged Particle detector - LECP, Magnetometer) has been relevant in measuring the plasma environment at Titan. Energetic electrons from the Saturnian magnetosphere provide a significant input to Titan's atmosphere, leading to production of nitrogenous compounds (such as HCN) which cannot be accounted for by photochemical production alone.

The magnetometer on Voyager also usefully characterised Titan's magnetospheric environment and interactions. An additional (but unsurprising) result, relevant for consideration of Titan's interior, was that Titan has no significant intrinsic magnetic field: a conservative upper limit of 30nT at the surface was obtained (Ness et al., 1981).

3.3 Overview

We may note from the foregoing discussion several key points:

• despite the opacity of the atmosphere and the brevity of the Voyager encounter, we know almost all of what we do know about Titan from the V1 results.

• the importance of synergistic (and, by implication, simultaneous) measurements cannot be overstressed - unambiguous interpretation of the RO experiment would be impossible without the contributions of the UVS and IRIS instruments. One of Cassini's main strengths is not the formidable capabilities of each of its instruments, but rather the fact that they are all present together.

• The quantity of data handled by these experiments (particularly the spectroscopic instruments) is formidable. While the information-processing equipment available is adequate to handle the data, the human element in data analysis is often in short supply. The law of diminishing returns (in terms of results/papers per man-hour of effort) applies to scientific data as to any other commodity: it is all too easy to sweep up the obvious or dramatic conclusions during an encounter and then move on to other missions and problems. The painstaking efforts required to refine models, narrow error bars, and investigate spectral features which may be either unrecognised compounds or just noise, are superficially less attractive than skimming 'quick look' data, but are ultimately equally important to science,

and perhaps personally even more rewarding. Clear exampes are the reanalysis of the IRIS and UVS data. The value of readily-accessible data archives should therefore be noted.

• the importance in assimilating all available scientific data to generate environmental models for spacecraft engineering is evident: uncertainties and over-generous error bars lead to system over-design and loss of performance - the argon and methane abundance questions (affecting the entry heat flux, and hence the thermal protection system design), and the zonal wind direction (affecting the landing point and hence the radio link) are cases in point for the Huygens mission .

Chapter 4

Titan Exploration by Spacecraft

Given ships or sails adapted to the breezes of heaven, there will be those who will not shrink from even that vast expanse.
Johannes Kepler
Dissertatio cum Nuncio Sidereo (1610)

4.1 Pre-Cassini Studies

Outer planet exploration became possible in the mid-70s. The Pioneer 10 (Jupiter 1973) and 11 (Jupiter 1974, Saturn 1979) missions were essentially engineering test vehicles, with modest (yet valid) scientific payloads: they successfully demonstrated the ability to build and communicate with a space vehicle at great distances and after flight times of several years (Wilson, 1987). These two missions paved the way for the much more ambitious Voyager 1 and 2 flights, the pertinent results of which have been mentioned in chapter 3. The Voyager and Pioneer spacecraft are illustrated in figure 4.1

Titan had been an object of intense interest, and even in 1976 (before any spacecraft had got near the Saturnian system!) NASA was sponsoring studies to identify options and required technologies for detailed Titan exploration. Unsurprisingly, since the Viking mission had recently taken place, and captured the public imagination in its search for life on Mars, the study (Martin-Marietta, 1976) includes many Viking-like elements (the contractor, Martin Marietta, was also prime contractor for Viking). Some remarkably exotic ideas are presented in the study, including helium balloons, hot-air balloons (using local air warmed by a flame using N_2O_4 oxidiser brought from Earth, and atmospheric methane!), a remote laser spectrometer (using a laser to vapourise samples at some distance from the lander, and deduce their composition by analysing their light emission), penetrators, synthetic aperture radar (from orbit) and artificial intelligence (for automatic site selection, and science planning, e.g. during a rainstorm to divert data rate from imaging to atmospheric measurements).

Once Voyager 1 and 2 were on their way, scientific planning (see Hunten, 1978) for subsequent missions began, and a favoured scientific concept was named SO2P - Saturn Orbiter and Dual Probe (one for Saturn, one for Titan). Such an ambitious mission anticipated improved transportation capabilitity, namely use of space shuttle with a nuclear-electric or solar-electric tug. The Saturn probe would probably have been based closely on Galileo, although the Titan probe was somewhat different.

A feature of Titan probe studies at this (pre-Voyager 1 Titan encounter) was that extreme atmosphere models had to be considered : a thin methane one, with a surface pressure of 17mbar, and a thick atmosphere, with a surface pressure of anything up to 20 bar. The design

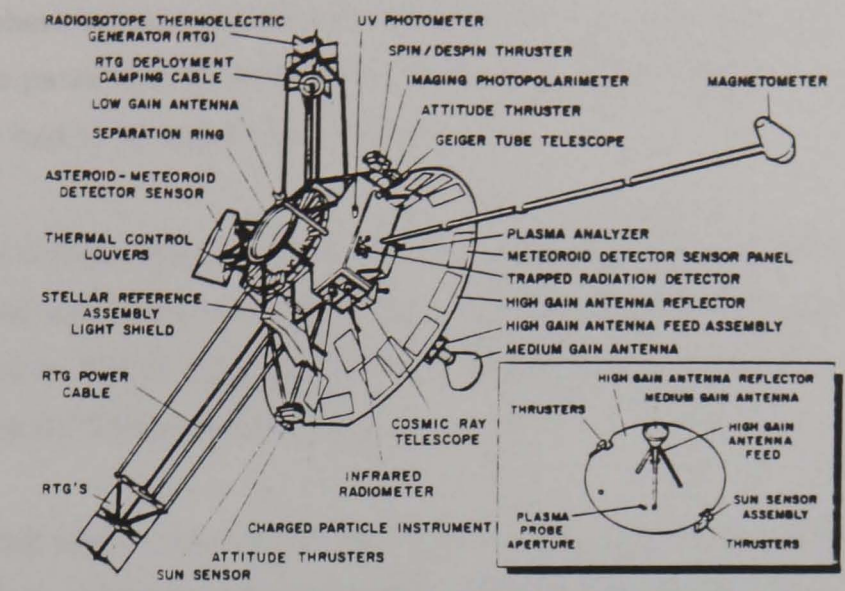

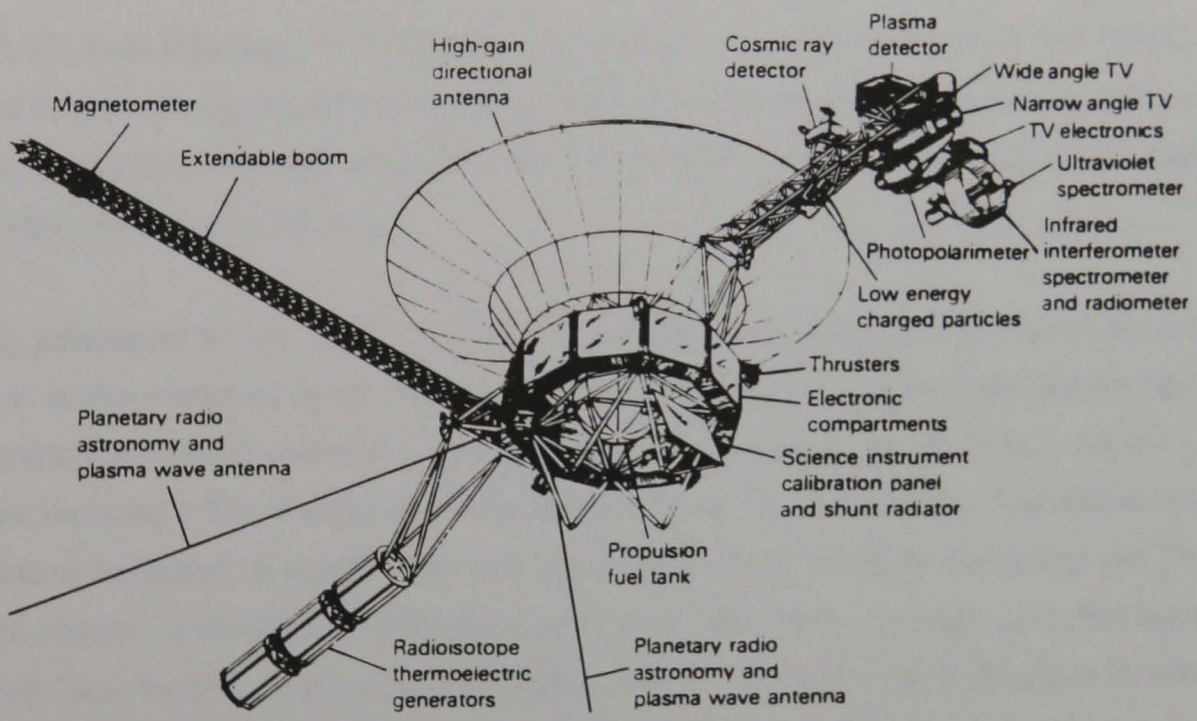

Figure 4.1 Pioneer 11 (above) and Voyager 2 (below) spacecraft From Wilson (1987)

Figures are approximately to scale (see also Cassini orbiter - Figure 5.9)

solutions (Murphy et al., 1981) for the two atmosphere models were slightly different - the thin atmosphere probe would require an 8m diameter parachute, whereas the thick atmosphere version would need to retain its 1.5m diameter entry shield for weight, and would have no parachute. Even then, its descent time to the surface could be up to 8 hours, and the battery had to be sized accordingly.

Surface science (impact accelerometry, alpha-backscatter and mass spectrometry of the surface material) was included in the 51kg payload, and with the impact velocity fixed at 20 ms^{-1}, the craft would be equipped with a crushable honeycomb impact attenuator, to limit impact loads on the 227kg probe to 300g.

A related Martin Marietta study (Castro 1980) identified required technologies (batteries, lubricants, magnetic bubble memory, etc.) for Titan exploration. A notable item is the need for materials that would be tough enough at cryogenic temperatures to be used in drill bits for the extraction of rock samples, although it was recognised that a liquid surface was also possible.

In 1983, NASA's Solar System Exploration Committee recommended that a Titan Probe/Radar Mapper be part of NASA's core programme, with a Saturn orbiter a candidate for a future mission (budgetary pressures, and the available transportation infrastructure, were making an SO2P-type mission unrealistic).

A study performed by the Science Applications International Corporation (SAIC) for NASA in 1983 (i.e. in the aftermath of the Voyager encounter) identified various concepts for advanced exploration (i.e. beyond that of a simple probe, as recommended by the SSEC). All the various concepts included a Titan orbiter for radar mapping, plus various probes (atmosphere probes, penetrators, balloons). A notable idea developed in some detail in the study was the Titan buoyant station - a dirigible or balloon (Friedlander 1984, 1985, although note that the idea of exploring Titan by balloon goes back somewhat further - see the work in France of Blamont 1978, Sable and Villaeys, 1982) and it was proposed that the dirigible might 'dunk' (using a tether) an instrument package onto the surface (or into any oceans).

4.2 Cassini Mission

The development of the Cassini mission, in context with other missons and studies, may be seen in table 4.1.

Following the success of the Voyager encounter with Saturn, and the participation of European scientists therein, a proposal was made to ESA in 1982 by Daniel Gautier and Wing Ip (leading a consortium of 27 co-proposers) for a mission they named Cassini. This would include a

Table 4.1 Development of Cassini in the context of other missions and observations

Date	Groundbased Observations	Other Missions and Studies	Pioneer + Galileo	Voyager	Cassini/Huygens
1969		<Apollo 11>	Approved Feb 1969		
1970					
1971		<Mariner 9>		Grand Tour cancelled	
1972	Trafton		P-10 Launch	Voyager (MJS) approved	
1973			P-10 Jupiter, P-11 Launch		
1974		Titan Atmosphere Workshop	P-11 Jupiter		
1975		<Viking>			
1976		MM Technology Study			
1977		Saturn System Workshop		V-1,V-2 Launched	
1978		<Pioneer Venus>	Galileo Planning begins		
1979	Fink & Larson		P-11 Saturn	V-1,V-2 Jupiter	
1980		Ames SOTP	Contractor selected (Hughes)	V-1 Saturn/Titan	
1981				V-2 Saturn	
1982					Mission Proposal to ESA
1983		SAIC Titan Exploration Study			NASA SSEC recommend Titan probe
1984			Asteroid flyby added to mission		NASA/ESA Assessment Study
1985					
1986		<Giotto>		V-2 Uranus	
1987					Phase A study (Marconi)
1988					ESA selection as M1
1989	Radar (Muhleman)		Galileo Launch	V-2 Neptune	
1990		<Ulysses Launch>			Payload,Contractor Selected
1991	IR window studies (Griffith)				Phase B Kick-Off
1992	Near-IR Variability		Gaspra flyby		
1993	Groundbased Adaptive Optics		Ida flyby		Phase C/D begins
1994	HST/WFPC-2 ?	<Mars-94, Clementine>			
1995		<MESUR Pathfinder,ISO>	Galileo Jupiter Arrival		
1996					
1997			Galileo Mission End ?		Nominal Launch date
1998	Arecibo Radar?				
1999					
2000					Jupiter Flyby
2001					
2002					
2003					
2004					Arrival at Saturn; Probe Delivery

European-built orbiter spacecraft and a US-supplied Titan probe (the US would also supply the RTGs, DSN support, and the launcher). The mission, as envisioned at this stage probably anticipated substantial heritage from the Galileo mission which was at advanced stages of development at this time.

Thus, with European space prowess growing (Spacelab was making its first flight around this time, and Giotto was in advanced stages of preparation) and with US and European thinking on outer planet exploration converging, the stage was set for collaborative study. A Joint Working Group (JWG) had been set up in 1982 by the European Science Foundation's Space Science Committee, and the Space Science Board of the US National Academy of Sciences, to study possible US-European cooperation : they recommended a Saturn Orbiter and Titan Probe mission , with launch foreseen for 1992 (see Johnson and Gautier, 1984).

A joint NASA/ESA assessment study (ESA 1985; Beckman & Scoon, 1985; Scoon 1985; see also ESA, 1986) was performed in 1984/1985 during which time it was decided to reverse the roles (as originally conceived) of the two partners, such that ESA would supply the Titan probe, with the orbiter to be supplied by NASA. In February 1986, ESA approved the Cassini 'Titan Atmosphere Probe' for a Phase A study.

The Phase-A study, performed in 1987-1988 by a consortium led by Marconi Space Systems, demonstrated the mission's feasibility. The study results are described in the Phase A report (NASA/ESA 1988, see also ESA 1989), and in various papers (e.g. Lebreton & Scoon, 1988). Key aspects are the use of a beryllium nose cap and a light carbon-carbon decelerator. The probe mass was 192 kg, including 40 kg of payload, and a 20kg decelerator.

A variety of technology studies were in progress following identification of technical challenges in the mission study phases. Among these included the use of expert systems (Ciarlo and Schilling, 1988) for science and engineering control during the mission, entry protection and parachute systems (Achtermann et al, 1986, Scoon et al, 1989), batteries etc.

The mission was adopted formally by its selection in November 1988 into ESA's Horizon 2000 science programme as the first Medium-class (M1) mission. The invitation to tender for Huygens Phase B was issued in April 1990, with two consortia delivering bids; one led by British Aerospace in Bristol, UK the other led by Aerospatiale of Cannes, France.

A change in the NASA schedule (reversing the priority of the CRAF and Cassini missions - see next chapter) was announced at about this point. The very tight Huygens development schedule imposed by a 1995 launch had particularly strong implications for the entry protection system on Huygens: to avoid schedule risk, less mass-efficient but conventional

insulator/ablator materials were preferred over more advanced technologies such as carbon-carbon.

The contrast between the high-technology, high-performance solutions suggested in the Phase-A study, and the less exciting, but pragmatic solutions eventually adopted by the project, is striking. In some senses this is disappointing, but in the opinion of this author, this caution is entirely appropriate owing to the fact that Titan is so unknown, and that failure of the Cassini mission would have a catastrophic impact on the progress of planetary science (e.g. while the science loss associated with the recent failure of the Mars Observer spacecraft can be recovered in perhaps 2-4 years, a Huygens reflight would take 10-15 years to put together, including its trip time (note also that after 1997 the non-availability of Jupiter gravity assist (see Murrow (1993) and Hechler (1990)) imposes a trip-time penalty of about 2 years; Jupiter swingbys become available again in 2014 - see also Appendix 1)

In the last days of September 1990 (when the author's involvement in the project began) the Scientific Payload for Huygens was selected, much as it is now (although many of the payloads were descoped somewhat from their original proposals - see chapter 6). Aerospatiale was officially selected in October 1990 as the prime contractor (ESA/IPC(90)129), with contract kick-off in January 1991.

Design and construction details of the probe and payload that are relevant to the study of Titan's surface are discussed elsewhere (chapters 5 and 6). Suffice it to say in general, however, that the early days saw much hard work on the part of ESA, industry and the science community, and were exciting and stimulating to be involved in. As paperwork turns slowly into hardware, the probe mass has grown considerably, partly as a result of the heavier entry protection system : at the time of writing, the probe descent module mass is 209kg, with the probe as a whole about 340kg.

It is pertinent to note here the annual budget review by US Congress and its impact on NASA programmes. There was extreme concern in early 1991 that Cassini would be sacrificed to pay for the space station; it survived. In 1992, budgets were again tight (see, e.g. Isbell 1992), and Cassini's sister mission CRAF was cancelled, with the Cassini launch slipped 2 years - increasing total cost, but decreasing the 1992 cost. Pressure was put on Cassini to de-scope and reduce costs when it was realised that halving the number of spacecraft in the Mariner Mk.2 series would not halve the costs: this cost-reduction exercise resulted in the deletion of the orbiter instrument scan platform and turntable and the probe relay antenna, with important implications for the probe mission (these aspects are discussed in more detail in chapter 5). At the time of writing (July 1994), the US Senate is debating once more NASA's budget, and whether Cassini should be cancelled.

As the launch date nears, and the peak of the Cassini spending profile is traversed, we may grow confident that the mission will take place, although it seems that in the current political/funding climate, with a focus on small missions, Cassini may be the 'last of the dinosaurs'. One of Cassini's strengths, however, is that its large payload ensures support from a broad cross-section of the planetary science community.

4.3 Post-Cassini Exploration

In the early 1990s, when the 'global ocean' was still the dominant model of Titan's surface, some studies were performed by the present author on possible submarines for the exploration of Titan's oceans and seabed. These studies (R Lorenz, unpublished manuscript 'Exploration of Titan's Oceans by Unmanned Submersible') were prompted by the inaccessibility of these interesting regions by other means, and by recent UK initiatives to develop autonomous submersibles for the exploration of the terrrestrial oceans and seabed (McCartney and Collar, 1990, and Collar et al., 1990).

Some notable conclusions of these studies are noted below:

- Improvement of RTG thermoelectric energy conversion by cooling of the cold junction by the ocean, leading to improved specific mass of the power system.
- The need for several centimetres of foam insulation, to balance the heat lost to the ocean with that produced by the RTG (typical RTG thermal output is 10-20 times the electrical output).
- The low increase of pressure with depth on Titan, due in part to lower fluid density, and mostly due to the lower gravity (a pressure of 20 bar is reached under 200m of water on Earth, but under 2.5 km of ethane on Titan), means a pressure hull, if needed at all - perhaps the interior could be pressurised with 'boiled' ocean, could be relatively light.
- The electric motor used to drive the screw could use high-T_c superconductors, cooled by the ocean, lowering the power required for propulsion.
- Care would be needed in both the screw and body design, to ensure that cavitation was minimised.Since an ethane/methane ocean is relatively close to its boiling point, cavitation problems might be severe.

As more and more ground-based data suggesting a solid surface became apparent, however, the concept was not pursued further.

Zubrin (1990,1991) advocated (as part of his crusade for nuclear thermal propulsion and in-situ propellant utilisation in general) exploration of the Saturnian system, using Titan as a base. He proposed a 10 ton (dry) rocket/aeroplane, powered by a nuclear reactor (300 MW_{th}), with the designation NIFTE ('Nuclear Indigenous Fueled Titan Explorer').

Exploration of the surface (and for an ocean, subsurface) regions would be accomplished by TERNs ('Titan Explorers and Retrievers to NIFTE'), small robot vehicles (helicopters, tilt rotor seaplanes, submarines, dirigibles, etc.) - Zubrin does not address the formidable control and autonomy requirements for such vehicles - which would bring samples to the large 'mother ship', capable of leaving Titan and visiting other Saturnian satellites.

Zubrin (1991) notes that due to its low gravity and dense atmosphere, Titan would be the 'aviation paradise of the solar system', and that like Icarus, any human settlers (equipped only with insulating suits and oxygen supplies) could strap wings onto their arms and fly.

While imaginative and stimulating, Zubrin's ideas are not relevant for the near-term exploration prospects of Titan.

As an aside, Clarke (1975) considered in fictional work that ground-effect vehicles (hoversleds) would be an effective means of transport in Titan's surface environment of low-g, high pressure.

Smith (1993) studied (superficially) various options for future Titan exploration, including RTG and battery-powered dirigibles and balloons, helistats, and sailplanes. Unaccountably, while he considered sailplanes (powered gliders) with an N_2H_4/N_2O_4 internal combustion engine and RTG or battery power with mission duration of 2 weeks, he did not examine any 'all-electric' options, which would certainly be possible on Titan, and could offer (in principle) unlimited mission duration. His conclusion that lighter-than-air vehicles are attractive for Titan seems reasonable, although he notes that overcoming winds are a significant problem with such vehicles.

Mitchell (1994) has given consideration to the investigation of deep oceans on Titan by means of an instrumented depth probe (i.e. an unpowered submarine) A novel feature here is the use of acoustic means to telemeter data through the ocean to a buoy which relays data to Earth by radio : however, until the acoustic environment on Titan (Lorenz and Svedhem, 1992) is better-known, this must be regarded as a speculative technique.

4.4 Conclusions

The exploration of Titan, as the rest of the outer solar system, is characterised by long lead times, and, owing to the expense and complexity of these missions, long development and decision times (times which have increased since planetary exploration began).
The unique and intriguing environment on Titan has prompted many exotic proposals for

exploration systems of varied types. None, however, is worth considering in much detail, until the Cassini/Huygens mission is completed and we know more about Titan's surface environment.

Chapter 5

The Cassini Mission, Orbiter and Huygens Probe

To define it rudely, but not inaptly, engineering is the art of doing well with one dollar that which any bungler can do with two, after a fashion.
Arthur Ellington, American Economist, 1887

The greedy touch of common-kissing Titan
William Shakespeare
Cymbeline

In this chapter I discuss the Cassini mission, and the design of the orbiter and probe which will, if all goes well, explore Titan in the period 2004-2008. While current descriptions of the mission exist (e.g. Murrow 1993 and others) no historical account of how the mission and spacecraft have evolved has yet been published, so this is discussed in detail. I briefly review the likelihood and duration of operation of the Huygens probe after impact on the surface of Titan.

5.1 Mission Design

5.1.1. Cassini Interplanetary Trajectory

The extreme distance of the Saturnian system makes even the delivery of a spacecraft there a challenge. Interplanetary mission design is a rich and interesting subject, involving trade-off between such factors as injected mass, flight duration, thermal and communications constraints, and science objectives.

In as much as Cassini's principal objective is the Saturnian system, pre- Saturn science objectives during cruise and planetary flybys are not allowed to influence the trajectory selection. However, even eliminating science from the considerations, the trajectory selection is still a complex area, and the Cassini trajectory has undergone substantial evolution during the development phase.

The current mission is described in detail in the Cassini Mission Plan (Murrow 1993), from which most of the following material is extracted, except where indicated.

Principal constraints are the capability of the Titan launch vehicle and the required delivered mass at Saturn. Launch energy is typically defined as C_3 (the square of the geocentric departure velocity). In order to fly directly to Saturn from Earth in 1997 from Earth

requires C_3>108 km^2s^{-2}, or with a Jupiter gravity-assist (JGA), C_3>83 km^2s^{-2}. The Voyager spacecraft, with a mass of ~1000 kg, were launched by Titan-IIIC boosters + solid upper stage to a C_3 of 1000 km^2s^{-2}. Cassini, however, has a considerably larger launch mass of >5000 kg, and even the more powerful Titan 4 with improved Solid Rocket Motor Units (SRMUs) is capable of providing a C_3 for this mass of only 22 km^2s^{-2}. It is clear, therefore, that a direct or JGA (i.e. Voyager-like) mission is impossible, attractive as it might be with a trip time of ~3 years. In any case, the arrival velocity of a direct or JGA trajectory at Saturn would be high, requiring a large amount of fuel to brake the spacecraft into Saturn orbit.

Thus, to deliver such a large spacecraft with currently-available US launchers requires the use of gravity-assists in the inner solar system. Inner solar system gravity assists were first used on an outer planet spacecraft by Galileo, after the original direct trajectory using a Shuttle launch with a high-energy Centaur upper stage was eliminated for Shuttle safety reasons. Note, however, that inner solar system gravity assists were identified in early studies as a way of increasing delivered mass to Saturn (e.g. SAIC, 1983).

The use of flybys of Venus and Earth (which make the required C_3 for a Saturn mission 16-20 km^2s^{-2}) imposes a number of constraints on the spacecraft system and mission design. First, in order to phase the flybys a longer mission is entailed, and second, the reduced distance to the sun (0.7AU at Venus) imposes large heat loads on the spacecraft. It is worth mentioning that the cross-US transport (Gibbons, 1991) required by Galileo to re-engineer the thermal design (install sunshades etc.) for the inner solar system is probably what led to the wear on the lubricant of the antenna release pins: these pins stuck, preventing the antenna from deploying, leading to a significant science loss at Jupiter. We see here how a political/management decision led indirectly to an engineering failure (at a microscopic level) and thence to a science loss: in outer planet exploration, the feedback of science loss to the political decision-makers is too weak and too slow to be useful, however.

The political theme is relevant at this point, since it has influenced the evolution of the interplanetary trajectory of Cassini. It is reminded that originally Cassini had a sister mission CRAF, which was (using the same spacecraft bus and similar instruments) to examine the primitive bodies of the solar system. The development of these spacecraft was to be parallel, and since they would use the same launch facility and DSN ground stations, their missions had to be carefully planned to avoid clashes in schedule. After the Phase A study, Cassini was to be launched after CRAF, in April 1996, with an EJGA (Earth-Jupiter Gravity Assist) trajectory which had a C_3 of 30 km^2s^{-2}, but included a large interplanetary manoeuvre after making an asteroid flyby. After an Earth flyby in 1998 and a Jupiter flyby in 2000, Saturn arrival would occur in October 2002, a total trip time of 6.5 years. (See Phase A study, NASA/ESA 1988). At the time, the 1996 opportunity was felt to be the best opportunity for the

next 20 years.

However, by 1991, a new baseline had evolved in part to allow CRAF to be launched as the second of the two missions (perhaps improving its chances of surviving funding cuts). This new trajectory had the virtue of allowing an increased mass at Saturn, but had two adverse effects:
1. the trajectory included a Venus flyby, requiring a revision of the thermal design, and imposing new high temperatures on the probe (which may lead to battery performance degradation). The orbiter is required use its HGA as a sunshade to protect the instruments and the probe.
2. the launch date of November 1995 made the development schedule extremely tight.

This new trajectory also included a large manoeuvre (690 ms^{-1}), this time on the outbound leg just after the Earth flyby in July 1998. After an asteroid flyby, the spacecraft would make the Jupiter flyby in April 2000, and Saturn arrival would occur in May 2004.

It may be noted at this point that there are two main drivers for setting arrival date. First is that critical mission events such as Saturn Orbit Insertion (SOI) should not occur near conjunction, when the collinearity of the Earth-Sun-Saturn would make communications difficult (the sun is a noise source with a high emission temperature). The second, less rigorous driver is Saturn's outermost known satellite Phoebe. This object, in an inclined (150°) orbit, is believed to be a captured satellite, but was only very poorly imaged by Voyager 1. Because Phoebe is so far from Saturn at 13 million km, Cassini's only opportunity to inspect it is on the inbound trajectory to Saturn. Further, since Phoebe's orbital period is so long (523 days), proximity of the inbound trajectory to Phoebe only occurs in brief windows spaced apart by 17 months. The 1995 launch would give a Phoebe flyby at 360,000km, allowing imaging at ~4km/line pair, about 10 times the resolution achieved by Voyager.

Funding pressure in the US came to the fore yet again. In order to minimise the yearly cost of Cassini, the development timescale was stretched to give a 1997 launch. Stretching the development phase increased total costs, but decreased peak cost which was the US Congress funding constraint. A side-effect was that costs to ESA and experimenters also increased, although the new launch date eased pressure on the development schedule.

The October 1997 opportunity made use of 2 Venus flybys, one of Earth, and one of Jupiter (VVEJGA) and has an arrival in June 2004, a trip time of 6.7 years. The relatively short trip time makes use of a very lucky planetary alignment, which allows the Earth flyby to occur almost immediately after the second Venus flyby (see figure 5.1). The trajectory includes a manoeuvre between the 2 Venus flybys, and a distant Jupiter flyby in December 2000 (Jupiter is now catching up with Saturn too much to be of use for significant gravity assist). Funding

considerations related to ground system development currently preclude pre-Saturn science, so no asteroid flybys are included (although in principle some pre-Saturn science could be included, particularly at Jupiter).

The Phoebe flyby distance for this trajectory, which is the current baseline, is 840,000km, somewhat degraded from the earlier mission scenarios: imaging resolution will be only ~4x better than Voyager.

The above mission relies on the availability of the advanced solid motors (SRMUs) for the Titan 4. These motors are still in the process of development, so the impact to the mission of using the less-capable existing solid rocket motors (SRMs) has been examined. The mission would be similar to that above, although the orbiter would have to carry less fuel to reduce the launch mass. The reduced fuel requirement would come from delaying Saturn arrival to December 2004 (when arrival velocity is lower, so the SOI fuel requirement is lower). Further, the number and proximity of Titan flybys would be reduced, reducing the manoeuvre fuel requirement. All of these measures allow the main goals of Cassini to be achieved, but there is significant science loss (Phoebe flyby, near-Saturn investigations at SOI, and Titan science). However, SRMU development is continuing, so it is hoped that this degraded (SRM) mission will not be required.

There was some concern that the 1997 SRMU opportunity had no backup, in case of development problems. JPL responded with several alternative missions. The first ('secondary') mission allows launch in December 1997, in case there is a short delay 'on the pad'. Even though the window occurs only two months after the nominal October window, because the fortuitous Venus/Earth phasing of the nominal mission is absent, the trip time (after a VEEGA trajectory - Jupiter is no longer encountered) is 8.8 years, giving arrival in October 2006.

If serious development problems arise (either for technical or 'programmatic' reasons, the latter usually a euphemism for funding cuts) backup launch opportunities exist in March 1998 and March 1999. Both these trajectories (EVEEGA and VEEGA, respectively) arrive in December 2008, after cruise of 10.8 or 9.8 years. Although these missions allow the full fuel load for a 4 year Saturnian tour with 35 Titan flybys (unlike the SRM launch option), the long trip times have adverse effects on science. First, the inclination of the ring plane to the sun is reduced, degrading ring science (having the sun, the rings and the spacecraft in the same plane makes high phase angle observations difficult), and second, the long trip time leads to decay of the RTG power source, reducing the number of instruments that can operate simultaneously (e.g. during a flyby). Longer trip times also increase the probability of failure, and increase operations cost.

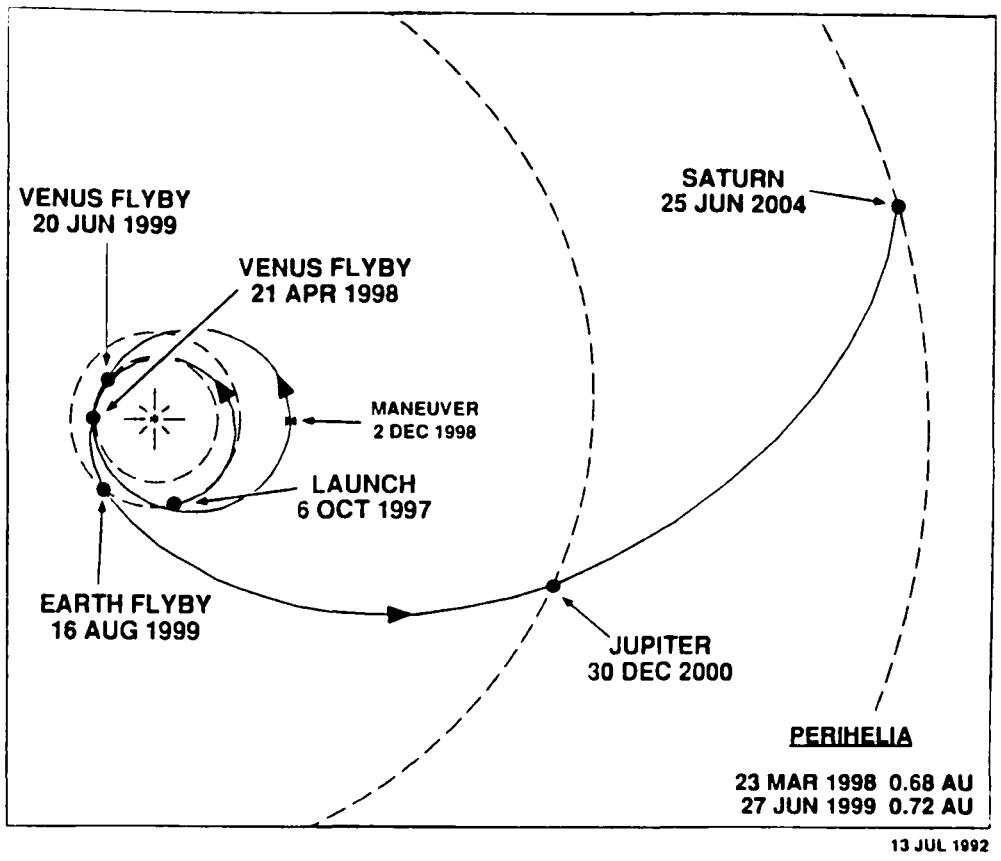

Figure 5.1 Cassini Interplanetary Trajectory (from Murrow 1993)

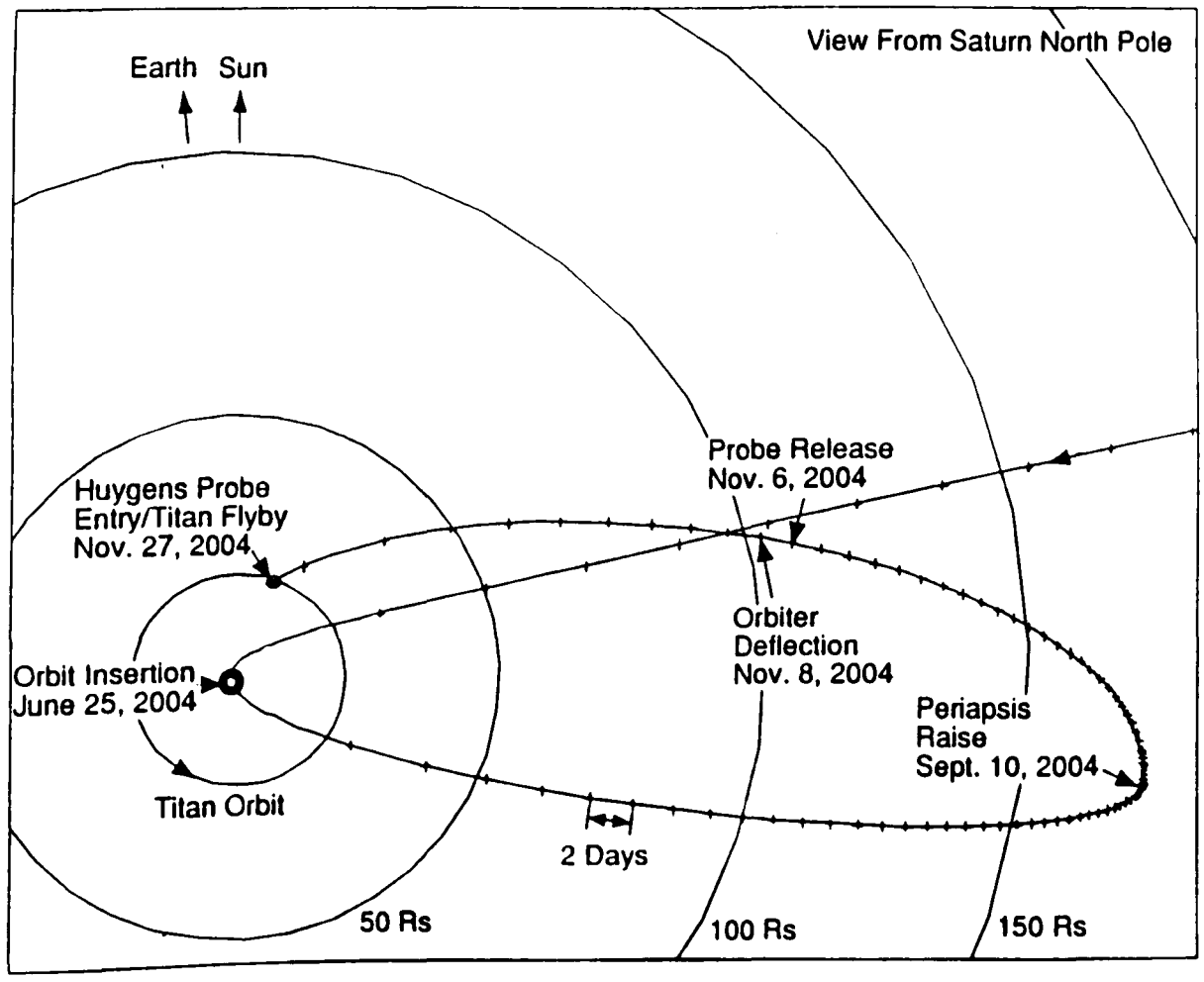

Figure 5.2 Cassini Saturn arrival orbit and Huygens Probe Delivery (from Murrow 1993)

It is interesting to reflect that, scientifically, Cassini has been 'pushed to the edge': funding limitations have delayed launch until the last practical moment, after which the quality of the mission (exciting nonetheless) degrades. Ironically, it is perhaps the extreme distance of Saturn, and the long interval between favourable mission opportunites, that have contributed to the preservation of the Cassini mission against US funding pressure. A generation of scientists knows that essentially it is 'now or never' (in terms of their own careers) to explore the Saturnian system. In contrast, mission opportunities exist for comets, asteroids and the inner planets virtually every year, making the schedules (or, indeed, continuation) of these missions perhaps more sensitive to budgetary pressures. Other factors that have contributed to Cassini's survival to date are the broad scientific support, and probably most importantly, the element of international collaboration.

5.1.2. Saturn Arrival and Orbiter Tour

The Saturn arrival part of the mission has changed little since the mission's inception, so will be decribed only briefly, except for the probe delivery considerations. The 4 year orbiter tour of the Saturnian system will be described in a little more detail, since this affects remote sensing of Titan.

Closest approach to Saturn occurs on 25 June 2004 - solar conjunction occurs not long afterwards, on July 8. The inbound trajectory (figure 5.2) is inclined to the ring plane, and crosses it in the gap between the F and G rings (to minimise the danger of colliding with a ring particle) at 2.6 Saturn radii (R_S). 1.8 hours later, the spacecraft reaches periapsis and commences the 550 ms^{-1} burn to allow the craft to be captured by Saturn. For the baseline mission, the capture orbit has a period of 152 days (apoapsis about 170 R_S, Perapsis 1.3R_S, inclination 17°). At apoapsis (September 10, 2004) a Periapsis Raise Manoeuvre is performed: this targets the spacecraft to Titan and reduces the Titan approach speed to 5.75 kms^{-1}.

Two questions naturally arise:

1. Why must the ring-plane be crossed so close to Saturn, exposing the spacecraft to the risk of dust impacts?
2. Why cannot the probe be delivered on the inbound leg of the Saturn approach trajectory?

SOI occurs at the closest approach reached by Cassini during the entire mission: all subsequent periapses are >2.7R_S. At 2.7R_S, the arrival velocity of 22.076 kms^{-1} would have to be reduced to 21.331 kms^{-1} to attain the initial orbit. On the other hand, at 1.3Rs, the velocity has to be changed from 31.402 kms^{-1} to 30.874 kms^{-1} Thus, the 1.3R_S arrival has a lower ΔV of by about 220 ms^{-1}; SOI outside the rings would invoke a ~300 kg fuel penalty (my calculations, assuming

coplanar orbits)

Saturnocentric escape velocity is about 7.7 kms^{-1} at 20 R_S, Titan's orbital distance. Thus, for an arrival velocity of 5 kms^{-1}, at Titan's orbit, the spacecraft would have a velocity of 9 kms^{-1}. Combining with Titan's orbital velocity of 5.5 kms^{-1}, gives an entry velocity (neglecting Titan's own gravitation) of 10 kms^{-1}. This would require a much higher performance entry protection system for the probe, since heat flux scales as V^3. Lower entry velocities at Titan could be obtained by aiming tangentially at the receding face of Titan; such a geometry, however, would be incompatible with a practicable SOI burn.

21 days before Titan arrival, the probe is spun up to 5 rpm for attitude stability and released on a trajectory which impacts Titan. During this 21 day coast, the only operating equipment is the 3 clocks, which will activate the probe systems just prior to entry. Surprisingly, these timers use a significant fraction (~20%) of the mission energy budget. The long coast is also a factor in sizing the delivery error ellipse.

Two days after probe release, the orbiter performs an orbiter delay manoeuvre (ODM) which delays its arrival at Titan relative to the probe (thereby allowing it to relay the probe's signals) and generates the required Titan miss distance. The size of this manoeuvre is dictated by the required orbiter delay time (ODT), and by the length of the coast phase: while a shorter coast would be desirable for the probe, to minimise entry point uncertainty and coast energy requirements, it would lead to a larger ΔV requirement for the ODM.

In the original scenario, where the probe signal was to be picked up by a dedicated antenna, the ODT was to be little longer than the probe mission duration. However, following the deletion of the Probe Relay Antenna (PRA) on the orbiter, the ODT had to be increased since the HGA used to pick up the probe signal had a much smaller footprint. The current ODT is between 4 and 4.7 hours.

During the probe mission, the orbiter points the HGA at the predicted probe location and receives the probe telemetry. 30 minutes after the latest touchdown time of the probe, it commences a turn to point the remote-sensing instruments at Titan until closest approach (~1500km during this first encounter with Titan) after which it turns to point the HGA at Earth to return the data.

Subsequently the orbiter tours the Saturnian system for 4 years, making a number of flybys of icy satellites, and performing remote sensing of Saturn, its satellites and rings. As it is the most massive satellite, Titan is used to change the energy and inclination of the orbit to allow the Saturn science objectives to be met (e.g. high inclination orbits are useful for ring studies

and investigation of high-latitude Saturn atmospheric dynamics and magnetosphere). Since Titan is instrumental for gravity assist in 'cranking' the orbit inclination and 'pumping' its energy up or down, most of the orbital tour's orbits include a Titan flyby. The reference tour to date, designated 92-01, is summarised in figure 5.3.

Titan flybys are divided into 4 types: optical remote sensing, radar, radio occultation and gravity field. In part, the need to specify these different modes results from the deletion of the scan platform for the remote sensing instruments.

In optical remote sensing flybys, the optical instruments (ISS, VIMS, UVIS, CIRS etc.) are pointed at Titan, or regions of it, and scanned over its surface. Note that (e.g. figure 5.4) most Titan flybys have closest approach on the nightside.

Radar flybys require the HGA to be pointed at Titan: details of the radar system and its operation are given in Chapter 6.

The radio occultation and gravity field flybys require the HGA to be pointed towards Earth. In principle, the two could be combined, although there are factors which argue that at least some flybys should be dedicated to each mode. Radio-occultation measurements require some slewing of the spacecraft, to allow limb-tracking: this requires that the spacecraft thrusters are used. Gravity field flybys rely on Doppler determination of the spacecraft velocity for ~2 hours before and after the occultation period. However, if the spacecraft uses its thrusters during the flyby, there is always the danger that the trajectory perturbation due to Titan's gravitational field (which is what is being measured) may be masked by thrust assymetry during the attitude manoeuvring: thus gravity flybys prefer attitude control using only momentum wheels, which are inadequate to perform the limb-tracking desired by the radio-occultation investigation.

The power limitations on Cassini become apparent here too: before radio science flybys can be performed, the UltraStable Oscillator (USO) on the orbiter must be warmed up to its steady operating temperature. For radio occultation flybys, the catalyst bed heaters on the thrusters must also be warmed up (thermal shock on operating a cold thruster degrades it) and it is not yet certain whether there is enough available power for both of these warmups to be performed simultaneously. If not, then the catalyst bed heating will take place earlier: this would preclude, however, the operation of the remote sensing instruments which could otherwise make observations until USO warmup.

The distribution of the various types of flybys is not yet decided, and will be discussed by the project science group (PSG), taking into account such details as flyby altitude (radar flybys

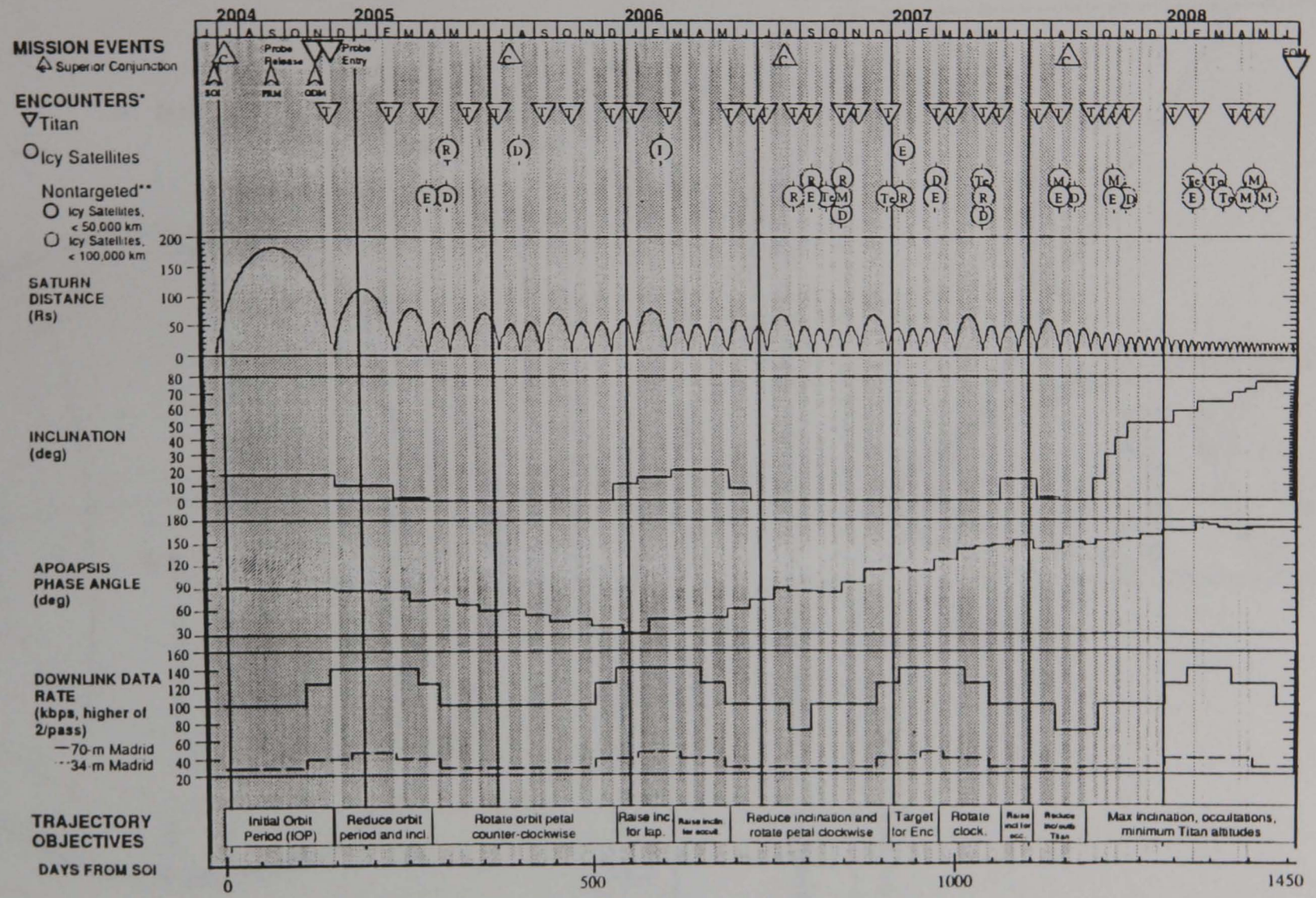

* M = Mimas; E = Enceladus; Te = Tethys; D = Dione; R = Rhea; T = Titan; H = Hyperion; I = Iapetus.

** Satellite symbols have been stacked in some areas where space is unavailable.

Figure 5.3 92-01 Tour Summary (from Murrow 1993)

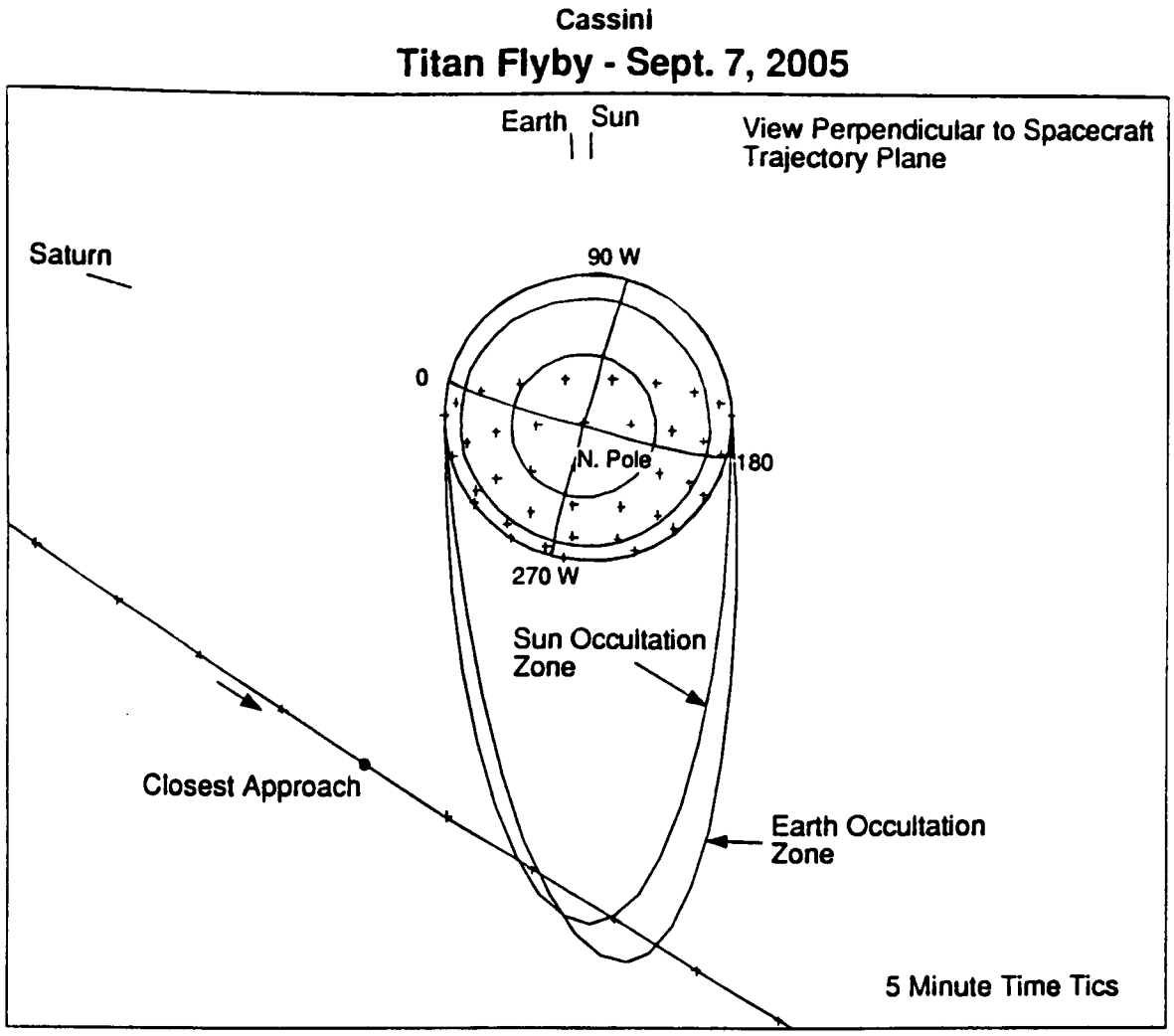

Figure 5.4 Typical Titan Flyby Geometry - note closest approach on nightside (from Murrow 1993)

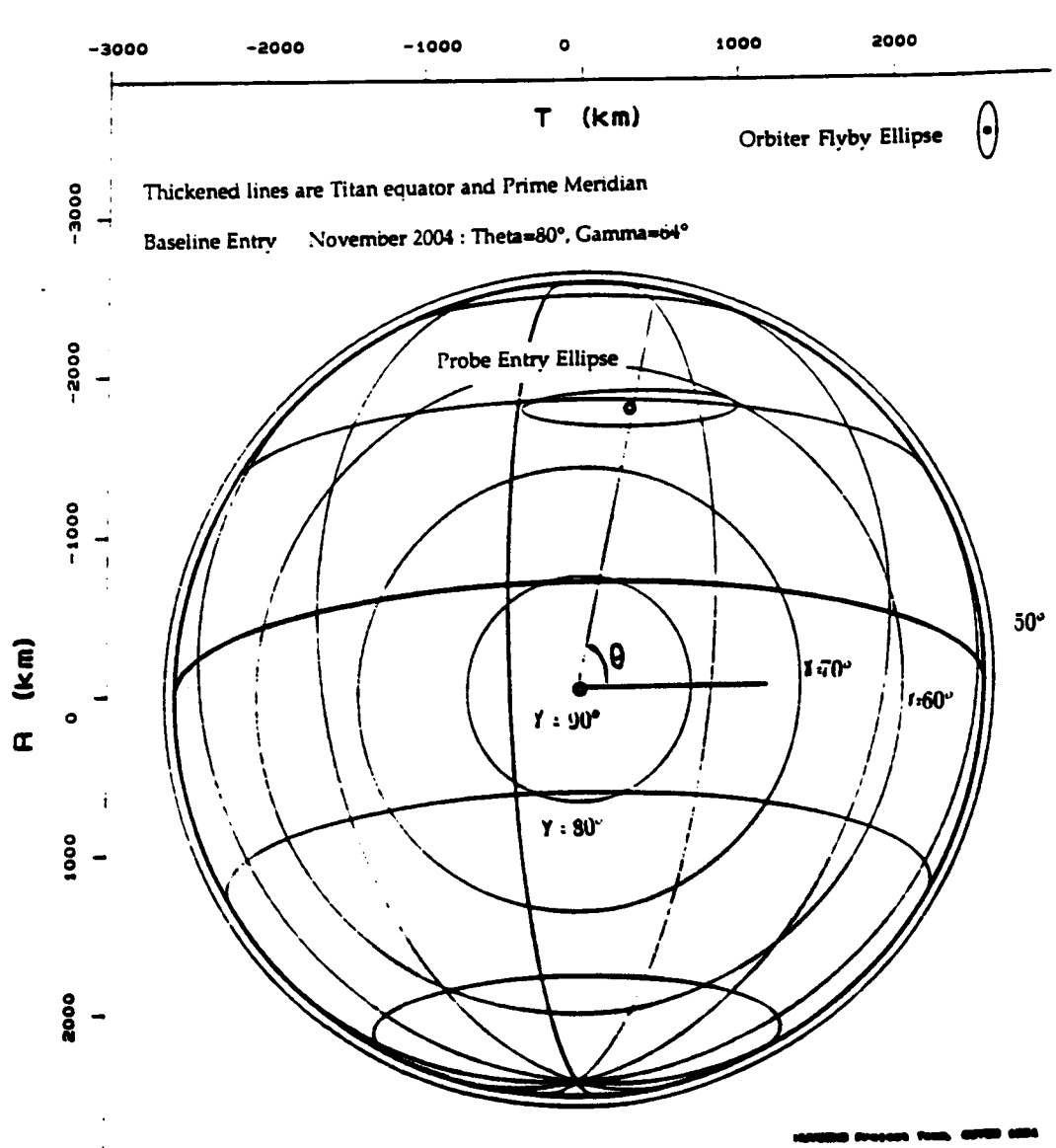

Figure 5.5 Huygens Probe Delivery Geometry From Ott (1991)

require low altitude flybys, for example). It is likely the details of the tour may be modified during the mission itself, in response to factors such as improved knowledge of Titan's atmosphere (which sets a lower limit on flyby altitude), fuel margins, and results of earlier flybys and the probe mission. For example, if optical imaging or radiometry on one flyby indicates a particularly interesting region (such as the edge of an ocean), a closer inspection of that area by radar might be requested.

5.1.3 Probe Entry

Probe mission analysis is described briefly in Ott (1992), and in rather more detail in Ott (1991).

The probe approaches Titan with an asymptotic hyperbolic velocity (V_i) of 5.75 kms^{-1}. Under Titan's gravity, this accelerates to a velocity at the entry interface (defined as 1270km above the surface of Titan). At such a velocity, entry into Titan's atmosphere can be accomplished at quite steep angles with modest entry protection : the flight-path angle (γ_{1270}) can be up to 90° (unlike, e.g. Jupiter entry for Galileo at 50 kms^{-1}, which must be performed with γ~10°). Entry angles shallower than 60° result in low peak heating, but increase the total heat load, 'heat-soak'. Lower γ still, ($\dot{\gamma}$<~35°), results in skip-out.

The centre of Titan's disk as seen (figure 5.5) from the incoming probe defines the γ=90 component. γ contours form circles around this point. The range of allowable entry locations is therefore first defined by the time of entry (i.e. what is the longitude of the γ=90 point) and second by the allowable γ range.

As design of the probe progressed and the entry protection system was defined, the allowable γ range narrowed to 55-75°, and eventially 60-66°, with the nominal value of 64°.

The other free parameter in defining the location of the entry site is the so-called 'impact parameter' Θ (see figure 5.5). This defines where along a given γ-contour entry takes place. As discussed by Ott (1990), this is largely constrained by the orbiter flyby geometry and the relay link.

Additional factors constraining the entry site are the scientific requirement for entry in the latitude range 60°N-60°S, but not the equatorial region (±5°), and the need to have the sun in the elevation range 25°-55° to allow the DISR to make solar aureole measurements, have enough illumination for imaging, but prevent the side- looking imager from being blinded. The combination of these factors, and consideration of the zonal wind's projection onto the line-of-sight to the orbiter (important for doppler measurement of wind speed) have led to a baseline

Θ=80.

Note that another significant reason for selecting large Θ is that the entry point uncertainty is dominated by uncertainty in spacecraft navigation and in the Titan ephemeris. The 1-sigma error ellipse has its longest axis in approximately the E-W direction, thus for a low Θ, the ellipse spans an unacceptably large range of γ contours. In principle, if improved navigation or ephemeris data became available (e.g. from orbiter imaging data during the first orbit), reducing the size of the error ellipse, a range of Θ values could become feasible.

The considerations described above not only summarise an interesting problem in mission design, but also explain why, even if groundbased imaging reveals areas (continents, oceans) of particular interest in the next few years, it will probably be impossible to target the probe to these areas.

5.1.4 Probe Descent

Some aspects of the mission design in connection with the descent sequence, are discussed in Lorenz (1993b). The current descent sequence is shown in figure 5.6.

After the entry phase, the probe has been slowed by aerodynamic drag to a velocity of ~400 ms^{-1} (Mach 1.5) at an altitude of ~170km. The parachute must be deployed at this point, since the entry configuration is unstable at transonic (M~1.2) speeds. The remarkably high deployment altitude in part determined the size of the entry shield, allowing braking to occur high in the atmosphere, and is due to the scientific requirement to sample the regions where the photochemical haze is generated.

The principal drivers for the descent sequence are the high parachute deployment altitude and the requirement to reach the surface within the mission duration

Mission duration is itself a parameter that has evolved during the probe development. During the mission, the probe suffers two limiting processes, namely its batteries become exhausted, and the probe cools down. Thus, probe 'lifetime' is 'bought' with the expenditure of resources (=mass) on thermal insulation and battery capacity. An additional constraint is the orbiter visibility (i.e. the mission duration cannot exceed the orbiter delay time). This latter factor is complicated by such aspects as the exact location of the probe relative to the orbiter flyby point (and near the end of the probe mission, its location will have been displaced from the entry point by the zonal winds, about which there is some uncertainty.)

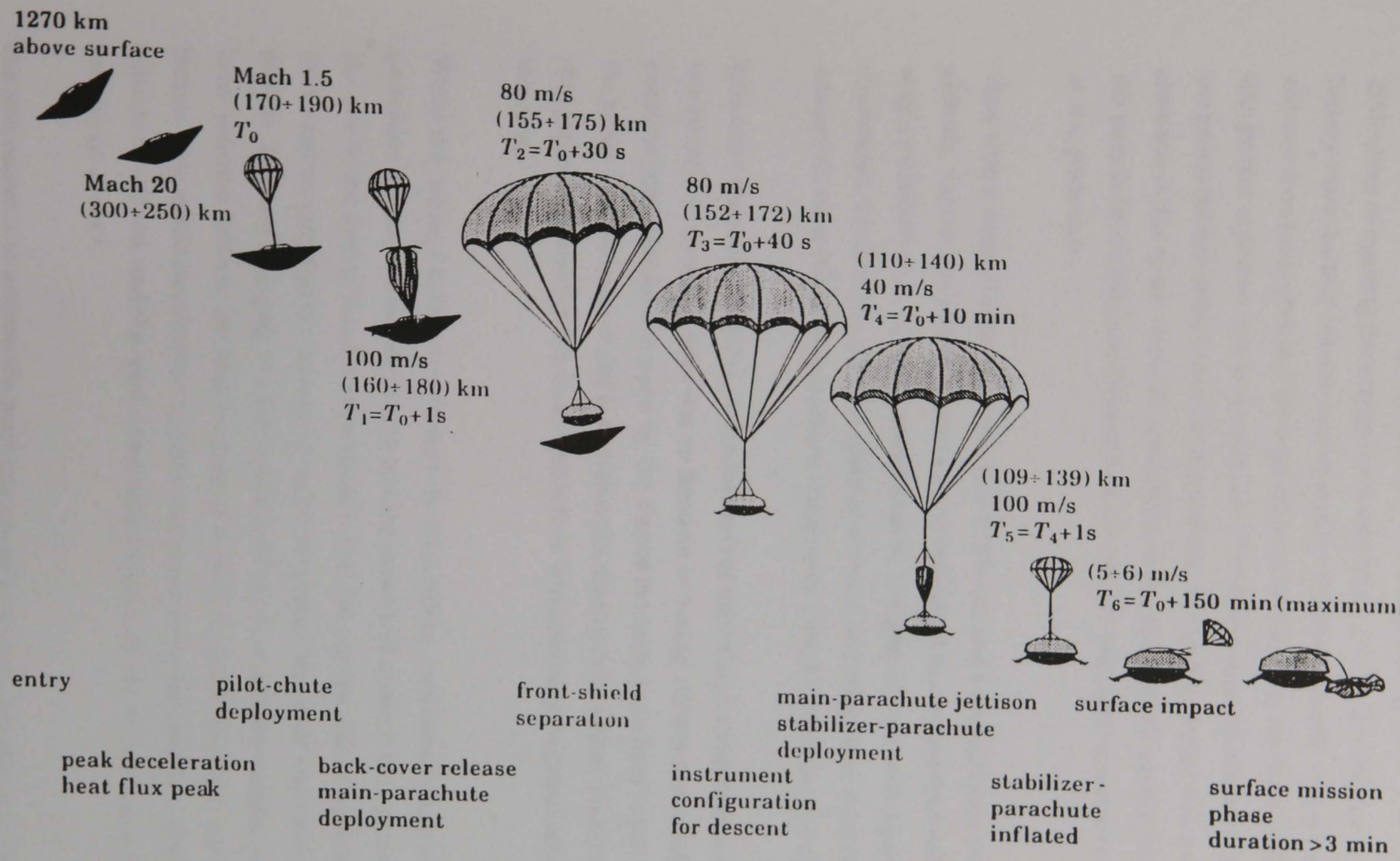

Figure 5.6 Schematic of Probe Mission (from Lebreton and Matson 1992)

Originally, the science requirement was for a descent duration of 2.5-3 hours. However, the difficulties of meeting the energy requirements for the 3 hour duration with a reasonable battery mass (battery mass is inconveniently quantised in units of one battery, of which there are now 5 on the probe) and the large dispersion in landing site location for a 3 hour descent (the project engineers had to consider zonal winds in either direction for mission analysis purposes) led to a reduction of the descent duration to 2-2.5 hours. The uncertainty in descent duration is due to the residual uncertainty in the atmospheric models (which couple into both the parachute deployment altitude and the descent rate) and uncertainty in drag performance of the parachute.

Thus with a nominal descent duration of 2.25 hours and a nominal parachute deployment altitude, the descent profile (altitude vs. time) should be a uniquely-determined function for a single parachute size. In early design phases, a staged descent with 2 parachutes was considered, to maximise the time spent at altitude, and there were even thoughts of adaptively controlling the parachute changeover time, to maximise the science return.

However, the project decided, in the interests of minimising complexity and risk, to use only one parachute, meaning there was no freedom in 'tuning' the descent duration. However, practical considerations stepped in: the size of the main parachute required to safely separate the probe from its entry shield is such that the descent from 170km would take 6 hours. Thus a changeover to a smaller (i.e. faster) parachute was necessary, re-introducing a degree of freedom.

While the average ballistic coefficient (β=mass/(drag coefficient*area)) of the probe-parachute system, a measure of how fast the probe will descend at a given altitude, is fixed, the size of the second (smaller) parachute is not. For a given size of parachute, the changeover time must be such that the average β meets the descent duration requirement. The tradeoff, then, is between changing to a large parachute early, or a much smaller parachute later. The latter solution (indeed, the limiting case of it, with no parachute) was the first studied by the project. This would have led to the main parachute being retained for ~100 minutes to an altitude of ~45 km, and the probe free-falling from there to the surface, with an impact velocity of ~7 ms^{-1}.

The alternative is to jetisson the main parachute as soon as possible (i.e. after the front shield had been safely separated) and switch to a parachute that would be only slightly smaller than the parachute sized for the whole descent.

The trade-off between these two options was driven in part by technical, part by scientific reasons. First, tests in the vertical wind tunnel in Lille in October 1991 indicated that the probe was insufficiently stable without a parachute (angular oscillations would lead to image blur for the DISR), so the free-fall option was ruled out. Thus the second parachute (known generally, but incorrectly, as the 'drogue' - strictly a drogue does work in extracting or deploying something: a more accurate term for the second parachute is 'stabiliser') could be sized for descent from about 140 km (10 minutes after main parachute inflation) or from about 60 km (lowest altitude compliant with the descent time constraint, with a canopy large enough to be an effective stabiliser). These mission options are illustrated in figure 5.7.

A higher (earlier) release would be better for Titan surface exploration, since it would spend a relatively long part of the mission near the surface (below the clouds) and would have a low impact velocity (improving chances of impact survival). On the other hand, a low, late release would be better for studies of the high-altitude aerosols. The question was debated at the HSWT, and the early release (favoured by DISR and SSP) was selected. This also had the engineering advantage of minimising the probe impact site dispersion by reducing the time spent at high altitude where the zonal winds are stronger.

The release time of the parachute is essentially a free parameter until the PROMs (Programmable Read-Only Memory) chips which store the flight sequence are set ('burned') in late 1994. The current descent profile (not now expected to change, following an examination of the implications of new atmospheric models) is illustrated in figure 5.8.

5.1.5 Surface Mission

Impact survival on a completely unknown surface has not been allowed to be a design driver of the Huygens probe. Nevertheless, it has always been recognised that impact survival is possible, allowing the spacecraft to make measurements from the surface. The mechanical loads on the probe and their survivability are discussed elsewhere (Section 5.3 of this chapter, Chapter 7 and Lorenz 1994 a), but I discuss here the mission-related parameters which define the available duration of the surface mission.

Mission energy and link budgets, and the performance of the thermal control system have always been required to permit probe operation for the maximum descent duration plus three minutes. Thus, in terms of resource budgets alone, we might expect the probe to support measurements from Titan's surface for about 18 minutes (nominal), or possibly 33 minutes (minimum descent duration). The maximum descent duration (corresponding to a 'thick' atmosphere, high drag performance of the parachutes, low topography, etc.) could mean only

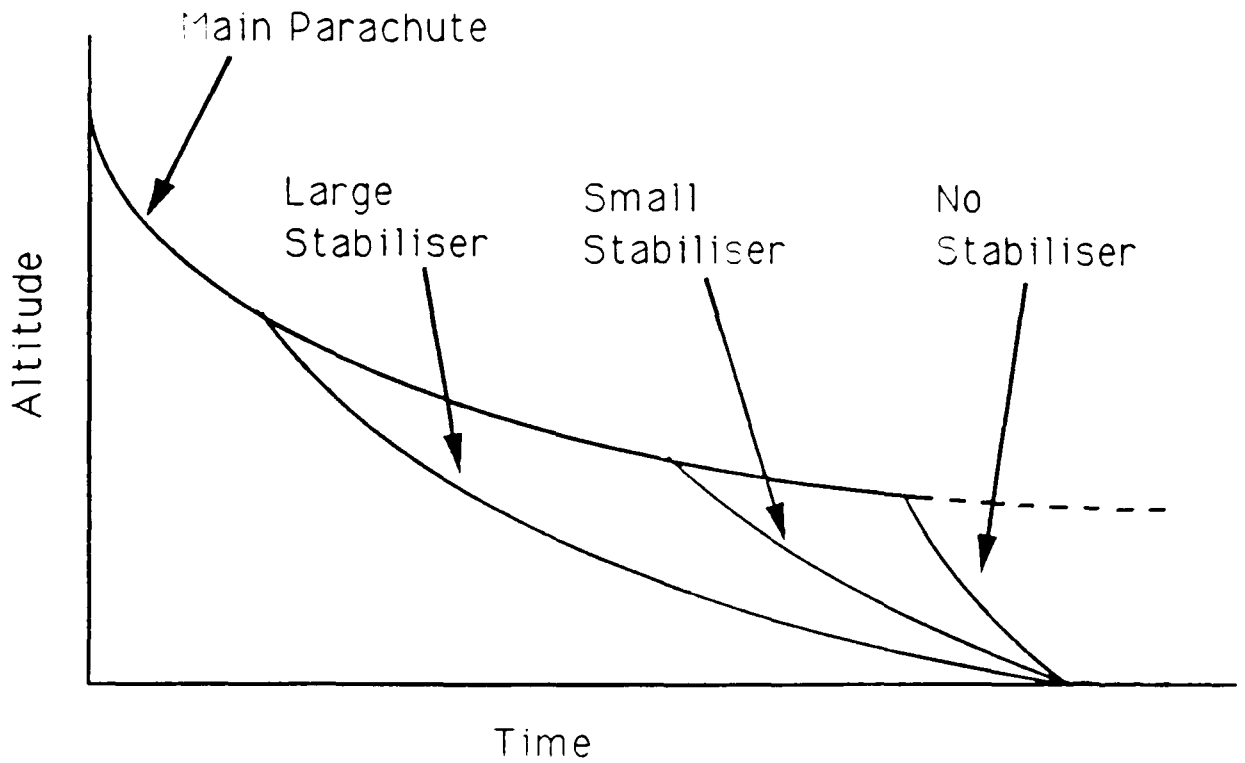

Figure 5.7 Descent Profile degree-of-freedom

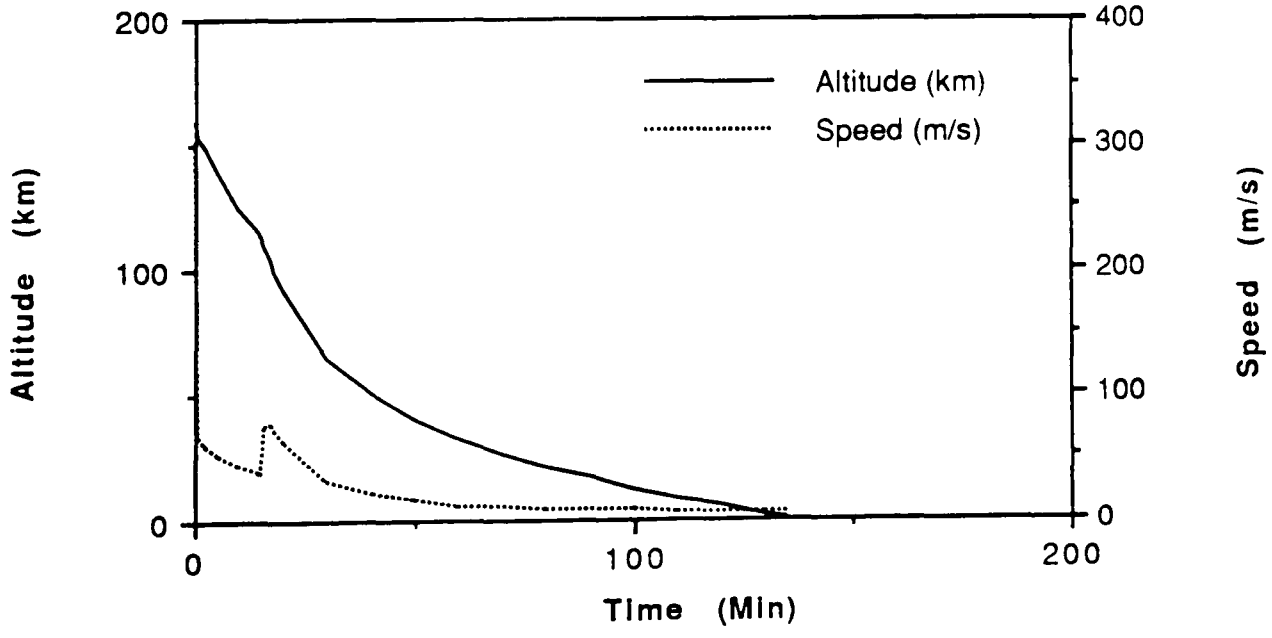

Figure 5.8 Current Descent Profile: velocity and altitude vs. time

3 minutes of resources are budgeted for surface operation, although a long descent duration would have the advantage of allowing a longer period in the low atmosphere for imaging of the surface.

The three minutes would allow a useful science return from the surface (see next chapter), including results from the SSP, DISR images and spectra of the surface, and a mass-spectrometer analysis of the surface material. A longer duration on the surface is required for such things as cloud-tracking by imaging, accurate wave-period monitoring and so on.

Assuming there is no significant damage at impact, the probe operation is constrained by the thermal, communications and energy margins.

Communications Limit

Margin on a spacecraft link budget should be >3 dB for reliable communication; currently (Aerospatiale 1994) there is a 7 dB margin on the link at end-of-descent (153 minutes, after 3-33 minutes on the surface). The availability of margin >3 dB after 183 minutes (i.e. the maximum surface mission) is uncertain, since it depends on the exact orientation and location (wind-dependent) of the probe, but prospects for several tens of minutes of link on the surface seem very good.

Energy Limit

The nominal (specified) energy to be provided by the batteries on the probe is 1476 Wh. The energy to be used during the maximum descent duration is 930 Wh, with an additional ~280Wh used by the coast timers. Most of the substantial margin arises from the requirement that no single-point failure (e.g. failure of one battery, an experiment failing and draining power - but just too little power to trip its current limiter, etc.) can degrade the mission. A little extra margin comes from the fact that the required worst-case energy budget would require 4.3 or so batteries. Non-integral numbers of batteries are of course impossible, so 5 batteries are carried.

Thus the energy margin to support the surface mission depends on :

1).the battery performance itself - as-built capacity may differ from the specification. Further, the energy budget assumes a certain degradation during cruise (especially during the high-temperature phase around Venus flyby), and a certain operating temperature during descent. These effects introduce a significant uncertainty in battery capacity. The available energy clearly also depends on whether a battery (or single cells within a battery) fails during the mission.

2. the energy consumed by the probe systems and experiments: power consumption of individual units may vary (e.g. depending on temperature) from that specified. Further, individual units may fail: if they fail completely (open-circuit, or closed-circuit leading to load disconnection by automatic current-limiters) the energy budgeted for those units will be available to allow other systems to continue operation. On the other hand, a 'soft' failure could lead to a higher-than-planned energy useage (although the nominal energy budget allows for this occurence for one experiment and one probe subsystem).

Thus, the energy available for the surface mission, being the difference between two large and uncertain quantities, is itself highly uncertain. However, a brief calculation shows that it is likely that battery energy will not be a constraint on surface mission duration: e.g. the current worst-case energy budget has a 10% margin giving ~20 minutes of surface operation, and if, for example, the allowed-for energy drain by a probe unit failure does not occur, the relevant margin (~125 Wh) would allow an additional ~20 minutes.

Thermal Limit

During the probe descent, the probe's interior cools from its initial value of ~10°C. The cooling is due to the forced convection of the cold atmosphere as the probe falls through it: the exterior of the probe rapidly attains the ambient temperature. Heat from the probe systems leaks slowly through the layer of foam insulation, and through those parts of the experimental payload which link to the outside.

The cooling of the probe is buffered slightly by the ~300W of electrical power dissipated in its systems, and the 30W of heat generate by the RHUs, but cooling is unavoidable: the probe's operation relies on its warm starting transient.

The temperature of the experiment platform at the end of descent is ~0°C, with a rate of cooling of ~5K/hour (Sainct and Clausen 1993). Thus, if we assume the acceptance operating temperature limits specified in the Huygens Experiment Interface Document (Part A) of -30°C, and if the rate of cooling remains the same on the surface as during descent, then the acceptance limit would not be reached for several hours.

However, the cooling rate assumption may not be valid. For landing in a liquid surface, heat loss is likely to be rather swifter, for the following reasons. First, the impact loads might crush the insulating foam, increasing its thermal conductivity. Second, immersion in liquid hydrocarbons at ~94K is likely to lead to somewhat faster heat loss than that due to forced convection during descent (although the heat budget of the probe as a whole is conduction-limited by the foam, some small areas such as the GCMS inlets, the SSP vent tube etc. are not,

and will increase their heat-leak on immersion). Thirdly, any rupture of experiment seals might allow ocean to leak in: it would instantly boil inside the probe, drawing away heat. Leaks are likely to be small, however.

On the other hand, some surface scenarios (such as porous ice) might lead to the heat-leak being lower than during the descent, since the convection is no longer forced. Thus, without considering specific landing scenarios, it seems relatively fruitless to investigate the heat budget further than the brief calculation above.

Thus, if the probe survives impact, there appears a good chance that it may continue to operate for some time. Ultimately, however, the probe mission will be forced to cease when the orbiter turns the HGA away from the probe to point the remote-sensing instruments at Titan, 30 minutes after the end of the longest descent of 2.5 hours.

5.2 Orbiter Design

In its original concept, the Cassini orbiter was to be just one member of a family of outer solar system probes in the Mariner Mark 2 series. This series would share common design features and components, to minimise recurring costs. Principal features were large manoeuvring capability, large communication antennae and RTG power generation.

Cassini's sister craft for the first 2 MM2 missions was to be CRAF, which to minimise cost would have had a part-solar part-RTG power system, and would have used a flight spare Viking dish for radio communications with Earth. Cassini, being so much further from the sun (10 AU, versus ~4 AU for CRAF) required a larger dish and all-RTG power. Both spacecraft were to be 3-axis stabilised, have a high-precision scan platform for remote sensing instruments such as imagers and spectrometers, and a lower-precision scan platform for particles-and-fields measurements. Both spacecraft were to carry an in-situ investigations platform, namely a comet penetrator for CRAF and the Titan probe for Cassini.

In concept, the MM2 series made sound engineering and scientific sense - the capabilities of these two missions for investigating the origin and evolution of the solar system would have been formidable, and by sharing many designfeatures, development costs would have been minimised. Further missions (e.g. Neptune/Triton) could have been built around MM2 vehicles for very modest incremental cost.

However, the cost of the two missions proved too high for the US to sustain, at a time when budgetary pressures have become extreme, particularly with respect to the Space Station programme. In 1991/2 the CRAF programme was cut back, then deleted. This move, however,

resulted in only marginal cost savings, since the design effort required for Cassini alone was only slightlyless than that for CRAF/Cassini. Further cost pressures led to a descoping exercise in 1992, with the deletion of the scan platforms and other less visible impacts.

The orbiter's dry mass is just over 2500 kg, including Huygens probe and payload. It is 6.8 m high, and 4 m in diameter. In appearance (figure 5.9) it is broadly cylindrical, topped by the 4m HGA. It carries 3000 kg of propellant, mostly in two spherical tanks, vertically stacked. Remote sensing instruments are mounted onto a pallet strapped to the cylindrical main body. Most electronic equipment is in the 12 bays of the electronics compartment just below the HGA (a similar arrangement was used on Pioneer and Voyager).

The HGA transmits X-band (8.4 GHz) telemetry at 19 W (at up to 140 kbits/sec, yielding about 4 Gbit of science data per day), and receives telecommands at 7.2 GHz. The HGA is also used for radio science at S and Ka band, and for the radar investigations at Ku band.

The orbiter carries a large data storage capability, driven by the large amount of data that is generated by the payload, during flybys (and in the intervals between groundstation passes). Unlike the Voyager spacecraftwhich used tape recorders (which cause small disturbance torques during operation) the Cassini data is held on SSR (Solid State Recorders), of which there are two, each of >1.8 Gbit capacity.

Electrical power is provided by 3 RTGs, supplying ~650W of electrical power to a 30V regulated bus, rather less at end-of-mission in 2008. Note that the loss in power is due only in part to decay of the Pu-238 source: a significant loss is due to the slow degradation of the thermoelectric energy converters - see e.g. Schock (1993) The thermal output of the RTGs is about 10x higher, so small shades protect the remote sensing instruments to allow them to run cold for maximum sensitivity and to minimise radiation damage.

Attitude control, with a capability of holding pointing to 2 milliradians, and rates as low as ~20 microradians/sec ('10 times slower than a watch's hour hand- Kohlhase, 1993) is performed by reaction wheels and monopropellant hydrazine thrusters. Attitude sensing uses star trackers, sun sensors and (for high rate manoeuvres) gyros.

Propulsion is by storable bipropellant, via clusters of 0.67 N thrusters and a (redundant) 450 N main engine. The monopropellant hydrazine tank (cylindrical) and the two bipropellant tanks (spherical, in the centre of the orbiter) are pressurised from a common helium supply. During the orbiter tour, the hydrazine system will perform some small ($<1 ms^{-1}$) burns, while the bipropellant system will be used for major burns. The total mission ΔV budget, including the interplanetary trajectory, is about 2100 ms^{-1}.

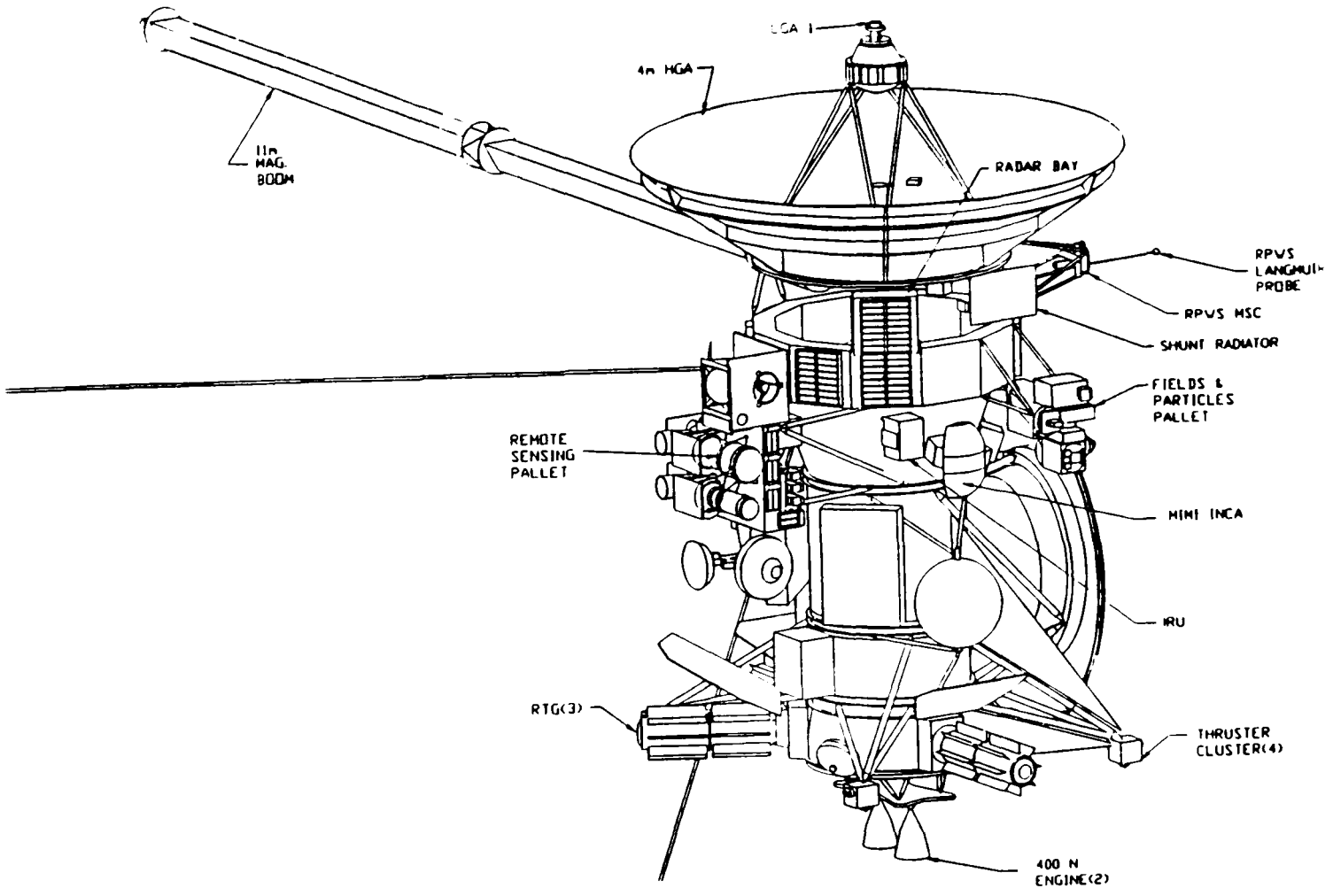

Figure 5.9 Side view of Saturn Orbiter (from Murrow 1993)

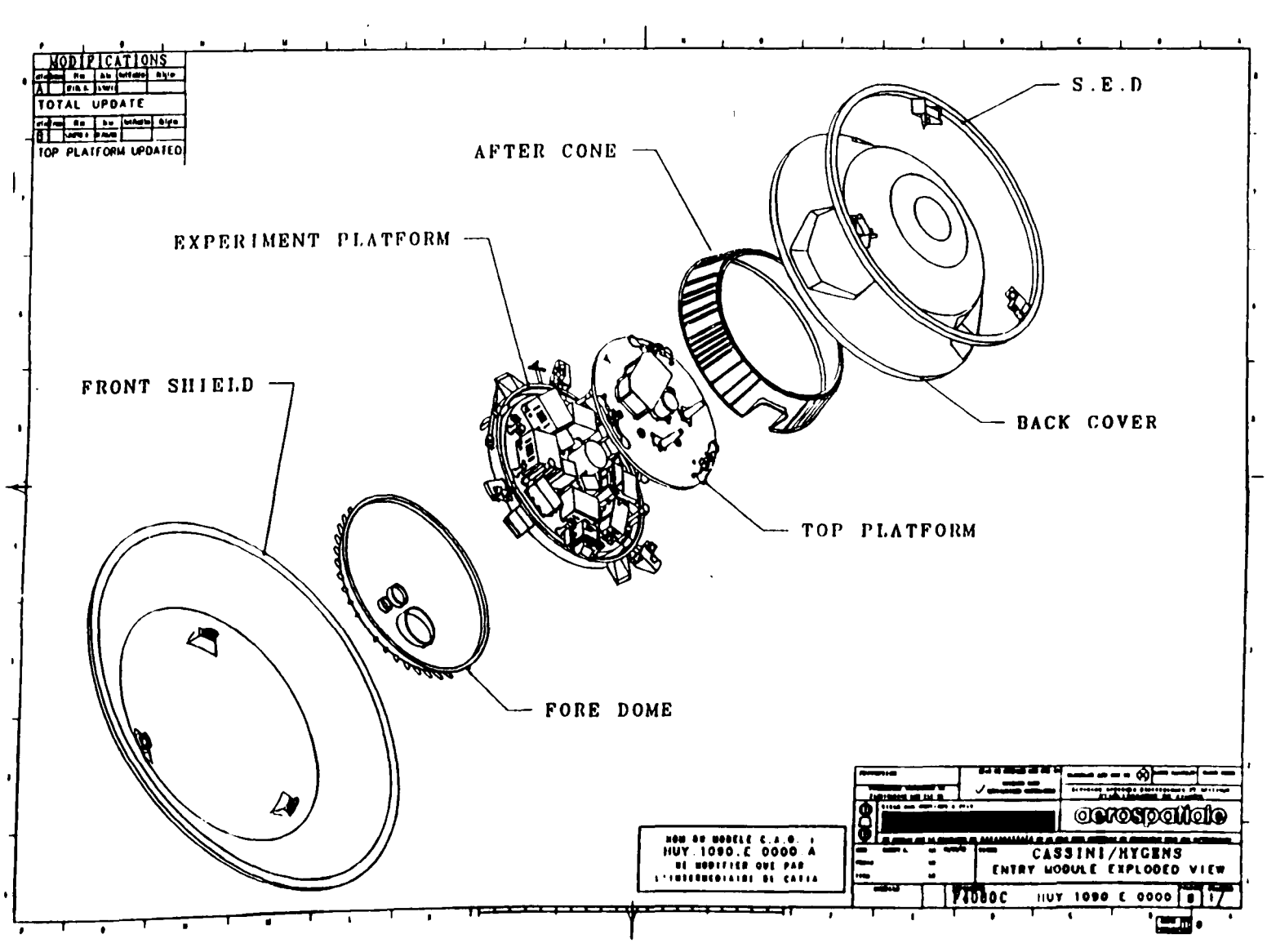

Figure 5.10 Exploded view of Huygens Probe (from Aerospatiale 1994)

Thermal control relies mostly on passive measures, such as MLI (MultiLayer Insulation) blankets. Automatic louvres, electrical heaters and RHUs are used in selected locations. The HGA must be used to shade the rest of the spacecraft in the inner solar system, placing constraints on the cruise attitude.

Thus the orbiter represents a natural evolution of earlier spacecraft (most notably Voyager). It is an impressive and highly capable vehicle, but uses mostly proven equipment. The many compromises in design, in particular the deletion of the scan platforms, and the use of Venus flybys, have made the vehicle cheaper to construct, but force the operation to be complicated and expensive.

5.3 Huygens Probe Design

The design of the Huygens probe is described briefly by Hassan et al. (1994) and in detail in Aerospatiale (1994). Some of the more novel features are also mentioned in Sainct and Clausen (1993). Descriptions of the probe design at earlier stages in the programme may be found in the following papers: Phase B3, Lebreton and Matson (1992); Phase B2, Lebreton (1992), Mooij (1992); Phase B1, Lorenz (1991); pre-Phase B, Lebreton (1990); Phase A (NASA/ESA 1988, Lebreton and Scoon 1988), Scoon et al (1989); Assessment study (Beckman and Scoon, 1985; Scoon 1985).

Only a brief summary will be given here, to provide background for the payload descriptions and impact dynamics (Chapters 6 and 7). There will doubtless be detailed descriptions of the probe systems published near the launch date.

The probe is built (figure 5.10) around a 75 mm thick experiment platform, made of a stiff sandwich of aluminium honeycomb, onto which most of the electrical equipment and payload units are bolted. A second, thinner and smaller platform is mounted on the top (rear) of the probe, and carries the parachutes and antennas. The two platforms are linked by three glass fibre struts and by the after cone, made of thin aluminium, with stiffeners. The after cone and the fore dome (0.8 mm thick aluminium) form a shell around the probe systems. Since the ambient pressure during descent reaches only 1.6 bar, the shell need be neither structurally stiff nor sealed (unlike Pioneer Venus and Galileo, whose structures must exclude pressures of 70 and 20 bar respectively). This decoupling of enclosure and structural function enables a more mass-efficient design, although it makes the analysis of impact accelerations rather difficult (see Chapter 7).

The after cone and fore dome are linked by a stiff equatorial ring around the probe : this is

attached by three radial titanium struts to the experiment platform. These struts and ring are the primary load path for launch and entry loads. The front shield and aft cover are attached (by their separation mechanisms) to this equatorial ring; the spin-eject device, which mates the probe to the orbiter, is attached to the front shield just next to the ring.

Within the shell is a 5 cm layer of foam insulation (foam must be used, since the more common MLI does not function efficiently in a non-vacuum environment) to retard the heat loss from the probe during descent. On the outside of the fore dome are a set of spin vanes which cause the probe to gently rotate to pan the DISR around, and the four planar antennas of the two radar altimeters are mounted on the equatorial ring.

The probe descent is controlled by a set of parachutes: the pilot, main and stabiliser. The pilot chute, ejected through a patch in the aft cover, inflates at Mach 1.5, to pull off the aft cover and deploy the main parachute. The main parachute slows the probe through the transonic region and allows an extended loiter at high altitude, although the main driver for its size is the requirement to release the front shield safely . After 10 minutes, the main chute is released, and the probe descends to the surface with the small stabiliser chute. The rotation of the parachutes and the probe are decoupled by a swivel. The parachute system and its development are described in Neal and Wellings (1993) and Lingard (1993).

The front shield, comprising about 30% of the probe mass, decelerates the probe from its entry velocity to parachute deployment speed. In doing so, the kinetic energy of entry is dissipated. The blunt shape of the shield leads to a strong shock wave, such that most of the energy is dissipated into the atmosphere (a more pointed shape, such as a missile re-entry vehicle, would have a weaker shock, such that the convective heat transport to the vehicle is higher). This shock layer at 12000K is incandescent, and heat transfer is predominantly radiative. The combination of methane and nitrogen in the atmosphere leads to non-equilibrium C-N chemistry in the shock layer, such that there is a significant radiative flux from the wake onto the rear of the probe (necessitating an insulating layer on the back of the front shield, and the aft cover). The C-N radicals give a large violet component to the radiation (indeed, the possibility exists of measuring the spectrum of the shock plasma to determine its composition in the otherwise difficult-to-access 200-400km region (Nelson et al., 1989)).

The uncertain presence of argon is also a strong driver on the upper limit of the predicted heat flux, again due to its radiative properties: in worst-case conditions, the peak heat flux is 1.4 MWm^{-2}. This peak heat flux drives the selection of the entry protection material (originally hoped to be Prosial, a spray-on resin of silica spheres used to protect the back of the front shield: this would have made the front shield easy to manufacture, and light.) However, the high heat loads would lead to temperatures above the decomposition temperature of Prosial,

so it had to be replaced with tiles of AQ60. AQ60 is a denser, stronger material developed by Aerospatiale for missile entry protection, and is made from silica fibres bound together by a resin. Although there is some mass loss during entry due to decomposition of the resin, the material is not strictly an ablator, but rather an insulator/radiator - it may be thought of as a non-reuseable version of the tiles used to protect the US space shuttle. (Interestingly, the Phase A study, which advocated a high-performance entry protection system using advanced technologies, namely beryllium and carbon-carbon, states that radiative heat transfer plays only a small role. As noted in Sainct and Clausen (1993), estimates of entry flux were doubled once relaxation times of molecules in the shock layer were taken into account in computing the radiative flux at the start of Phase B (see e.g. Velazquez et al, 1991): aerothermodynamics is a challenging and complicated field, critical for the probe design, and an area where European expertise is still developing. The entry protection system accordingly carries large design margins {which may be useful if methane is unexpectedly supersaturated in the atmosphere: models assume that methane abundance in the upper atmosphere is limited by the saturation value at the tropopause 'cold trap' - if this is not the case, the higher methane abundance could give higher entry heat fluxes }, and a large testing programme (see, e.g. Rock et al, 1993) has been neccessary.

The tiles of AQ60 are bonded to a structure made of a carbon-fibre/honeycomb sandwich via a flexible material to allow for thermal distortion. The thickness of the tiles is driven by their insulation performance: the structure must be kept below 423K, even though the front reaches ~1500K. The heat pulse (~20 seconds long) from entry penetrates through the tiles, causing the structure to reach ~400K just when the front shield is released (the analogy of a 'hot potato' springs to mind.)

In electrical terms, the probe is fairly straightforward. 5 Primary batteries ($LiSO_2$, giving excellent specific energy) supply power via battery discharge regulators (BDR) to a power bus, although power for pyrotechnic operations (such as parachute deployment) is taken directly from the batteries. Although the bus is not redundant, the mission can survive the failure of a battery or BDR.

Over the cruise phase of the mission, power for checkouts is supplied by the orbiter, and a coating builds up on the battery electrodes. This coating must be removed by 'depassivation': a short pulse of high discharge current just prior to separation.

During coast the batteries power triple-redundant timers. These power up the probe after the nominal coast duration, and the Command and Data Management (CDMS) commences the probe mission sequence. The first event is the warmup of the DWE USO, which requires a stable operating temperature to maintain frequency stability: the warmup begins 15 minutes

prior to entry.

During entry, g-switches arm the pyrotechnic systems. An accelerometer monitors the deceleration : simulations indicated that a measure of 0.8g, after the peak entry deceleration, correlates well with a speed of Mach 1.5. On detection of this g-level, the descent sequence begins with pilot chute deployment.

The CDMS distributes timing and other information (altitude, spin rate) to the experiments, and collects their telemetry packets in a 'round robin' fashion. If an experiment fails, such that its 'data ready' flag is not up, the CDMS moves onto the next experiment in its list. Thus, although it relies on flexibility of the experiments' own processors, it is possible that the portion of the probe telemetry stream devoted to a failed experiment could be used by another experiment (e.g. the DISR has essentially unlimited capability to generate data). The experiment packets are in turn assembled, together with housekeeping data, into probe packets and passed to the uplink transmitter.

Apart from the g-detection and data-handling functions, the CDMS essentially performs a sequencing function (a function that used to be performed by clockwork timers on satellites), in the nominal case. There are, of course, additional capabilities, such as the running of checkout sequences during cruise, which rely on the flexibility of the CDMS. However, in computing terms the probe CDMS tasks are relatively undemanding.

Each CDMU, of which there are two, running in hot redundancy, is based around the MAS 281, a processor built to MIL-STD-1750, using silicon-on-sapphire architecture. This architecture is required for its radiation hardness.

The telemetry chains from each experiment through the two CDMUs and their transmitters are independent. One chain, however, is delayed by 4s relative to the other, such that if the radio link were lost intermittently (e.g. due to excessive attitude motion) the overlap between the two channels means that no data is lost, assuming the interruption is less than 4s.

The data is transmitted to the orbiter by two S-band transmitters, using solid-state amplifiers to give 10W RF output power. Each transmitter has a separate antenna on the top platform of the probe, and the two links are separated in both frequency and polarisation. One transmitter has its freqency slaved to the USO of the DWE.

Thermal design of the probe is relatively challenging, with 4 principal design environments. The descent and entry aspects have already been mentioned. During the coast phase, the probe would become too cool, and relies on the 30 RHUs to maintain an acceptable temperature. In

contrast, during the perihelion passage close to the Venus flyby, the probe is exposed to high temperatures, despite shading by the orbiter's high gain antenna.

5.4 A Surface-Optimised Huygens Probe

The Huygens probe was designed to carry a payload to meet the stated objectives of the mission, of which study of Titan's surface was only one. The atmospheric objectives imposed design constraints, such as minimum parachute deployment altitude. It is interesting to consider as a *Gedankenexperiment* how the probe might have been designed were surface measurements the only objective, assuming the same cost and mass constraints, a similar payload and mission duration.

A steeper entry trajectory (γ up to 90°) and a smaller diameter would lead to a much deeper entry : the Mach 1.5 altitude (at which reduced aerodynamic heating makes parachute deployment possible) would be much lower, although peak entry loads and heating would be considerably higher. These larger loads would require a stiffer structure, and possibly a higher performance entry protection material, such as carbon. However, due to the shorter duration of heating, and the smaller probe diameter, the entry protection mass could probably be rather lower, allowing a larger payload.

For a lower deployment altitude and the same mission duration, the descent speed would be lower than for the current design (i.e. requiring a larger parachute than the stabiliser). This would lead to an extended loiter at low altitude, allowing better vertical resolution for atmospheric structure and composition measurements, and a lower impact velocity. With a lower descent velocity, however, the influence of surface topography on the time of impact would be rather larger.

Since winds are lower at low altitudes, the wind-induced dispersion on landing site would be reduced, perhaps allowing improved link margins and hence higher data rate. Correspondingly, however, the area under the probe that is available for imaging would be reduced.

A stiffer structural design of the probe would make interpretation of impact deceleration rather easier, since the rigid probe would force the acceleration signal to be due exclusively to the deformation of the surface material. On the other hand, a lower impact velocity would increase the uncertaintly on the attitude at impact (the influence of a sideways component of velocity, due to winds, increases if the vertical component is reduced): impact acceleration would have to be measured in 3 axes. Implementation of a single penetrometer would also be difficult.

It might therefore be better to jetisson the parachute prior to impact : even without the parachute impact velocity would be modest (of order 10 ms^{-1}), and a probe with a rigid structure would be likely to survive most impact scenarios. The probe shape would need to take the impact attitude (and any bounce from the surface) into account, to assure appropriate orientation of payload sensors.

A rigid probe might be expected to have a rather denser design: that of Huygens is about 300 kgm^{-3}, and may be compared with Pioneer Venus and Galileo at ~1000 kgm^{-3}. A probe with such a density would sink in a hydrocarbon ocean, unless some kind of flotation device were provided.

Thus, all things considered, the gains in surface mission performance of a 'surface-optimised' Huygens probe would be relatively modest. The Titan surface science community should be pleased with how the actual Huygens probe design has evolved.

Chapter 6

Cassini/Huygens Payload Capabilities for Surface Measurements

Equipped with his 5 senses, man explores the universe around him, and calls the adventure 'Science'

Edwin Hubble, American Astronomer

Get your facts first, then you can distort them as much as you want

Mark Twain, American Writer

The Huygens payload is described briefly in Lebreton et al. (1994), although a much fuller description document is currently in preparation in the ESA Special Publications series. Here only a brief summary will be made, but the capabilities for measurements relevant to surface conditions are described in detail, for both the probe and the orbiter. Additionally, the development of the Surface Science Package (SSP) is reviewed comprehensively , and the combination of SSP measurements for ocean composition determination is assessed. Finally some more general thoughts on the value of various measurements, and on the payload selection process, are given.

Tables 6.1a,b and 6.2 list the orbiter and probe payloads, their Principal Investigators and current best estimate (CBE) masses. Also shown are the corresponding masses estimated in the Phase A and assessment studies.

The mass growth of the orbiter payloads is remarkable. This is in part because many instruments have been developed as combinations of what were seen as separate instruments (e.g. CIRS is a combination of the original pressure-modulated IR sounder and far-IR spectrometer). Additionally, the deletion of the scan platforms meant that in some cases pointing hardware had to be incorporated onto the instruments, increasing their mass.

The process of assimilation is less obvious on the probe. The total payload mass for the payload has remained remarkably constant, compared with the orbiter. This is in part due

Investigation · Acronym	Scientist/Affiliation	Brief objectives
Cassini Plasma Spectrometer (CAPS)	D. Young, (PI), Southwest Research Institute, San Antonio (USA)	*In situ* study of plasma within and near Saturn's magnetosphere.
Cosmic Dust Analyzer (CDA)	E. Grün, (PI), Max-Planck-Institut für Kernphysik, Heidelberg (Germany)	*In situ* study of ice and dust grains in the Saturn system.
Composite Infrared Spectrometer (CIRS)	V. Kunde, (PI), GSFC, Greenbelt (USA)	Temperature/composition of surface/atmosphere within the Saturn system.
Ion & Neutral Mass Spectrometer (INMS) (Facility)	J. H. Waite Jr., (TL), Southwest Research Institute, San Antonio (USA)	*In situ* composition of neutral and charged particles in Saturn's magnetosphere and Titan's ionosphere.
Imaging Science Subsystem (ISS) (Facility)	C. Porco, (TL), University of Arizona, Tucson (USA)	Multispectral imaging of Saturn, Titan, rings and icy satellites to observe their properties.
Dual Technique Magnetometer (MAG)	D. Southwood, (PI), Imperial College, London (UK)	Study of Saturn's magnetic field and solar wind interactions.
Magnetospheric Imaging Instrument (MIMI)	S. Krimigis, (PI), Johns Hopkins University, Baltimore (USA)	Global imaging and *in situ* measurements of Saturn's magnetosphere and solar-wind interactions.
Cassini Radar (RADAR) (Facility)	C. Elachi, (TL), JPL, Pasadena (USA)	Radar imaging, altimetry and backscatter of Titan's surface.
Radio & Plasma Wave Science (RPWS)	D. Gurnett, (PI), University of Iowa, Iowa City (USA)	Study of plasma waves and radio emissions in the Saturn system.
Radio Science Subsystem (RSS) (Facility)	A. Kliore, (TL), JPL, Pasadena (USA)	Study of atmospheric and ring structure, gravity fields and gravity waves.
Ultraviolet Imaging Spectrograph (UVIS)	L. Esposito, (PI), University of Colorado, Boulde (USA)	Spectra and low resolution imaging of atmospheres and rings for structure, chemistry and composition.
Visual & Infrared Mapping Spectrometer (VIMS) (Facility)	R. Brown, (TL), JPL, Pasadena (USA)	Spectral mapping to study composition and structure of rings, surfaces and atmospheres.

Table 6.1a Cassini Orbiter Payload as selected

Name (in Assessment Study)	Acronym (where selected)	Mass (kg) Ass.	Phase A	Current
Solid State Imager	ISS	31	36.3	64.8
Near IR Spectrometer	VIMS	12	18.5	36.5
Pressure-Modulated IR Sounder		6		
Far IR Spectrometer		15		
Composite IR Spectrometer	CIRS		22.9	38.4
Ultraviolet Spectrometer	UVIS	4.1	8.0	13
High Speed Photometer		1.5	1.5	
Dust Analyser	CDA	5.0	5.0	14.9
Plasma/Radio Waves	RPWS	5.7	6.8	33.8
Magnetometer	MAG	5.0	3.0	7.4
Hot Plasma Detector			8.0	
Magnetospheric Imaging Instrument	MIMI		16.0	21.6
Radio Science	RSS	6.3	6.3	12.6
Ion/Neutral Mass Spectrometer	INMS	5.0	6.0	9.3
Energetic Gas		2.0		
Langmuir Probe/Retarding Potential Analyser		2.5	3.4	
Plasma Spectrometer	CAPS	12.5	12.5	17.8
Microwave Radiometer/Spectrometer		12	17.0	
Radar	RADAR	18.0	18.0	46.6
TOTAL		150.9	181.2	316.7

6.1b Cassini Orbiter Payload Mass History

Instrument	PI / Comments	Assessment Study (1985)	Phase A Study (1989)	Phase C/D October 1993
Atmospheric Structure Instrument	M. Fuclhignoni University of Rome Italy	3.8	3.8	6.7
Gas Chromatograph/ Mass Spectrometer	H Niemann GSFC USA	13	16	19.5
Aerosol Collector/Pyrolyser	G Israel Service d'Aeronomie, CNRS France	4.71	4.7	6.8
Descent Imager/ Spectral Radiometer	M Tomasko University of Arizona USA	4	6	8.5
Surface Science Package	J Zarnecki University of Kent at Canterbury UK	3.95 (I/SS)	1.2 (RITO)	4.2
Lightning and Radio Emission Detector	Not Selected - some functions performed by HASI/PWA	2.15	2.15	
Nephelometer	Use of Galileo flight spare investigated in Phase B - too difficult to re-engineer for Huygens. Science overlap with DISR	4.4	0 (PIRLS)	
Radar Altimeter Science	Not selected as PI instrument. Signal from engineering altimeter processed by HASI/PWA	0.25	0	(HASI)
Probe IR Laser Spectrometer	Not selected - space-rated laser diode technology too immature?		4.4	
Probe Doppler Tracking Science	M Bird Astronomisches Institut, Universitat Bonn Germany	1	0.7	2.3
TOTAL		40.66	38.95	48

to the tighter mass constraints on the probe, and also to the reduction in the number of payloads (e.g. the nephelometer was initially included in the payload: after it was deleted, its mass of 4.4kg was released to other experiments, allowing them some mass growth, but preventing the total payload mass from increasing). The process of payload selection is discussed in a later section.

Of particular interest is the history of surface science. Originally, in ~1985 during the assessment study, when the surface of Titan was largely unknown, about 4kg was allocated for Impact/Surface Science (I/SS), perhaps a small package to be dropped from the probe just prior to impact. Such a package could survive impact on liquid or solid surfaces and relay its information by radio to the probe. The probe itself need not survive impact in this scenario. At the end of the Phase A study, the global ocean model had taken hold, and atmospheric chemistry was the prime focus of Titan science: surface science was reduced to a refractive index measurement (RITO) to determine the ocean gross composition and the use of the ASI accelerometers, with 'possibly other investigations'. The mass allocated for RITO was 1.2kg. Now, in the hardware phase, Titan's surface composition is once more uncertain, and the Surface Science Package (SSP) is back to ~4kg.

Figure 6.1 illustrates the Titan surface coverage and resolution of the selected payloads. It illustrates that, while probe imaging achieves high spatial resolution, it only covers a small fraction of Titan's surface. Orbiter payloads will achieve coverage of a large fraction (all?) of Titan's surface, but at poorer resolution. Note that the coverage areas for imagers apply to single frames - mosaicing allows more extensive coverage, although this is limited to the area under the groundtrack of the probe for the DISR.

6.1 Probe Payload

6.1.1 DWE

While DWE is not intended as a surface measurement, the results are relevant to the understanding of surface conditions. Further, the discussion of the relay link geometry hereunder is relevant for assessing the survivability of the probe on the surface.

The Doppler Wind Experiment (DWE) comprises a rubidium Ultrastable Oscillator (USO) on the probe, by which one of the probe telemetry links is driven. The USO holds the

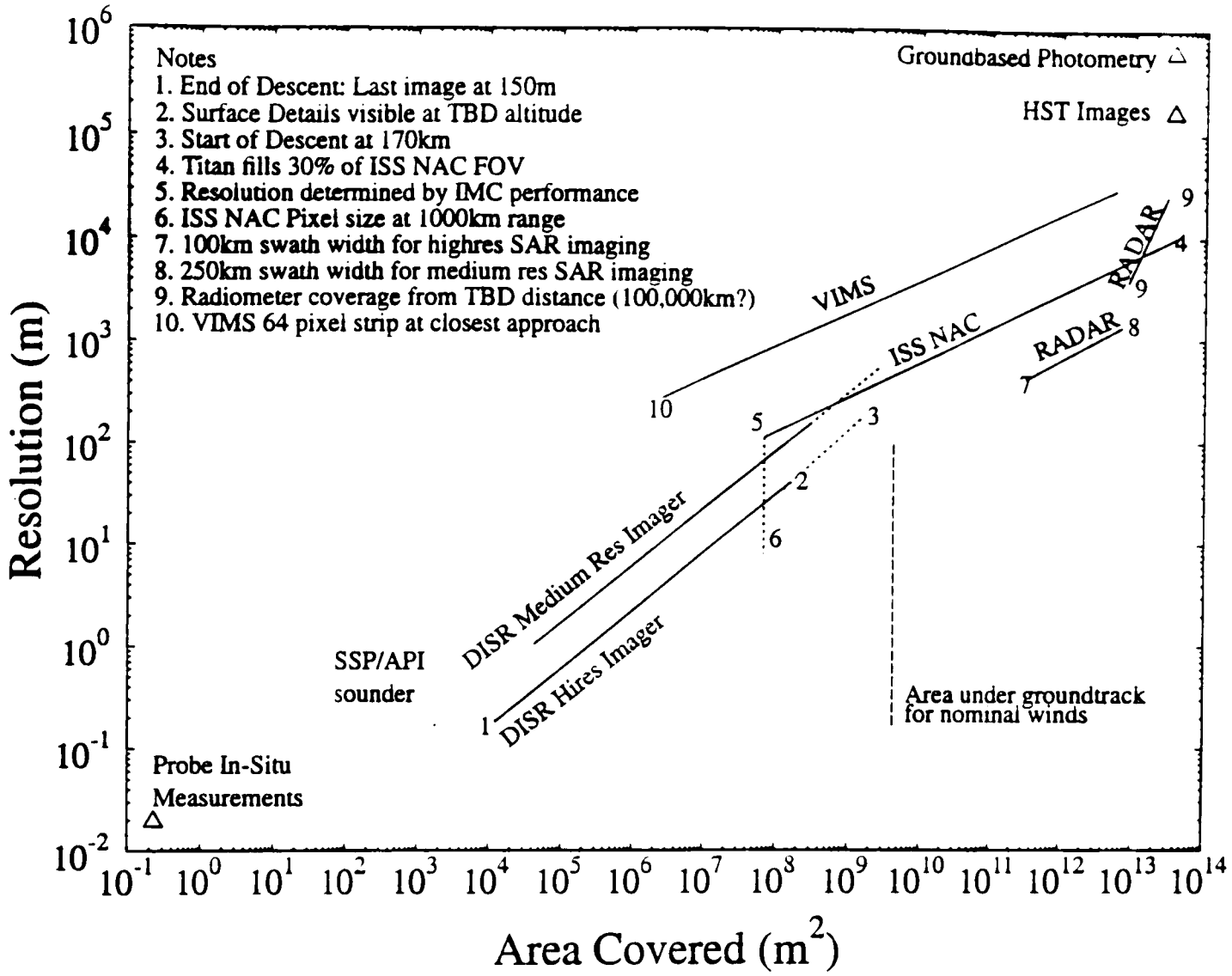

Figure 6.1 Cassini Payloads - Titan Coverage and Resolution (Lines show coverage of individual images - mosaicing can increase coverage)

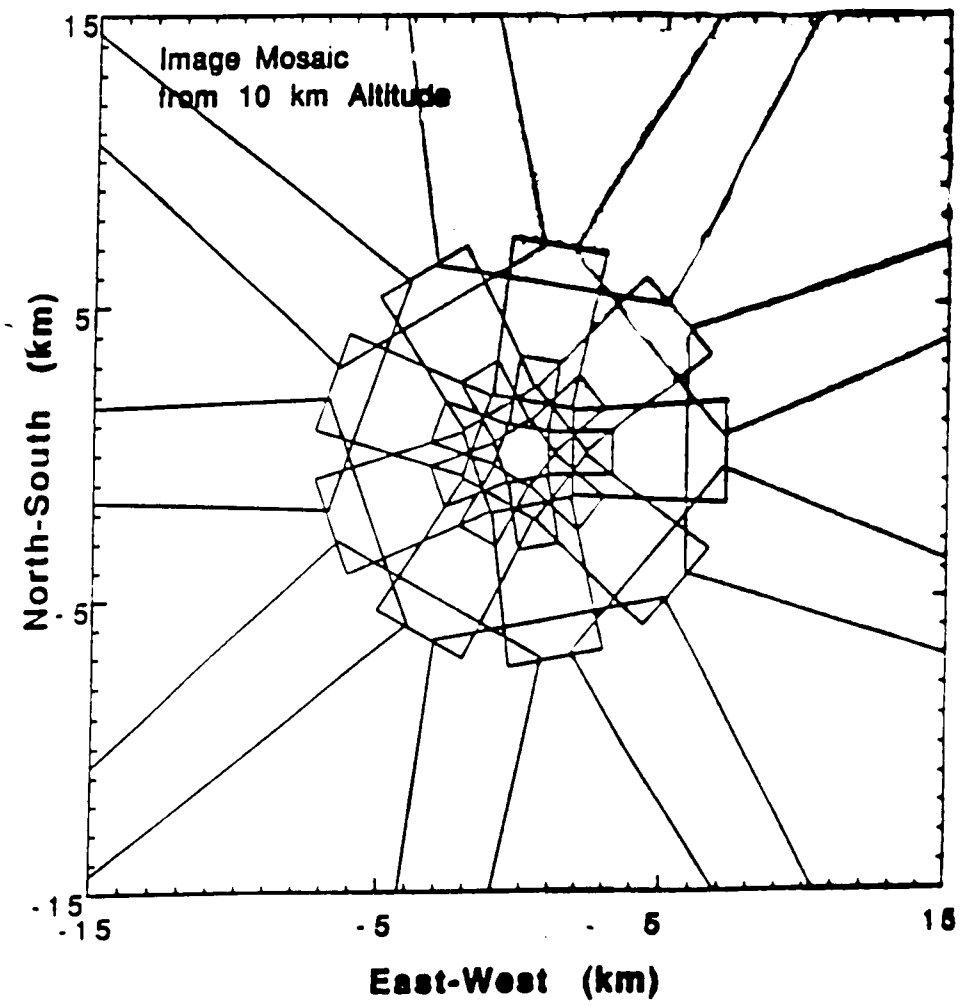

Figure 6.2 DISR imaging footprint during descent (by DISR team, from HSWT minutes)

carrier frequency of the radio link constant (with a drift over the duration of the mission of the order $\Delta f/f \sim 10^{-11}$) The frequency of the signal received by the orbiter is compared with a reference (another USO) and the difference in frequency is measured. This frequency difference is dominated by the Doppler shift due to the range rate between probe and orbiter (there are other, much smaller shifts due to General Relativity effects etc. - see e.g. Pollack et al. 1992). This range rate in turn includes a large component due to the (fast) motion of the orbiter relative to Titan, and a small component due to the probe's motion relative to Titan. For details of the scientific rationale, an error-analysis and the radio link geometry, see Atkinson et al. (1990).

The probe's motion relative to Titan may be broken down into three components, a vertical one, a meridional one (N-S) and a zonal one (E-W). The projection of each of these axes onto the range vector is determined by the orbiter-probe geometry, the 'Probe Aspect Angle' (PAA) being the angle between the range vector and the vertical. To maximise the effect of horizontal motions on the range rate, this angle should be minimised (i.e. the probe should be on the limb of Titan as seen from the orbiter, or conversely the orbiter is just on the probe's horizon.)

Since the dominant wind direction on Titan is believed (see chapters 2 and 3) to be zonal, the stated objective of the experiment is to measure zonal winds. Thus the meridional component of probe velocity on the range rate should be minimised, implying the probe should be on Titan's limb, as seen from the orbiter. This, however, is a rather impracticable relay geometry, suffering strong atmospheric attenuation, for example. The engineering constraints (see Ott, 1990) on entry angle, relay link geometry, and solar zenith angle (for the DISR) have led to a geometry that is not favourable to DWE, with a PAA of 25°-50° during the descent. The largest component of the range-rate is therefore that due to the probe's vertical descent velocity (which at least is predictable, and so can be eliminated from the data to retrieve the zonal motion). Worse, because the entry point is only slightly to the East of the incoming asymptote's meridian, the projection of zonal winds onto the line-of-sight is small: see figure 5.5.

The frequency is measured on the orbiter 8 times a second. Additionally, the strength of the received signal can be estimated by a measurement of the automatic gain control (AGC) on the receiver 8 times a second. Since these are the only measurements made, it will not be possible to detect, for example, the reflections of the radio signal from the surface (as was

done on the Pioneer Venus mission (Croft, 1980), possible since the probe signals were able to be recorded directly on Earth, rather than via a relay).

The short-term variation of frequency (the root Allen Variance) affects how probe dynamics may be measured. For example, since the probe antennae are displaced 20cm from the axis, there is a spin modulation imposed on the frequency of the link. For a 3rpm rotation, this leads to range-rates (noting that the orbiter is 60° above the horizon) of ~3cm s^{-1}. While this is about the level of the expected frequency 'noise' (M Bird, personal communication) the slow rate of change of spin should make it possible to detect the spin rate using fourier analysis. Detection of pseudo-random or rapid movements of this magnitude (e.g. ocean currents, or waves) is less likely.

6.1.2 ACP

The Aerosol Collector and Pyrolyser (Israel et al., 1992) deploys a filter through a sampling tube to the front of the probe. A fan forces the atmosphere through the filter, onto which aerosol particles are captured. After a sampling interval of some tens of minutes, the filter is withdrawn into the instrument, where an oven warms the sample. First, volatile components are evaporated, then at higher temperatures more refractory (and probably more complex) compounds are thermally decomposed (pyrolysed). The products of evaporation and pyrolysis are passed along a heated tube to the GCMS for analysis.

The ACP does not, in its final configuration, contribute to understanding Titan's surface directly, but since aerosols are ultimately precipitated onto the surface, it will provide valuable information. Also, since condensation processes are an important factor in photochemical models, the ACP will assist in understanding the Titan-atmosphere system.

The PI had intended to use the two inlet tubes as electrodes to measure the dielectric constant of the surface material (indeed the PI was also associated with an unsuccessful RITO (Refractive Index of Titan Ocean Proposal - see Badoz et al. (1992)) - the dielectric constant is diagnostic of, for example, the composition of binary CH_4-C_2H_6 mixtures (Ulamec et al., 1992) but following descoping in 1991-1992 to only one inlet tube, this measurement became difficult, and in the face of some development problems, attention was focussed on the experiment's primary objective, that of atmospheric aerosol sampling.

An additional obstacle to ACP operation on the surface is its large power consumption (for the ovens): concern over the probe mission energy budget led to the incorporation of an ACP switch-off in the descent sequence after the second pyrolysis, about 20 minutes before touchdown. Without this switch-off command, in a failure case where the ovens or fan remained on, the batteries might be exhausted before the surface was reached, compromising surface investigations.

6.1.3 DISR

The Descent Imager/Spectral Radiometer will perhaps be the most exciting instrument on the probe, taking images of the surface throughout descent. While gas compositions, detection of gravity waves in the atmosphere, and so on are of great planetological importance, the 'man in the street' most readily understands images. Thus the results of imaging payloads such as DISR are the most accessible to the general public, who by paying taxes, ultimately fund space exploration.

The instrument uses a CCD detector, with areas of the CCD mapped to different functions by fibre-optic bundles. It comprises 3 imagers - two down-looking for imaging the surface and/or cloud deck, and one side-looking to detect haze layers, distant clouds, and perform imagery on the surface.

One downward imager (Hi-res) has a FOV of 9.6°, with 160x256 pixels, each 0.06° across. Thus the ground resolution is about 20cm from the altitude at which the last pre-impact image is taken (150m). The other (medium res) imager has 176x256 pixels, each about double the size of those on the hires imager: its FOV is therefore 21° across. Hence, if atmospheric opacity is low enough to permit imaging from the start of descent, a single image would cover a square about 60km across.

The intention, however, is to cover a much larger area by mosaicing. The imagers are boresighted about 30° from the vertical, so as the probe slowly spins, the DISR FOV is slowly panned around (see figure 6.2) - indeed, DISR is the source of the requirement for the probe's rotation. Thus DISR will actually 'see' hundreds of square kilometres during the descent, due to the probe's spin, and its drift over the surface due to the zonal winds.

The side-looking imager extends the field imaged on the surface out to infinity (although clearly, atmospheric opacity and the curvature of Titan's surface prevent this from being literally true) in narrow strips. The resolution of the side-looking imager is quite poor, at 0.2° per pixel, with 128x256 pixels: the main function of this imager is to search for haze layers during descent (by adding the horizontal rows of pixels to form a vertical strip image one pixel across, signal-to-noise is improved to allow the detection of layers of very low optical depth (Peter Smith, personal communication)). Post-impact imaging is another function.

All the imagers are sensitive to the spectral range 600-1000 nm (i.e. red and near-IR). Colour information may be added in processing the images, since parts of each image field will be covered by a surface reflectance spectrometer, covering the regions 480-960nm and 870-1700nm with spectral resolutions of 4.8 and 12.6nm respectively. These spectra will allow the identification of surface materials (e.g. ices - see Schmitt et al. 1992). In order to get enough signal-to-noise for the surface material identification, surface spectra are made continuously during the last 150m of descent, and a 20W lamp is used to illuminate the ground below (since ambient lighting is too poor for good spectral work).

The DISR also makes radiometric measurements of the upward and downward flux in the atmosphere. These measurements will refine radiative models of the atmosphere, and by helping to profile the variation of opacity with depth, will aid in the interpretation of orbiter and groundbased images of Titan.

A final function is the solar aureole measurement, which measures the angular variation of sky brightness around the sun: this allows the scattering properties of the atmospheric aerosols to be measured, and hence their size and shape to be constrained. A clear requirement for this measurement is that the sun is not obscured by the parachute: this imposed the mission analysis constraint that the probe should descend more than 20° away from the sub-solar point on Titan, although ideally not too much more, to ensure adequate illumination for imaging.

Interestingly an alternative proposal for a DISR-type instrument had a broadly similar concept, although with more pixels/image. The proposed 'Descent Imaging Spectrometer and Large Format High Resolution Camera' (M Malin, personal communication) used a 800x800 pixel CCD imager, with a ground resolution of 50m from 20km altitude. Like DISR,

it would also have made side-looking images to detect haze layers, and have made solar aureole measurements.

6.1.4 GCMS

The atmosphere of Titan has so many different compounds in it that a simple gas analyser would be unable to discriminate between them. Thus, to determine the abundances of all its consituents requires the ablity to 'cut' in two dimensions: by polarity/adsorbability in a gas chromatography column, and by molecular mass in the mass spectrometer. For example, the common gases CO and N_2 are not easy to separate in either technique alone, but the combination of GC and MS allows them to be untangled. The Huygens GCMS instrument will be capable of measuring the abundances of constituents with masses of 2-146 atomic mass units, for all compounds abundant at levels (mole fraction) of above 10^{-8}, and selected compounds at levels down to 10^{-10}.

The GCMS will measure the isotope ratios D/H , O^{18}/O^{16}, C^{13}/C^{12} and N^{15}/N^{14} , helping constrain theories of Titan's atmospheric origin and evolution (see chapter 9.) If Argon is sufficiently abundant, its isotope ratio will also be measured, and will be a useful constraint on the origin and evolution of Titan's atmosphere.

The GCMS system performs several (of order 8) GC analyses, each of which takes several minutes. Direct MS measurement is more rapid, and is performed frequently.

Accurate measurement of the atmospheric composition near the surface will be useful in constraining surface-atmosphere interactions, such as possible ocean-atmosphere equilibrium.

6.1.5 HASI

The Huygens Atmospheric Structure Instrument (HASI) comprises 4 principal subsystems, aimed at making a determination of the structure of Titan's atmosphere (Fulchignoni, 1992).

The accelerometers' prime function is the measurement of atmospheric density during the entry phase (since the radio link is not open, this data is stored and transmitted after

parachute deployment). The technique is standard and has been applied successfully to the atmospheres of Venus, Earth and Mars (e.g. see Seiff, 1991) and will be used on the Galileo mission to Jupiter. Its application to Titan has been investigated by Fabris et al. (1992).

The original accelerometers baselined (piezoresistive types) have a sensitivity of ~1mg, leading to a threshold detection altitude of ~700km . However, this type of sensor suffers significant crosstalk and temperature-dependent offsets. Further, it was desired to extend the threshold altitude upwards to overlap with orbiter in-situ measurements (navigation, and the INMS which would measure gas composition). The corresponding threshold is met with an electromagnetic servo-type accelerometer on the x-axis of the probe, with piezoresistive sensors on x,y,z.

Extreme atmospheric turbulence during descent can be detected with the piezoresistive accelerometers, although their sensitivity is poor. The better sensitivity of the servo accelerometer will allow it to *detect* (but probably not *characterise*) rather weaker turbulence.

The temperature sensors are essentially platinum resistance thermometers, with a considerable design heritage from those developed by Seiff for Viking, Pioneer Venus, and Galileo (although note that following the failures of all 4 Pioneer Venus sensors at 12km, possibly due to an electrical phenomenon, the Galileo sensors are equipped with Faraday-cage shields.) The accuracy that might be expected from the sensors is ~0.5 K (see, e.g. Seiff 1976). Their response time is 0.1s or less (Cornaro and Castelli, 1991), leading to an altitude resolution of better than ~50m; in flight altitude resolution will probably be limited by data rate.

The pressure sensors are derived from devices used for terrestrial measurements on balloon sondes. They measure the total pressure (i.e. static pressure plus dynamic pressure) which corresponds closely to the ambient pressure. The pressure is sampled inside a small pipe called a Kiel tube - this (and the measurement of total rather than static pressure) minimises the variation in the measurement due to attitude motion of the probe. Note also (Lorenz, 1993b) that the dynamic pressure is essentially constant, and is directly related to the parachute parameters.

The PWA (Plasma Wave Analyser), the most visible part of HASI (being mounted on the long, deployable booms) bears a strong heritage from space plasma measurements. To the author's knowledge, it is the first flight of such an instrument on a Western planetary lander, although some related experiments have flown on FUSSR Venus probes. The instrument essentially comprises electrodes mounted ~40cm from the probe body, and the conductivity and permittivity between them is measured, giving a measurement of atmospheric conductivity (diagnostic of aerosol area (Borucki and Fulchignoni, 1992). On the surface, the electrodes can be used to measure the dielectric constant of the surface material (Grard 1992b,1992c), diagnostic of composition and porosity.

By searching for electric fields, the experiment also hopes to investigate atmospheric electricity. A stated objective is the search for lightning, although neither available evidence nor theoretical arguments support its existence (as discussed in chapter 3).

In principle, the experiment could get a 'sniff' of the surface dielectric constant while being 1-2 metres above it, allowing a surface detection before impact. However, such a measurement is probably not quantitatively useful, and in any case, for the measurement to be taken, processed, packetised by HASI, collected by the probe, repacketised and transmitted in the <0.4s before actual impact seems unlikely.

The PWA also incorporates an acoustic sensor (i.e. a broadband microphone) to search for thunder. However, since (Brock, 1991; Lorenz and Svedhem, 1992) the dominant aeroacoustic noise of the probe will be at the low frequencies, as for thunder (Hill, 1977), unambiguous detection of thunder may be difficult. A search for lightning activity on Venus with the 'Groza' instrument on Venera 11 and 12 was performed using electrical and acoustic sensors. However, (Ksanfomality et al. 1983a) the output of the acoustic sensors was attributed to aeroacoustic noise. Other acoustic signals may be detected (e.g. on the surface) but these remain highly speculative - see chapter 8. In any case, the time history of signals will not be transmitted (due to data rate limitations), only the power spectrum. The spectrum is computed using a digital signal processing (DSP) chip that is part of the PWA electronics. The availability of this facility for performing DSP on signals led to the inclusion of a link between the probe radar altimeter and HASI.

6.1.6 Radar Altimeter

Although there were several radar altimeter PI proposals, none was selected. One example is ASTRA, proposed by P Kamoun (1992). This was a frequency-modulated continuous wave (FMCW) radar, operating at S-band (2 GHz) with a 3 dB (FWHM) width of 28°. Its altimetric range resolution was to be better than 25 m and would detect the first reflection (for a layered surface) at levels down to -20 dB. Its penetration in an ocean (assuming loss tangent of 10^{-4}) would be 1.2 km, allowing a useful lower bound on depth to be placed. The stated data rate requirement was 50 bits/sec at 170 km altitude, 1 kbit/sec at 500 m.

The selection committee did suggest the examination of the use of the probe altimeter (required for sequencing some payload operations, although not, as it turns out, for probe system functions such as parachute deployment) for scientific purposes. The selected altimeter is also FMCW, although its scientific capabilities are still under review/development. The operating frequency 15.8 GHz is usefully close to that of the orbiter RADAR, allowing comparative measurements.

Detection of the surface reflection may be possible above even 50 km, although the FM ramp frequency means range is unambiguous only below 33 km. The altimeter will probably saturate below an altitude of 150 m, assuming a -10 dB surface target reflectivity. Altimetric resolution is 5-10 m, or 0.0025 times the altitude, whichever is the greater. (NB these figures are still under review.) The shape of the return pulse will allow some constraints to be placed on topography - see chapter 8 for the analogue process for acoustic sounding.

It is unlikely that the altimeter will function on the surface - reflection from a close solid surface would saturate the receiver, while in an ocean the poor antenna matching would give reflections in the waveguides which would disrupt the altimeter operation (L H Svedhem, personal communication).

6.1.7 SSP

The Surface Science Package (SSP) is described in detail here for two reasons; first, it is the instrument with which the author has been most closely involved, and second (and more importantly) it is the only probe experiment explicitly designed to study the surface. The

instrument is described briefly in Zarnecki et al. (1992) and Zarnecki (1992). Additionally, a BBC/OU programme (Balburnie 1994) gives a useful introduction, and shows some early ACC-E and DEN development work in graphic detail.

The original Titan probe studies did not envisage a substantial surface role for the probe (see chapter 4, where a Galileo-evolved design was anticipated). However, it was realised as the studies went on that surface survival might be possible, and the notion of the global hydrocarbon ocean was taking hold. Thus a limited surface science component was included (e.g. see Phase A study) comprising, for example a refractive index measurement, and the use of the impact acceleration of the probe to determine the solid or liquid nature of the surface.

Thus the model payload (Phase A) included a small surface science package (SSP) - one scenario involved a small sub-probe that would be released just prior to impact of Huygens, using Huygens as a relay (a similar concept was once proposed for the Moon - see McCarty et al., 1964).

When the Huygens payload selection was made, the proposal due to Zarnecki et al. was selected. This included the following elements

XRF - an X-ray fluorescence spectrometer, for the measurement of the abundance of surface material with molecular weights >12 . This instrument, proposed by US Co-I W. Boynton, would have used a $^{55}Fe/^{109}Cd$ source and a silicon PIN diode detector. The gross composition of a 10% silicate/ice mixture would be determined within a few tens of seconds, with elemental abundances of Mg, Si, S, K, Ca, Ti, Cr, Mn, Fe and Ni possible within a few minutes.

REF - a critical angle refractometer (see Geake and Mill, 1992, Birchley 1992) and references therein) to measure the refractive index of any liquid that the probe might land in. Refractive index was identified as a useful diagnostic of ocean composition in the Phase A study: the refractive index varies from ~1.38 for 100% ethane, to ~1.28 for all methane/nitrogen (Badoz et al.,1992)

ACC-A - a set of 3 orthogonal piezoresistive accelerometers, to measure entry accelerations, and motion on the surface due to waves. These sensors were essentially identical to those proposed as part of the HASI experiment

ACC-B - a piezoelectric accelerometer (along the probe X-axis, mounted near the base of the probe) to measure impact accelerations

DEN - a capacitive sensor to measure the level of liquid in a vent tube (the vent allowing the 'Top-Hat' sensor structure to fill with liquid after impact), thereby inferring the depth of immersion of the probe, and hence (from Archimedes' principle) the density of the ocean (believed to be a diagnostic of composition, owing to the difference in density of ethane and methane). This sensor would also measure the dielectric constant of the ocean.

ACP - Acoustic Properties. This sensor would measure the speed of sound in the atmosphere and ocean, and acting as a depth-sounder, place a lower bound on ocean depth.

TIL - two axis tilt measurement. Simple fluid-in-tube sensors would measure the angle of repose of the probe on a solid surface, and would measure rocking and motion due to waves on an ocean.

THP - a thermal properties measurement. Here the temperature, thermal conductivity and thermal diffusivity (=conductivity/density*specific heat capacity) of the atmosphere and ocean would be measured using a transient hot wire sensor. A simple platinum wire, or a thin substrate with a deposited conductor, was envisaged.

The SSP as proposed had a mass of 3.13 kg, with a possible extra 0.72kg for the Acc-A sensor; this may be compared with the Phase A strawman payload allocation of 1.2kg.

Thus the SSP as proposed would have made useful composition measurements of solid and liquid surfaces, although the question of how ocean composition might be constrained beyond the methane/ethane ratio was not addressed. Many of the measured parameters (refractive index, thermal conductivity) are themselves of minimal interest; the intention was presumably that the combination of the measurements would allow composition to be constrained.

For solid surfaces, the XRF would have identified z>12 elements, constraining the exogenic and endogenic resurfacing processes that may have taken place. Organic composition of solid surfaces was not addressed.

It should be stressed, however, that when the proposal was written, there was virtually no direct information on Titan's surface; Muhlemann's radar observation had not yet appeared in print and was regarded with some suspicion due to its poor signal-to-noise ratio. Perception of Titan's surface was largely dominated by the global ocean model. It is worth noting also that the probe configuration at Phase A differed significantly from that proposed by the two bidders for the Huygens contract.

In September 1990 (when the author became involved in the project) the Huygens payload selection was announced. From the rough-hewn designs in the various proposals, some 'trimming' was required, to meet mass, cost and other constraints: among some features of the payload that were lost in this rescoping exercise were the window covers of DISR (an issue later to cause some concern over contamination during entry) and the XRF subsystem of SSP, due to US funding difficulties (since the large US DISR and GCMS experiments had been selected for the probe, NASA funds for probe experiments became strained and support for XRF was withdrawn).

Additionally, certain elements of SSP and HASI had to be rationalised: the ACC-A accelerometers on SSP were identical to those baselined for HASI (the PIs of HASI and SSP being Co-Is on each other's experiment). Further, the potential utility of an acoustic sounder for making surface measurements was pointed out to the project by Hakan Svedhem (doubtless influenced by the ideas on acoustic measurements developed by J-P Lebreton [in an office only metres away from Svedhem's] and by his own background in radar). The possible utility of the DSP device on HASI/PWA for this measurement was noted, and stressed by Dr Grard.

By February 1991, the SSP ACC-A sensor had been deleted, such that the entry and ocean wave accelerometry would be performed by HASI. The acoustic sounder would be incorporated onto SSP, although a passive microphone was retained on HASI (with the principal justification of listening for thunder).

Throughout 1991, the details of SSP (and the accelerometry portion of HASI, to be provided by the University of Kent) remained in a state of flux, most notably due to funding pressure from SERC, which supported UK experiments on Cassini. ESA concerns over the ability of SSP to meet ESA requirements and the science objectives with a greatly (~50%) reduced budget nearly resulted in the deletion of the experiment. To the credit of the PI and SSP team, work-around solutions to the funding problems were devised, and the experiment retained.

As part of the ESA payload team, the author was tasked with evaluation of certain aspects of SSP. For example, the DEN measurement technique was judged inappropriate, and alternatives were sought; the two options favoured by the author in a November 1990 study ('Methods of Titan Ocean Density Determination', unpublished memo) were a vibrating-vane sensor and a float/arm buoyancy sensor. Other aspects studied were the scientific value of the TIL and PER sensors, and the optimum location and type of sensor for the ACC-B sensor (PER was the part of the original DEN sensor to measure the relative permittivity, or dielectric constant, of the ocean material).

At the time of writing (Spring 1994, during the integration of the engineering model of SSP) the SSP experiment configuration is essentially fixed. The status and capabilities of the various subsystems is described below.

ACC-A - now part of the HASI experiment

ACC-B - this sensor will be discussed in more detail in chapter 7. The impact accelerometry function was essentially split in two, with a penetrometer (ACC-E ; 'accelerometer-external') mounted near the apex of the probe, on a mast from the Top Hat, and an accelerometer (as originally envisaged for ACC-B, now redesignated Accelerometer-Internal, or ACC-I) now mounted on the experiment platform, on the SSP electronics box.

DEN - shortly after payload selection, the SSP team (independently of the study by the author, but in concurrence with it) decided to use a commercial aerospace fuel-density sensor using the vibrating-vane principle (aircraft fuel density in fact varies significantly from airport to airport, reflecting different hydrocarbon compositions). The baselined sensor, by GEC, would have required some re-engineering to allow cryogenic operation, with a significant cost impact (£30,000+).

This cost, coupled with the financial pressure on the SSP programme, led to yet another evaluation of alternative techniques, by Mark English. He examined hydrostatic pressure measurement and buoyancy gauges. The small vertical separation between pressure sensors means that the pressure difference (equal to the product of density, gravitational acceleration and vertical separation) would be too small to be reliably measured. Thus a buoyancy sensor (resembling that suggested in the author's 1990 study as a promising alternative), where the upthrust on a small, light float would be measured by strain gauges on a small flexible arm, was designed . This sensor, with the remarkably low mass of 10g and volume of $3cm^3$ is intended to measure the ocean density with a resolution of 5 kg/m^3, although this capability has yet to be demonstrated at cryogenic temperatures.

In spring 1992, an alternative sensor became available at low cost, namely another vibrating-vane sensor, developed by the Space Research Institute in Warsaw. This sensor was comparable in mass and performance with the buoyancy sensor, but more robust and less likely to be affected by probe motion. Further, since the strain gauges on the buoyancy sensor are bonded onto a thin epoxy beam, and immersed in a cryogenic liquid, drift in strain gauge resistance is a possible error source.

However, the advanced stage of development of SSP, made the replacement of the DEN sensor with the new one awkward (the strain gauge bridge circuit would have had to have been replaced with the phase-locked loop counter of the vibrating vane sensor, plus the mechanical accomodation would have had to have been revisited.)

In any case, density turns out to be a relatively poor diagnostic of composition, since (especially in the low-temperature models favoured in the light of the refined atmospheric argon abundance) the nitrogen content of the ocean may be quite high ; about 0.16 of the methane content at Titan's surface temperature (Kouvaris and Flasar, 1991, Thompson et al. 1992). Since the densities of methane, ethane and nitrogen are approx 450, 650 and 800 kg m^{-3} respectively, the incorporation of nitrogen largely offsets the low density that might be expected of a methane-rich ocean. Thus the density contrast between a 10 and 90% ethane ocean changes from 469:623 to only 509:626 (see figure 6.3). Further, the addition of unknown quantities of argon (0-6%) and propane (few %), the dissolution of other organics, and the suspension of bubbles and/or sediments mean that density is subject to a bewildering number of factors. (Note that the densities computed in Lorenz (1992) of 605

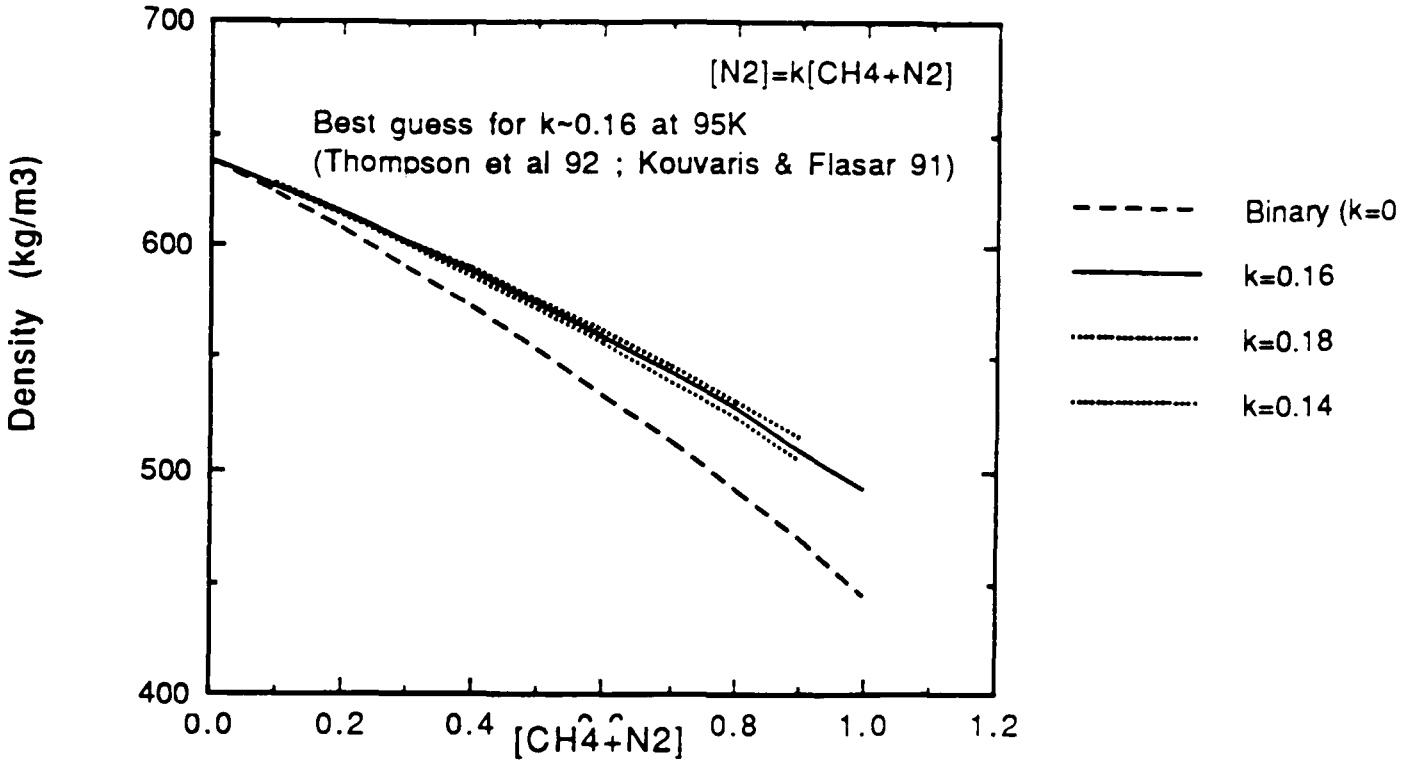

Figure 6.3 Density as function of ocean composition

Abscissa is mole fraction of methane+nitrogen : remainder is ethane
Curves are for different values of equilibrium nitrogen:methane mix k

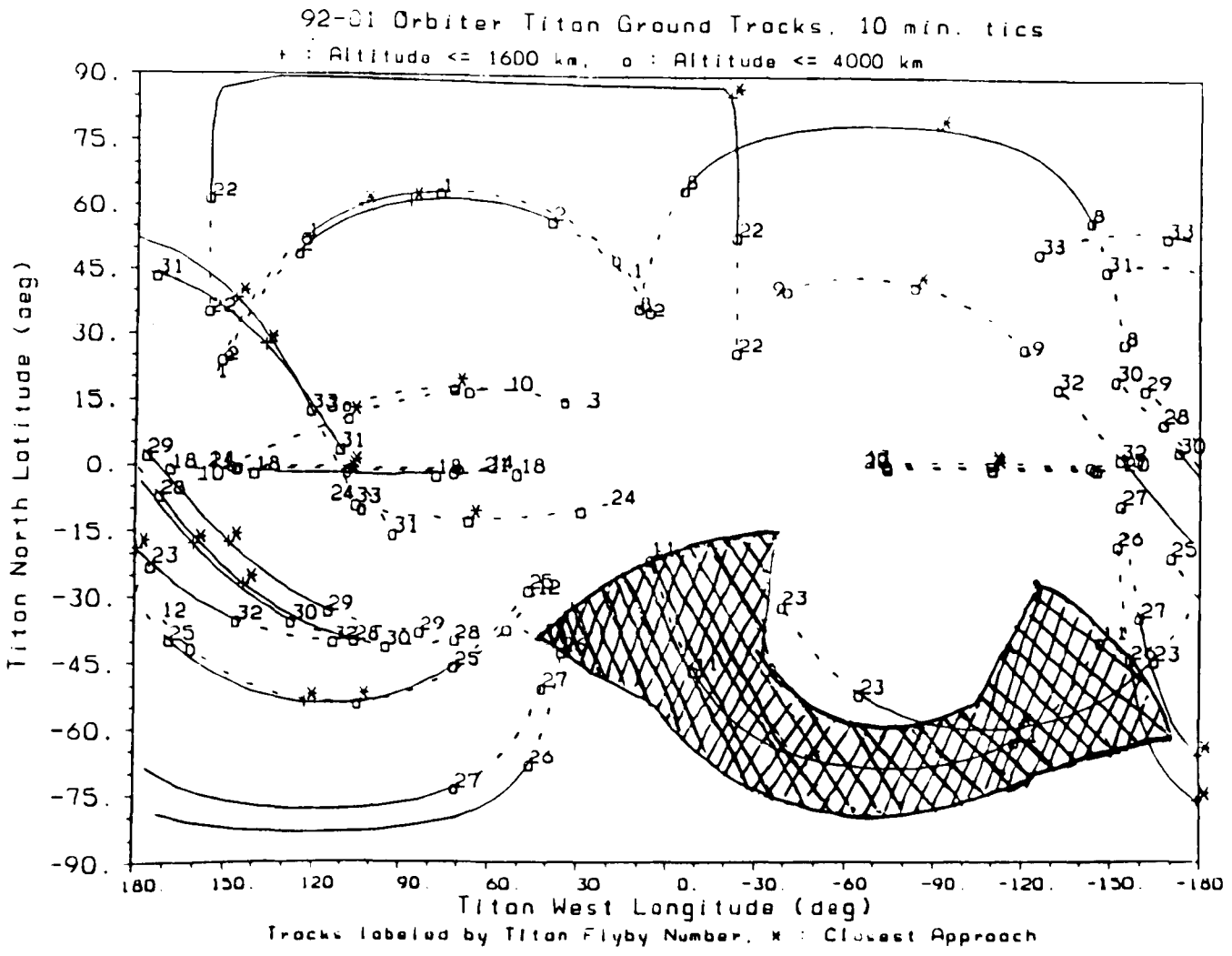

Figure 6.4 Orbiter Radar ground track and sample swath (adapted from Murrow 1993)

and 645 for the two 'end member' ocean cases of Dobouloz et al (1989) do not correspond to ocean density extremes, since their temperatures and argon abundances are not treated independently).

THP - in an effort to maximise the scientific return from SSP (and, in part, to justify its retention on the probe for atmospheric measurements when it became questionable whether a global ocean was a likely surface model for Titan) the sensor design was made rather more complex and delicate than originally proposed; this gave it the ability to measure atmospheric thermal conductivity. While it offers an additional application of the experiment, the planetological utility of the measurement of thermal conductivity may be questioned. The current configuration comprises 4 wires 2 of 6μm diameter, 2 of 25 μm, each in its own capsule (to protect the fine wires against damage). The sensor requires rapid sampling at high accuracy (see, for example, Birchley 1992) and in its present form has used a large fraction of SSP resources (top hat volume, circuit board space, manpower etc.).

Since the dominant heat transport phenomenon in lakes and seas is rarely conduction, it is unlikely that the thermal conductivity of the fluid is itself of particular interest. With the stated accuracy of 0.001 W/mK, it would be capable of measuring the composition of a binary C_2H_6,CH_4 mix with ~1% accuracy, although (see later) the addition of nitrogen and other solutes degrades this accuracy. Further, see Birchley et al (1992), 'real-world' measurements where convection and other effects may be taking place give the data considerable scatter, perhaps 10%, or 0.01 W/mK.

Why is this measurement being made? Even the PI is less than specific : 'to constrain models of the ocean and atmosphere by reducing the number of free parameters of direct relevance to particular models and providing properties which must be satisfied by any postulated surface structure or composition' (Zarnecki, 1992)

A coarse measurement of ocean thermal conductivity is in principle useful as a broad constraint on ocean composition, although THP is no better in this respect than many other (smaller, simpler) sensors. In the present author's opinion, the resources devoted to it are out of proportion to the scientific return.

PER - This became two plates, forming part of a capacitive bridge. These enable the measurement of the dielectric constant of any material filling the gap between them.

Dielectric constant is a possible diagnostic of ocean composition, and a relatively simple measurement to make. Note that this measurement will also be performed, albeit over a larger distance scale and at a different frequency, by the HASI PWA. A point worthy of note is that while the dielectric constant depends broadly on the ocean bulk composition, it is also sensitive to relatively small amounts of polar material (HCN - see Thompson and Squyres 1990)

REF - a problem with the originally-proposed design was that the CCD detector (which records the light/dark transition on the prism, indicating the onset of total internal reflection) would be degraded by radiation dose during cruise. Instead a photodiode array was selected, although there were some early problems in getting the photodiode array to work at low temperature, and the originally-selected device (manufacturered by EG&G) had to be replaced with one by Hammamatsu. The transducer is in principle able to measure refractive index with an accuracy of 0.001, and so is a relatively efficient diagnostic of ocean composition.

A useful by-product of REF is that the externally-illuminated mode gives an indication of how much suspended material is in the ocean liquid (e.g. photochemical aerosols).

API-V - this took the form of two bimorph piezoelectric elements facing each other across the top of the top hat. The speed of sound measurement is directly useful for interpreting data from the API-Sounder, and is an additional diagnostic of ocean composition. Further, its capability of measuring atmospheric speed of sound allows the recovery of a temperature profile (for an assumed composition) with very high vertical resolution.

API-S - this became an array of 10 bimorph piezoelectric elements, mounted on the flat end of the tophat facing vertically downwards during descent. At the operating frequency of 15kHz, they have a half-power beamwidth of 8 degrees.

The API-S measurement is described in more detail in chapter 8, but for the purpose of this chapter, it may be mentioned that the API-S will be able to constrain ocean depth to a minimum of 300m (depending on the scattering and absorption of the ocean)

6.2 Orbiter Payloads

During its 4 year tour of the Saturn system, the orbiter will make a large number of flybys of Titan. Some of these will be devoted to remote sensing with the imaging and spectral instruments, others to radar observations. In addition, as soon as the 30-minute extended surface mission of the Huygens probe is over, the orbiter is slewed around to point the imaging instruments at the landing site.

6.2.1 RSS

The RSS (Radio Science Subsystem) comprises those scientific investigations using the orbiter radio link with the Earth. While telemetry is sent on an X-band downlink, S and Ku-band carriers can also be monitored.

Radio Occultation

The details of the analysis of the Voyager 1 radio-occultation data are given in Chapter 3. One may assume that the measurements from Cassini will be somehat more precise than Voyager, due to improvements in technology (signal-to-noise at the ground station, and so on) and due to our current knowledge of Titan's radius and atmosphere (recall that the occultation geometry at the Voyager 1 encounter was designed to cope with a surface pressure of 20 bar, making the measurement less sensitive than would be possible for 1.6 bar).

Further, since there are several flybys, occultation measurements of the atmosphere at several points on the surface will be performed, allowing the investigation of how temperature structure may vary with latitude.

Spacecraft Tracking

Tracking of the Voyager and Pioneer spacecraft, as well as observations of the perturbations of the orbit of Hyperion, have enabled Titan's mass to be fairly well-

constrained. This, in turn, allows the density to be estimated, which gives a clue as to the proportions of ice and rock in the interior.

Because the orbiter is in orbit around Saturn, the flyby velocity relative to Titan is considerably lower than during the Pioneer and Voyager encounters, so the effect of Titan's gravity is correspondingly larger (indeed, the gravity of Titan is being used to change the orbital period and inclination to allow the orbiter to explore the Saturnian system more fully.)

Thus accurate tracking of the spacecraft should help to refine estimates of the harmonics of Titan's gravitational field (J2, J4 etc.) These, in turn, place constraints on the distribution of mass in the interior of Titan, for example deducing the extent of differentiation, or the radius of the core. Comoretto et al. (1992) estimate that tracking will be able to measure the J4 (quadrupole) coefficient of Titan's gravitational field to within 1%. Also, since flybys will occur at different parts of Titan's orbit, measurements of the field will be made at different points in Titan's tidal cycle, allowing the response of Titan's interior to the varying tidal potential to be made. This will enable the determination of Titan's Love number, a measure of the rigidity of the interior (see chapter 9).

6.2.2. ISS

The ISS (Imaging Science Subsystem) incorporates two CCD cameras, each using 1024x1024 pixel devices. The narrow-angle camera has a field of view of 0.35°, giving an angular resolution of ~6 μrad, while the wide-angle camera has a FOV of 3.2°. The narrow-angle camera is sensitive to radiation from 200-1100 nm; as a result of the 1992 NASA descoping exercise, the wide-angle camera uses spare Voyager optics, which cuts the transmission range to 380-800nm. Both cameras are equipped with wavelength and polarisation filters.

Although it was not realised early (see e.g. Murray, 1992) the narrow angle camera will be therefore sensitive to the 0.94, and possibly 1.08 μm window regions: efforts are being made (C Porco, personal communication) to ensure that the appropriate filters are installed and image sequences performed.

Notionally the best ground resolution for a 1000 km flyby is of the order of 6m/pixel, although due to the difficulties of image motion compensation and non-zero atmospheric

scattering (even in the window regions) a more realistic figure might be ~20-100 m. (Note also that closest approach for most Titan flybys occurs on the nightside of Titan - see figure 5.4, so even with effective image motion compensation, the ground resolution on illuminated areas would be about double the 6m mentioned above).

As well as detecting albedo contrasts, it may be possible to examine shadows of topographic features such as mountains or crater rims, or 'glitter' from waves on seas (Griffith and Owen, 1992). These measurements, however, depend on how diffuse or direct the surface illumination is (i.e. exactly how transparent the atmosphere is in the window regions). Note that topography estimation from shadowing generally requires low sun angles; this implies low illumination levels and high atmospheric scattering, so signal-to-noise is poor. It is probably unlikely that we will know for sure how much (if anything) these measurements will tell us until Cassini arrives, although the forthcoming HST observations may give us some clues.

6.2.3 VIMS

The Visual and Infrared Mapping Spectrometer (Baines et al., 1992; see also Formisano et al. 1992) will allow spectral maps of satellite surfaces, including that of Titan, to be made. The VIMS instrument covers two wavelength ranges, visible (0.35-1.0μm) and IR (0.85 to 5.1μm), thus covers all the near-IR window regions where it is currently believed to be possible to see to the surface or deep atmosphere.

Resolution is poorer than ISS (0.5 mradian at IR, 0.17 mrad at visible), but since the spectral coverage is so much better (in the IR range, the spectral resolution is 0.167 μm, approximately the width of the window regions - see figure 2.1) the detection of surface albedo contrasts will be more effective.

Thus, dayside images of Titan from a close flyby at 1000 km should yield spectral maps identifying features as small as 500 m across. Since measurements at several windows are possible, discrimination between different surface compositions can be made: H_2O ice or NH_3 hydrates have reflectivities which fall with wavelength, while tholins have a flat spectrum in the 1-2 μm range.

Note that the interpretation of VIMS and ISS images depends largely on the profile of optical depth with altitude: for example, as noted by Griffith and Owen (1992) and Griffith et al. (1991), the absolute albedo of the surface is modified by the possible existence of C_2H_6 mist.

The instrument will also be used to observe Titan's nightside to search for active volcanism. Baines et al. (1992) have noted that the emissive flux for fresh water-ammonia cryolava (at 167K) in the 5 μm atmospheric window is 20 times that for the 94K background, assuming a radiating area larger than the footprint of a single VIMS pixel. Improved detection of volcanic activity, and in particular the discrimination between large warm areas and small hot ones, can be achieved by using radiance measurements at two wavelengths (Rothery and Lawrence, 1993): since the flux at 167K in the shorter-wavelength IR windows will be very small, perhaps a combination of VIMS and microwave radiometry would be the best way of measuring the temperature.

A second nightside VIMS imaging objective is to search for possible lightning (many of the species expected to be produced in a lightning strike have emissions in the window regions), although as discussed earlier, this is speculative.

VIMS will also be able to measure abundance profiles of methane, acetylene, carbon dioxide and carbon monoxide in the atmosphere, although with less precision than CIRS (see below).

6.2.4 CIRS

The CIRS (Composite Infrared Spectrometer) will perform high spectral resolution measurements over the range 7 to 1000 μm (Calcutt et al., 1992), improving greatly on the performance of the Voyager IRIS instrument. Using both limb-sounding and nadir-viewing modes, it will be able to make profiles of the mixing ratios of various atmospheric constituents with excellent altitude resolution.

Since the wavelength coverage of this instrument does not include the near-IR windows, no direct surface information is expected, although the atmosphere profiles will validate photochemical models.

6.2.5 RADAR

The impenetrability of Titan's atmosphere, like that of Venus, makes it a natural target for study by radar (cf some of the studies cited in chapter 4 which mention a 'Titan Radar Mapper' as a mission option). The recent success of the Magellan spacecraft in revealing the exciting features on the surface of Venus adds to the interest in this instrument.

Essentially the high-gain antenna is used as a radar transmitter and receiver at Ku-band (13.8 GHz). The details of the investigation are described by Elachi et al. (1991), with some additional theoretical detail on radar reflection from various surface models in Picardi et al. (1992).

Signal-to-noise considerations restrict radar imaging to ranges of 4000 km and below (resolution of 660x2500 m) and high-resolution (380x600 m) below 1600 km. Clearly, high-resolution coverage of Titan is maximised by maximising the number of close flybys.

The high ground resolution is achieved using only a modest antenna by employing the Synthetic Aperture Radar (SAR) technique, whereby the orbiter's motion is used to synthesize a large aperture (cf. groundbased interferometric aperture synthesis, such as on the VLA). The radar investigation uses offset feeds on the HGA to generate seven fan-shaped radar beams (one nadir, six off-nadir). The huge amounts of data generated are compressed with the same quantisation scheme as used on Magellan.

The SAR will generate maps of swaths of Titan's surface (see figure 6.4) showing radar reflectivity (which may vary due to both topography and surface composition : the interpretation of even terrestrial SAR data from ERS-1 is only now being fully explored). It is the stated requirement of the radar investigation to image 30% of Titan's surface.

The radar has two additional modes: altimetric (which will measure topography - see the chapter on SSP acoustic measurements) and scatterometric (measuring radar cross section). These two modes use a narrow 'pencil' beam, formed by illuminating the HGA with a single Ku-feed at its focus. The difference between the two modes is simply in the method of processing. Altimetric resolution is of the order of 80 m (Elachi et al. 1991). Altimetry begins from a range of 25,000 km.

The HGA is also used passively, as a microwave radiometer. Radiometric measurements may be made from as far out as 100,000 km, although 25,000 km is the baseline. By scanning the antenna (most probably in a conical fashion, such that the footprint - 61 km diameter at 10,000 km range - describes a spiral on Titan's disk) a map of brightness temperature will be built up (indicating temperature and/or emissivity variations over the surface).

Thus the radar will map Titan's entire surface (at all latitudes) with resolutions of the order of 10km, with some swaths (making up ~30% of the surface, in the current mission plan) imaged at sub-km resolution.

6.3 Probe Measurements Post-Impact

Post-impact measurements are summarised in tables 6.3, 6.4 for landings on liquid and solid surfaces, respectively.

It is the feeling of the DWE PI (M Bird, personal communication) that the impact deceleration may cause a perturbation to the USO reference frequency during the impact, but afterwards will return to its nominal value. If this is the case, then post-impact drift measurements will be possible (with a resolution, depending on direction, of perhaps 0.1~1 ms^{-1}, although it is repeated that the geometry means the doppler signal is also sensitive to vertical motion (waves, bobbing).

The DISR will be able to make images using the side-looking imager, whose FOV stretches 6° above the horizon. What these will show is entirely speculative, but weather monitoring (cloud-tracking) is an obvious possibility. If the probe lands in a liquid and drifts around, the area observed by the imager will be increased.

The DISR lamp is cycled on and off for a short time after impact - the thermal effects of this are probably small, however. An intriguing possibility, if the probe begins to sink in a liquid, is undersea images. Due to suspended particulates, however, opacity is likely to be so high as to prevent anything being seen.

Table. 6.3 Huygens Surface Measurement Scenario (Liquid Surface)

	Impact	3 mins	5 mins	15 mins	30 mins
SSP	I..impact data.....I I + preimpact .....I I tilt sensor (wave period determination).....(time variability).....> I API-S depth determination .....(drift measurement, change of depth).....> I other sensors.....I.....(time variability).....>				
HASI	I...impact data....I(ACC, PWA) I..ACC.wave period determination.....(time variability).....> I.....PWA search for acoustic emissions (wind), lightning.....> I.....(drift measurement: detection of shallows, bubble clouds, etc).....> I..TEM,PRE surface conditions.....(time variability).....>				
DWE	I zero pointI (to calibrate wind curve) I.....(drift measurement: winds and currents).....>				
GCMS	I..MS (1 min).I.....Full GC (11mins).....I.....GC cycle(11 mins).....I.....GC cycle(11 mins).....I I rough composition I.....accurate composition.....I.....(time variability).....>				
DISR	I..pre-impact..I I...local images.....weather (cloud-tracking).....> 20-30 images in 1st 15mins (0.8 m/s winds resolved at 10km) (0.4 m/s winds resolved) .....(field of view drifts around?).....> I.....surface science lamp cycled on-off.....I .....(undersea images, if sinking?).....I				

Table 6.4 Huygens Surface Measurement Scenario (Solid Surface)

	Impact	3 mins	5 mins	15 mins	30 mins
SSP	I..impact data.....I I + preimpact .....I I tilt sensor .....(time variability - subsidence).....>				
HASI	I...impact data....I(ACC, PWA) I..ACC.detection of seismic signals?.....> I.....PWA search for acoustic emissions (wind), lightning.....> I..TEM,PRE surface conditions.....(time variability).....>				
DWE	I zero pointI (to calibrate wind curve)				
GCMS	I..MS (1 min).I.....Full GC (10mins).....I.....GC cycle(11 mins).....I.....GC cycle(11 mins).....I I rough composition I.....accurate composition.....I.....(time variability).....>				
DISR	I..pre-impact..I I...local images.....weather (cloud-tracking).....> 20-30 images in 1st 15mins (0.8 m/s winds resolved at 10km) (0.4 m/s winds resolved) I.....surface science lamp cycled on-off.....I (changes in spectral characteristic of surface due to lamp-induced thermal changes)				

Just after impact, the upward radiometer may detect a dust cloud thrown up by the wake of the probe (Lorenz, 1993a). Detection of such a cloud may allow constraints on particle size and cohesion to be made.

The inlets of the GCMS are heated, so if it and the probe survives impact, volatile components of the surface material (ices etc.) will be vapourised and their composition indicated. A direct MS analysis of the surface will take about 1 minute. After this, repeated GC analyses are made (each taking ~11 minutes). If GCMS is able to operate in the event of a liquid landing, several of the SSP functions (REF,DEN, THP) are redundant.

The SSP systems will be able to make ocean measurements in a few seconds (compared with ~1 minute for the MS analysis). However, it seems likely that if the probe survives for a few seconds, it will probably survive rather longer (see chapter 5).

Further, the utility of the measurements DEN, THP and REF has not been demonstrated for ocean composition. These systems were developed on the assumption that the ocean would be a binary methane-ethane mixture, with the physical properties of refractive index etc. varying monotonically between ethane mixing ratios of 0 and 1. However, methane and ethane form a ternary mixture with nitrogen, with high nitrogen content (up to ~10%) associated with methane-rich seas, and other organic compounds are likely to be present in unknown quantities. This problem is discussed more fully in the next section.

The PER instrument also fits into the above category, except it has the useful additional function of possibly detecting polar compounds (e.g. HCN) in the ocean.

6.4 Ocean Composition Measurement using SSP

One of the principal objectives of the SSP experiment is to determine the composition of Titan's surface at the probe landing site. Most of the SSP subsystems are designed to address this question in the context of the prevailing model of Titan's surface when SSP was proposed, namely the global ocean.

The composition measurements (PER,DEN,THP,REF,API-V) can make useful measurements with liquids only, since the intimate contact between sensor and sample that is needed for

the measurements is improbable with solid surface materials. Note, however, that the liquid need not be an 'ocean' : a puddle of modest depth (~30cm) will be enough to immerse the transducers.

Ocean composition measurement allows valuable constraints to be placed on the delivery and inventory of methane to the surface, and on the photochemical evolution of Titan's atmosphere, particularly when these measurements are combined with a measurement of ocean depth (by API-S, orbiter radar, or the radar altimeter) and areal extent (by radar or imaging from orbit). In the classic ocean model (Lunine et al, 1983) an initially methane-rich ocean would decrease in depth over geologic time, becoming increasingly richer in ethane.

Thus the fundamental quantity to be estimated by SSP is the ethane:methane ratio, and the accuracies of most of the SSP sensors were specified to enable the ethane mole fraction to be estimated to ~1%, assuming the ocean to be a binary mixture. The proposal (Zarnecki et al. 1990) suggested that 'correction for propane content could be made by assuming the 2.4% of ethane abundance predicted by photochemical models' and that 'the quantities of dissolved nitrogen, argon and other hydrocarbons are also related to the methane abundance'.

These corrections, however, are model-dependent. The crux of the matter is *how* model-dependent are the SSP measurements and their interpretation? In one limit, confidence in models of Titan's photochemistry and ocean-atmosphere evolution is absolute, and only one of the following measurements would be needed : ocean depth, ocean composition, or sea-level atmosphere composition. In the other limit, where model confidence is poor, atmospheric composition only poorly constrains ocean composition, with depth an independent parameter altogether . In this case, ocean composition may be considered as 4 parameters, namely X_E, X_{Ar},X_{N2}, X_{so} (the mole fractions of ethane, argon, nitrogen and solutes, mainly propane, respectively). The methane abundance X_M is given simply by

$$X_M=1-X_E-X_{Ar}-X_{N2}-X_{so} \qquad (1)$$

Thus the bulk composition of the ocean has 4 unknowns, and would require 4 independent measurements to solve uniquely. This would rely, however, on impossibly high accuracy for

the SSP sensors: to unravel a complex mixture such as Titan's ocean (or, indeed, its atmosphere) requires a sophisticated analytic instrument such as GCMS.

In reality, the situation is an intermediate one: the ocean and atmosphere are coupled, and the mole fractions of ocean constituents can be at least partly constrained by models. Here I attempt to assess how accurately ocean composition can be determined by SSP, using reasonable model assumptions.

Assume X_E, X_{Ar}, X_{so} as free parameters. Due to the high solubility of nitrogen in methane (but poor solubility in ethane), we can define the binary CH_4-N_2 mixture to have a mixing ratio X_b, so

$$X_b=1-X_E-X_{Ar}-X_{so} \qquad (2)$$

and

$$X_M=(1-k)X_b,\ X_{N2}=kX_b \qquad (3)$$

where k is the equilibrium mixing ratio of nitrogen in the binary CH_4-N_2 system. According to Thompson et al (1992), k=0.16 at Titan's surface conditions (94K). A different thermodynamic model of the CH_4-N_2 system (Kouvaris and Flasar, 1991) gives k=0.17 (see, e.g. fig 4 in Thompson et al, 1992 for a comparison of the two models). Further, k is temperature-dependent, decreasing by about 0.01 for every 1K increase in temperature (see previous two references, and also Thompson, 1985). Thus, nominally I take k=0.16±0.01, or as a pessimistic case 0.16±0.02.

X_{Ar} is less certain. First, argon has yet to be detected in the atmosphere, so it may be present in only very small quantities. While constraints on the origin of argon and the rest of the atmosphere require measurement of its abundance in both the atmosphere and ocean (Lunine 1990), it is probably safe to assume that if it is absent as a major constituent in the atmosphere, it is also absent in the ocean. Detection of significant quantities of atmospheric argon can be inferred by a molecular mass constraint imposed by API-V, although direct measurement by GCMS will be more accurate.

For an argon-rich (20%) atmosphere, Dubouloz et al (1989) found X_{Ar} could be 0.056. Since more recent constraints (Strobel et al, 1993) pose an upper limit of 10%, if argon is detected, I assume $X_{Ar}<0.04$. If argon is not detected, I constrain $X_{Ar}<0.005$.

X_{so} is the least certain of the model-dependencies. Yung et al (1984) found a production rate (f_{C3H8}) of propane (a liquid at Titan surface temperatures, and miscible with ethane) equal to 2.4% that of ethane (f_{C2H6}). However, a more recent model by Lara (1993), see also Lara et al. (1993) found f_{C3H8}/f_{C2H6}~0.0008. Although Lara's model gives excellent agreement with the observed stratospheric abundances of many compounds, it fails by an order of magnitude to reproduce the observed propane abundance , and Yung et al . are probably slightly closer to the mark for this particular compound. The problem remains, however, that there is clearly some uncertainty in these models.

Propane is not the only solute that might affect ocean physical properties: Raulin (1987) investigated the solubility of various compounds in putative Titan oceans. The abundance of some compounds in an ocean is limited by their solubility (after saturation is reached, additional inputs of these compounds simply sink to the sea floor); others are limited by their availability (= photochemical production). Potentially the most abundant additional solutes after propane are ethene and butane, with production-limited (i.e. uncertain) limits of ~1 and ~0.1 moles/litre, or (since ocean compositions have densities of about 25 moles/litre) X_{so}~0.04. (Including propane as well as ethene could lead to higher values still, but a maximum X_{so} value of 0.04 is probably representative. While very large quantities of ethyne (C_2H_2) and its polymers are produced, the very low solubility of these compounds probably prevents them from affecting ocean properties significantly, except as suspended sediments).

Given these constraints, I now attempt to evaluate how accurately SSP measurements can determine ocean composition. I assume that physical properties can be derived for ocean mixtures simply by linear combination of the values for the pure components, or

$$z_{mix}=\sum_{i} X_i z_i, \text{ with } i=\{C_2H_6,CH_4,Ar,N_2,Solutes\} \qquad (4)$$

This method is not strictly valid for ratio quantities, such as density or speed of sound, but is used here as a first approximation. Birchley (1992) examined various ways of predicting physical properties for mixtures, and found that linear combination by mass ratio was

reasonable (though this relies on the non-polar nature of these compounds). The pure-component z_i values used in the present study are listed in table 6.5: values are at 95K. Values for propane have been used for solutes, where available, otherwise the methane:ethane trend has been simply extrapolated. Note that the variability in the precision of the values listed in the tables reflects the variability (of absolute value, as well as variability of precision) of the values found in the literature.

Note that I have not undertaken an exhaustive search for these physical properties: the aim here was simply to get some working values in order to assess the contribution of different measurements. It was noted that considerable variations (of order 10%) exist in the published values for some of these properties. If the full potential of the SSP sensors is to be realised, a considerable campaign of laboratory measurements is required.

The 'nominal' ocean for which these properties are computed is 70% ethane, 25% methane and 5% nitrogen, with no argon or solutes.

By allowing a tolerance on each of the properties (i.e. simulating the accuracy of each SSP transducer) a range of ocean compositions is allowed. This range could be large if the component abundances were unconstrained, but the model constraints on k, X_{Ar} and X_{so} mean each measurement gives a manageable composition range.

As an example, the refractive index of this nominal ocean is 1.346. If, however, the accuracy of the REF subsystem is ±0.001, then ocean compositions with a refractive index of 1.345-.347 would be allowed , corresponding to an ethane mixing ratio of 65-71%, for $X_{Ar}<0.005$, and $X_{so}<0.04$.

Note that the uncertainty on ocean composition from a measurement is also dependent on the composition: ethane-rich oceans have relatively low methane+nitrogen content, so the influence of the uncertainty of the nitrogen:methane ratio k is quite small. For methane-rich oceans, the corresponding influence would be higher.

At the time of writing, calibration of these SSP sensors has not taken place, so no 'as-built' performance figures are available. Thus the instrument performances assumed in this study are estimated in table 6.6.

Table 6.5 Physical Properties of Titan Ocean Liquids

	Dielectric Constant	Thermal Conductivity ($Wm^{-1}K^{-1}$)	Density (kgm^{-3})	Refractive Index	Speed of Sound (ms^{-1})
Methane	1.6	0.215 (0.18)	445	1.28	1533
Ethane	1.8	0.3 (0.23)	645	1.38	1977
Solutes	1.9 *	0.4 *	720	1.4 *	2000 *
Argon	1.53	0.114	1400	1.2	1500 *
Nitrogen	1.54	0.096	710	1.346	744
Ocean	1.737	0.269	597	1.346	1805

Data are from CRC Handbook of Chemistry and Physics, Birchley et al. (1992), Ulamec (1987), Badoz et al (1992), Abbiss et al (1965), Thompson & Squyres (1990). Asterisked values are my own estimate. Thermal conductivity of methane was assumed 0.215 in the SSP science requirements document, with that of ethane ~0.3. Birchley (1992) has since measured these at 0.18 and 0.23 $Wm^{-1}K^{-1}$ respectively.

Table 6.6 SSP Sensor Accuracy Estimates

Sensor	Accuracy	Justification
PER	±0.003 ±0.001	1% ethane/methane ratio specification modest enhancement of accuracy
THP	±0.001 $Wm^{-1}K^{-1}$ ±0.005 $Wm^{-1}K^{-1}$	1% ethane/methane ratio specification Degraded accuracy due to real-world effects (turbulence etc.) See scatter in Birchley et al (1992)
API-V	±5 ms^{-1}	Sound speed 2000ms^{-1}: transducer separation (~140mm) known to ±0.5mm
DEN	±2 kgm^{-3} ±10 kgm^{-3}	1% ethane/methane ratio specification Susceptibility to bobbling, strain gauge drift and performance at cryogenic temperatures
REF	±0.001	1% ethane/methane ratio specificatio, and as-built performance of prototype

Clearly, the more accurately a given property can be measured, the closer ocean composition can be constrained. However, there is another factor: the combination of sensor data. In mathematical terms the ocean composition is a four-dimensional space, and each physical property a function of that space. Constraining the value of a given function by measurement allows a permitted region of the ocean composition space to be defined. Ideally, the physical properties would be vastly divergent functions of the ocean composition space, such that the regions permitted by the various measurements intersected in a very small region. If, on the other hand, the properties are similar functions of the space, the corresponding intersection regions are large, and ocean composition is less effectively constrained.

The situation may be more readily envisaged if the composition space is 2-dimensional. A constraint imposed by a physical measurement may be thought of as a curve in this space, with the width of the curve corresponding to the accuracy of the measurement. The intersection of two curves (for 2 different measurements) corresponds to the composition allowed by the combination of the two. For a fixed curve width (accuracy) the intersection area is smallest if the gradients of the two curves are very different (e.g. orthogonal). On the other hand, if the gradients are similar (a shallow intersection, like a very flat X) the intersection region is large, and composition is poorly constrained.

Composition ranges for the nominal ocean model allowed by the various measurements are shown in figure 6.5.

It is seen:
1. that the error bars are dominated by model uncertainty.
2. most of the sensors' error bars are in the same region (i.e. there are few partial overlaps, where combining measurements from more than one sensor would result in a composition determination much improved over that for a single sensor).

It will not be possible to improve on this accuracy, even if models improve, unless :
a:the corresponding physical properties of the pure components can be measured to better than 1%,
b: the method of combining these values to determine the corresponding property for an assumed ocean composition can perform better than 1% (for example, Birchley 1992 cites

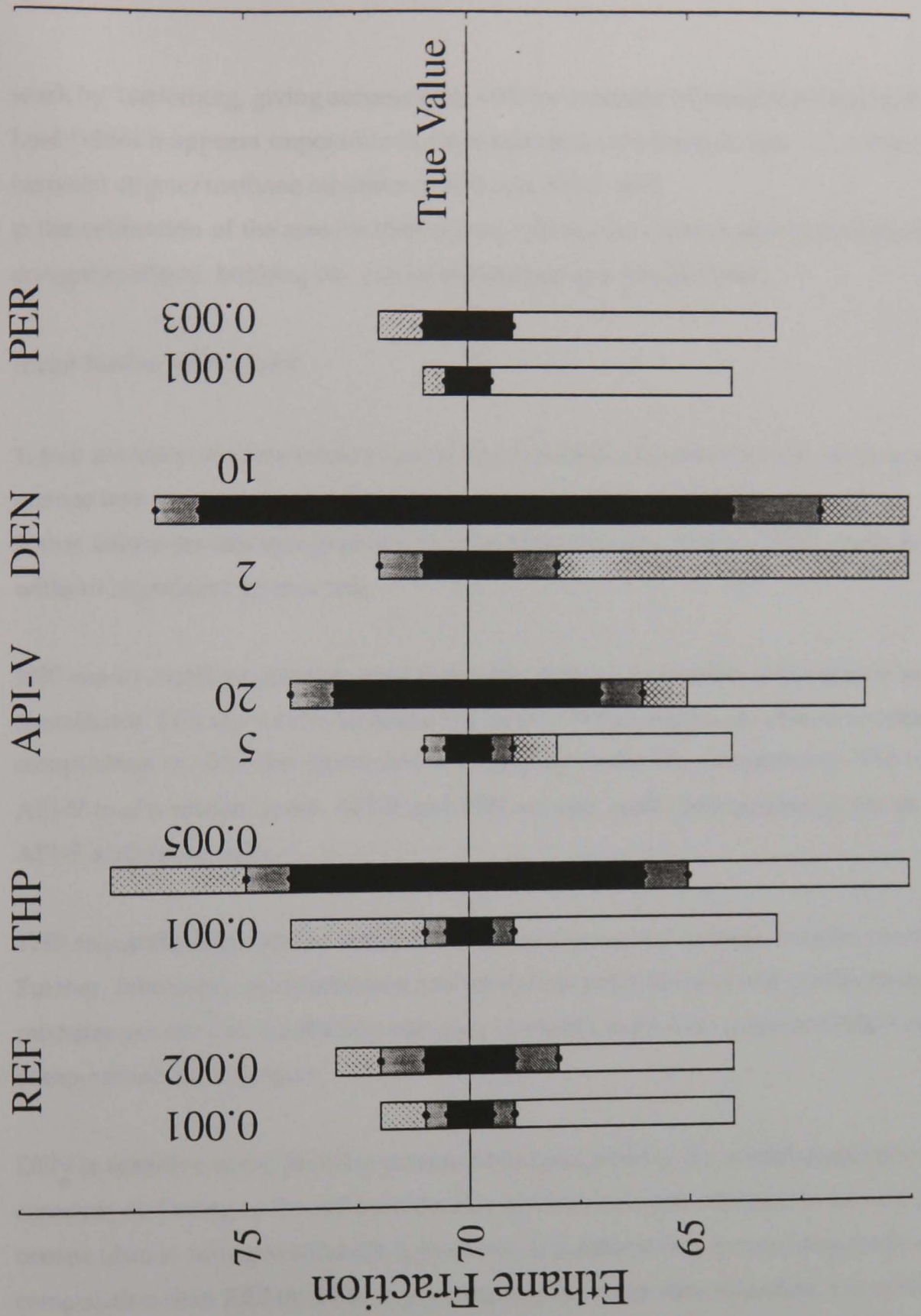

Figure 6.5 Accuracy of ocean composition determination by SSP subsystems. Real value of ethane mole fraction is 70% : black bars indicate range of composition compatible with each measurement, for stated accuracy (units -, $Wm^{-1}K^{-1}$, ms^{-1}, kgm^{-3},- respectively, assuming k=0.16, no solutes and no Argon. Grey bars represent same, if k is uncertain between 0.14 and 0.18; shaded bars for $0.14<k<0.18$ and up to 4% Argon allowed; white bars for same and up to 4% solutes permitted

work by Tsederberg, giving accuracies of ~4% for mixtures of non-polar liquids. Also, in Van Loef (1986) it appears impossible to discriminate on the basis of thermal conductivity between ethane/methane mixtures of 35% and 50%) and
c: the calibration of the sensors themselves, taking into account ageing, radiation dose, cryogenic effects, bobbing etc. can be maintained to a similar level,.

It can further be inferred:

1. that accuracy of some sensors can be degraded from the specification without significant science loss.
2. that failure (or descoping) of one or more of the sensors, notably THP, could be tolerated without significant science loss.

REF shows excellent promise, confirming the early identification of the sensor as a useful contributor. PER shows similar potential: both of these sensors are able to constrain ocean composition to ~5%, this figure driven largely by model (X_{so}) uncertainty. The accuracy of API-V is of a similar order. API-V and PER are also useful independently for interpreting API-S and radar data.

THP requires a high (and as yet undemonstrated) accuracy to make a useful contribution. Further, laboratory measurements and analytical predictions of the conductivity of mixtures are not yet of sufficient accuracy to enable more than a coarse (~10%) estimate of ocean ethane mixing ratio.

DEN is sensitive to the possible presence of argon, making it a useful diagnostic of this component. Owing to the reduced density contrast between ethane-rich and methane-rich oceans (due to nitrogen solubility), however, it is otherwise a poorer diagnostic of composition than REF or PER. If performance is poorer than specified, the utility of the measurement may be questioned, although its resource requirements are very modest.

6.5 What should be measured ?

The foregoing discussion of the interpretation of SSP data brings to mind the philosophical question, what should be measured? How much resources should be devoted to each

measurement. The direct answer to these questions is of course subjective: an atmospheric scientist may give an altogether different answer from that of a geologist.

Consensus is the only current method of tackling this problem. However, even when obvious questions are agreed upon, such as 'what is the argon abundance in the atmosphere', the value of the measurements to address these questions can often only be determined *a posteriori* .

For example, hundreds of images of Titan were transmitted by Voyager, but yielded very little information, since the disk was virtually featureless. In this sense, the incremental value of images after the first was very small. In contrast, a single Voyager image identified a ring around Jupiter : a profound discovery. An informal theorem exists in information theory that may be expressed as 'the value of a piece of information is directly proportional to its improbability'.

An even more striking example is the detection of a radar echo from Titan. This discovery may, in a sense, be reduced to one bit of information: an echo or not. Sagan and Dermott (1982) suggested that detection of an echo would deny the existence of a global, deep ocean, and Muhlemann et al.'s 1990 detection started the 'sea-change' in the model of Titan's surface from global liquid to heterogenous solid, and represents a very valuable bit.

Similarly, theories of the origin of Titan's atmosphere may be discriminated by a coarse measurement of the argon abundance (Owen, 1987, see also chapter 9). A very simple measurement such as speed of sound could detect large argon abundances, although probably not unambiguously. Unambiguous measurement requires a more sophisticated instrument, such as a mass spectrometer.

The situation is complicated yet further by the combination of measurements (cf. the previous discussion on SSP ocean determination). If one instrument tells the same thing as another (e.g. the SSP estimate of the range of ocean composition spans the estimate made by GCMS), then the incremental value of that measurement is low; i.e. the data is redundant. More formally, the value of a scientific measurement may be estimated (Szabo, 1994) by the incremental Kolmogorov complexity of the data it yields. Kolmogorov complexity (Li and Vitanyi, 1993) is essentially the smallest possible representation for a piece of information (the 'minimum description length' - strictly, the smallest possible

Turing machine that could reproduce the data). Science may be expressed as taking the widest range of data and explaining it with the most concise models : redundant data is data that can be explained by existing models, so its incremental Kolmogorov complexity is small (i.e. the new redundant data does not require new models to explain it). Thus, it has been proposed (Szabo, 1994) that a value measure using Kolmogorov complexity may be a useful and objective criterion with which to estimate how much resources should be devoted to given projects or measurements.

The above discussion assumes that an assessment of the value of various instruments can be objectively assessed, further that the resources required to make that measurement can be assessed in advance. In the real world, additional constraints (such as political pressure) apply: see next section. Further, a redundant measurement offers some resilience against instrument failure.

Thus, until some kind of objective assessment of the value of a measurement can be made, *and that assessment acted upon without constraint,* the selection of which bodies to visit, with what instruments, and how mass and data allocations should be shared between these instruments, will continue to depend on an imperfect process of lobbying and compromise. Since exploration, and science in general, are fundamentally human activities, however, it is perhaps not inappropriate therefore that these decisions rely on the preferences, prejudices and enthusiasms of individuals.

6.6 Winners and Losers

A rarely-discussed aspect of spacecraft payloads is their selection process. This usually takes the form of competitive bids, with intended PIs delivering detailed technical and scientific proposals, together with management/financial plans. After evaluation by an independent panel, some are selected, while the others are not.

The definition of 'independent' in this context is interesting, since those people most acquainted with the scientific aspects are themselves the most likely to be associated with proposals. Thus those performing the selection are often not directly involved in the scientific topic .

On purely statistical grounds, those scientists involved in the study/definition phases of a project, appear to stand a better chance of selection than 'outsiders' (e.g. on Huygens 5 of the 6 selected PIs, and all 3 IDS's are mentioned in the Phase A report). This is natural: these study scientists are likely to be better-prepared for the AO. (Compare, for example, with Giotto - of 8 scientists mentioned in the Phase A report (ESA SCI(80)4), 6 became co-Is on flight instruments, and 2 were PIs).

From a programmatic point of view, proposals based on mature or proven designs are favoured, since schedule risks are minimised. The proposing PI may also favour repeating proven designs, since development costs are reduced and experience gained in previous missions may be usefully applied (although given the long intervals between planetary missions, staff turnover may erode this advantage). These two effects have the disadvantage, however, of discouraging technical innovation: a balance must be sought between novelty (high performance) and maturity (high confidence) : see chapter 4.

Additionally, since resources are limited, proposals with modest mass, power, volume etc. requirements stand a better chance of selection. Note that while most payloads grow in mass (sometimes dramatically) from their mass as stated in the proposal (see tables 6.1b, 6.2) , the proposal should still be credible. Project engineers, being (as they should be) risk-averse, will also prefer to avoid interface headaches such as large mechanisms or pyrotechnics.

A sound technical proposal to build an instrument is, of course, worthless without the capability (=manpower, facilities and money) to build it. A credible cost, and reliable support to meet that cost, are the obvious, but rare, solution. In scientific terms, for example, the ASTRA proposal mentioned in section 6.1.6 (this example is chosen, as the technical details have been published openly, and are not locked in a confidential proposal) is a very interesting instrument, and technically appears credible (indeed resembling somewhat the current probe radar altimeter). However, the instrument was not selected. One must therefore assume that the proposal was simply ranked too low to be selected on at least partly non-technical grounds.

There is yet another consideration, that of geographical distribution. While there is no formal policy on the matter in ESA (as with the 'juste retour' system for industrial contracts), an all-British payload on an ESA mission would be just as inappropriate as an

all-Danish one, or all-American one. A suitable distribution is required, not only to ensure a wide participation, but also to prevent the financial burden of payload development falling on only one nation (c.f. XRF, the US portion of SSP mentioned earlier). Thus the selection process (like most business or even personal relationships) is one of compromise, which attempts to address the stated scientific objectives of the mission, while remaining within mass, energy etc. constraints, and still maintain some kind of geographical balance. Doubtless, however, some political pressures are applied. The situation may be further complicated by international collaboration on an individual instrument.

These latter two aspects are perhaps the most delicate areas of payload development. It is clear that to be a successful PI requires not only scientific/technical ability, but also resourcefulness and, at times, guile. Such secrets as the author has learned in these areas, however, he will not write here.

But what of those scientists not selected? In the DISR section, another (unsuccessful) proposal was mentioned, that of Mike Malin. In addition to his unsuccessful Huygens camera proposal, Dr Malin (personal communication) had also proposed a camera for the Galileo probe , but data rate limitations (when Galileo was being designed, modern data compression devices were not available) meant that it was not selected. Dr Malin was PI of a flight instrument, the camera on the ill-fated Mars Observer spacecraft, which was lost just prior to Mars Orbit Insertion. Dr Malin may be commended for his perseverance.

This is a reminder that for every PI on the Cassini mission, there are several unsuccessful bidders who worked hard to produce proposals. By setting a standard for the evaluation of other proposals, they too contribute to the quality of the mission.

Some papers have been published on unselected (or even unproposed) Huygens payloads: Oberbeck et al. (1987) suggested a combined impactor + electrostatic precipitator for aerosol collection in Titan's atmosphere. Webster (1988) described gas composition measurement from terrestrial stratospheric balloons using tunable diode laser spectroscopy and describes details of a possible application for a Titan probe (PIRLS - Probe InfraRed Laser Spectrometer) which would have made abundance measurements of selected atmospheric constituents with high (~km) altitude resolution, as well as performing nephelometry. Nelson et al. (1989) suggested a simple 2-channel radiometer measuring the radiance of the entry shock layer would allow composition measurement in the difficult-to-access 200-

400km altitude range. Technical difficulties with these payloads may have included uncertainties in electrostatic collector performance in Titan's atmosphere, unavailability of space-qualified laser diodes, and integration concerns with an entry radiometer. Additionally, all these payloads were developed in the US: with GCMS and DISR (or equivalent instruments) already selected, the US financial envelope didn't permit further US probe experiments.

One 'survival strategy' that is worth mentioning is that of the 'cross Co-I'. The planetary science community is small enough that one is likely to know one's competitors. An informal agreement may be made whereby the successful PI will make his 'opponent' a Co-I on his experiment; this at least guarantees some participation in the mission, and in principle strengthens the scientific/technical expertise available to the successful experiment.

Another (obvious) strategy is to be involved directly in several proposals: this naturally increases the probability that at least one will be selected. On the other hand, this exposes the scientist to the risk of extreme workload : for example Dr Athena Coustenis is a co-I on DISR, HASI and CIRS: all three of the proposals with which she was allied were selected.

Lessons that may be learned from the above section for successful participation in a space mission are as follows:

- be involved as early as possible (definition study team).
- be involved in more than one proposal.
- ensure credibility of all aspects of the proposal (financial/management, as well as technical).
- don't give up.
- avoid competition : select a country and/or investigation where there are few competing proposals. Alternatively, neutralise competition by merging with it.

Chapter 7

Impact Measurements

'Why, then the world's mine oyster, which I with sword will open'
William Shakespeare
The Merry Wives of Windsor

'For my part, I travel not to go anywhere, but to go. I travel for travel's sake: the great affair is to move, to feel the needs and hitches of this life more nearly, to come down from this feather-bed of civilisation and find the globe granite underfoot and strewn with cutting flints'
Robert Louis Stevenson
Travelling Upon a Donkey in the Cevennes

7.1 Introduction

The assessment and Phase A studies both identified impact accelerometry as a useful surface measurement, in part because of the assumed presence of accelerometers for entry dynamics measurements. Both the HASI and SSP experiments carry accelerometers, although little in the way of preparatory theoretical or experimental work was done on assessing what science could be determined from the measurements, with 'probe response to impact' being the stated measurement objective. In part, this is due to lack of manpower (actual development of the instrumentation being perceived as more important than considering its interpretation) and in part due to the paucity of information on the structural properties of the final probe design.

The present author played a large role in predicting the expected impact profiles for both solid and liquid impacts, and specifying the required measurement ranges and sampling frequencies for both the SSP and HASI accelerometers. As mentioned in the previous chapter, it was decided to optimise the SSP accelerometers for an impact on a solid, with those on HASI optimised for impact (and post-impact) dynamics for liquid surfaces.

7.2 Review

As described in Lorenz (1994b) the landing loads for spacecraft on liquid surfaces is fairly well-documented as a result of work on the Mercury, Gemini and Apollo programmes. A fairly simple 'added mass' method can be used to compute decelerations; this method is also used for evaluating ditching loads on aircraft (Leigh, 1988).

Literature on spacecraft impact loads on solid surfaces is rather more scattered: a list of relevant references may be found in Lorenz (1994b). The subject is further complicated by the large amount of work on penetrators (i.e. long, slender vehicles) designed to penetrate a significant distance into the surface material. The dynamics of such vehicles are complicated, since they are acted upon by frictional forces along their length as well as by forces at their tip. Although empirical relations (Young, 1967) exist for predicting their depth of penetration and deceleration loads, the deceleration profiles are complicated, even for uniform surface materials.

The influence of a 'penetrator' mindset is evident in the evolution of the SSP accelerometers. This is perhaps unsurprising, since before the ESA M1 mission selection of Huygens, effort at UKC had been focussed on an asteroid mission, Vesta. When Vesta (which featured a number of asteroid penetrators) was not selected, efforts to utilise or 'recycle' development work on Vesta instruments (accelerometers and thermal properties) led to these instruments playing a large role in SSP.

7.3 ACC-E

Originally the concept for an impact accelerometer on SSP was to place a piezoelectric accelerometer on a short stub (on which was also mounted the XRF subsystem). As the SSP and probe design evolved in Phase B1, with a glass-fibre top-hat and thin fore-dome, a 'pylon' was envisaged - a slender but stiff structure to put the accelerometer as far forward as possible, yet have it as strongly-coupled as possible to the experiment platform.

In Phase B2, in summer 1991, the author (then part of the ESA project team) was asked to examine whether this location and mounting was suitable. I found (R Lorenz, unpublished memo 24/9/91) that the location was acceptable, but that the transducer was inappropriate. Ultimately it is force that is the desired measurement, since it is this quantity (an 'effort' variable in transducer theory) which is generated by the surface material. Usually, in a rigid body such as a penetrator, this force produces an acceleration (a 'flow' variable in transducer theory), with the two quantities related by Newton's Second Law.

However, the acceleration of the pylon does not depend only on the soil force acting on it, but also due to the force at its mounting on the experiment platform. While in shape the pylon may resemble a penetrator, in dynamic terms it does not. If the pylon were perfectly rigid, the accelerometer could equally well (and more safely) be put at its base, near the

experiment platform, although both there and in its original location it would be susceptible to structural oscillations.

Thus, to eliminate these uncertainties in dynamics, it was proposed (Lorenz 24/9/91) to use a force transducer on the tip of the pylon, thereby measuring the force directly. A force measurement at the tip helpfully eliminates the effect of frictional forces along the pylon's length.

In order to minimise the changes to the SSP electronics design, a piezoelectric force sensor was suggested (strain gauges may have worked, although it was not certain that their bandwidth would have been adequate). Commercial force washers were expensive and presented some materials compatibility problems: it should be remembered that low outgassing, coupled with operation at cryogenic temperatures, was required. Thus it was decided to develop the transducer at UKC.

The initial development configuration used a piezoelectric disc (made of Lead Zirconate Titanate - PZT) sandwiched between two brass screw fittings, with the assembly held together with an epoxy adhesive. The brass screw fittings allowed experimental penetrator tips (conical and hemispherical) to be attached, and different pylons (kevlar- or carbon-reinforced plastic tubes, of 8 and 14mm diameters) to be used.

Signals from the transducer were amplified and passed to a home-made A/D converter, sampled by a BBC microcomputer (the BBC's internal ADC was too slow). Data was extremely noisy, but it was determined that the hemispherical tip gave a better (stronger) signal, with less structural ringing.

It was also noted, during the many breakages of the transducer, that a design held together with adhesive was not adequately robust. Thus the second generation of designs had a PZT washer as the sensing element, with the tip held onto the base by a bolt. These tips were 28mm in diameter, and were made of steel. An innovation suggested by Z Krsynski was the incorporation of a small electrode on the PZT washer to allow stimulation of the sensor for in-flight health verification. Two heads were made, one with the PZT washer exposed, the other with a lip which restricted sideways movement (at the suggestion of Al Seiff). These two sensors gave much better results. Additionally, a great improvement in reproducability was gained by using a more reliable and less noisy PC-based data acquisition system, the SMU (Stimulus and Monitoring Unit).

Interestingly, by examining the Fourier transform of the sensor's response to hammer blows, it was possible to discriminate between a hammer tap on the apex and on the side of the sensor. These taps presumably excited different oscillation modes of the support pylon.

Assembly of the sensor with the lip was very difficult, and the device gave no performance improvement, so the unlipped design was adopted. The next and final step in the ACC-E's evolution (summarised in figure .1) was the scaling down and the substitution of materials to reduce mass. Scaling to 14mm diameter reduced the transducer's mass by a large factor (although by forcing the relative sizes of the stimulus and sense electrodes, it rather complicated the calibration of the sensor : see later). Also aluminium was used as the material for the support collar and pylon, and titanium for the penetrator head (which could suffer rough treatment during test and calibration). An additional design aspect was that the pylon was now mounted on the top hat, rather than directly on the experiment platform.

The detailed design of the ACC-E subsystem, and its calibration, is described in Lorenz et al. (1994). The following comments describe small changes since that paper was submitted.

First, as details of the electronics emerged from RAL, it was realised that the stimulator circuit which would allow in-flight health checks of the system itself needed protection from the possible high voltages developed during test or accident. Thus a large capacitance was put between the stimulus and ground lines: the effect of this is effectively to remove the charge generated across these electrodes by the transducer. Since this charge is coupled capacitively to the sense electrodes, the force-voltage characteristic of the transducer is affected.

Second, an improvement has been made in the absolute calibration. Under my direction, Mick Willett wrote a program (Willett, 1994) to simulate the force-time profile of an impact of a lump of material onto the ACC-E transducer. This allows the prediction of the peak force produced by the ACC-E calibration jig, if the material properties (Young's Modulus E) are known. However, the quoted values for this quantity vary (e.g. 7-70 MPa in the Southampton Engineering Data Book). Since the peak force is proportional (McCarty and Carden, 1962) to $E^{0.4}$, this leads to a 60% uncertainty in the value of the force produced by the jig.

However, since the program generates a force profile, as does the instrument, these profiles may be compared. The force profile (for the rubber impactor, dropped from position 4 on the

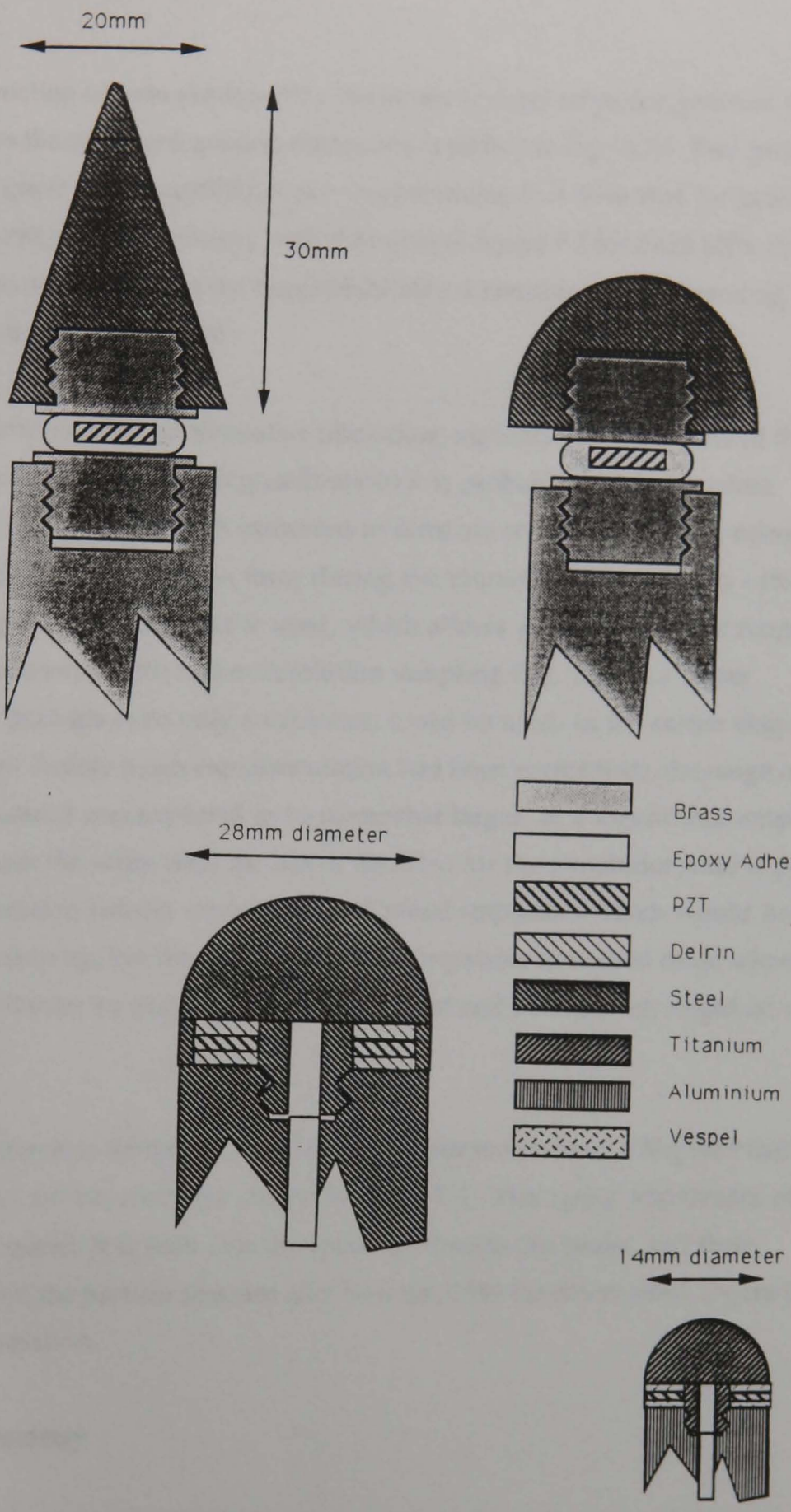

Figure 7.1 ACC-E Impact penetrometer evolution (top to bottom) First adhesive-bonded mockups, then large bolt/washer type, eventually scaled down to flight size

The intermediate stage and flight versions are seen in the TV programme (Balburnie, 1994)

calibration jig i.e. impact speed 1.3 ms^{-1}) varies as a function of the assumed value of E (see figure 7.2)

The voltage as a function of time produced by the sensor (rubber impactor, position 4, with a 8nF capacitor across the sense and ground electrodes) is shown in figure 7.3. Two profiles are shown, indicating good reproducibility of the measurement. It is seen that the profile falls to zero is ~3.5 ms, corresponding closely with the curve in figure 7.2 for E=20 MPa. Further numerical experiments suggest that the range 18-20 MPa is consistent, corresponding to values of the peak force of 142-148 N.

Considering the various other uncertainties (including, significantly, the value of the capacitor used across the sensor during calibration) it is probable that the absolute calibration is good to ~5%. (Note that variations in force are measured to 8 bits using a logarithmic amplifier, so variations in force during the impact are measured to ~1%) Note that although a logarithmic amplifier is used, which allows a useful dynamic range with only an 8 bit measurement, with higher resolution sampling (e.g. 12 bit), a linear amplifier/filter, or perhaps even only a capacitor, could be used. In the earlier stages of the ACC-E development (before much experimentation had been performed), the range of forces that should be measured was expected to be somewhat larger, so a logarithmic amplifier was selected. In much the same way, the use of titanium for the penetrator head is probably 'vestigial': the calibration stimuli envisaged used metal impactors which would have damaged an aluminium tip, but the teflon and rubber impactors now used could allow the substitution of aluminium for titanium, although the cost and mass saving would be very modest.

Some sample measurements for drops (5 ms^{-1}) of the sensor mounted on a 5kg steel mass by a small pylon into various materials are shown in figure 7.4 . The 'spiky' appearance of drops onto gravel may be noted. It is seen that the spacing between the peaks, and their magnitude depend on the particle size (see also Newton, 1994 for discussion). Figure 7.5 illustrates this correlation.

7.4 Internal Accelerometry

Impact accelerometry in general, and the impact dynamics of the Huygens probe have been investigated in some detail by myself (Lorenz 1994b). Here I describe only the accelerometry instrumentation itself, and the work performed on interpretation methods.

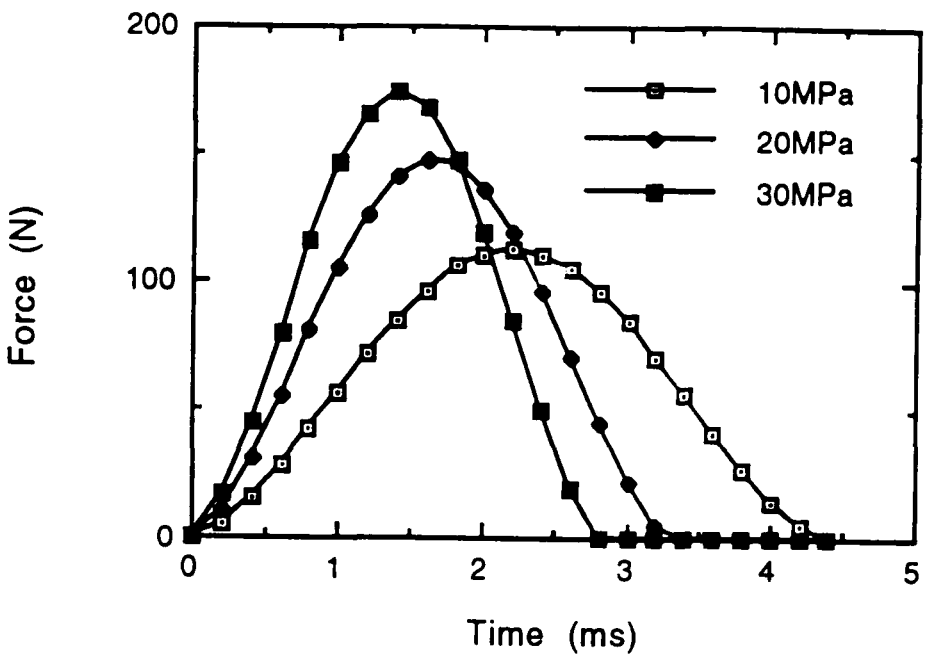

Figure 7.2 Theoretical force profiles produced by calibration jig with rubber impactor dropped from position 4, as a function of assumed rubber Young's modulus E

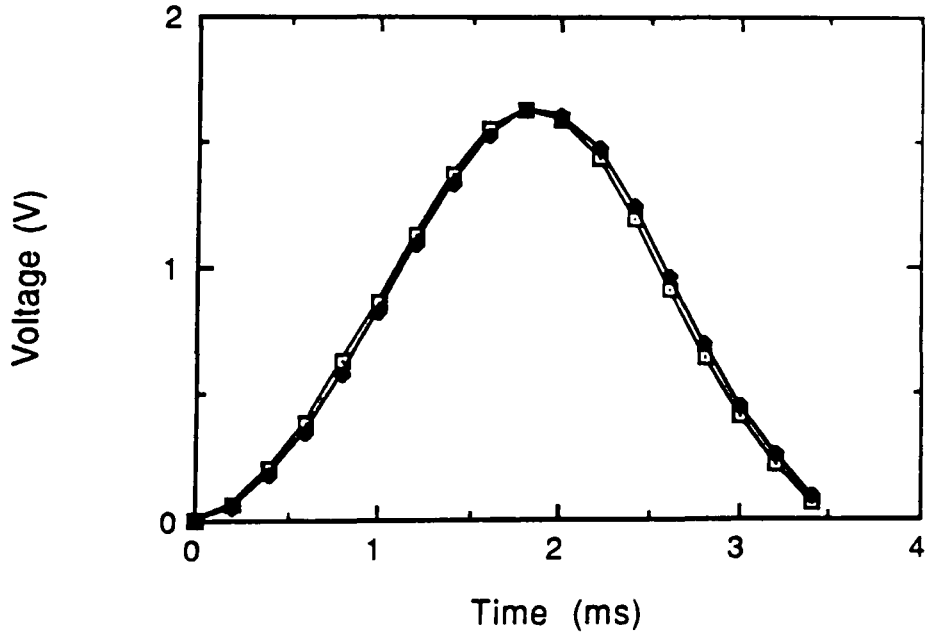

Figure 7.3 Transducer response to calibration force pulse (rubber impactor, position 4). Reproducibility is very good - the two examples here are virtually identical.

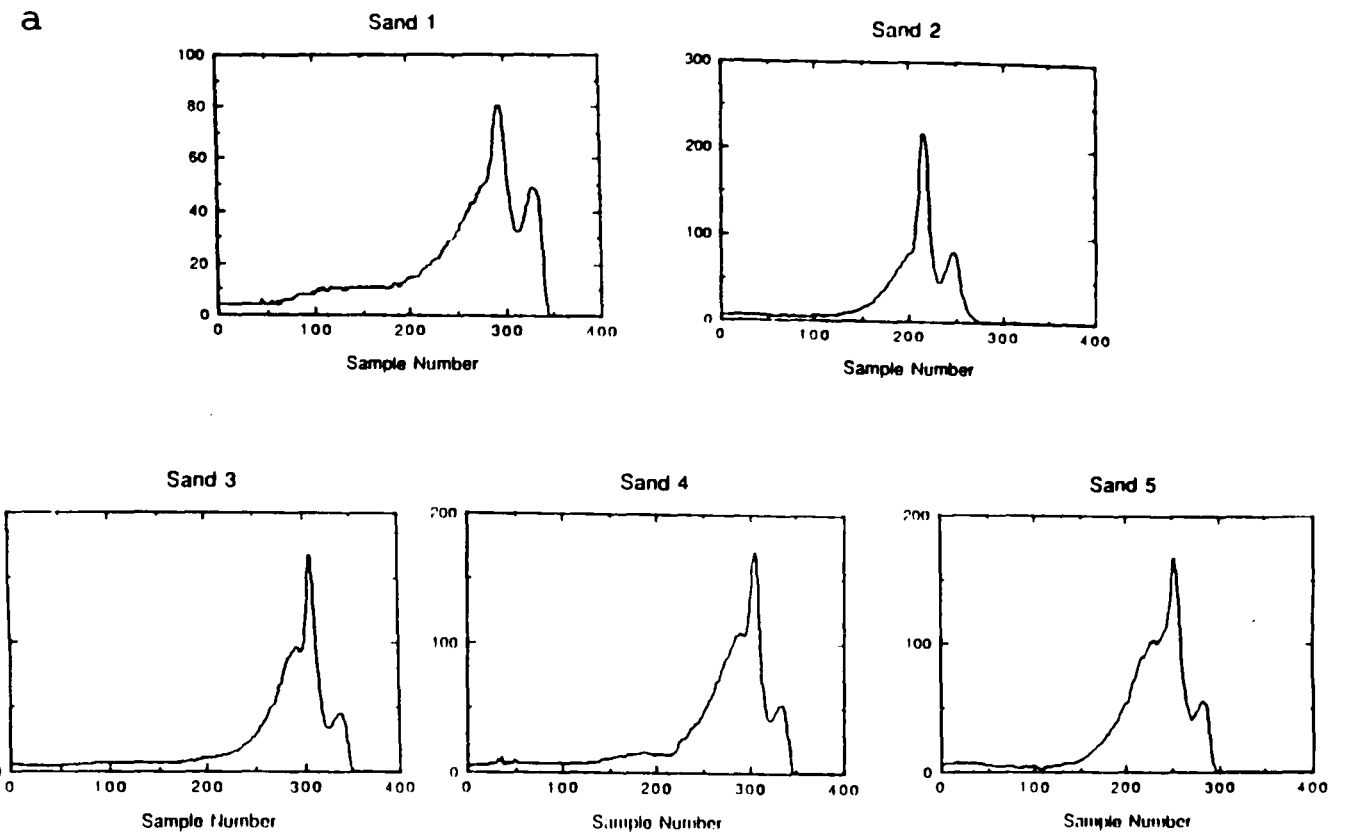

Figure 7.4 Penetrometer force profiles (arbitrary units) after pseudolog amplification. Abscissa is time, sampling at 10kHz, so sample 200=20ms. Profiles (a) for sand show a power-law rise, with a final wiggle due to impact of the drop weights. Profiles (b) show impacts into grey stone clay, and show a broadly constant resistance

c

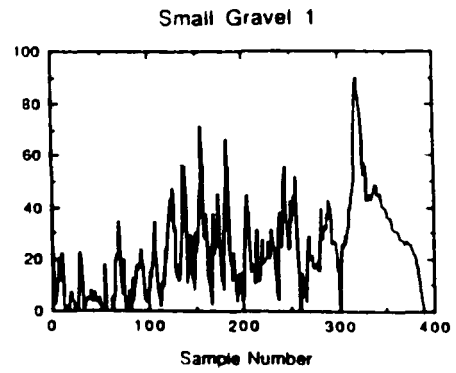

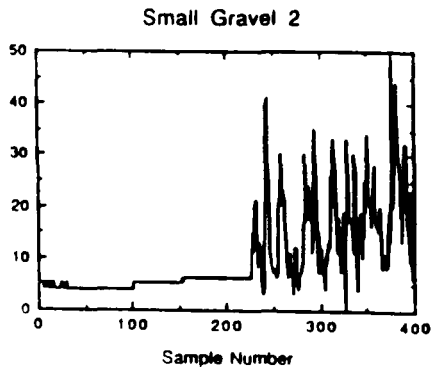

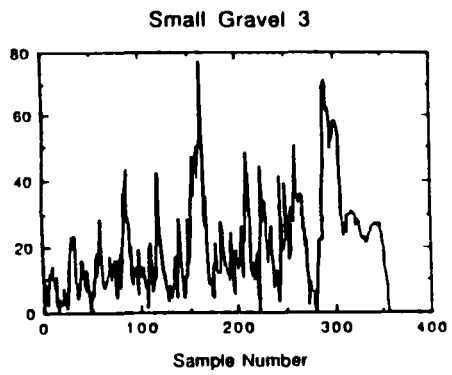

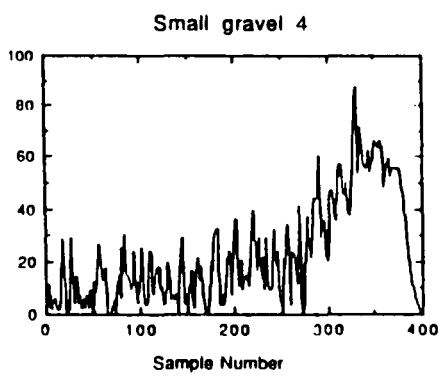

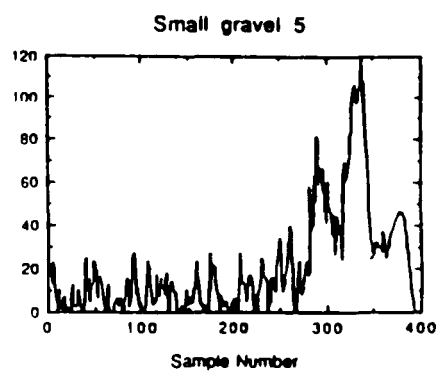

d

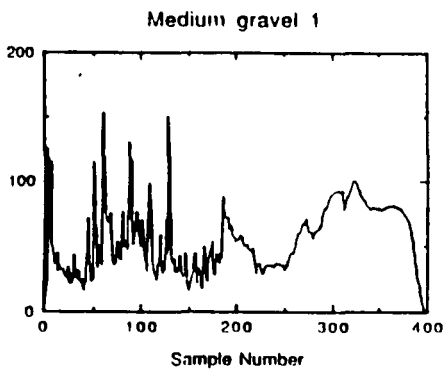

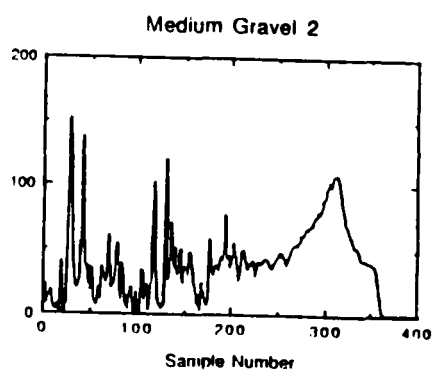

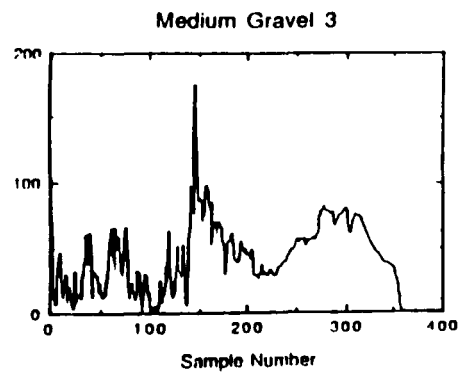

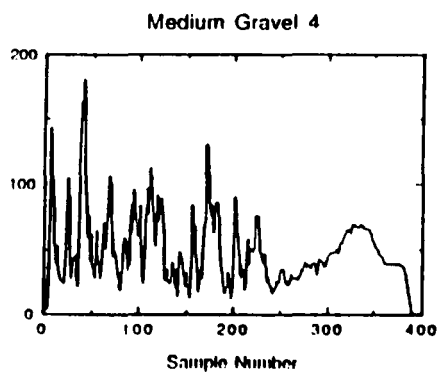

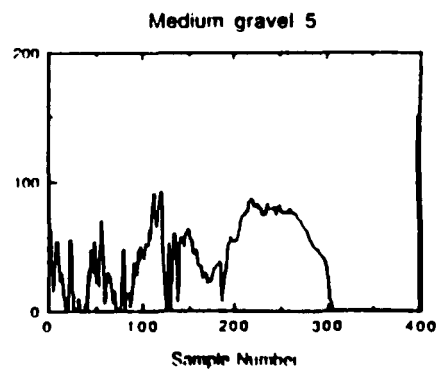

Figure 7.4 (continued) Axes as before. Drops (c) into fine gravel, with mean particle diameter of 8mm. Drops (d) are into coarser gravel, with mean diameter ~15mm - note the greater amplitude of the peaks, as well as their fewer number compared to (c). Broad bump at end of profile is 'bottoming out' of drop weights.

The HASI accelerometers are the following:
1 Sunstrand QA-2000-030 electromagnetic servo accelerometer, mounted at the cg of the probe along the X axis (i.e. the spin axis of the probe, nominally vertical at impact), and 3 Endevco 7264A-2000T piezoresistive accelerometers, also mounted at the probe cg, measuring in three orthogonal axes.

The servo accelerometer is sensitive (few μg resolution) for entry measurements, but has a range of only 25 g, and its bandwidth is limited (by the servo loop) to 100 Hz. Thus the servo accelerometer is not used for impact measurements, as it would respond too slowly to impact accelerations.

The piezoresistive accelerometers are sampled during descent at 50 samples/second, with data averaged over 1 second intervals and telemetered. Near the surface, the measurement rate is increased to 400 samples/second along the X-axis, and 50 samples/second in the Y and Z axes to characterise accurately the splashdown and subsequent bobbing in the event of a liquid landing . These transducers are able to measure to ~2000 g, but due to the configuration of the sampling electronics (designed to maximise entry sensitivity to give 50 mg resolution), their upper limit is 20 g. Thus, the HASI sensor suite will characterise liquid impacts well (~10 g), but do not have sufficient range to cover impacts on regolith or harder materials.

However, SSP carries an Endevco 2271A piezoelectric accelerometer, mounted on the SSPE box, about 25 m from the probe centre. This accelerometer is sampled at 500 samples/second, giving a good profile of both liquid and solid impacts, and allowing (hopefully) the identification and removal of features in the accelerometer profile due to structural oscillations of the probe.

Since this accelerometer is near the edge of the probe, angular accelerations at impact may give an additional component to this signal. Hopefully, however, combination of HASI and SSP ACC data, with that of SSP TIL, should allow the extraction of this component.

Interpretation of accelerometry relies on the ability to discriminate the effects of the mechanical properties of the probe on the accelerometer signal from the effects of the mechanical properties of the surface material. Thus knowledge is required of the effect of the coupling of soil mechanical properties to the probe (largely a problem of geometry - see section 7.2, and Lorenz 1994b) and the probe's response, which depends on the strength and stiffness of its structure.

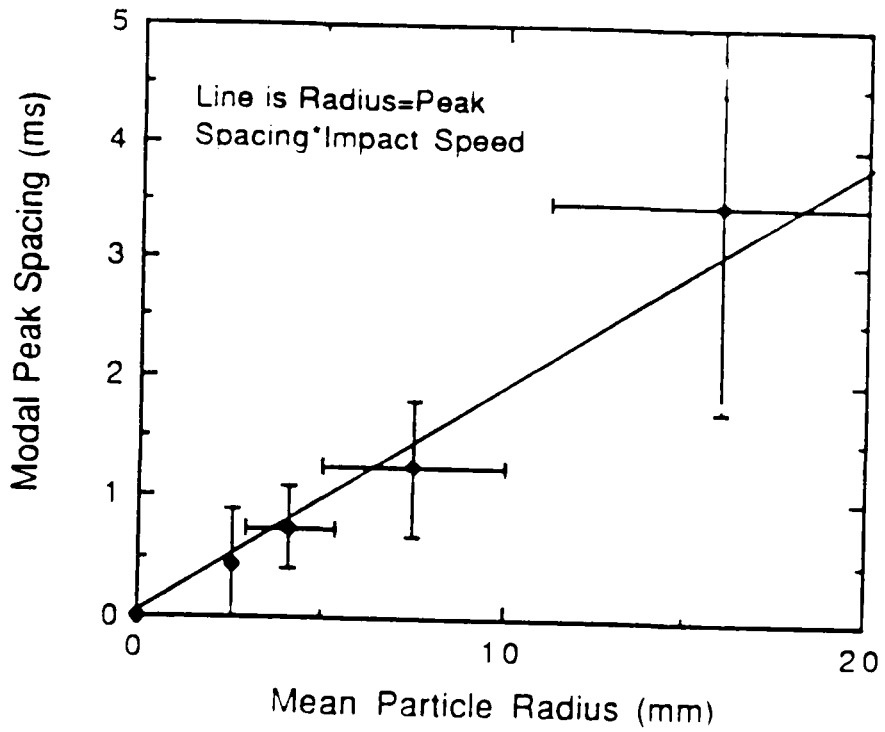

Figure 7.5 Correlation of Peak spacing and Particle size : Although statistics are poor, the peak spacing multiplied by the impact speed correlates well with the particle size

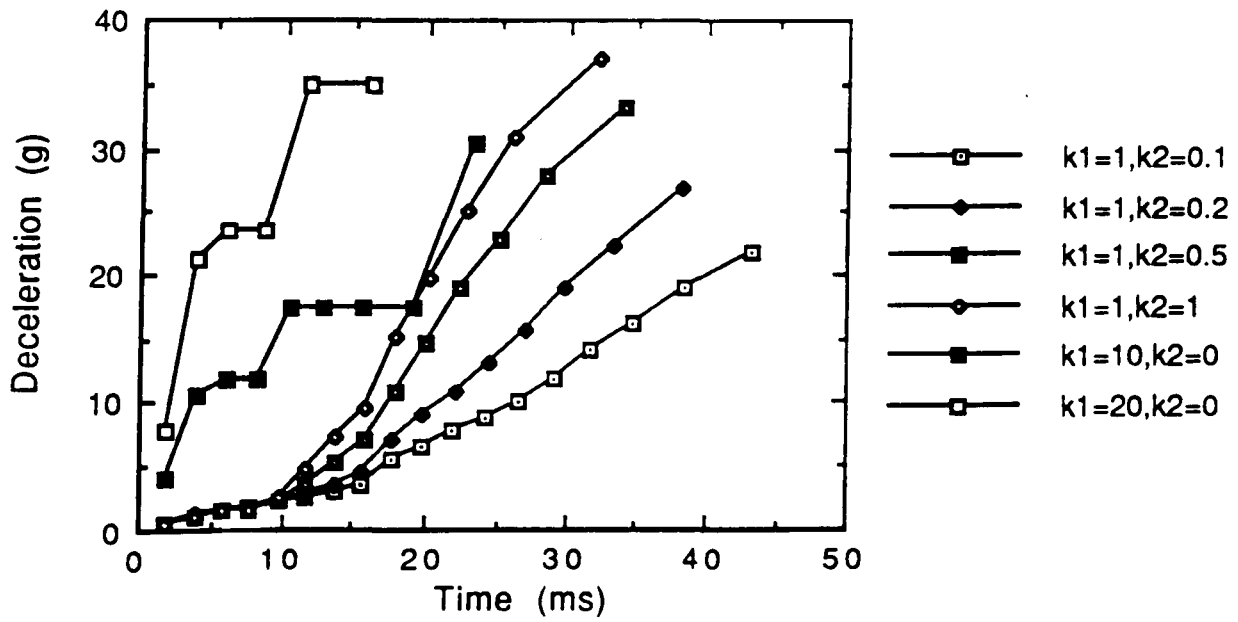

Figure 7.6 Probe Deceleration profiles for various solid materials : k1 is the bearing strength of the soil, k2 the subgrade modulus, or increase of bearing strength with depth. k1=20 corresponds to a sludge surface, k1=1,k2=0.2 corresponds to sand or regolith

The concept for interpretation of the probe response envisaged in the SSP proposal was to use a physical model of the probe, named DYN ('dynamic'), in drop tests. This would have required flight-representative models of the main probe structural elements, such as the experiment platform and fore-dome. These would have been expensive to procure, and many of the drop tests would have been destructive (although it should be noted that the proposal was based on the Phase A design of the probe, which was somewhat more rigid than the eventual configuration - see chapter 5).

As the probe design evolved, it emerged that the fore-dome would not sustain a large load: thus the main load path for loads due to the soil on the bottom of the probe at impact would be through the equipment boxes on the underside of the experiment platform, rather than through the fore-dome and its attachment points. Obtaining or building boxes with flight-representative structural characteristics (which would require the cooperation of experiment teams and the various probe subsystem contractors - not just the inner structure subsystem contractor CASA, who supply the fore dome and experiment platform) would be impracticably expensive.

Thus a numeric model was set up, modelling the probe boxes as a set of (non-linear) springs, making engineering guesses as to the structural properties of the various boxes. The model is described in detail in Lorenz (1994b). Setting up the model with realistic parameters relied on the availability of engineering drawings of the GCMS, ACP and SSP structures, and that of the large PCDU box; the author's close association with the project team was useful in obtaining these drawings. In the (unlikely) event of test data, or spare models of these boxes, becoming available, it will be useful to update the model parameters.

The model also includes the load path due to the fore dome. A linear law was assumed, first for simplicity, and second, model test data on the Apollo heat shield structure (Stubbs, 1967) indicated a broadly linear force-deformation characteristic. It was further found, during numerical experiments with the model (Appendix in Lorenz 1994b) that the acceleration profiles are relatively insensitive to realistic variations in the force-deformation characteristic of the fore-dome.

Acceleration profiles are indicated in figure 7.6.

7.5 Analysis and Interpretation

The Huygens instruments will provide acceleration or force profiles as a function of time during the impact event.

The Surveyor landing loads were investigated to deduce soil parameters by generating simulated force profiles for different soil parameters and comparing visually with those actually measured (Sperling and Galba 1967). Such a method is probably the most appropriate for Huygens, since there is only one set of data to examine, and depending on the other mission results, an appropriate effort invested in analysing the data. In principle a small catalogue, either on hard copy or in software form, could be built up and compared with the flight dataset as soon as it is received (assuming, of course, that Huygens survives the impact).

Given that the probe might not survive, and that liquid impact is possible, and that there will be only one set of data to investigate, development of a software catalogue of impact profiles with some kind of least-squares fitting is probably not justified.

Note that in missions where large sets of data are to be analysed, an automated approach is worthwhile. For example, the accelerometers on the 'snake' guiderope of the Russian Mars 94 balloon used to measure its speed (Powell et al. 1993) of traverse across the ground give a signal that is indicative of the surface that the snake is traversing, and a neural network method has been found to be an effective way of classifying surfaces ('rocky', 'sand', etc.).

Generating some characteristic parameters for the various impact signatures is a useful way of classifying impact types, and of deriving quantitative (albeit uncertain) properties of the surface material.

Two obvious parameters, which are transmitted in the 'quick-look' dataset, are the magnitude of the peak acceleration signal, and the rise time (the time for the signal to go from 10% to 90% of its peak value) or the time of the peak relative to the start of impact. The materials which correspond to various combinations of these parameters are indicated in figure 7.7.

For the ACC-E signal, for broadly smooth signals, the profile indicates the cohesion of the material. For low-cohesion materials (suchas sand) the force builds up with time: mechanical strength increases with depth. Cohesive materials (clay is the extreme

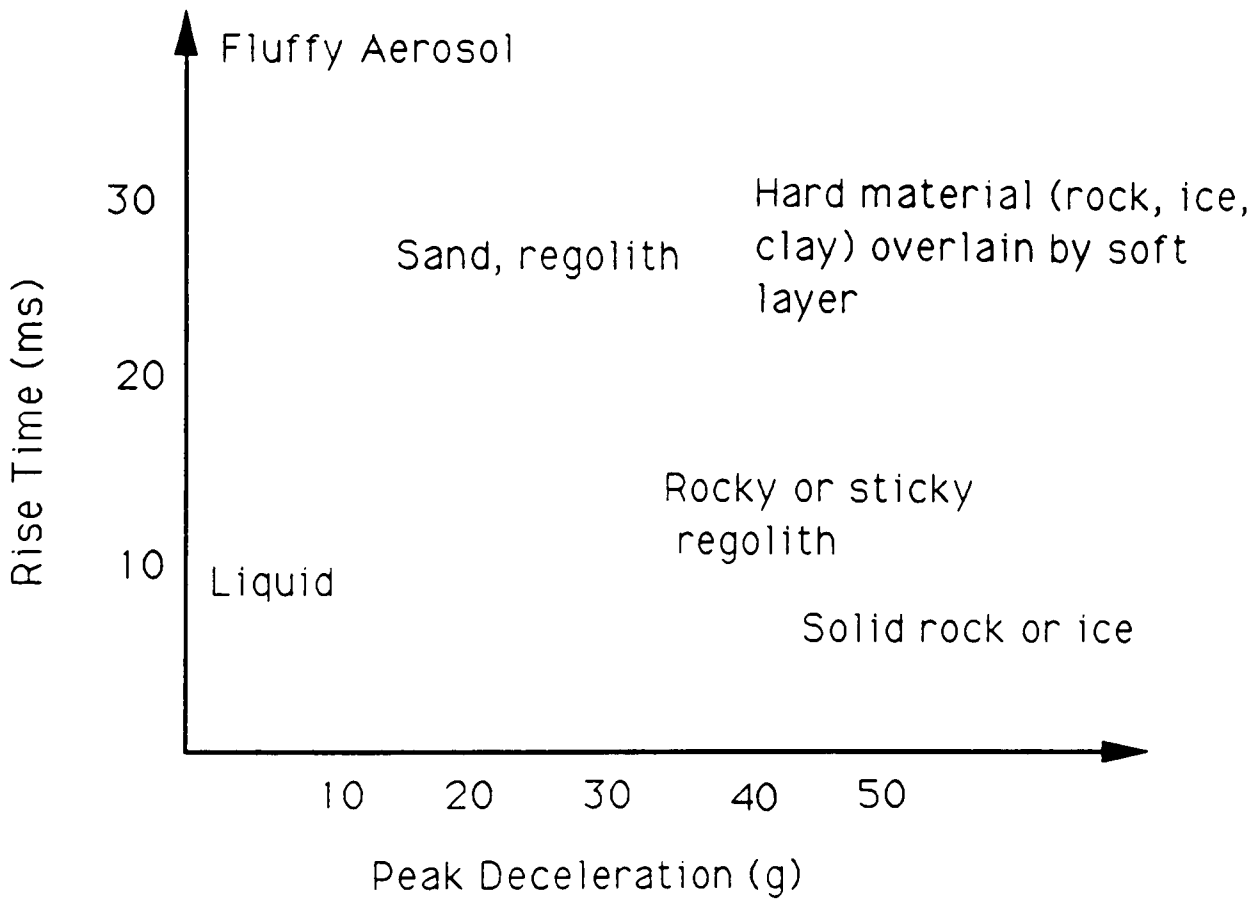

Figure 7.7 Surface material identification map : rise time and peak deceleration allow simple identification of the surface material

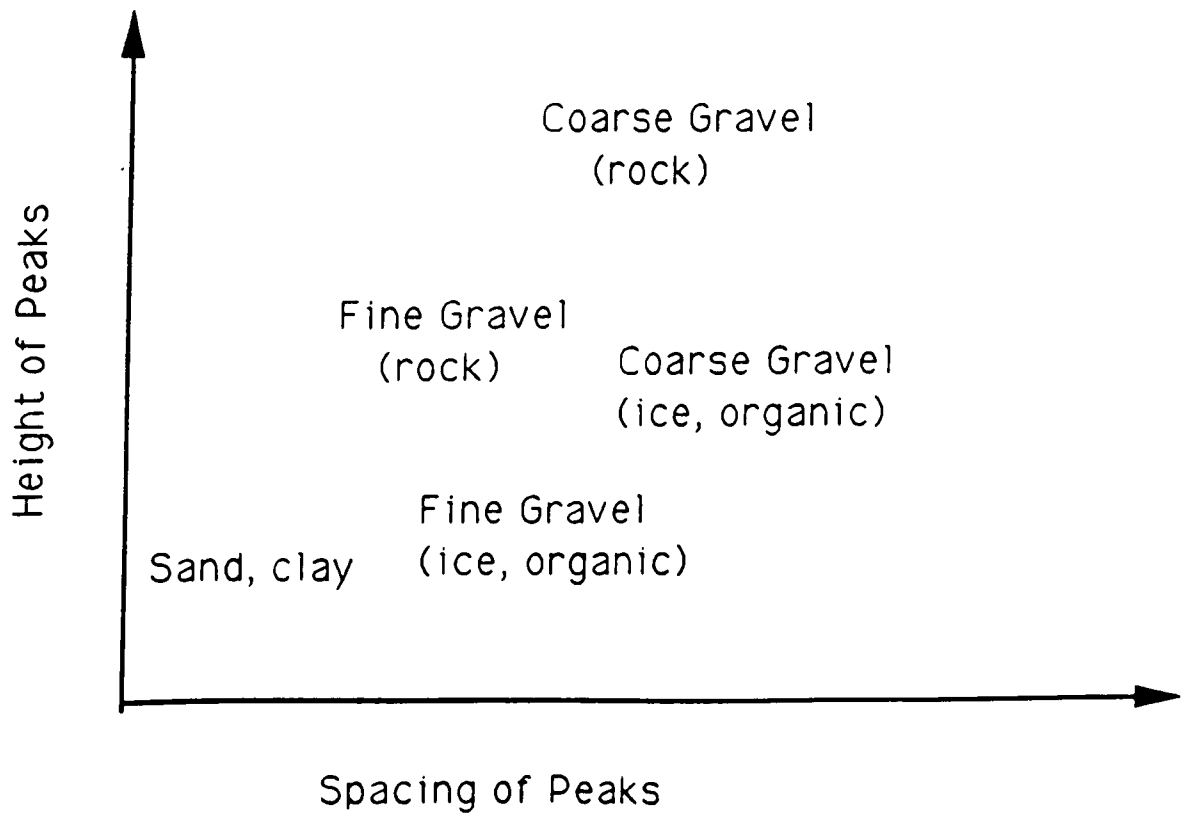

Figure7.8 Particle density determination from penetrometer data: use of peak height and spacing may allow discrimination of low-density materials (e.g. ice) from high density (rock)

example) jump to an essentially constant value, related to the 'flow pressure' of the material.

Note that, in principle, the ACC-E and accelerometer datasets do not necessarily have to be mutually consistent. The accelerometer signal is sensitive to surface properties averaged over 0.1-1 m^2, whereas ACC-E only probes a small fraction of this area. Scenarios can be envisaged where, for example, ACC-E probes a gravelly gully where fluvial sorting has removed small particles, yet the probe as a whole 'feels' a surface dominated by small cohesive particles.

7.6 Future Work

The work conducted by myself and reported here and in Lorenz 1994b,1994c has shown that the accelerometry and impact penetrometry measurements allow a qualitative identification of the surface materials. Further, if the material is well-sorted in terms of particle size, analysis of the ACC-E profile gives a quantitative indication of particle size, although the measurement suffers from small-sample statistical errors.

As may be seen from the graphs of ACC-E response (figure 7.4) , both the spacing and magnitude of the peaks in the signal correlate with the particle size. Since the magnitude of the peaks presumably depends on the mass of the particles (rather than their size per se), it may be possible to discriminate between particles of a given size with low or high density. After estimating the particle size from the peak spacing, the peak magnitudes for this size may be compared with those expected for materials of various densities (see figure 7.8)

Thus, a set of impact profiles for various particle sizes and densities would be valuable: obtaining such a dataset would be a task commensurate with the effort required in a typical undergraduate project. Steel ball-bearings of a variety of sizes are available (ρ=7900 kgm^{-3}); glass spheres (ρ=2900 kgm^{-3}) can be obtained as toy marbles; plastic spheres (ρ~1000 $kg\ m^{-3}$) are available also as toys (5mm diameter spheres are used as ammunition in toy guns, for example) and finally, expanded polystyrene spheres (ρ~100 kgm^{-3}) are used in making chemical models. Impact profiles (and the corresponding peak-height and peak-spacing histograms) for these materials, and combinations of them, would be useful.

Additionally, combinations of particle sizes (e.g. a bimodal one of large particles interspersed in a finer medium) and combinations of various particle sizes with binders of varying viscosity (e.g. water, glycerol, clay) would be interesting. Such experiments would

be useful not only for Huygens, but also in the context of preparations for measurements on the comet Surface Science Package of the Rosetta mission.

During the experiments reported here (see figure 7.4) the attitude of the penetrometer has been controlled by dropping down a tube. This is quite inconvenient, since the cable must also go down the tube. False triggering due to tube friction occurs, and it is difficult to vary the impact speed. Additionally, it is not possible to vary the orientation of the penetrometer independent of its velocity (i.e. the penetrometer always points directly along its velocity vector). To allow independent investigation of non-vertical orientation and non-vertical velocity, apparatus shown in figure 7.9 is suggested for future experiments.

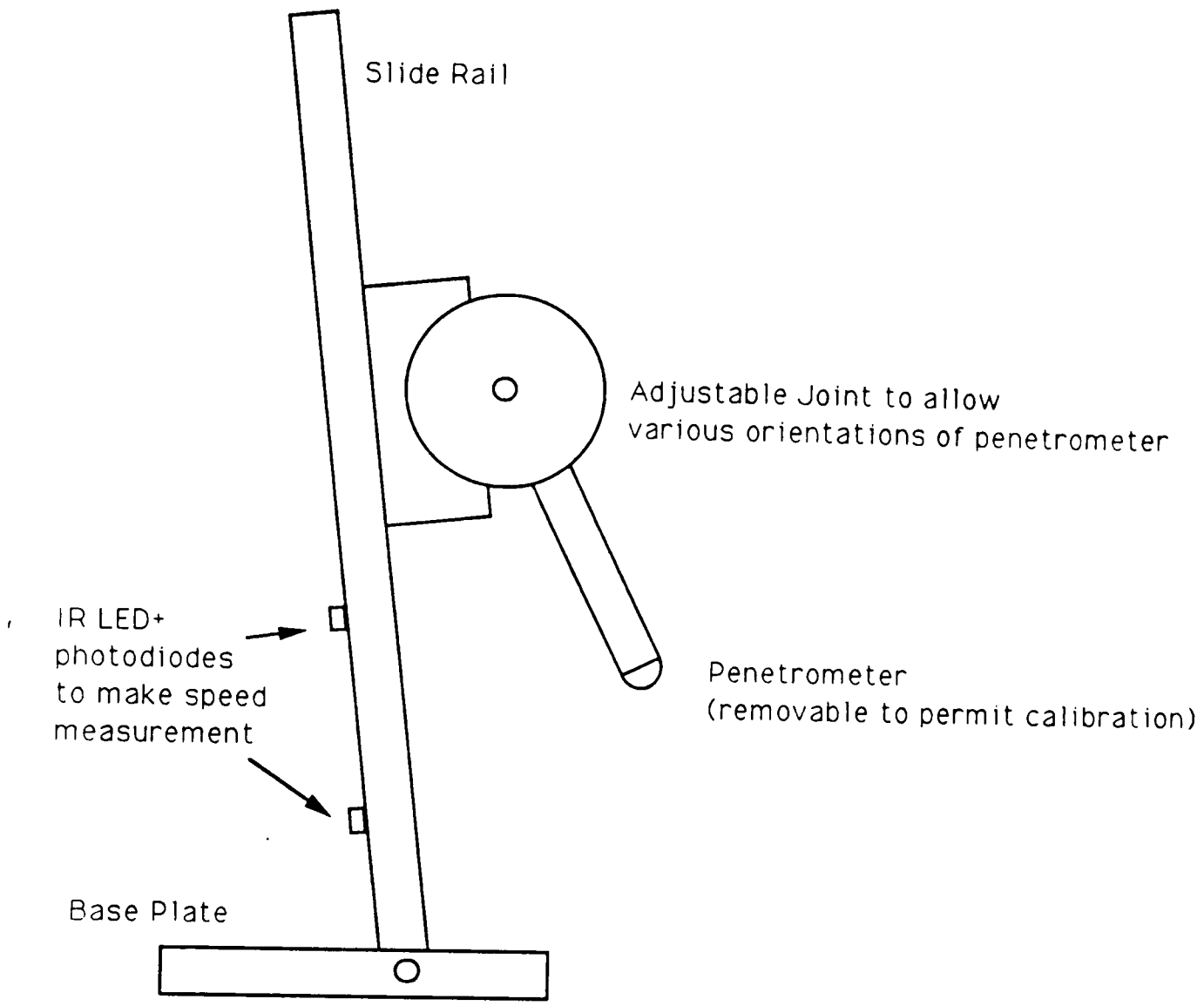

Figure 7.9 Suggested apparatus for future experimentation with penetrometer. Joints allow attitude and direction of motion to be varied. Direct speed measurement allows easy examination of sensitivity to impact velocity. Open rail design allows easy cabling access.

Chapter 8

Acoustic Measurements

The observer listens to nature: the experimenter questions and forces her to reveal herself

Georges Cuvier, French Zoologist

Noise proves nothing. Often a hen who has merely laid an egg cackles as if she had laid an asteroid

Mark Twain, American Writer

The potential utility of making acoustic measurements with Huygens was realised early in the study phase, and the project scientist J-P Lebreton encouraged some interest in this area. Ulamec performed some studies (Ulamec 1987, 1990) of the backscatter coefficient of various materials, as well as an investigation of the speed of sound and attenuation coefficient in liquid hydrocarbons.

As mentioned in Chapter 6, the passive acoustic sensing function (with the primary stated aim of searching for lightning) was adopted by HASI, since it already had a DSP function in its electronics. Active acoustic sensing (sounding, and speed of sound measurement) was adopted by SSP in early 1991, with the development being undertaken by L H Svedhem of ESTEC/SSD.

Here I discuss briefly the speed of sound measurement, and then go on to describe the sounder, and how its data may be used to derive information on the surface topography. Some computer simulations and field tests are illustrated. Finally I make some comments on passive acoustic sensing and the acoustic environment on Titan.

8.1 Speed of Sound

In a perfect gas, the speed of sound is given by

$$c=(\gamma R_0 T/M)^{0.5}$$

where γ is the ratio of specific heats (1.4 for nitrogen) R_0 is the universal gas constant (8314 Jkg^{-1} mol^{-1}), T is the absolute temperature and M is the mean molecular weight of the gas. Substituting M=28, T=287 gives c=340 ms^{-1}, the standard value for the speed of sound in air.

In Titan's atmosphere, M~28, T=94K near the surface, so c~200 ms^{-1}. The profile of sound speed as a function of altitude is dominated by the variation in temperature: see figure 8.1. Measurement of the speed of sound poses a constraint on $\gamma T/M$: if temperature is known, then composition (γ/M) can be constrained. Since T should be known with high accuracy by HASI measurements, then measurement of c allows the molecular mass of the atmosphere to be constrained e.g. the range allowed by the V1 RO experiment is 28.3-29.2 at the surface (Samuelson et al., 1981), suggesting nitrogen as the dominant constituent, with the range driven by the mixing ratios of argon (M=40) and methane (M=16). For small mixing ratios of these compounds, the variation in γ (1.4 for nitrogen, 1.313 for methane, 1.667 for argon) is small, and the variation in M controls the sound speed: 20% argon leads to a sound speed ~3% lower than if no argon is present.

Thus a measurement of c gives a useful constraint on atmospheric composition, although it does not determine it uniquely. Further, since the methane abundance in the troposphere is controlled by its vapour pressure (and hence is a function of temperature, and altitude) variation in c, where T is known, allows the methane mixing ratio profile to be determined to a useful accuracy, which is important for understanding moist convective processes, for example.

Because a speed of sound measurement is very brief, it can be made frequently - much more frequently than the GCMS can sample atmospheric composition. Thus the vertical resolution of the methane mixing ratio obtained with a speed of sound measurement can be considerably higher than that derived from other instruments such as GCMS (although a PIRLS-type instrument would be considerably better).

The speed of sound measurement on SSP is performed between two transducers mounted at the bottom of the top hat, at the base of the probe. The transducers are separated by ~14cm, leading to a 1 way trip time of ~0.7ms.

The altitude at which these measurements can start is driven by the efficiency of coupling between the transducers (bimorph piezoelectric elements) and the atmosphere, this coupling being driven by the ratio of acoustic impedances (acoustic impedance = density*speed of sound). Thus at high altitude (low atmospheric density) the impedance is very low (see figure 8.2), and the coupling is inefficient, so the signal-to-noise ratio for reception of the signal becomes too low. (This problem is in part exacerbated by the fact that the transducer design is a compromise

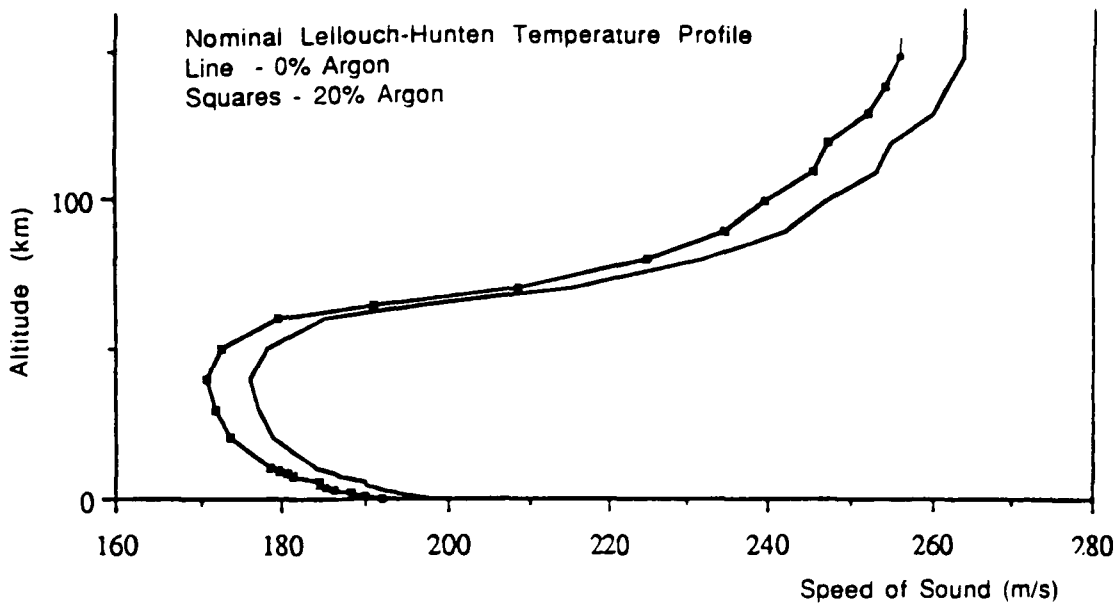

Figure 8.1 Speed of Sound in Titan's Atmosphere, with and without Argon

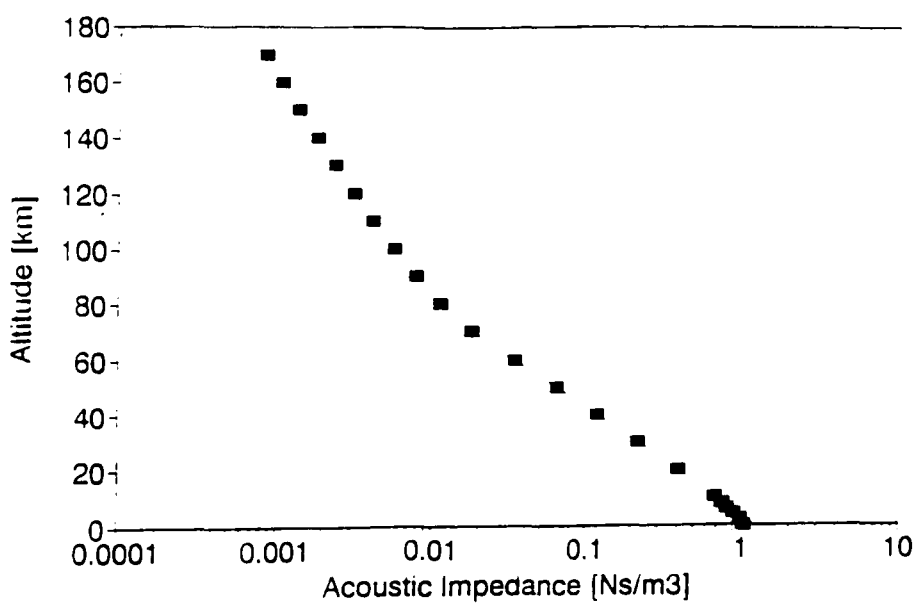

Figure 8.2 Acoustic Impedance of Titan's Atmosphere

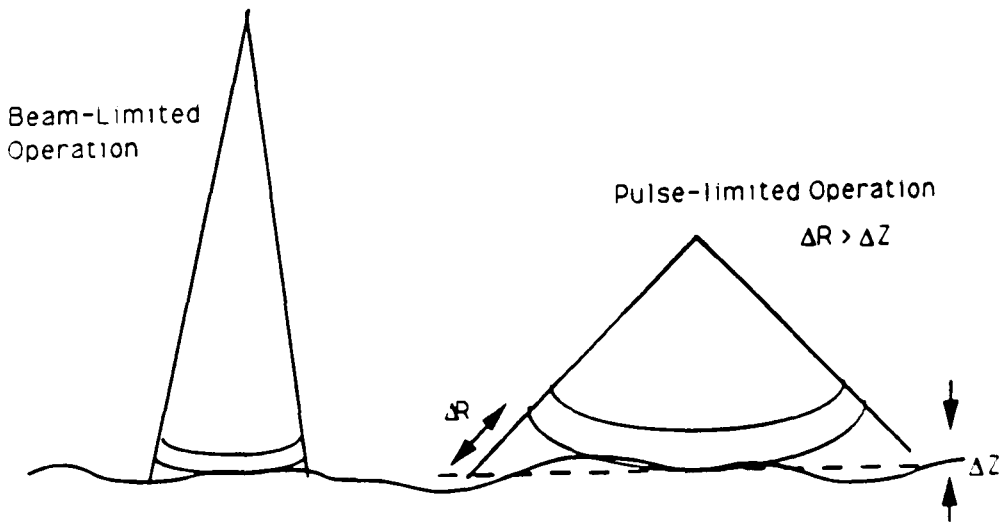

Figure 8.3 In beam-limited operation, a sounder illuminates only a tiny patch of the surface. When the beam is wide enough that the slant range ΔR exceeds the surface roughness scale ΔZ, the sounder is termed 'pulse-limited'.

between atmospheric performance and performance in an ocean). Currently it is anticipated that speed of sound measurements will be able to take place from an altitude of ~100 km.

The altitude resolution is dictated by data rate constraints, which limit the frequency with which the measurements can be made. Measurements are recorded once per second, leading to an altitude resolution profile that mirrors the descent velocity (see Figure 5.8), reaching about 5m near the surface.

The time of flight of the signal is measured with an accurate clock . Assuming the transducer-transducer distance is known to 0.5mm (recall that the transducers distort in order to function, and there may be some slight deformations of the probe and SSP structure due to aerodynamic loads and temperature effects) then the speed of propagation of the sound pulse will be known with an accuracy of ~0.3%. An additional problem (Svedhem, private communication) is that to keep the pulse bandwidth sufficiently narrow, the pulse itself must be quite wide. Thus an accuracy of ~0.5% may be expected.

The speed of propagation in one direction could be influenced by the component of any wind velocity in the propagation direction (indeed acoustic anemometers are quite widely used in meteorological applications, and especially in measuring turbulence for pollution or gas transport studies, due to the high rate of measurement). However, the measurement is made in both directions to counter this potential problem, and the transducers are recessed slightly from the front of the probe in any case, minimising the influence of wind on the measurement.

In an ocean, the speed of sound measurement is a useful diagnostic of composition. Ulamec (1987) evaluated the speed of sound for various ethane/methane mixtures, varying between 1535 ms^{-1} for methane and 1977 ms^{-1} for ethane, although he did not investigate the effects of argon, nitrogen and other solutes. Taking these factors into account, and assuming the speed of sound can be measured to an accuracy of 0.5%, then the ethane mole fraction can be determined with an accuracy of the order of ~ 5% (see chapter 6).

In addition to providing a constraint on ocean composition, the speed of sound measurement is of direct relevance to the interpretation of data from the sounder, both in the atmosphere, and more importantly in the ocean, where the sounder will constrain the depth.

8.2 Sounder

The original rationale for the sounder was as a means of establishing a lower limit on ocean depth. However, it was realised that sounding measurements of the surface could be performed shortly before impact, to evaluate surface topography.

The principle of the sounding measurement is simple: a pulse of sound is transmitted, and the reflected signal received, and its time-of-flight noted. At its most simple level, if the beam from the transducer is considered to be small, the measurement gives the range between the transducer and the 'illuminated' spot on the surface: an altimetric profile could be built by allowing the spot to traverse the surface due to the horizontal displacement of the probe by winds. The spot could also be 'painted' around by pendulum motion of the parachute.

However, such 'beam-limited' operation has disadvantages: first, the spot only samples a small region of the surface. Second, while a narrow beam gives good range performance due to the high transmit and receive gain, this requires good attitude control of the probe (to a first order, the attitude of the probe should not change by an angle of the order of the half-beamwidth of the transducer during the propagation time of the signal. The attitude specification for the descent control system on Huygens is 0.6°/s, imposed by DISR to prevent motion blur, and would correspond to a half-beamwidth of about 1° for a measurement from 200m altitude.

On Huygens the beamwidth question is largely academic, since antenna theory shows that to generate a beamwidth of θ requires a transducer diameter D of the order of θ/λ. In the low sound speed environment on Titan, with c~200 ms^{-1}, and for realistic frequencies ~10kHz (see later) λ~2cm. For straightforward accommodation on SSP, D is limited to ~10cm, so the beamwidth is at least ~0.2 radians, or ~10°. With such a large beamwidth, the sounder is no longer 'beam-limited', but 'pulse-limited'. For a discussion of these two modes in the context of radar altimeters, see Rapley (1990) : see also figure 8.3.

In pulse-limited operation, the footprint (spot) of the transducer is relatively large. However, because the range to the centre of the spot is considerably less than that to the edge of the spot, and the propagation times are correspondingly different, the echo of the transmitted pulse is smeared out. The altimetric accuracy of a beam-limited device is clearly better, since the echo pulse is unsmeared, but the shape of the echo from a beam-limited device contains information on

the topography within the footprint. For a detailed description of the smearing process, see Brown (1977), and the following section.

The choice of operating frequency for the sounder is driven by a compromise between strong attenuation of high-frequency sound (and the thermal generation of noise at these frequencies) in the atmosphere, and the likely aeroacoustic noise generated by the flow around the probe (see figure 8.4). The optimum operating frequency was felt initially to be around 35 kHz (Svedhem 1990), but a subsequent study (Brock 1991) suggested 20 kHz. Transducer performance is also a factor, so the implemented frequency is around 15 kHz.

8.3 Computer Simulations of Sounder Operation

In order to investigate what can be learned from the shape of the echo signal from Titan's surface, and to define the useful sampling rates and digitisation accuracy for the sounder, computer simulations were performed.

The acoustic sounder function on Huygens carries an important complication, not found with classical radar altimeters: the platform (probe) velocity is a significant fraction of the propagation speed of the signal, such that the transmission point of the sound pulse, and its reception point cannot be considered to be co-located. E.g. for a 200 m altitude, the sound pulse takes 2 s to return, during which time the probe has descended 10 m. Since this distance is appreciable compared with the footprint size and the expected topographic variation, a correction must be applied. Where the transmitter and receiver of a radar or sonar system are colocated, the isochrones (or contours of equal propagation time) are spherical: where the two are displaced by some distance, the isochrones become ellipsoidal.

For these initial simulations, the probe is assumed to be descending vertically with a speed v. The transmit pulse is d wide, and is transmitted and received by a transducer whose gain G for an angle ϕ is described by

$$\left.\begin{aligned} G &= G_0 \cos(\pi\phi/2\theta) \text{ for } \phi<1.5\theta \\ G &= 0 \text{ for } \phi>1.5\theta \end{aligned}\right\} \quad (1)$$

with G_0 the boresight gain, and 2θ is the FWHM beamwidth mentioned earlier

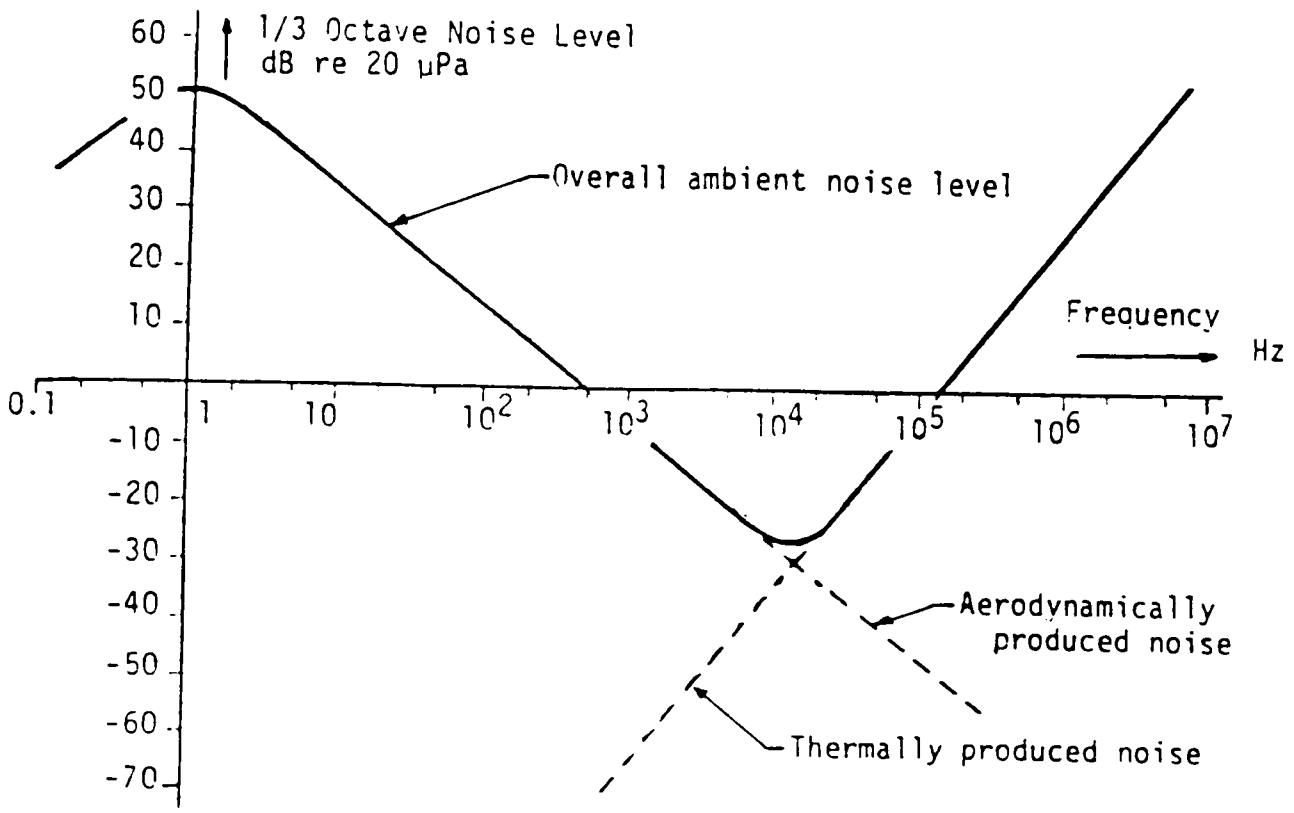

Figure 8.4 Acoustic environment during probe descent. API-S operation occurs near the noise minimum at about 20kHz (Figure taken from Broch 1991)

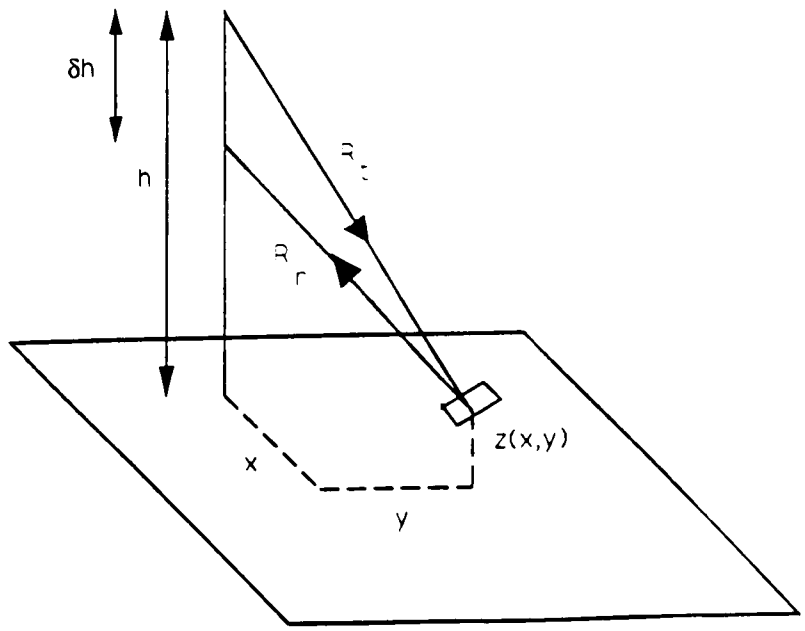

Figure 8.5 Geometry for echo simulations : signal from probe at altitude h bounces from surface element at height z(x,y) and returns to probe, which has descended by a height δh during the transit time

The boresight is assumed to be vertical. The probe is assumed to be a height h above the nominal surface. The surface topography is described by a function z=f(x,y) where x and y are orthogonal coordinates in the horizontal plane, with the sub-probe point at the origin: see figure 8.5.

Thus the transmit range to a point is

$$R_t = ((h-z(x,y))^2 + x^2 + y^2)^{0.5} \qquad (2)$$

and the one-way propagation time =R/c. To a first order, during the two-way trip of the sound pulse, the probe will have descended a distance δh, where

$$\delta h \sim 2vR_t/c \qquad (3)$$

and the corresponding receive range is

$$R_r = ((h-\delta h-z(x,y))^2 + x^2 + y^2)^{0.5} \qquad (4)$$

Thus the two-way trip time is

$$t = (R_t + R_r)/c \qquad (5)$$

(strictly speaking, since $R_r < R_t$, $\delta h < 2vR_t/c$ these expressions slightly underestimate t, but the error is of order $(v/c)^2$, and can therefore be ignored).

The magnitude of the echo component from this point z(x,y) is computed as follows. The transmit pulse has an energy P. The transmit angle ϕ_t is given by

$$\tan \phi_t = ((x^2+y^2)^{0.5}/(h-z(x,y))) \qquad (6)$$

and the transmit gain G_t computed from equation X above. The signal is attenuated by a free space loss (atmospheric attenuation is ignored) of $1/R_t^2$, and intercepted by the scattering area dA at (z,x,y). It is assumed the surface has a unity reflection coefficient, and scatters isotropically, so the return echo is attenuated by a factor $1/2\pi R_r^2$, and multiplied by a gain G_r, determined from equ.1 above using

$$\tan \phi r = ((x2+y2)^{0.5}/(h-dh-z(x,y))) \quad (7)$$

Thus the echo strength S is

$$S=PG_tG_rdA/R_t^2R_r^2 \quad (8)$$

The echo shape is formed as follows: a set of echo time bins E(t) are set up (e.g. 1ms wide) and a computer program steps through an array of surface positions (x,y) calculating the echo times and strengths as above. For each (x,y) position, the corresponding time bin has its value incremented by the echo strength S(x,y). The resultant profile is then smoothed by convolving with a square window dt wide, to take account of the finite width of the transmit pulse.

Note that I have not been rigorous in preserving conventions of definitions of gain, backscatter coefficient etc., and units are arbitrary: the object of the exercise was to see how the *shape* of the echo pulse was influenced by the topography, and thereby to define sampling rate and resolution requirements for the flight instrument.

For the simulations, performed in Autumn 1991, a 30x30 grid of (x,y) points was assumed, with $dA=1m^2$. These values correspond approximately to the footprint defined by the probe 100m above the surface. Processor speed and memory limitations prevented higher-fidelity simulations being performed (in principle, it would be useful to have an (x,y) grid with spacing equivalent to the altitude resolution of the sensor, namely ~10cm.). However, these simulations showed that useful topographic information could be recovered if the echo was sampled at ~1kHz, with the relative magnitude of the signal (it was assumed the sensor would have some kind of automatic gain control (AGC) to limit the dynamic range needed) measured to ~6 bits : these allowed practicable data rate and volume allocations to be defined for the API-S

Some sample surfaces and their echoes are shown in figures 8.6 and 8.7.

The response from the flat, horizontal surface (figure 8.6a) is quite short (like the transmit pulse), but slightly rounded and smeared due to the combined effect of beam shape and range spread within the footprint. As the slope of the surface is increased (figures 8.6b-8.6d) the decay part of the echo pulse becomes shallower. Correlation of the probe attitude, measured with TIL, and the decay slope, should be able therefore to indicate the surface slope.

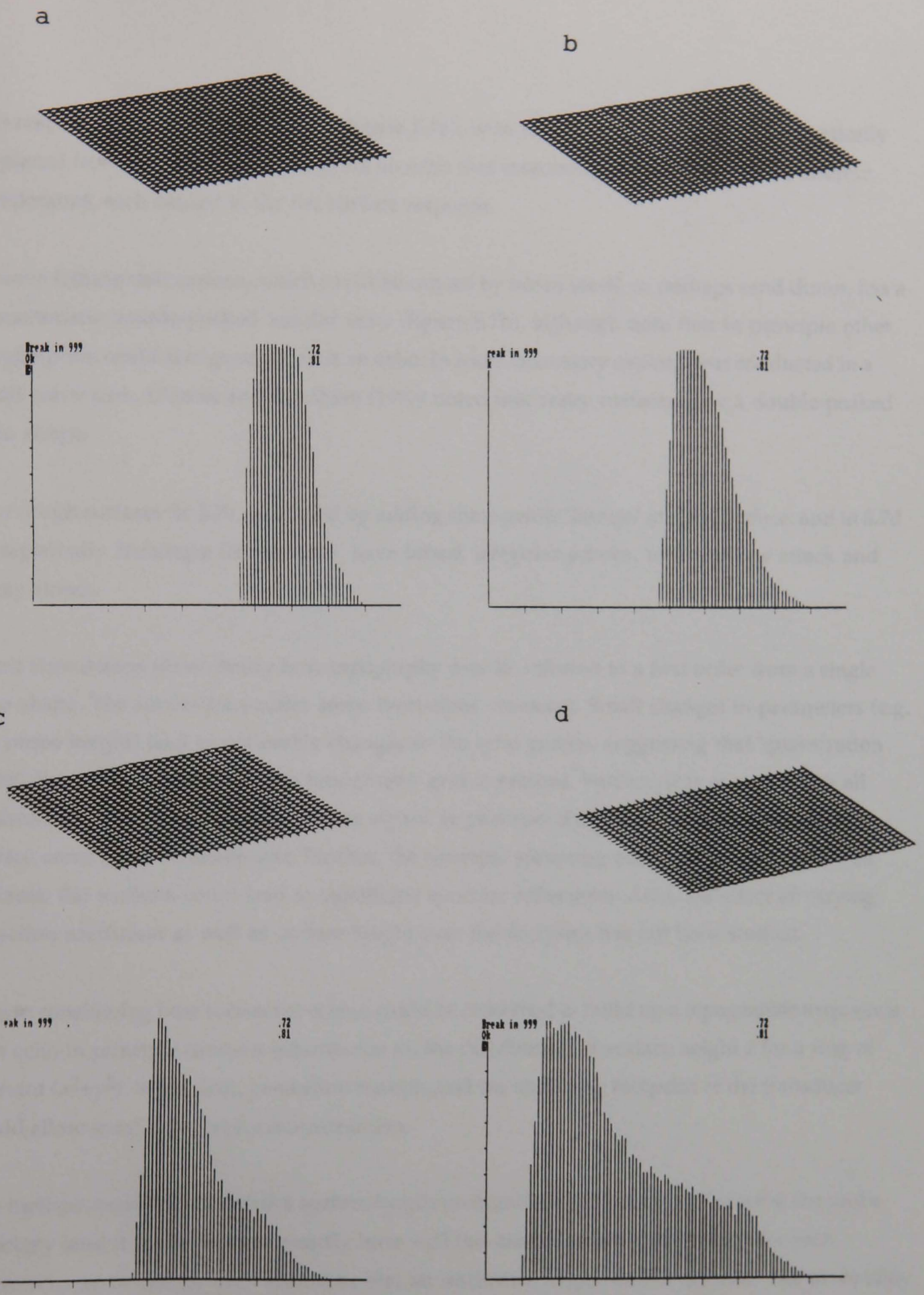

Figure 8.6 Simulated echo shapes from various flat surfaces. Each panel shows the simulated surface, and the amplitude profile of the returned echo. The surface is 30m square: echo amplitude is in arbitrary units. Echoes are for h=100m; the abscissa (echo time) runs from 0.72 to 0.81 seconds on each graph. Surfaces are flat, with slopes 0 (a), 1 in 20 (b), 1 in 10 (c) and 1 in 5 (d)

The response from a faulted surface (figure 8.7a), with two flat, horizontal sections vertically displaced from each other by 3 m, gives an echo that essentially comprises 2 almost discrete components, each similar to the flat surface response.

A wavy (sinusoidal) surface, which could be caused by ocean swell, or perhaps sand dunes, has a characteristic double-peaked 'saddle' echo (figure 8.7b), although note that in principle other topographies could also generate such an echo. In some laboratory experiments conducted in a small wave tank, Ulamec and Svedhem (1992) noted that wavy surfaces gave a double-peaked echo shape.

Two rough surfaces (in 8.7c, generated by adding some gentle 'bumps' to a flat surface, and in 8.7d by repeatedly faulting a flat surface) have broad, irregular echoes, with shallow attack and decay slopes.

These simulations show clearly how topography may be inferred to a first order from a single echo shape. The simulations suffer some limitations, however. Small changes in parameters (e.g. the probe height) lead to noticeable changes in the echo profile, suggesting that 'quantization noise' due to the relatively coarse topography grid is present. Further, it is assumed that all surfaces are illuminated by the transmit signal: in principle if the topography is steep, some surface areas could be shadowed. Further, the isotropic scattering assumed is not valid for all surfaces: flat surfaces could lead to significant specular reflections. Also, the effect of varying reflection coefficient as well as surface height over the footprint has not been studied.

I began considering how successive echoes could be combined to build up a topographic map: since each echo in principle contains information on the distribution of surface height z for a ring of constant (x^2+y^2). Wind drift, pendulum motion, and the shrinking footprint of the transducer would allow some topography reconstruction.

One method would be to define a surface height probability space p(x,y,z). Knowing the probe trajectory (and it is not yet clear exactly how well this can be reconstructed) then for each transmit location and for each echo time bin, an isochronic ellipse can be defined. The probability of a scatterer (e.g the surface) being present at a location (x,y,z) is presumably higher if (x,y,z) is on one of these isochrones. Thus each element p(x,y,z) on each isochrone for each transmit pulse should be incremented by a quantity related to the strength of the echo, range, uncertainty on

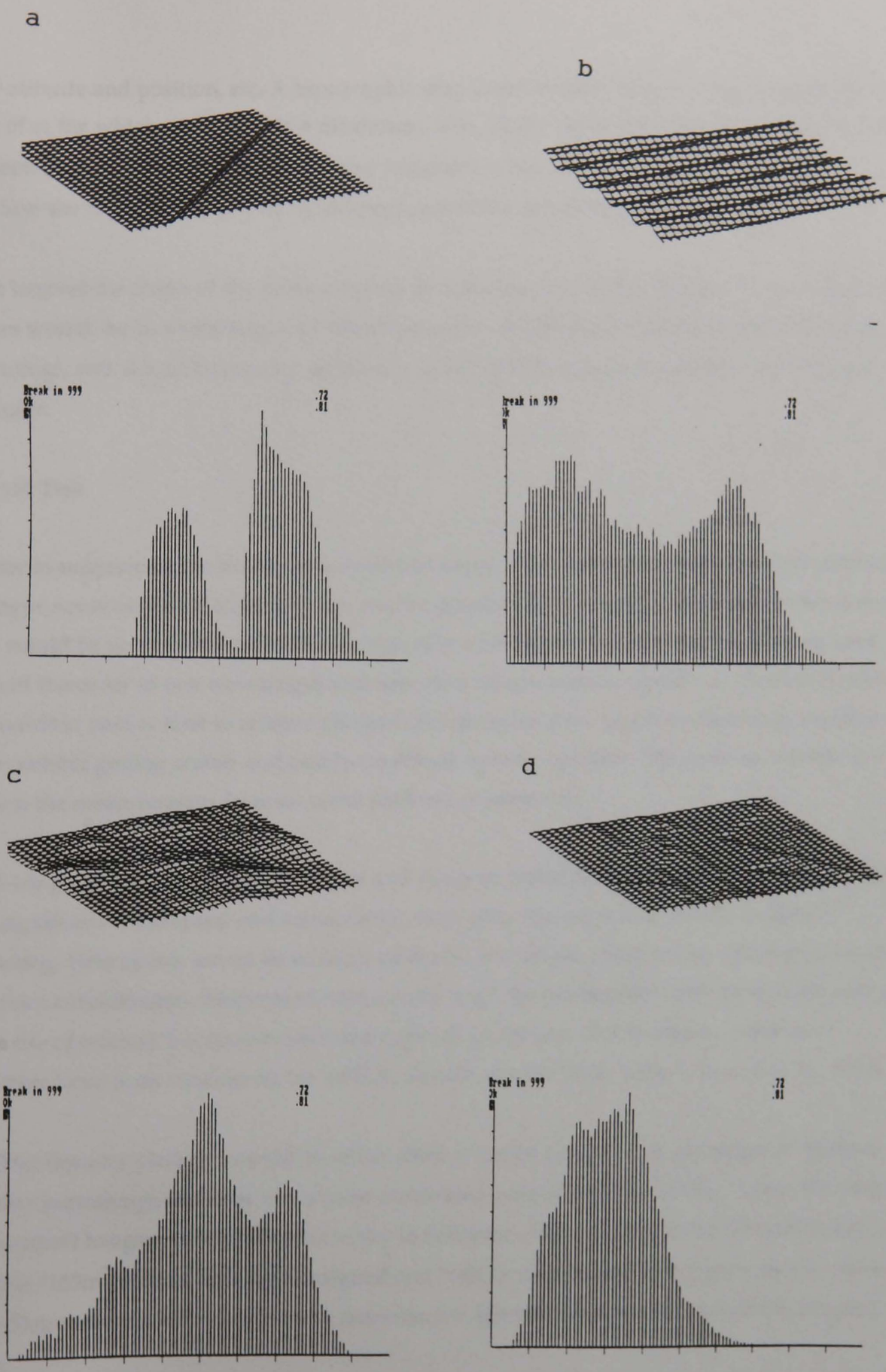

Figure 8.7 Simulated echo shapes from various 'textured' surfaces. Conditions and graph axes as in figure 8.6. Panel a shows a surface with a 3m fault. Panel b shows a sinusoidal surface wavelength ~7m, peak-to-trough height 6m . Panel c shows a surface with bumps, maximum height 6m. Panel d shows a 'cliffy' surface, formed by multiple faulting, again maximum height 6m.

probe attitude and position, etc. A topographic map could be derived by setting z(x,y) equal to the value of z_i for which $p(x,y,z_i)$ was a maximum, after all the increments for all available echoes had been applied. The method is attractive because it would also offer a measure of how uncertain the topographic profile is, although would be computationally intensive.

While beyond the scope of the present thesis, an investigation of this topography reconstruction process would be an interesting and valuable exercise (especially for someone with a talent for computing), and would be directly applicable to API-S data reduction, and that for the radar altimeter.

8.4 Field Test

In order to supplement the simulations described above, outdoor experiments were planned for a prototype sounder. Small-scale tests are readily possible, but it is not clear how representative these would be of real outdoor surfaces, especially when model surfaces have variations over scales of the order of one wavelength and near-field effects become significant. A natural problem with outdoor tests is how to achieve clutter-free separation from target surfaces (e.g. buildings, cliffs) without getting scatter and multipath effects from the ground. The obvious solution is to perform the measurements from an aerial platform of some sort.

Fixed-wing aircraft are generally too fast and noisy to make this practicable. Even hang-gliders have significant wind-speed and aeroacoustic noise, plus operation of a sodar would be distracting. Helicopters would be an ideal platform , but are also very noisy, and expense is an important consideration. Suspension from a crane might be practicable if one were found near a target site of interest, but convenience and expense are factors. (Interestingly, ultrasonic altimeters have been considered for VSTOL aircraft, despite their noise - Maeda et al., 1970)

A lighter-than-air platform would be ideal, since it can be placed over any target of interest (weather permitting) and does not require continuous propulsion. The author visited the Vosper Thorneycroft hangar on Southampton water in February 1992 and flew in the D2 human-powered dirigible ($165m^3$ helium capacity) designed and built by Dr Graham Dorrington and his students of the Department of Aeronautics and Astronautics, University of Southampton (Dorrington, 1994).

There were considerable delays in the manufacture and procurement of suitable portable sonar and data logging equipment, and the Southampton airship programme was interrupted by a fatal accident in Sumatra in March 1993. Thus the planned campaign of airborne measurements never took place.

In summer 1994, portable sonar equipment was finally ready, but using large-beamwidth transducers (tweeters for stereo music speakers). The operating frequency was set at 10kHz, to be comparable with the API-S performance, but with lower atmospheric attenuation, and to be easily audible to verify correct experiment operation. The 10kHz signal was sent as a 5ms burst. As with radar equipment, the receiver (even though it used a separate transducer) had to be suppressed by a transmit gate, to prevent saturation as the transmit pulse was sent. The received echo is amplified and sampled by an ADC mated with a portable PC. The whole equipment is battery powered.

The low directionality implies low gain, so only large targets could be 'pinged', and only at ranges of a few metres. Indoor experiments proved to be unsatisfactory, due to multiple echoes. Outdoor experiments were performed under cover of darkness, to ensure low ambient noise, and to minimise embarrassment to the experimenter.

Results are shown in figure 8.8 . Although reproducability was sometimes poor, especially due to false triggering (cf figures 8.8a and b) and the shapes almost defy interpretation, qualitative discrimination between targets is at least possible. No attempt has been made to model these echoes with the simulation method above, in part due to the poorly-controlled conditions (pointing of the transducers and their beamshape) and the variability of the shape of the transmit pulse (often saddle-shaped, rather than square).

Figures 8.8a and b show echoes from the front of the UKC physics building, which is flat The echo is quite spread, in part due to the large beamwidth of the transducers. Note, however, the steep attack of the echo shape. The slow decay or after-echo may be in part due to multipath involving ground reflection.

Figure 8.8c shows an echo from a bushy tree. The 'scattering volume' nature of this target, and its rounded shape, give a much shallower attack slope.

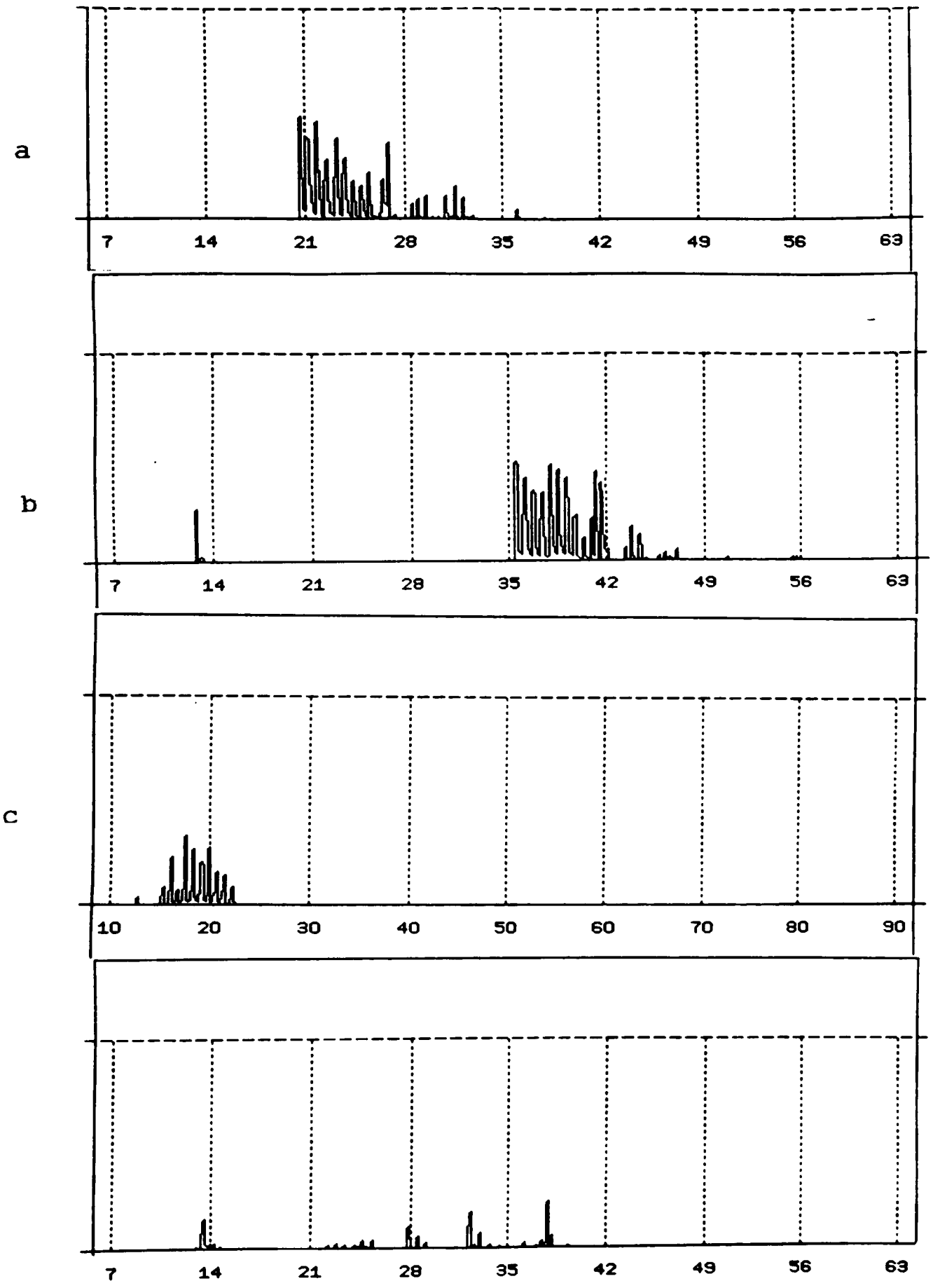

Figure 8.8 Field test echo measurements; abscissa is time in milliseconds. Panels a and b show echoes from the flat wall of the UKC physics building at ~4m (note in panel b that the timing of the return pulse looks incorrect, as the sampling system has been spuriously triggered. The small spike at ~12ms is the tail end of the transmit pulse which has not been suppresed by the receiver gate. The difference between this spike and the start of the echo at 35ms is ~21ms, the same as in panel a) Panel c shows echo from a bushy tree at ~2m. Panel d shows the echo from the UKC library building's 'castellated' wall.

Figure 8.8d shows a barely-detectable echo from the side of the UKC library. This building has a 'boxy' buttressed wall, resembling a mortice, or castellation. There are essentially two reflection targets, spaced in range by about 1.5m, leading to the multiple echo (consider two attenuated echoes like 8.8a, spaced by ~10ms, and the result superficially resembles figure 8.8d).

Thus, the field measurements broadly show that, as indicated by the simulations, useful topographic information can be inferred from echo shape. However, the field tests to date are somewhat unsatisfactory. Future experiments, using more powerful (and more importantly, more directional) transducers, would be of great benefit. Further, airborne measurements would aid interpretation by eliminating multipath effects.

8.5 Passive Acoustic Sensing

The SSP API-S subsystem is able in principle to record background or ambient noise within its passband (currently ~15 kHz+/-500Hz, the bandwidth dictated by doppler shift expected by the probe's motion near the surface, with an appropriate margin)

Additionally, the HASI PWA system includes a wideband microphone, able to record (by using the DSP chip of PWA) the power spectrum of ambient noise from a few Hz to 5 kHz, with a resolution of the order of 50 Hz.

What might these instruments record? Clearly during descent (see figure 8.4) there will be a substantial aeroacoustic component. On the ground, however, this noise will cease. Probe-generated noise on the surface is likely to be small - the ACP pump will have been shut down, so the only piece of moving equipment on the probe is the tiny shutter on the DISR infrared channels, which is unlikely to produce a large acoustic signal.

Ksanfomality et al. (1983b) were able to infer near-surface windspeeds on Venus by comparing the amplitude of noise recorded by a microphone on the Venera 12 and 13 landers with that obtained by microphones on models in a wind tunnel. A similar surface windspeed measurement might be possible on Huygens, and would be extremely valuable, especially if a landing-induced dustcloud was present.

Other noise sources such as rain, distant volcanoes, thunder etc. can be speculated upon, but one noise source is worth investigating, namely that of undersea bubbles. Rainfall and wave action can lead to the entrainment of bubbles of atmosphere, which eventually float upwards and burst at the surface, often yielding small aerosol particles. These bubbles play an important role in transporting materials across the ocean-atmosphere interface.

Bubbles oscillate like little bells, and it is this oscillation that leads to the pleasant musical 'tinkling' sound of water familiar to us on Earth. The frequency of the oscillation f of a bubble was investigated by Minnaert (1927), who gave the following expression

$$f = (1/\pi d)(3\kappa P_o/\rho)^{0.5}$$

with d the bubble diameter, κ the polytropic exponent (~ratio of specific heats), ρ the gas density and P_o the ambient pressure. The dominant frequency observed on Earth in the oceans during periods of moderate rainfall (Scrimger, 1985) is ~13.5kHz, corresponding to a bubble size of 0.5mm.

Taking the same bubble size (admittedly a sweeping assumption) and imposing Titan conditions gives a frequency of ~20 kHz, interestingly close to the API-S passband. However, as suggested in the following chapter, rainfall is unlikely to be heavy on Titan's oceans. Spilling breakers could be another source of bubbles, however.

The presence of large quantities of bubbles in liquids on Titan may be inferred from the liquid's density, it's reflectivity (measured by DISR) and turbidity (inferred from SSP REF external illumination measurement). Large numbers of bubbles with natural frequencies within the API passband are likely to make ocean depth measurement difficult - both due to increased ambient noise, and enhanced scattering of the sonar signal. On the other hand, detection of bubbles would be interesting for understanding atmopsphere-ocean coupling on Titan.

Chapter 9

Planetological Modelling of Titan

There is something fascinating about science. One gets such wholesome returns of conjecture out of such trifling investment of fact
Mark Twain

Mathematical formulas took on the quality of fun-filled games, and the physical world became an enchanted kingdom whose every secret seemed worth exploring.
Samuel Florman
The Civilized Engineer

The question of the nature of Titan's surface and its evolution is addressed in the comprehensive, although now slightly dated, review of Titan by Hunten et al. (1984). Knowledge and theories concerning Titan's surface have been reviewed regularly by Lunine (1990,1992,1993,1994). Additionally, my own review (Lorenz, 1993d) is found in an appendix to this thesis. In this chapter I enlarge upon some subjects treated briefly in that review, particularly where I have made a contribution. Additionally, some brief comments on Titan's origin and evolution are given.

9.1 Tides

In late 1991, when I commenced study at UKC, the only evidence of a solid surface was the radar observation by Muhlemann, which was difficult to reconcile with the need to account for an inventory of ethane and other hydrocarbons (Lunine et al, 1983; Dobouloz et al. 1989) of global depth ~1km required by photochemical models (Yung et al, 1984).

Additionally, Sagan and Dermott (1982) pointed to Titan's relatively high orbital eccentricity (0.029) - not high in itself, but unexpectedly high for a satellite in a regular orbit with no perturbing resonances. They suggested that if shallow oceans were present, dissipation due to bottom friction in response to tidal currents would tend to damp the eccentricity to much lower values. They computed a minimum depth of ~400m compatible with plausible initial eccentricities at the 'start' of the solar system, or suggested that oceans would not be present at all. Deep oceans have low dissipation, since the currents required to respond to the changing tidal potential are small.

It was further argued that since the solubility of water ice in methane was believed (Rebiai et al, 1983) to be fairly high, any oceans would rapidly erode topography to become a global ocean (Sagan and Dermott, 1982; Lunine and Stevenson 1985).

Lunine (personal communication, 1991) suggested that the tidal dissipation argument of Sagan and Dermott (1982) needed detailed re-examination, and tasked a graduate student with developing a numerical model of dissipation in oceans of various configurations. The results of this numerical model have recently been submitted for publication (Sears, 1994) for a number of depths and configurations (global, or global with a continent, or polar). Qualitatively, the results agree with Sagan and Dermott (1982), in that oceans much shallower than ~400m lead to tidal dissipation that, for plausible values of eccentricity at the start of the solar system, would lead to much lower eccentricity than is presently observed. Thus, as suggested by Sagan and Dermott (1982), if the eccentricity is primordial and oceans have existed on Titan's surface over the age of the solar system, then the oceans must be deep.

However, the issue is not so simple. I noted pre-Voyager work by Peale et al (1980) who suggested (long before notions of oceans became widespread) that tidal dissipation in the interior of Titan would make preservation of such a large eccentricity marginal. Two co-workers and myself computed the dissipation in the interior of Titan for various internal models (Sohl et al, 1994) and found that, even without any oceans, dissipation is sufficient to make primordial eccentricity implausible for some interior scenarios. We also developed an analytical model of ocean dissipation which agrees to within 20% of Sears' (1994) numerical results (Sagan and Dermott use an incomplete formulation of the tidal dissipation, treating the radial component only, and not the component due to Saturn's libration).

If the eccentricity is indeed primordial, and there are no oceans present, or if they are very deep, or have only existed on Titan's surface for a short time, then the model (Sohl et al. 1994) suggests Titan's interior must be differentiated and volatile poor (i.e. layers of ice, with no liquid mantle of water-ammonia). If the interior is undifferentiated (unlikely) or has a liquid mantle, or a shallow ocean is present (unlikely, given observations), then the eccentricity cannot be primordial.

Stevenson (1992) suggested that the eccentricity could have been generated by a collision with a body equal in size to one of the other Saturnian satellites. Sohl et al. (1994) also considered 'near-miss' scenarios, where momentum exchange by gravitation during a near collision leads to the observed eccentricity: assuming the relevant body escaped the Saturnian system, it must have been at least 1000 km in diameter.

Thus Titan's eccentricity remains a mystery: explaining it with current models requires improbable events, although it should be noted that the models are somewhat uncertain, since the rheological properties of high-pressure ice phases as a function of temperature are poorly known. However, the principle conclusions remain :

1. Even for the case that the interior is differentiated and rigid, dissipation due to liquids must be low (suggesting either deep oceans, patchy seas, or a buried ocean (Stevenson 1992)).
2. Since internal dissipation is significant, but poorly constrained, the tidal argument is of little use in trying to constrain allowable ocean depths, which in any case will have evolved over the age of the solar system.

A small, but important, point in shaping the perception of Titan's surface is the alleged high solubility (~10^{-5}) of water ice in methane (Rebiai et al, 1983). As the solubility is considerably higher than would be expected from theoretical considerations (Raulin, 1987; Lunine and Stevenson, 1985; Lunine 1993), it was suggested (Lunine, personal communication 1991) that the experimental result of Rebiai et al be checked. As this work was performed in Southampton (my old university) I was able to follow this up in a visit in December 1991 : Dr Tony Rest (one of the co-authors of the Rebiai paper) advised me (Rest, personal communication, 1991) that the measurement was erroneous. The dissolved ice content was estimated by IR spectroscopy: it seems that the wings of a CO_2 absorption band led to absorption which was mistakenly taken to be due to water, so the solubility was overestimated. More careful measurements (Rest et al. 1987) established an upper limit for water solubility in methane of 10^{-7}, although theoretical arguments suggest it could be orders of magnitude lower (Lunine, 1993) .

Thus solubility of ice bedrock in oceans (and for that matter, rivers or raindrops) is therefore small. Lunine (1994) did note, however, that ammonia hydrate ice might be eroded significantly by methane, due to the higher solubility of ammonia in methane. If erosion is significant, then seas and lakes on Titan may show preferential migration antipoleward, towards the sub- and anti-Saturnward points due to tidal effects (Lorenz, 1994b).

Lakes on Titan (Clarke (1974) describes a hydrocarbon lake on Titan named 'Loch Hellbrew') could also offer insight into the crustal thickness and rheology, since lakes are likely to form in impact craters. Craters in icy surfaces tend to relax, or dome upwards, which would tend to make lakes into ring- or horseshoe-shapes (Lorenz, 1994b). The depth and extent of the lake would allow an estimate of the relative rates of lake filling (due to ethane deposition) and relaxation.

9.2 Photochemistry

The photochemical processes in Titan's atmosphere, in particular methane photolysis, yield more complex molecules which condense and settle onto the surface. Hunten (1978) suggested that ~1 km of photochemical debris would cover the surface of Titan. The global ocean concept was driven by the result of Yung et al.'s (1984) photochemical model, which suggested that ~600 m of

ethane had to be accounted for. Essentially *all* subsequent work was based around this result, including the bounds on ocean depth suggested by Dobouloz et al. (1990).

However, these photochemical models suffer from considerable uncertainty in rate coefficients at low temperatures (and, indeed, even the dominant reaction pathways are poorly known - for example Mordaunt et al. (1993) recently overturned the accepted wisdom that the primary pathway of methane photolysis is the CH_2 radical: they found instead CH_3 was the dominant product). Additionally, the production and deposition rate of ethane is very sensitive to the way condensation processes are treated in the model. Lunine (1993) noted that the observed ethane abundance in Titan's atmosphere measured by Coustenis et al. (1989) was three times lower than Yung et al.'s model suggested, and therefore suggested that a factor ~3 uncertainty should be considered for the modelled ethane production, and hence ocean depth.

A more comprehensive photochemical model of Titan's atmosphere has been developed by Lara (1993), including updated reaction coefficients, the effect of magnetospheric electrons (important for nitrogen chemistry) and improved treatment of condensation and eddy diffusion. With this model, we (Lara et al. 1994 - Appendix 5 to this thesis) demonstrated that the ethane production on Titan over geologic time is rather less than previously supposed: perhaps 250 m at most. (This is within the factor ~3 uncertainty associated with the Yung et al. (1984) estimate, as suggested by Lunine (1993)).

Such an ethane inventory (even when supplemented by methane, giving up to ~4 km) is considerably easier to conceal than the ~1-10 km previously supposed.

9.3 Meteoric Materials

Since Titan's surface is essentially hidden at present, an informed discussion of its impact history is impossible. However, the atmosphere allows some investigation of current meteoric activity, since in Titan's reducing atmosphere, oxygen compounds are unexpectedly observed. The low temperature means these compounds have very low vapour pressure, such that there is a very strong condensation sink acting to remove compounds such as carbon dioxide. However, carbon dioxide has been detected from V1 IRIS measurements with an abundance of 1.3×10^{-9} (Coustenis et al. 1989).

As discussed in Samuelson et al. (1983), and English et al. (1994) such an abundance requires either that we are looking at an atypical episode in Titan's history, or that there must be an influx of water vapour. Thus the oxygen species in the atmosphere act as a tracer for meteoric activity. The required influx of water , according to English et al. (1994) is ~10-200 times the

expected interplanetary meteoroid deposition, but ejecta from interplanetary particles on Iapetus and Hyperion could perhaps provide this amount. (Note that outward diffusion of ice particles from Saturn's E-ring is unlikely, as there is substantial blocking by the other inner satellites).

There should be, for the observed CO_2 abundance, a CO_2 deposition flux of ~.01-.001 times the ethane flux, plus silicate dust (which would have been dehydrated by the high temperatures encountered during entry)

Note that the CO_2 flux determined by English et al. (1994), using Lara's (1993) photochemical model, is about 10 times higher than that determined by Samuelson et al. (1983) and Yung et al. (1984), even though the CO_2 abundance in the models is the same (in agreement with observations). This is largely due to the different treatment of condensation and transport between the Yung/Samuelson and Lara models, and in particular the selection of a value for the eddy diffusion coefficient, a parameter which describes how efficiently compounds are transported away from their formation sites. It is in part the treatment of this transport in the model that leads to the lower predicted ethane deposition flux and the 'disappearance' of the global ocean, a conclusion that rests more comfortably given recent IR and radar observations. However, this same condensation and transport treatment gives a higher CO_2 deposition flux than earlier models, and compels us to look for more plentidul supplies of oxygen to the atmosphere, perhaps due to ejecta from Saturn's outer satellites. An increased water influx might make it easier to explain the existence of water ice in Titan's stratosphere, identified recently by Coustenis et al. (1994).

If this oxygen source (or, perhaps, a large, recent impact) is found, it will represent a triumph of the predictive power of models. On the other hand, the sensitivity of models to parameter changes (such as the eddy diffusion coefficient), and the experience with the ethane inventory, suggests that maybe in a few years an updated model may predict altogether different things.

One additional aspect examined by English et al. (1994) is that of meteoric ionisation. Even with a higher meteoric input than earth, owing to the larger atmospheric scale height on Titan and the lower entry velocity of meteoroids, the ionisation produced should be small compared with that on Earth. Consequently, there seems little justification for Grard's (1992) ionised layer, nor for lightning hidden beneath it.

9.4 Aeolian Processes and Surface Texture

The presence of a dense atmosphere on Titan coupled with low gravity suggests it may be easy to levitate materials from the surface (indeed Zubrin (1989) has suggested that a human might be able to strap wings onto his/her arms, and fly). The notion of aeolian processes naturally arises.

Greeley (1987) computed the threshold speed for saltation (the process by which surface particles may jump about and migrate under the influence of wind to form dunes and other features) at ~2 cms^{-1} for 180μ diameter particles . Allison (1992) and Grier and Lunine (1993) obtained similar results, and Allison (1992) noted that this speed is comparable with the frictional wind speed (the maximum near-surface windspeed expected from a consideration of the planetary boundary layer).

Thus it was concluded (on the basis of gravity, gas density etc. considerations) that 'windblown dust may be an occasional feature of Titan meteorology' (Allison 1992). Note that rather higher wind speeds are required to actually levitate particles from the surface (i.e. to suspend them: saltating particles are on short semi-ballistic trajectories).

The influence of liquids or regolith compaction processes may increase the particle cohesion such that the results mentioned above do not apply (these computations use a semi-empirical parameter, the Bagnold number, which implicitly assumes a certain value of particle cohesion). Thus, if ethane rainout is uniformly distributed over Titan, there may be no aeolian transportation at all.

ACC-E data and impact accelerometry (chapter 7) should indicate whether the surface material at the landing site is grossly cohesive or not. An additional piece of information is the presence and duration of a dust-cloud following landing. Such clouds have been observed on Venus and Mars (see Lorenz, 1993a{Appendix 3},1994a; Garvin 1982 and references therein) These clouds are believed to be largely due to the ring vortex about a lander levitating surface materials, although it has been suggested (Garvin, personal communication) that additional factors, such as aerodynamic heating of a probe wake, may also play a role).

The duration of the cloud allows constraints to be placed on the particle fall times (and hence their size) and on the behaviour (viscosity, and windspeed) of the atmosphere near the surface. If small particles are inferred from ACC-E measurements, for example, failure to observe a dust cloud may imply that the particles are cohesive, due to ethane moistening, for example. The acoustic reflectivity of the material will depend strongly on how 'fluffy' it is.

Imaging or detection (by API-S, for example) by the probe instruments would be fortunate, since these instruments (see figure 6.1) will only cover a tiny fraction (10^{-3}~10^{-6}) of Titan's surface. Detection of aeolian features from orbit by ISS, VIMS or the radar would that the features are rather large-scale (>100 m).

9.4 Rainfall

In the context of erosive processes, rainfall may be a significant modification agent of Titan's surface. The expected photochemical deposition flux of ethane is too small to be significant for weathering, but the vapour pressure of methane at Titan's surface temperature is such as to allow a methane cycle, with vapour convecting upwards until it reaches cooler regions where the methane saturates into droplets. Even though the lower 3km or so of Titan's atmosphere are undersaturated with respect to methane, the possibility was considered (Lunine 1990) that large raindrops could reach the surface before evaporating.

I examined this question quantitatively, having already taken an interest in methane droplets to assess the hazard to the Huygens probe of methane icing: in the altitude range 17-40km, the stable state of methane-nitrogen is solid, although supercooled droplets might be possible. If clouds of supercooled drops exist, they could freeze onto the probe (Lorenz and Zarnecki, 1992). One major input to such studies is how large can individual drops be, and how fast do they fall.

Toon et al. (1988) examined Voyager IR data and concluded that if methane clouds were present, they were of large droplets (of order 1 mm in diameter) and also computed descent rates for drops and estimated the maximum size of a Titan methane raindrop (on the basis of hydrocarbon's surface tension being lower than that of water) at 3mm diameter.

With this result in mind, I began to develop a quantitative model of raindrop behaviour (Lorenz 1995) which is described in detail, together with some of the results that follow, in Lorenz (1993c - Appendix 4) .

This model, which uses a classical aerodynamics approach by computing the drag of a drop assuming initially it is a sphere using an empirical relation for drag coefficient as a function of Reynolds number, then modifying the drag coefficient to take into account the deformation of the drop into a non-spherical shape (with the deformation assumed to be proportional to the ratio of aerodynamic forces to surface tension forces). This approach was found to give excellent agreement with experimental measurements of the terminal velocity of terrestrial raindrops (aerodynamic drag equals the drop's weight at terminal velocity).

Further, when the ratio of aerodynamic to surface tension forces (defined by the Weber number) reaches 4, the drop is statistically likely to break up. This occurs for terrestrial drops of diameter about 6.5mm, again in agreement with experimental data for details.

Substituting appropriate environmental parameters (liquid properties, gas density, gravitational acceleration etc.) into the model allows predictions to be made about Titan : it was found that near the surface, the aerodynamic/ surface tension balance allows drops of up to 9.5mm diameter, which would fall at only 1.6 ms^{-1}.

It is interesting to contrast these results with those of Toon et al (1988). Toon's team considered the raindrops essentially as large aerosol particles, and apparently applied the same methods (e.g. Stokes' Law to estimate terminal velocity) for aerosols to raindrops as well. In fact, raindrops (see Lorenz 1993c) are too large for Stokes' Law to apply, since drag is due more to inertia forces than to viscous ones (i.e. the Reynolds' Number is too high). This is not a problem for my methodology, since the drag coefficient's variation with Reynolds' number is treated correctly. We see here an interesting example of how an investigator's previous experience can shape his or her approach to a problem : my own background as an aerospace engineer led to an approach that was more appropriate to the raindrop parameter regime than an aerosol physics method. Doubtless the converse process could also apply.

The evaporation of raindrops during descent was then computed, using standard relations, modified by an empirical factor to take account of the enhancement of evaporation due to ventilation by the airstream. The coupled descent/ evaporation model (as a drop evaporates, it shrinks, so falls slower, giving it more time to evaporate) allowed the examination of the question whether raindrops could reach the surface. It was found, considering methane only, that for equatorial conditions (where the surface humidity is restricted to 70% or less - see chapter 3) even the largest drops released from a cloudbase of 3km altitude could not reach the surface. When non-ideal solubility of nitrogen in methane was considered, some drops (shrunk to less than 0.5mm diameter) could get to ground level.

This has important implications: unless rainfall is extremely frequent (unlikely, since the interpretation of IR data (Griffith et al. 1991, Toon et al 1992) is that methane clouds are either patchy or thin) then no rivers can exist on Titan, at least for present equatorial conditions. (In a past epoch, or near the poles, where the methane humidity may be higher, rivers could perhaps exist).

However, if there is substantial topography on Titan (and Ganymede has mountains 2km high) highland regions may receive substantial rainfall, since when released from 3km altitude, drops have only shrunk by ~30% when they reach 1km altitude. Rainfall may erode dark organic material more than ice (although the dark organic material ('tholin') is poorly soluble in methane (McDonald et al. 1994) it is probably more soluble than ice is - see section 9.1) leading to white mountain tops. (J Caldwell, in a meeting in Baltimore in May 1994, suggested that should Cassini find such a mountain, an appropriate name would be 'Mauna Kea' - Hawaiian for 'White Mountain').

Further work remains to be performed on rain studies on Titan: exploration of the sensitivity of rainfall to updraughts, simulation of the formation of 'rain shafts' (locally-enhanced humidity due to previous rainfall), and simulation of raindrop formation in convecting clouds would all be fruitful tasks.

An additional implication of raindrop evaporation before reaching the surface is that their condensation nuclei (ethane droplets or aerosol particles) are not necessarily deposited directly onto the surface, but may remain suspended in the lower troposphere for some time, forming a fog or 'rain ghost' (Lorenz, 1993c). Samuelson (private communication) has pointed out, however, that the globally-averaged optical depth of such a fog must be low, or the surface of Titan would be much cooler than is observed, so such a fog must be patchy or thin.

9.6 Regolith Processes

Investigation of the possible properties of regolith on Titan has become of interest for several reasons. First, since data is available for impact dynamics on sand and regolith surfaces on the Earth and Moon (Lorenz, 1994a), it is a useful model surface to consider for Huygens impact dynamics. Second, regolith could be susceptible to aeolian transport (see section 9.4). Finally, and perhaps most importantly, a porous regolith allows the concealment (Stevenson, 1992) of the ~200m ethane inventory from groundbased radar and IR observation.

Considerations of Titan's impact history (Thompson and Sagan, 1992) suggest over 300 m of regolith could be produced, although as pointed out in Lara et al. (1994) and Lorenz (1993d), proto-Hyperion debris could produce around 10 km of regolith - see next section. Such a thickness could easily accommodate the hydrocarbon inventory.

However, since a regolith is highly insulating due to its porosity, regolith thickness is self-limiting. Lower layers, warmed by radiogenic heat from the interior, anneal and sinter faster, reducing their porosity. In collaboration with K. Kossacki and M. Banaskiewicz of the Space

Research Centre in Warsaw, I have begun to examine whether this process would destroy the porosity sufficiently to prevent the concealment of the hydrocarbon inventory, using a coupled conduction/densification model developed by Kossacki.

Preliminary results confirm an initial suspicion (Lorenz, 1993d) that Titan is sufficiently cold that densification is very slow. After ~$5x10^8$ years, only the bottom ~200 m has lost its porosity, and subsequent densification is slower still. Further, the model assumes only conductive heat transport - a 'heat pipe' effect due to hydrocarbon vapours percolating through the regolith will allow lower layers to remain cooler and hence maintain their porosity (Lorenz, 1994d).

9.7 Origin of Titan's Surface and Atmosphere

This, perhaps more so than the other subjects considered in this chapter, is a deep and broad subject, and only the briefest overview is presented here, to put the investigations of Titan's surface into context.

Current theories on the formation of planets and satellites suggest that they accreted from smaller bodies named planetesimals. As accretion proceeds, the gravitational potential energy gained by the infalling planetesimals increases as the satellite's mass grows. The fraction of this energy that is deposited onto the body (rather than being radiated away) is unknown, but estimates of 0.1-0.4 are frequently used.

Assuming the planetesimals are made of rock and ice, the initial core of Titan would have been mixed (since the core was unmelted), but the outer layers, depositing more energy would have melted and differentiated. This would lead to an unstable situation with the rock-ice core overlain by rock in turn covered by a warm water/ammonia magma ocean. The core would soon overturn, with most silicates falling to the core, and the outer layers consisting mostly of ice. Following this scenario, it would follow that the silicates on the surface suggested by Coustenis et al. (1994) are of more recent origin, having been deposited on the surface after the magma ocean began to freeze.

Note that the incorporation of large amounts of methane clathrate and water/ammonia ices was suggested by Lewis (1971). The vapour pressure of ammonia over a warm water/ammonia magma ocean would be significant, and photolysis of this ammonia is the most likely source of the thick nitrogen atmosphere on Titan: see, for example, Lunine (1989) for a more extensive discussion.

If the nitrogen was formed by photolysis of ammonia released from ices, it is expected (Lunine, 1990) that argon should be a minor (<1%) constituent, since argon would have competed

unfavourably with methane for trapping sites in the ice. On the other hand, if the atmospheric nitrogen has its origin as molecular nitrogen in the preplanetary nebula, solar abundance considerations suggest an argon-to-nitrogen ratio of the order 1-10%. Current observations have been unable to discriminate between these two scenarios, although Huygens GCMS will determine the atmospheric composition accurately.

One important discrepancy between theory and observation is the small amount of CO in Titan's atmosphere. If, instead of forming from NH_3, the nitrogen is primordial, then there should also be 1-20 bar of CO on Titan. Some mechanism to destroy this is required, and it is not clear that photolysis (into CO_2, which would form a ~100 m thick layer of solid) is adequate (Owen 1987, Lunine 1989). A significant CO atmosphere might be expected if the atmosphere was delivered by late-veneer impactors (Zahnle et al. 1992), since CO is found in comets, however, these authors suggest that although the CO destruction mechanism is unknown, it must exist. Although many opinions are leaning toward the NH_3 orgin of the atmosphere, the question is still an open one.

The D to H ratio is another diagnostic of Titan's history, as are other isotopic ratios. D/H on Titan is enriched by ~7 relative to solar abundances, and is similar to that in comets or terrestrial seas. Pinto et al. (1986) considered various enrichment mechanisms, and found that the largest potential enrichment is by atmospheric evolution by photochemistry, although such a large enrichment seems unlikely. One mechanism that neatly explains the D/H ratio is that the atmosphere is made of cometary material - i.e. the atmosphere was formed by volatiles brought by a late veneer of impactors (Zahnle et al. 1992.)

If argon is present, its isotope ratio is also an important constraint on evolution : Ar^{36} is primordial, while Ar^{40} is produced by the decay of potassium. Its presence in the atmosphere implies that gases from the interior can reach the surface - Ar^{40} is a tracer of the coupling between the interior of a body and its atmosphere, via volcanism perhaps. If Titan's atmospheric methane was supplied from the interior (Lunine and Stevenson, 1987), then we might expect it to coexist with, and be released by the same mechanisms as, radiogenic argon.

Such gas release could be quite gentle, occurring at the base of the regolith, hidden from view. On the other hand, it is tempting to speculate on volcanic activity, especially after the detection of active geysers on Triton, which in many respects resembles a cold Titan, with its atmosphere frozen (much, indeed, as Titan's atmosphere may have been in the past (McKay et al. 1993, Lunine and Rizk, 1989)).

Ammonia-water cryovolcanism on the surface relies on the crust being more dense than the magma: i.e. containing a significant silicate component. It is difficult to imagine water-ammonia cryovolcanism producing an anhydrous silicate surface as suggested by Coustenis (1994): first silicates would make the magma less buoyant, and second it is difficult to see how they could remain unhydrated if they are intimately mixed with aqueous liquids.

Once scenario for a silicate-rich crust involves the deposition of the bulk of the material from a large proto-Hyperion. Hyperion is believed (Smith et al., 1981) to be a collisional remnant of a much larger body, and most of the debris from the fragmentation event would have fallen onto Titan (Farinella et al. 1990), leading to a resurfacing of Titan with a rock-ice layer with thickness of a few hundred metres to ~8km (Lorenz, 1993; Lara et al. 1994).

9.8 Conclusions

Modelling of Titan's surface has been, and remains, a powerful tool for identifying gaps in our knowledge that need to be filled by observation. On one hand, models make remarkable predictions about Titan's surface and atmosphere , and fuel our enthusiasm for making closer examination of Titan, perhaps to find whitecap mountains, ring-shaped lakes, or an abundance of watery meteoroids raining into the atmosphere. On the other hand, models are susceptible to small changes in parameters, many of which have to be guessed. There is a great temptation to 'tune' a model to obtain a desired conclusion : models, like the scientists who build them, are subjective.

This subjectivity is a crucial point: we as humans base our views and approaches on our experiences and associations. Just as 'microscopic' phenomena such as condensation can affect the output of photochemical models, so can such trivia as a worker's previous affiliation affect his/her success in tracking down information.

How to deal with this subjectivity? In the absence of unambiguous data, the only way of attempting to obtain some kind of objectivity is by a diversity of opinions, and the free and open exchange thereof. It is the richness of diversity of backgrounds and opinions that makes working in this field so interesting.

Chapter 10

Conclusions

Where oil is first found, in the final analysis, is in the minds of men. The undiscovered oil field exists only as an idea in the mind of some oil finder. When no man any longer believes more oil is left to be found, no more oil fields will be discovered, but so long as a single oil-finder remains with a mental vision of a new oil field to cherish, along with the freedom and incentive to explore, just so long new oil fields may continue to be discovered

Wallace Pratt

Towards a Philosophy of Oil-finding

At a scientific level, this thesis has reviewed our knowledge of Titan from models and available data, and found it to be intriguing, but sorely lacking. The next step, then is to obtain more data, and the capabilities of instruments currently under development have been examined. While, as history shows us, the data to be returned in the middle of the next decade will probably raise yet more questions, the most pressing debates on Titan's surface and atmosphere will be resolved. The development of new impact and acoustic instruments has been described, and these offer excellent prospects for providing useful data.

More philosophically, an unexpected conclusion in an interplanetary endeavour that includes the efforts of thousands of workers and billions of dollars processed through faceless bureaucracies, is the remarkable role played by individuals. Not only theoretical paradigms, but also the shape of investigations, and even such tangible engineering aspects as the configuration or type of instruments or the shape of connectors used, can be traced to the preferences, previous experiences, or even 'best guesses' of individuals. Although in engineering there may notionally be some 'most efficient' way of fulfilling requirements, and even (as discussed in chapter 6) some objective way of assessing scientific investigations may exist, it is as it should be that individuals play significant parts, albeit imperfect ones. Exploration is an expression of the human spirit: to undertake exploration in some mechanistic, optimised fashion would be to deny the pleasure and reward that exploration and discovery bring.

Of the three elements in the exploration triad mentioned in the introduction, the most fundamental is that of the mental paradigm. Data from earth-based instruments or in-situ probes means little while it is locked in magnetic tape, or tables or graphs in some journal. It only becomes worthwhile when a concept or picture takes root in the mind of people. Such thoughts

may blossom, prompting further models or investigations, which in turn may seek further observational data. The shorter turnaround time for observational versus in-situ measurements means that for the most part, the former are what are used to constrain evolving models. In this sense, observations represent an intermediate step between the (mental) start of an investigation, and its resolution by in-situ measurement. All three elements are indispensible: it is models and mental pictures which tell us which bodies are interesting enough to merit expensive in-situ investigation. This expensive and time-consuming enterprise seeks constraints from observations (e.g. the wind direction on Titan) to make it practicable, although ironically it suffers from additional constraints imposed upon it by policymakers.

Despite the formidable technical and programmatic difficulties and risks involved in in-situ investigation, compared with the sedate and unrestricted fields of modelling and observation, I am led to concur with Mr Huygens, who says in the closing words to 'The Celestial Worlds Discover'd' (Huygens, 1698):

But indeed all the whole story of Comets and Planets, and Production of the World, is founded upon such poor and trifling grounds, that I have often wonder'd how an ingenious man could spend all that pains in making such fancies hang together. For my part, I shall be very well contented, and shall count that I have done a great matter, if I can but come to any knowledge of the nature of things, as they now are, never troubling my head about their beginning, or how they were made, knowing that to be out of the reach of human Knowledge, or even Conjecture.

While remote observations have made remarkable contributions to our understanding of Titan's atmosphere, they have provided only the most tantalising hints of what the surface may be like. Similarly, modelling of the surface evolution processes (admittedly both instructive and fun) has only made speculations about Titan's surface more educated than they might otherwise be; they remain, as Huygens says, 'fancies'.

Ultimately, then, the only way to know the true nature of Titan's surface is to go there, or at least send our automated proxy, the Huygens probe. I regard it as an exciting privilege to have been involved in its development.

References

Abbiss C P, Knobler C M, Teague R K and Pings C J, Refractive Index and Lorentz-Lorenz Function for Saturated Argon, Methane and Carbon Tetrafluoride, *J. Chem. Phys.* vol.42 pp.4145-4147, 1965

Achtermann E, Kapp R and Lehra H, Parachute Characteristics of Titan Descent Modules, ESA CR(P)2438, February 1986

Aerospatiale , Huygens Hardware Design Report, HUY-AS/c-100-RP-0180 (NB Project Document - circulation may be restricted) 1994

Allison M A, An Assessment of Titan's Boundary Layer, Symposium on Titan, Toulouse, September 1991 *ESA SP-338* pp.113-118, 1992

Atkinson D H, Pollack J B and Seiff A, Measurement of a Zonal Wind Profile by Doppler Tracking Cassini Entry Probe, *Radio Science* vol.25 pp.865-881, 1990

Badoz J, Nahoum R, Israel G and Raulin F, Experimental Determination of the Refractive Index of Liquified Gas Mixtures. Applications to Hypothesized Titan Oceans, *ESA SP-338*, pp.303-305, 1992

Baines K H , Brown R M, Matson D L, Nelson R M, Buratti B J, Bibring J-P, Langevin Y, Sotin C, Carusi A, Coradini A, Clark R N, Combes M, Drossart P, Sicardy B, Cruikshank D P, Formisano V and Jaumann R, VIMS/Cassini at Titan: Scientific Objectives and Observational Scenarios, ESA SP-338, pp.215-219, 1992

Balburnie C (producer), Design for An Alien World, programme TV5 in S281 course 'Images of the Cosmos', BBC Televison, Milton Keynes, 1994

Beckman J and Scoon G E N, Project Cassini - A Potential Collaborative ESA/NASA Saturn Orbiter and Titan Probe Mission, IAF-85-396, also published in *Acta Astronautica*, Vol.14 pp.185-194, 1986

Birchley, P N W, Development of a Refractometer and Thermal Properties Instrument for the Cassini Mission, PhD Thesis, University of Kent, 1992

Birchley P N W, Daniell P M, Zarnecki J C, Parker D J, Laboratory Determination of the Thermal Conductivity of Liquid Methane and Ethane, *ESA SP-338*, pp.311-314, 1992

Birchley P N W, Wright M J, Zarnecki J C, Ratcliff P R and Mill C S, Laboratory Determination of the refractive indices of Liquid Methane and Ethane at Temperatures Appropriate to the Surface of Titan, *ESA SP-338*, pp.307-310, 1992

Blamont J, A Method of Exploration of the Atmosphere of Titan, in D M Hunten and D Morrison (eds), The Saturn System, NASA CP-2068, 1978

Borucki W J and Fulchignoni M, Huygens-ASI Capabilities for Aerosol Measurements, in *ESA SP-338*, 1992

Broadfoot A L, Sandel B R, Shemansky D E, Holberg J B, Smith G R, Strobel D F, McConnell J C, Kumar S, Hunten D M, Atreya S K, Donahue T M, Moos H W, Bertaux J L, Blamont J E, Pomphrey R B, Linick S, Extreme Ultraviolet Observations from Voyager 1 Encounter with Saturn, *Science*, vol.212 pp.206-211, 1981

Broch J T, Acoustical Sensors for the Huygens Probe - The Acoustic Altimeter, Sintef/Delab report STF40 F91179, December 1991

Brown G S, The Average Impulse Response of a Rough Surface and Its Applications, *IEEE Transactions on Antennas and Propagation* AP-25, pp.67-74, 1977

Budden N A, Spudis P D, Evaluating Science Return in Space Exploration Initiative Architectures, NASA Tech. Paper 3379, 1993

Calcutt S, Taylor F, Ade P, Kunde V and Jennings D, The Composite Infrared Spectrometer, *Journal of the British Interplanetary Society*, vol.45 pp.811-816, 1992

Caldwell J , Cunningham C C, Anthony D, White H P, Groth E J, Hasan H, Noll K , Smith P H, Tomasko M G and Weaver H A, Titan: Evidence for Seasonal Change - A Comparison of HST and Voyager Images, *Icarus*, v.97 pp.1-9, 1992

Castelli A and Cornaro C, A Temperature Sensor for the Cassini/Huygens Probe, ASI Science meeting, Paris March 7-8, 1991

Castro A J, Titan Probe Technology Assessment and Technology Development Plan Study, NASA CR-152381, 1980

Chicarro A F, Coradini M, Fulchignoni M, Liede I, Lognonne P, Knudsen J M, Scoon G E N, Wanke H, Marsnet Assessment Study Report, ESA SCI(91)6, 1991

Ciarlo A and Schilling K, Application of Expert System Techniques to the Cassini Titan Probe, *ESA Journal* vol.12, pp.337-351

Clarke A C, Imperial Earth, Victor Gollancz, London, 1975

Collar P G, Packwood A R and Blane D D, Autosub - The NERC Community Research Project to Develop Autonomous Underwater Vehicles for Marine Science in the Deep Ocean, in proceedings of Oceanology Technology '90, Brighton, March 1990

Comoretto G, Bertotti B, Iess L and Ambrosini R, Doppler Experiments with the Cassini Radio System, *Il Nuovo Cimento*, vol.15C pp.1193-1198, 1992

Coustenis A , Spatial Variations of Temperature and Composition in Titans Atmosphere: Recent Results *Annales Geophysicae* vol.8 p.645-652, 1990

Coustenis A, Bezard B and Gautier D, Titan's atmosphere from Voyager Infrared observations. I. The gas composition of Titan's equatorial region, *Icarus*, vol.80, pp. 54-76, 1989

Coustenis A, Bezard B and Gautier D, Titan's Atmosphere from Voyager 1 Infrared Observations II. The CH_3D Abundance and D/H Ratio from the 900-1200 cm^{-1} Spectral Region, *Icarus* vol.82, pp.67-80, 1989

Coustenis A, Lellouch E, Maillard J P and McKay C P, Titan's Surface: Composition and Variability from the Near Infrared Albedo, Icarus (submitted) 1994

Coustenis A, Schmitt B, Samuelson R E and Khanna R K, Water Ice and Other Condensates in Titan's Stratosphere, submitted, 1994

Coustenis A,Bezard B, Gautier D and Marten A, Titan's Atmosphere from Voyager 1 Infrared Observations III. Vertical Distributions of Hydrocarbons and Nitriles near Titan's North Pole, *Icarus* vol.89, pp.152-167, 1991

Croft T A, Surface Reflections of Pioneer Venus Probe Radio Signals, *Geophysics Research Letters*, vol.7 pp.521-524, 1980

Cruikshank D P, The Development of Studies of Venus, in D M Hunten et al. (eds) Venus, University of Arizona Press, 1983

Desch M D and Kaiser M L , Upper Limit Set on Level of Lightning Activity on Titan, *Nature*, vol.343, pp.442-444,, 1990

Dorrington G E, Development of Human Powered Airships at Southampton 1991-1993, International Airship Conference , Stuttgart, Germany, June 1990

Dubouloz N, Raulin F,Lellouch E and Gautier D, Titan's Hypothesized Ocean Properties: The influence of Surface Temperature and Atmospheric Composition Uncertainties' *Icarus* 82 pp.81-96, 1989

Elachi C , Eastwood I M , Roth V L and Werner C L , Cassini Titan Radar Mapper, *Proceedings of the IEEE* vol.79 pp.867-879, 1991

English M A, Lara L M, Lorenz R D, Ratcliff P R and Rodrigo R, Ablation and Chemistry of Meteoric Materials in the Atmosphere of Titan, *Advances in Space Research*, submitted, 1994

ESA, Proposal to Place a Contract, ESA/IPC(90)129, 30 October 1990

ESA, Cassini Mission : Huygens Probe. Announcement of Opportunity, ESA SCI(89)2, October 1989

Eshleman V R , Radar Glory from Buried Craters on Icy Moons, *Science* vol.234 pp.587-590, 1986

Eshleman V R, The Radar-Glory Theory for Icy Moons with Implications for Radar Mapping, *Advances in Space Research* vol.7 No.5 pp.(5)133-(5)136, 1987

Eshleman V R, Lindal G F andTyler G L, Is Titan Wet or Dry, *Science* vol.221 pp.53-55, 1983

Fabris M, Marzari F, and Vanzani V, Titan's Atmospheric Structure from Huygens-ASI Measurements, *ESA SP-338*, pp.339-342, 1992

Farinella P, Paolicchi P , Strom R G, Kargel J S and Zappala V, The Fate of Hyperion's Fragments, *Icarus* vol 83 pp.186-204, 1990

Flasar F M, Oceans on Titan, *Science* vol.221 pp.55-57,1983

Flasar F M and Conrath B J , Titan's Stratospheric Temperatures: A Case for Dynamic Inertia?, *Icarus* vol.85, pp.346-354, 1990

Flasar F M, Samuelson R E and Conrath B J , Titans Atmosphere: temperature and dynamics, *Nature* vol.292 pp.693-698, 1981

Formisano V, Adriani A and Bellucci G, The VNIR-VIMS Experiment for CRAF-Cassini, *Il Nuovo Cimento*, vol.15C, pp.1179-1192, 1992

Friedlander A L, Titan Buoyant Station, *J. Brit. Interplan. Soc.*, v.37, pp.381-387, 19841959

Friedlander A L, Buoyant station Mission Concepts for Titan Exploration, IAF-85-417, 1985

Froidevaux F and Ingersoll A P, Temperatures and Optical Depths of Saturn's Rings and a Brightness Temperature for Titan, *Journal of Geophysical Research*, vol.85 pp.5929-5936

Fulchignoni M, The Atmosphere of Titan and the Huygens Atmospheric Structure Instrument, *Il Nuovo Cimento* vol.15C pp.1163-1177, 1992

Furlong R, Cassini RTG Program: Cassini Project Review, in Cassini Project Mission and Spacecraft system delta preliminary design review (D-PDR), JPL 1699-0135, 1992

Geake J E and Firth C S, The Huygens SSP Refractometer, *ESA SP-338*, pp.343-346, 1992

Gibbons A, Has Challenger knocked out Galileo?, *Science* vol.253 pp.846-847, 1991

Goldstein R M and Green R R, Ganymede: Radar Surface Characteristics, *Science* vol.207, pp.179-180, 1980

Grard R J L, The significance of Meteroic Ionisation for the Propagation of Lightning Spherics in the Atmosphere of Titan, *ESA SP-338* pp.125-128, 1992

Grard R J L, A quadrupolar array for measuring the complex permitivity of the ground: application to Earth prospection and planetary exploration, *Measurement Science and Technology*, vol.1 pp.295-301, 1990a

Grard R J L, A quadrupole system for measuring in situ the complex permittivity of materials: application to penetrators and landers for planetary exploration, *Measurement Science and Technology*, vol.1 pp.801-806, 1990b

Grard R J L, Svedhem H, Brown V, Falkner P and Hamelin M , An Experimental Investigation of Atmospheric Electricity and Lightnign Activity during the Descent of the Huygens Probe on Titan, submitted 1993 .

Greeley R, Planetary Landscapes, Unwin Publishers, Winchester USA, p.66, 1987

Griffith C A, Evidence for surface heterogeneity on Titan, *Nature* vol.364 pp.511-514 , 1993

Griffith C A and Owen T C, Observing the Surface of Titan through Near-Infrared Windows in its Atmosphere, *ESA SP-338*, pp.199-204, 1992

Griffith C A, Owen T and Wagener R, Titans Surface and Troposphere, Investigated with Ground-Based, Near-Infrared Observations, *Icarus* 93 pp.362-378, 1991

Grossman A W and Muhleman D O, Observations of Titan's Radio Light-Curve at 3.5cm., (abstract) *Bull. Amer. Astron. Soc.* vol.24 No 3 p.954, 1992

Grundy W, Lemmon M, Fink U, Smith P and Tomasko M, Windows Through Titan's Atmosphere, (abstract) *Bulletin of the American Astronomical Society* vol.23 p.1186, 1991

Gurnett D A, Grun E, Gallagher D, Kurth W S and Scarf F L, Micron-sized particles detected near Saturn by the Voyager plasma wave instrument, *Icarus*, vol.53, p.236 ,1983

Gurrola E M and Eshleman V R, On the Angle and Wavelength dependencies of the radar backscatter from the icy Galilean moons of Jupiter, *Advances in Space Research* vol.10 No.1 pp.(1)195-(1)198, 1990

Hagfors T, Gold T and Ieric H M, Refraction Scattering as origin of the anomalous radar returns of Jupiter's Satellites, *Nature* vol.315, p.637-640, 1985

Hanel R , Conrath B, Flasar F M, Kunde V, Maguire W, Pearl J, Pirraglia J, Samuelson R, Herath L, Allison, M, Cruikshank D, Gautier D, Gierasch P, Horn L, Koppany R, and

Ponnamperuma C, Infrared observations of the Saturnian system from Voyager 1, *Science* vol.212 pp.192-200, 1981

Hapke B and Blewett D , Coherent backscatter model for the unusual radar reflectivity of icy satellites, *Nature* v.352, pp.46-47, 1991

Hassan H, McCarthy C and Wyn-Roberts D, Huygens - A Technical and Programmatic Overview, *ESA Bulletin* 77, pp.21-30, 1994

Healy G J, Aircraft Far-Field Aerodynamic Noise: Its Measurement and Prediction, in I R Schwartz, H T Nagamatsu and W C Strahle (eds, Aeroacoustics: STOL noise; airfrane and airfoil noise, Vol.45 in Progress in Astronautics and Aeronautics, 1975

Hechler F, Cassini-Huygens Interplanetary Trajectories and Initial Orbits about Saturn, MAS Working Paper No.307, ESOC, 1990

Hill R D, Thunder, pp.385-406 in Golde R H (ed), Lightning, vol.1, Academic Press, 1977

Hubbard W B , Hunten D M, Reitsema H J, Brosch N, Nevo Y, Cerreira E, Rossi F and Wasserman L H,, Results for Titan's Atmosphere from its Occultation of 28 sagitarii, *Nature*, vol.342, pp.353-355, 1990

Hubbard W B, Sicardy B , Miles R, Hollis A J, Forrest R W, Nicolson I K M, Appleby G, Beisker W, Bittner C, Bode H-J, Bruns M, Dezau H, Nezel M, Riedel EE, Struckman H, Arlot J E, Roques F, Sevre F, Thuillot W, Hoffman M, Geyer E H, Buil C, Colas F, Lecacheux J, Klotz A, Thouvenot E, Vidal J L, Cerreira E, Rossi F, Blanco C, Cristaldi S, Nevo Y, ReistsemaH J, Brosch N, Cernis K, Zdanavicius K, Wasserman L H, Hunten D M, Gautier D, Lellouch E, Yelle R V, Rizk F, Flasar F M, Porco C C, Toublanc D and Corugedo G, The Occultation of 28-Sgr by Titan, *Astronomy and Astrophysics* vol.269, No.1-2 pp.541-563, 1993

Humes D H, Results of Pioneer 10 and 11 Meteoroid Experiments: Interplanetary and Near-Saturn, *Journal of Geophysical Research,* vol.85 No.A11 pp.5841-5852, 1980

Hunten D M, The Atmosphere of Titan, NASA SP-340, 1974

Hunten D M, A Titan Atmosphere with a Surface Temperature of 200K, in The Saturn System, NASA CP 2068, pp.127-140, 1978

Hunten D M, The Thermal Structure of the Atmopshere of Titan, Proceedings of the Symposium on Titan, Toulouse September 1991 (*ESA SP-338*) pp.37-40, 1992

Hunten D M, Tomasko M G, Flasar F M, Samuelson R E, Strobel D F and Stevenson D J, Titan in Gehrels and Matthews (eds) Saturn, University of Arizona Press, Tucson, 1984

Huygens C , De Saturnii Luna Observatio Nova, March 1656

Huygens C, The Celestial Worlds Discover'd, 1698

Ip W H, Gautier D et al., Project Cassini: A Proposal to the European Space Agency for a Saturn Orbiter/Titan Probe Mission, 15th November 1982

Isbell D, Budget Alarms Scientists, *Space News* vol.3 No.5 February 10-16, 1992

Israel G, Chassefiere E, Niemann H B, Boon J J, Muller C, Raulin F, Cabane M, and Sable C, Huygens/ACP: An Instrument for Aerosols Chemical Composition Measurements, *ESA SP-338,* pp.225-228, 1992

Jaffe W, Caldwell J and Owen T, Radius and Brightness Temperature Observations of Titan at Centimetre Wavelengths by the Very Large Array, *Astrophysical Journal*, v.242, pp.806-811, 1980

Jeans J H , Dynamical Theory of Gases, 4th ed. pp.346-348, Cambridge 1925

Johnson T V and Gautier D, Saturn Orbiter/Titan Probe Mission, in Planetary Science in Europe, European Science Foundation, 1992

Kamoun P , Anne J C and Ford P, ASTRA : Altimetry and Sounding of Titan with a radar on a descending craft, Proceedings International Symposium on Radars and Lidars in Earth and Planetary Sciences, Cannes, France 2-4 September, 1991 (*ESA SP-328*) pp.71-78 ,1992

Kim S J and Caldwell J , The abundance of CH_3D in the atmosphere of Titan, derived from 8- to 14-micron thermal emission, *Icarus* vol.52, 473-482, 1982

Kohlhase C, Meeting with a majestic Giant, *The Planetary Report* vol.13, July 1993

Kouvaris L C and Flasar F M, Phase Equilibrium of Methane and Nitrogen at Low Temperatures: Application to Titan, *Icarus* vol.91 pp.112-124, 1991

Ksanfomality L V, Scarf F L and TaylorW W L , The Electrical Activity of the Atmosphere of Venus' in D M Hunten et al. (eds) 'Venus' University of Arizona , 1983a

Ksanfomality L V, Goroshkova N V and Khondryev V K, Wind Velocity Near the Surface of Venus form Acoustic Measurements, *Cosmic Research* vol.21 pp.161-167 (translated from *Kosmicheskii Issledovania* vol.21 pp.218-224), 1983b

Kuiper G P, Titan - A Satellite with an Atmosphere, *Astrophysical Journal*, vol.100 pp.378-383, 1944

Lara L M, Estudio Fotoquimico de los componentes neutros de la atmosfera de Tita, PhD Thesis, University of Granada, Spain, 1993

Lara L M, Lorenz R D and Rodrigo R, Liquids and Solids on the Surface of Titan, *Planetary and Space Science*, vol.42 pp.5-14, 1994 (Appendix 6)

Lebreton J-P , The Huygens Probe, Proceedings of the Symposium on Titan, Toulouse, 9-12 September 1991, *ESA SP-338* pp.287-292, 1992

Lebreton J-P and Matson D, Cassini - A Mission to Saturn and Titan, Proceedings of 24th ESLAB Symposium on the Formation of Stars and Planets and the Evolution of the Solar System, Freidrichshafen 17-19 September 1990 (*ESA SP-315*) pp.7-12, 1990

Lebreton J-P and Matson D L, An overview of the Cassini Mission, *Il Nuovo Cimento* vol.15C, pp.1137-1147, 1992

Lebreton J-P and Scoon G E, Cassini - A Mission to Saturn and Titan, *ESA Bulletin* 55, pp.24-30, 1988

Leigh B R, Using the Momentum Method to Estimate Aircraft Ditching Loads, *Canadian Aeronautics and Space Journal*, vol.24 pp.162-168, 1988

Lellouch E and Hunten D M, Titan Atmosphere Engineering Model, ESLAB 87/199, ESA Space Science Department, 1987

Lellouch E, Hunten D M , Kockarts G and Coustenis A, Titan's Thermosphere Profile, *Icarus*, vol.83, pp.308-324, 1990

Lemmon M T, Karkoshka E and Tomasko M, Titans Rotation: Surface Feature Observed, *Icarus* vol.103 pp.329-332, 1993

Lemmon M T, Karkoshka E and Tomasko, M, Titan's Rotational Lightcurve, *Icarus* (submitted) 1994

Letourneur B and Coustenis A, Titan's Atmosphere from Voyager 2 Infrared Spectra, *Planetary and Space Science*, vol.41 pp.593-602, 1993

Lewis J S, Satellites of the Outer Planets: Their Physical and Chemical Nature, *Icarus* vol.15 pp.174-185, 1971

Li M and Vitanyi P, An Introduction to Kolmogorov Complexity and Its Applications, Springer-Verlag, New York, 1993

Lindal G F, Wood G E, Hotz H B, Sweetnam D N, Eshleman V R and Tyler G L, The Atmosphere of Titan: An analysis of the Voyager 1 Radio Occultation Measurements, *Icarus*, vol.53, pp.348-363, 1983

Lingard J S and Underwood J C, Wind Tunnel Testing of Disk-Gap-Band Parachutes Related to the Cassini-Huygens Mission, RAeS/AIAA Aerodynamic Decelerator Systems Technology Conference, AIAA-93-1200, London, May 1993

Lorenz R D, The Huygens Mission to Titan, Estec Internal Working Paper EWP-1628, September 1991

Lorenz R D, Huygens Probe - The Surface Mission, Symposium on Titan, Toulouse, September 1991, *ESA SP-338* pp.359-364, 1992a

Lorenz R D, Gravitational Tide in the Atmosphere of Titan, Proceedings of the Symposium on Titan, Toulouse, September 1991 (*ESA SP-338*) pp.119-123, 1992b

Lorenz R D, Wake-Induced Dust Cloud Formation following Impact of Planetary Landers, *Icarus* vol.101 pp. 165-167, 1993a (Appendix 3)

Lorenz R D, Scientific Implicationd of the Huygens Probe Parachute System, AIAA-93-1215, 12th RAeS/AIAA Aerodynamic Decelerator Systems Technology Conference, London, May 1993b

Lorenz R D, The Life, Death and Afterlife of a Raindrop on Titan, *Planetary and Space Science*, vol.41 pp.647-655, 1993c (Appendix 4)

Lorenz R D, The Surface of Titan in the Context of ESA's Huygens Probe, *ESA Journal* vol.17 pp.275-292, 1993d (Appendix 5)

Lorenz R D, Huygens Probe Impact Dynamics, *ESA Journal* vol.18 pp.93-117, 1994a (Appendix 8)

Lorenz R D, Crater Lakes on Titan: rings, horseshoes and bullseyes, *Planetary and Space Science*, vol.42 pp.1-4, 1994 b (Appendix 9)

Lorenz R D, Raindrops on Titan, *Advances in Space Research* , vol.15 pp.(3)317-(3)320, 1995

Lorenz R D, Bannister M, Daniell P M, Krysinski Z, Leese M R, Miller R J, Newton G, Rabbets P and Willett D M , An impact penetrometer for a landing spacecraft, *Measurement Science and Technology*, vol.5 pp.1033-1041, 1994 (Appendix 7)

Lorenz R D and Svedhem L H, Acoustic Environment on Titan, poster presented at EGS Conference, Edinburgh, April 1992 (Abstract in *Annales Geophysicae*, vol.10, Supplement No.3, p.C487)

Lorenz R D and Zarnecki J C , Precipitation on Titan and the Methane Icing Hazard to the Huygens Probe, Presented at the European Geophysical Society, Edinburgh, Scotland, April 1992 (Abstract in *Annales Geophysicae*, vol.10, Supplement No.3, p.C487)

Low F Jand Rieke G H, Infrared Photometry of Titan, *Astrophysical Journal*, vol.190 pp.L143-145, 1974

Lucey P G and Clarke R N, Spectral Properties of Water Ice and Contaminants, in J Klinger et al. (eds) Ices in the Solar System, p.155-168, D Reidel Publishing Co. 1985

Lunine J I, Titan's Surface: Nature and Implications for Cassini, in The Atmospheres of Saturn and Titan, *ESA SP-241*, 1985

Lunine J I, Origin and Evolution of Outer Solar System Atmospheres, *Science* vol.241 pp.141-147, 1989

Lunine J I, The Urey Prize Lecture: Volatile Processes in the Outer Solar System, *Icarus*, vol.81, pp.1-13, 1989b

Lunine,J I, Evolution of the Atmosphere and Surface of Titan, *ESA SP-315*, pp.159-165, 1990

Lunine J I, Plausible Surface Models of Titan, *ESA SP-338* pp.233-239, 1992

Lunine, J I, Does Titan Have an Ocean? A Review of Current Understanding of Titans Surface, *Reviews of Geophysics* vol.31 pp.131-149, 1993

Lunine, J I, Does Titan Have Oceans, *American Scientist*, vol.82, pp.134-143, 1994

Lunine J I and Rizk B, Thermal Evolution of Titan's Atmosphere, *Icarus* vol.80, pp.370-389, 1989

Lunine J I and Stevenson D J, Evolution of Titan's Coupled Ocean-Atmosphere System and Interaction of Ocean with Bedrock, in J Klinger et al. (eds), Ices in the Solar System, pp.741-757, Reidel, 1985

Lunine J I and Stevenson D J, Clathrate and Ammonia hydrates at high pressure : Application to the Origin of Methane on Titan, *Icarus* vol.70 pp. 61-77, 1987

Lunine J I, Stevenson D J and Yung,Y L, Ethane Ocean on Titan, *Science* vol.222 pp. 1229-1230, 1983

Lutz B L , DeBergh C and Owen T , Titan: discovery of carbon monoxide in its atmosphere' *Science*, v.220 pp.1374-1375, 1983

Maeda H, Umeda Y and Arihara N, An Ultrasonic Altitude-Velocity Sensor for Airplanes in the Vicinity of the Ground, *Memoirs of the Faculty of Engineering*, Kyoto University vol.32 pp.249-259, 1970

Martin-Marietta, A Titan exploration Study - Science, Technology, and Mission Planning Options (vol.2), NASA-CR-137847, 1976

McCarty J L, Beswick A G and Brooks G W, Application of Penetrometers to the Study of Physical Properties of Lunar and Planetary Surfaces, NASA TN D-2413, 1964

McCarty J L and Carden H D, Impact Characteristics of Various Materials Obtained by an Acceleration-Time-History Technique Applicable to Evaluating Remote Targets, NASA TN D-1269, 1967

McCartney B S, and Collar P G, Autonomous Submersibles - Instrument Platforms of the Future, *Underwater Technology*, vol.15 pp.19-25, 1990

McDonald G D, Thompson W R, Heinrich M, Khare B N and Sagan C, Chemical Investigation of Titan and Triton Tholins, *Icarus*, vol.108 pp.137-145, 1994

McKay C P, Pollack J B and Courtin R, The Thermal Structure of Titan's Atmosphere, *Icarus* vol.80, pp.23-53, 1989

McKay C P, Pollack J B, Lunine J I and Courtin R, Coupled Atmosphere-Ocean Models of Titan's Past, *Icarus*, vol.102, pp.88-98, 1993

Minnaert M, On Musical Air-Bubbles and the Sounds of Running Water, *The London, Edinburgh and Dublin Philosophical Magazine and Journal of Science* vol.16, pp.235-248, 1933

Mitchell B J, Conceptual Design of a modified XBT Telemetry System for Use in the Oceans of Titan, submitted to International Telemetry Conference, 1994

Mooij E, De Cassini-missie, *Ruimtevaart* June 1992 pp.2-8, 1992

Mordaunt D H, Lambert I R, Morley G P, Ashfold M N R, Dixon R N, Western C M, Schneider L and Welge K H, Primary product channels in the photodissociation of methane at 121.6nm, *J. Chem. Phys*, vol.98, pp2054-2065, 1993

Muhleman D O, Grossman A W, Butler B J and Slade M A, Radar Reflectivity of Titan, *Science* vol.248 pp.975-980, 1990

Muhleman D O, Grossman A W , Slade M A and Butler B J, The Surface of Titan and Titan's Rotation: What is Radar Telling Us?, *Bull. Amer. Astron. Soc.* vol.24 No.3, 1992

Muhleman D O, Grossman A W, Slade M A and Butler B J, Titan's Radar Reflectivity and Rotation, *Bulletin of the American Astronomical Society*, vol. 25, p1099, 1993

Murphy J P, Cuzzi J N, Butts A J, and Carroll P C, Entry and Landing Probe for Titan, *J. Spacecraft and Rockets*, vol.8 pp.157-163, 1981

Murray C D, The Cassini Imaging Science Experiment, *Journal of the British Interplanetary Society*, vol.45 pp.359-364, 1992

Murrow D W, Cassini Mission Plan, PD 699-100-2 rev B, JPL, May 1993

NASA/ESA , Cassini - Saturn orbiter and Titan Probe, ESA/NASA Assessment Study, ESA SCI(85)1, August 1985

NASA/ESA, Cassini, Supplement to the Assessment Study, ESA SCI(86)5, December 1986

NASA/ESA, Cassini Phase A study ESA/SCI 88(5)

Neal M F andWellings P J, Descent Control Subsystem for the Huygens Probe, !2th RAeS/AIAA Aerodynamic Decelerator Systems Technology Conference, AIAA-93-1221, London, May 1993

Nelson H F, Park C and Whiting E E, Titan Atmospheric Composition by Hypervelocity Shock Layer Analysis, AIAA 24th Thermophysics Conference, AIAA-89-1770, Buffalo, June 1989

Ness N F, Acuna M H, Lepping R P, Connery J E P, Behannon K W abd Burlaga L F, Magnetic Field Studies by Voyager 1: Preliminary Results at Saturn, *Science*, vol.212 pp. 211-217, 1981

Newton G P, Cassini Mission Project Penetrometer, Final Year Project Report (Physics with Computing) University of Kent, 1994

Noll K S and Knacke R F, Titan: 1-5um photometry and spectrophotometry and a search for variability, *Icarus* vol.101 pp.272-281, 1993

Oberbeck V R, O'Hara D and Carle G C, Concepts for Collection of Aerosols in Titan's Atmosphere, *Journal of Geophysical Research*, vol.92 No.B4 pp.E717-E722, 1987

Ostro S J , Campbell D B, Simpson R A, Hudson R S, Chandler J F, Rosema K D, Shapiro I I, Standish E M, Winkler R, Yeomans D K, Velez R and Goldstein R M, Europa, Ganymede, and Callisto: New Radar Results From Arecibo and Goldstone, *Journal of Geophysical Research*, vol.97 No.E11 pp.18,227-18,244, 1992

Ott S, Analysis of the Targeting Requirements for the Huygens Mission, Estec Internal Working Paper EWP-1640, December 1991

Ott S, Cassini Mission : The Targetting of the Huygens Probe, IAF-92-0067 Presented at the World Space Congress, Washington DC, September 1992

Owen T, How Primitive are the Gases in Titan's Atmosphere, *Advances in Space Research*, vol.7 pp.51-54, 1987

Owen T and Gautier D, Titan: Some New Results, *Advances in Space Research*, vol.9 pp.(2)73-(2)78, 1989

Peale S J, Cassen P and Reynolds R T, Tidal Dissipation, Orbital Evolution and the Nature of Titan's Inner Satellites. *Icarus* 43 pp.65-72, 1980

Picardi G, Seu R , Coradini A, Zampolini E and Ciaffone A, The Radar System for the Exploration of Titan, *Il Nuovo Cimento*, vol.15C pp.1149-1161, 1992

Pinto J P, Lunine J I, Kim S J and Yung Y L, D to H ratio and the origin and evolution of Titan's Atmosphere, *Nature* vol.319, pp.388-390, 1986

Pouliquen M, 1992, Space Transportation Systems, Presentation at International Space University (Engineering Department) Summer Session, Kitakyushu, Japan.

Pollack J B, Atkinson D H, Seiff A and Anderson J D, Retreival of a Wind Profile from the Galileo Probe Signal, *Space Science Reviews*, vol.60 pp.143-178, 1992

Powell G, Schurmeier B and Murray B, Measuring Speed on the Mars-96 balloon guiderope System, IAF-93-U.6.585, presented at 44th International Astronautical Federation Congress, Graz, Austria, October 1993

Prange R, The Cassini Mission - Complementary Observations with the Space Telescope, in The Atmospheres of Saturn and Titan, *ESA SP-241*, pp.209-217, 1985

R O Fimmel, L Colin and E Burgess, Pioneer Venus, *NASA SP-461* , 1983

Rapley C, Satellite Radar Altimeters, in R A Vaughan (ed), Microwave Remote Sensing for Oceanographic and Marine Weather-Forecast Models, pp.45-63, Kluwer Academic Presss, 1990

Raulin F, Accaoui B, Razaghi A, Dang-Nhu M, Coustenis A and Gautier D, Infrared Spectra of gaseous organics : Application to the atmosphere of Titan - II. Infrared intensities and frequencies of C4 alkenenitriles and benzene, *Spectrochemica Acta* vol.46A, pp.671-683, 1990

Raulin F, Frere C, Paillous P, de Vanssay E, Po L and Khlifi M, Titan and the Exobiological Aspects of the Cassini/Huygens Mission, *Journal of the British Interplanetary Society* vol.45 pp.257-271, 1992

Rebiai R , Rest A J and Scurlock R G, The Unexpectedly High Solubility of Water in Cryogenic Liquids, *Nature* vol.305 pp.412-413, 1983

Rest A J , Scurlock R G and Wu M F, The Solubilities of Nitrous Oxide, Carbon Dioxide, Aliphatic Ethers and Alcohols, and Water in Cryogenic Liquids, *The Chemical Engineering Journal* vol.43 pp.25-31, 1990

Ringwood S D, Looking over Galileo's Shoulder, *Astronomy Now*, vol.8 No.4 , pp.48-52, 1994

Rock W, Auweter-Kurtz M, Dabal P, Fruholz H, Habiger H and S Laure, Experimental Simulation of the Entry of Huygens into the Titan Atmosphere for the Thermal Protection Qualification, IAF-93-I.3.227, IAF Congress, Graz, Austria, October 1993

Rothery D A and Lawrence G, Remote Sensing for the Study of Volcanoes and Earthquakes, *Geoscientist*, vol.3 No.6, 1993

Sable C and Villaeys J, Choix des Materiaux d'enveloppe pour vehicules d'exploration planetaire (Venus-Mars-Titan), in Materials in the Space Environment, *ESA SP-178*, 1982

Sagan C, Structure of the Lower Atmosphere of Venus, *Icarus*, vol.1, pp.151-169, 1962

Sagan C and S F Dermott, The Tide in the Seas of Titan. *Nature* vol. 300 pp.731-733, 1982

SAIC, Titan Exploration with Advanced Systems, a study of future mission concepts, NASA-CR-173499, 1983

Sainct H and Clausen K, Technologies New to Space in Huygens Probe Mission to Titan, IAF-93-U.4.564, Presented at 44th IAF Congress, Graz, Austria, October 1993

Saint-Pe O, Combes M, Rigaut F, Tomasko M and Fulchignoni M, Demonstration of Adaptive Optics for Resolved Imagery of Solar System Objects: Preliminary Results on Pallas and Titan,*Icarus* vol 105, 263-270, 1993

Samuelson R E, Cassini/CIRS Capabilities for Aerosol, Cloud and Surface Measurements, *ESA SP-338*, pp.221-214, 1992

Samuelson R E , Hanel R A, Kunde V G and Maguire W C, Mean Molecular Weight and Hydrogen Abundance of Titan's Atmosphere, *Nature*, vol.292, pp.688-693, 1981

Schmitt B, Quirico E and Lellouch E, Near Infrared Spectra of Potential Solids at the Surface of Titan, *ESA SP-338* pp.383-388, 1992

Schock A, Effect of Mode-Switching on Output of Mariner/Mark-2 RTGs, IAF-92-0571, 43rd IAF Congress, Washington DC, September 1992

Scoon G E , Cassini - A Concept for a Titan Probe, *ESA Bulletin* 41, pp.12-20, 1985

Scoon G, Whitcomb G, Eiden M, and Smith A, Cassini Huygens Entry and Descent Technologies, IAF-89-028, presented at 40th IAF Congress, Malaga, Spain, October 1989

Scrimger J A, Underwater Noise Produced by Precipitation, *Nature* vol.318 pp.647-649, 1985

Sears W, A Numerical model of Tidal Dissipation on Titan, *Icarus*,(submitted) 1994

Sears W, Lunine J I and Greenberg R, Equilibrium Nonsynchronous Rotation of Titan, *Icarus*, v.105 pp.247-252, 1993

Seiff A, The Viking Atmosphere Structure Experiment - Techniques, Instruments, and Expected Accuracies, *Space Science Instrumentation*, vol.2 pp.381-423, 1976

Seiff A, Atmospheres of Earth, Mars and Venus, as Defined by Entry Probe Experiments, *J. Spacecraft and Rockets*, vol.28 pp.265-275, 1991

Seiff A, Juergens D W and Lepetich J E, Atmospheric Structure Instruments on the Four Pioneer Venus Entry Probes, *IEEE Transactions on Geoscience and Remote Sensing*, vol. GE-14, pp.1105-11, 1980

Seiff A and Knight T C D, The Galileo Probe Atmospheric Structure Instrument, *Space Science Reviews*, vol.60, pp.203-232, 1992

Sicardy B, Brahic A, Ferrari C, Gautier D, Lecacheux J, Lellouch E, Roques F, Arlot J E, Colas F, Thuillot W, Sevre F, Vidal J L, Blanco C, Cristaldi S, Buil C, Klotz A and Thouvenot E, Probing Titan's Atmosphere by Stellar Occultation, *Nature*, vol.342 pp.350-353, 1990

Smith B A , Soderblom L, Beebe R, Boyce J, Briggs G, Bunker A, Collins S A, Hansen C J, Johnson T V, Mitchell J L, Terrile R J, Carr M, Cook A F II, Cuzzi J, Pollack J B, Danielson G E, Ingersoll A, Davies M E, Hunt G E, Masursky H, Shoemaker E, Morrison D, Owen T, Sagan C, Veverka J, Strom R and Suomi V E, Encounter with Saturn: Voyager 1 Imaging Science Results, *Science* vol.212 pp.163-191, 1981

Smith K, Titan Probe Options: A study of Future Mission Concepts, B.Eng. Honours report, Department of Aeronautics and Astronautics, University of Southampton, May 1993

Smith P H, The Radius of Titan from Pioneer Saturn Data, *Journal of Geophysical Research*, vol.85 No.A11 pp.3943-3947

Smith P and Lemmon M, HST Images of Titan, (abstract) *Bulletin of the American Astronomical Society* vol.25 p.1105, 1993.

Sohl F, Sears W, and Lorenz R D, Tidal Dissipation on Titan, *Icarus* (submitted July 1994)

Sperling F and Galba J A, Treatise on the Surveyor Lunar Landing Dynamics and an Evaluation of Pertinent Telemetry Data Returned by Surveyor 1' Technical Report 32-1035, Jet Propulsion Laboratory, 1967

Srokosz M A, Challenor P G, Zarnecki J C and Green S F, Waves on Titan, *ESA SP-338*, pp.321-323, 1992

Sromovsky L A, Suomi V E, Pollack J B, Krauss R J, Limaye S S, Owen T, Revercomb H E, Sagan C, Implications of Titan's North-South Brightness Assymetry, *Nature* vol.292, pp.698-702, 1981

Stammes P, The detectability of Titans Surface in the Near-Infrared, *ESA SP-338* pp.205-210, 1992

Stevenson D J, Interior of Titan. Proceeedings of the Symposium on Titan, Toulouse, September 1991 (*ESA SP-338*) pp.29-33, 1992

Stevenson D J and Potter B E, Titan's Latitudinal Temperature Distribution and Seasonal Cycle. *Geophysical Research Letters* vol.13 pp.93-96, 1986

Strobel D F , Hall D T, Zhu X and Summers M E, Upper Limit on Titan Atmospheric Argon abundance, *Icarus* vol.103, pp.333-336, 1993

Stubbs S M, Dynamic Model Investigation of Water Pressures and Accelerations Encountered during Landings of the Apollo Spacecraft, NASA TN D-3980, 1967

Szabo N, Measuring Scientific Value, article 5272 on Usenet newsgroup sci.research, 1994

Tanguy L , Bezard B, Marten A, Gautier D, Gerard E , Paubert G and Lecacheaux A, Stratospheric profile of HCN on Titan from Millimetre observations, *Icarus* vol.85 pp.43-57, 1990

Thompson W R and Sagan C, Far IR and Microwave Remote Sensing of Titan's Methane Clouds and Organic Haze, *Icarus* vol.59, pp.133-161, 1984

Thompson W R and Sagan C, Organic Chemistry on Titan - Surface Interactions, Symposium on Titan, Toulouse, September 1991 *ESA SP-338* pp.167-176, 1992

Thompson W R and Squyres S W , Titan and other Icy Satellites - Dielectric Properties of Constituent Materials and Implications for radar Sounding, *Icarus* vol.86 pp.336-354, 1990

Thompson W R, Zollweg J A and Gabis D H, Vapor-Liquid Equilibrium Thermodynamics of N_2+CH_4: Model and Titan Applications, *Icarus* vol.97 pp.187-199, 1992

Tomasko, M G, Preliminary Results of Polarimetry and Photometry at large Phase Angles from Pioneer 11, *Journal of Geophysical Research,* vol.85 No.A11 pp.5937-5942

Toon O B, McKay C P , Courtin R and Ackerman T P, Methane Rain on Titan, *Icarus* vol.75 pp.255-284, 1988

Toon O B, Mckay C P, Griffith C A and Turco R P , A Physical Model of Titan's Aerosols, *Icarus* vol. 95, pp.24-53, 1992

Tyler G L, Eshleman V R, Anderson J D, Levy G S, Lindal G F, Wood G E and Croft T A, Radio Science Investigations of the Saturn System with Voyager 1: Preliminary Results, *Science* vol.221, pp.201-206, 1981

Ulamec S, Stagiaire Report, ESTEC 1987

Ulamec S, Possible Applications for an Acoustic Instrument aboard the Huygens Probe, ESTEC Internal Report, 1990

Ulamec S, Badoz J and Lebreton J-P, Dielectric Constant Measurements in Simulated Titan Ocean Liquids, *ESA SP-338,* pp.401-405, 1992

Ulamec S and Svedhem L H, Reflection of Acoustic Pulses from a Simulated Titan Liquid Surface, unpublished note 1992

Van Helden A , Saturn through the Telsecope : A Brief Historical Survey, in T Gehrels and M S Matthews (eds), Saturn, University of Arizona Press, pp.23-43, 1984

Van Loef J J, On the Thermal Conductivity of Methane-Ethane Mixtures, *Physica B*, vol.141, pp.213-215, 1986

Velazquez A, Huot J-P and Molina R C, Aerothermodynamics Effects during the Huygens Entry Phase, Symposium on Aerothermodynamics for Space Vehicles (*ESA SP-318* pp.61-66), July 1991

Webster C R, Stratospheric Composition Measurements of Earth and Titan using High-Resolution Tunable Diode Laser Spectroscopy, *J. Quant. Spectrosc. Radiat. Transfer*, vol.40 pp.239-248, 1988

Wenkert D D and Garneau G W, Does Titan's Atmosphere have a 2-day rotation period, (abstract) *Bulletin of the American Astronomical Society* vol.19 p.875, 1987

Wild W J and Fugate R Q, Untwinkling the Stars, *Sky and Telescope*, vol.87 No.6, pp.20-27, 1994

Willett D M, Calibration of Cassini SSP Penetrometer, Third Year Project Report, University of Kent, 1994

Wilson A, Solar System Log, Janes, London 1987

Young C W, The Development of Empirical Equations for Predicting Depth of an Earth-Penetrating Projectile, SC-DR-67-60, Sandia Labs, May 1967

Yung Y L, Allen M and Pinto J P, Photochemistry of the Atmosphere of Titan: comparison between model and observations, *Astrophysical Journal (Supplement Series)* vol.55 pp.465-506, 1984

Zahnle K, Pollack J B and Grinspoon D, Impact-Generated Atmospheres over Titan, Ganymede and Callisto. *Icarus* vol.95 pp.1-23, 1992

Zarnecki J C , Surface Science Package for the Huygens Titan Probe, *Journal of the British Interplanetary Society*, vol.45 pp.365-370, 1992

Zarnecki J C, McDonnell J A M, Green S F, Stevenson T J, Birchley P N W, Daniell P M, Niblett D H, Ratcliff P R, Shaw H A, Wright M J, Cruise A M, Delderfield J, Parker D J, Douglas G, Peskett S, Morris N, Geake J E, Mill C S, Challenor P G, Fulchignoni M, Grard R J L, Svedhem H, Clark B, Boynton W V, A Surface Science Package for the Huygens Titan Probe, *ESA SP-338*, pp.407-409, 1992

Zubrin R, Missions to Mars and the Moons of Jupiter and Saturn Utilizing Nuclear Thermal Rockets with Indigenous Propellants, AIAA-90-0002, 28th Aerospace Sciences Meeting, Reno, Nevada Januray 1990

Zubrin R, The Case for Titan, *Ad Astra*, pp.26-30, June 1991

If Disaster Happens.....

Still mousie, thou art no thy lane
in proving foresight may be vain,
The best-laid schemes o' mice an' men
gang aft agley,
and leave us naught but grief an' pain
for promis'd joy

Robert Burns, Scottish Poet
To a Mouse

The Cassini mission forms the principal reason for the interest of the foregoing thesis. However, the arrival date of 2004 is yet distant, and exploration is a hazardous business. In the early days of planetary exploration (indeed until Voyager [1977] for the US, and Mars 94 [1996] for Russia) spacecraft were launched in pairs, such that if one failed, the other could recover the mission objectives. The financial climate of the 1980s and 1990s (and perhaps a perception that improved spacecraft reliability obviated the need for dual launches) means that only single spacecraft can be afforded today.

Of the many perils that might befall Cassini, the launch is perhaps the most threatening. While catastrophic in-flight anomalies are not unheard-of in planetary missions (c.f. the recent Mars observer failure, attributed either to leak of oxidiser through valves in the pressurisation circuit, or to failure of the spacecraft clocks), they have proven thankfully rare in non-FUSSR deep space missions. However, it is a simple fact that rocket launch vehicles (of any spacefaring nation) have been unable to demonstrate reliabilities in excess of 90-99%.

Concern following the failure of a Titan 4 in 1992 led to the re-examination of the option of launching Cassini and the required Cantaur upper stage on two space shuttle missions, with in-orbit assembly. The examination of this option (which would, by rational accounting practices, not have been cheaper; and little more reliable if at all) was probably to prompt Martin Marietta (the Titan 4 contractor) to improve its efforts. Overall Titan reliability has been 92% (for the 160 launches of all Titan variants until May 1992 (Pouliquen 1992)), and current Titan 4 /Centaur reliability is assessed by NASA Lewis Research Centre as 0.91 (Mark Adler, personal communication 10/5/94).

Thus we may expect a chance, on the order of 8%, that the Cassini mission may end in 1997 in a cloud of debris somewhere between Florida and parking orbit. What would be the implications for Titan exploration?

An obvious response to the destruction of Cassini at launch in 1997 is that flight spare equipment could be assembled into a second, complete Cassini spacecraft, and launched in the

1999 launch opportunity. While not impossible, this seems highly unlikely: the principal technical problem is the unavailability of flight spares for certain elements (e.g. the WAC of the orbiter ISS, itself a Voyager flight spare) and in particular the RTGs and RHUs. Only 4 RTGs (3 for Cassini + 1 spare) are called for in the Cassini RTG programme (Furlong, 1992), and since the lead time for production is >3 years, it seems unlikely that the 1999 opportunity could be met.

Technical considerations, however, would probably not be the driving ones. Stronger arguments are that a rebuild would entail considerable expense, with the second launch alone costing of the order of $500M, a sum that is difficult to imagine could be obtained within a couple of years. The fiscal and technical challenges to build and launch a spare Cassini would require a political committment to space that has not been seen since the Apollo era.

Further, Cassini does not fit in with the 'faster, cheaper, better' doctrine brought to NASA by its administrator Dan Goldin. While Mr Goldin has resisted pressures to cancel Cassini, he has stated publicly that Cassini 'has too much risk', and that such a project would not have been started under his administration. It seems more than likely that other programmes would seize upon the ~$700M Cassini Mission Operations and Data Analysis budget that would effectively be released by the cancellation of Cassini.

Thus a short-term reflight of Cassini seems extremely unlikely. The costs to ESA of a second Huygens probe would be relatively modest (since a full set of spares should exist, except RHUs), and the funds might (after much painful political wrangling) become available for the assembly of a flight spare. However, the probe is useless until delivered to Titan and its data relayed to Earth; without the NASA orbiter, this would require some kind of carrier/relay spacecraft. However, such a spacecraft would still be expensive and the development time (including non-negligible political decision time) would fail to meet the 1999 launch window. It might be further pointed out that the scientific value of an in-situ measurement by the probe without the comprehensive remote-sensing survey made possible by the huge orbiter payload would be relatively modest.

Thus sending Huygens II to Titan seems essentially impossible, even if the carrier could be built light enough to fly on available launchers. Aerothermodynamic considerations would rule out sending the probe Jupiter (and perhaps Venus), but Mars might be marginally achievable (comparing the heat loads and decelerations for shallow entry (γ=-15°) for the MARSNET mission (Chicarro et al. 1991), which has a similar arrival velocity and ballistic coefficient to Huygens). However, even retaining the main parachute, a Huygens descent on Mars would only be a few minutes, and the payload is poorly-optimised for Mars operation : the money for a rebuild and a carrier spacecraft would be better spent on a dedicated small mission to Mars (although using a flight-spare Huygens entry shield might be a cost-saving measure).

A medium-term (say 5-10 years later) development of a new mission to Titan seems improbable, since the Jupiter/Saturn planetary alignment is not ideal, leading to large trip times (~10 years). Long trip times impose severe reliability demands, add operations costs and present problems in providing power (due to decay of the RTG fuel). More importantly, long missions are unattractive on a human level, since those investing effort in the development of the mission are less likely to see its fruition during their careers (whether political, engineering or scientific). Thus, unless there is some unforeseen development in propulsion technology, allowing shorter trip times, there would be a strong temptation to delay launch until planetary alignments became favourable for a more rapid mission.

Thus a second attempt at the exploration of Titan would (and should) probably wait until ~2014, when the availability of a Jupiter gravity assist would allow a large combined orbiter/probe mission with a modest trip time. This also gives enough time for the public outcry at a visible and expensive Cassini failure to decay before development begins. Technological improvements between now and then will probably allow higher payload mass, so perhaps a multiprobe mission (see also the concepts in chapter 4) would be possible. Improved knowledge of Titan's surface and winds from Earth and space-based observation might allow optimisation of probes for land or sea surfaces (perhaps one for each, if observations reveal large landmasses or oceans.)

It is the author's earnest hope, having invested his entire graduate career in the project, that all goes well with Cassini. If the worst should happen, however, we have the consolation of having learned much in the last few years, knowledge that can be usefully applied in improving our next efforts.

Titan has waited 4.5 billion years to reveal her secrets; she would wait another 17.

Appendix 2

List of Conferences and Meetings Attended

International Astronautical Federation Congresses
41st, Dresden, Germany, October 1990
42nd, Montreal, Canada, October 1991
43rd, Washington DC, USA, September 1992
44th, Graz, Austria, October 1993
45th, Jerusalem, Israel, October 1994

European Geophysical Society (EGS)
Edinburgh, Scotland, April 1992
Wiesbaden, Germany, April 1993
Grenoble, France, May 1993

Huygens Science Working Team meetings:
Cannes, France, April 1991
Toulouse, France, September 1991
ESTEC, Noordwijk, The Netherlands, April 1992
ESTEC, Noordwijk, The Netherlands, October 1992
ESTEC, Noordwijk, The Netherlands, October 1993
ESTEC, Noordwijk, The Netherlands, February 1994
DASA, Ottobrun, Germany, October 1994

Athena Coustenis et al. 'Committee for the Investigation of Aerosols' (CIA) meetings
Meudon, October 1992
Meudon, May 1993
Meudon, June 1994

Commitee on Space Research (COSPAR)
Washington DC, USA, September 1992
Hamburg, Germany, July 1994

- Many SSP instrument development meetings
- Royal Astronomical Society/European Astronomical Society Meeting, Edinburgh, April 1994
- International Telemetry Systems Conference, Las Vegas, October 1993
- International Conference of Physics Students (ICPS) Bodrum, Turkey, September 1993
- 12th Royal Aeronautical Society/American Institute of Aeronautics and Astronautics (RAeS/AIAA) Aerodynamic Decelerator Systems Technology Conference, London April 1993
- Workshop on Scientific Preparations for the Cassini/Huygens Mission, Warsaw, Poland
- American Astronomical Society Department of Planetary Sciences (DPS) Munich, Germany, October 1992
- American Geophysical Union (AGU) meeting, Baltimore, USA, May 1994
- Geological Society Planetary Tectonics Meeting, London, May 1994
- Royal Society meeting on Results from Planetary Missions, London, January 1994
- Royal Astronomical Society meeting on Cometary Impacts with the Planets, March 1994
- Huygens Atmospheric Science Instrument Scientific Meeting, Paris, France, March 7-8, 1991
- Symposium on Titan, Toulouse, September 1991
- Symposium on Comparative Planetology and the Origins of Life, Creteil, France, September 1993
- Meeting on the Small Bodies of the Solar System and Their Interaction with the Planets, Mariehamm, Aland, August 1994

Courses Attended

- International Space University, Kitakyushu, Japan, June-August 1992
- 1st European Research Course in Atmospheres, Grenoble, France, January-February 1993
- Austrian Space Agency, Summer School on Comparative Planetology, Alpbach, Austria July 1993

Sites Visited

Morgan Matroc (Vernitron Div., Southampton)	(PZT material for ACC-E)
IGG Ltd (Portsmouth)	(Huygens Parts Procurement)
Irvin (GB) Limited (Letchworth)	(Huygens Parachutes)
Martin-Baker Aircraft Limited (Uxbridge)	(Huygens Descent Control System)
MBA Chalgrove Airfield	(Huygens Parachute drop test)

Faculty of Aerospace Engineering, Delft University of Technology, The Netherlands
Rutherford Appleton Laboratory, Didcot, England
Observatoire de Meudon, Paris, France
Aerospatiale, Cannes, France
Deutsche Aerospace (DASA), Ottobrun, Germany
Lunar and Planetary Laboratory, University of Arizona, Tucson, USA
Deutsche Forschungsanstalt fur Luft- und Raumfahrt , Oberpfaffenhofen, Germany
Laboratoire de Glaciologie et Geophysique de l'Environment, Grenoble, France
Hans Ramberg Tectonics Laboratory, University of Uppsala, Sweden

IRAM 3x15m mm-wave Interferometer, Plateau de Bure, France
IRAM 30m mm-wave telescope, Sierra Nevada, Spain
Nuffield 76m radio telescope, Jodrell Bank, England

Publications Generated

(in addition to those in Reference List)

'Design of the Scientific Payload for the UK Student Rocket ASPIRE' IAF-ST-92-0010, Presented at the IAF Congress, Washington DC, September 1992

'A Deep Jupiter Probe' IAF-93-Q.5-412 (co-authored with D Gautier and J-P Lebreton), Presented at the IAF Congress, Graz, Austria, October 1993

'In-situ exploration of the Kordylewski Clouds' (co-authored with J C Zarnecki) Workshop on Hypervelocity Impacts in Space, Canterbury, July 1991

'Dunes on Titan and their Detectability' (co-authored with J Grier and J Lunine) In Preparation

'Impact Dynamics and Measurements on a Comet Lander' presented at COSPAR meeting, July 1994 and submitted to Advances in Space Research

'Assessment of Lightning and Triboelectric Charging Hazard to the Huygens Probe', to be included in ESA Special Publication on Huygens Probe Environment Models and Payload

'Titan: Unveiling an Icy Giant' to appear in special remote sensing/tectonics issue of 'The Geoscientist'

'Descent and Impact Dynamics of the Huygens Probe' Paper IAF-94-A.1.004, presented at the IAF Congress, Jerusalem, Israel, October 1994

Appendix 3

ICARUS 101, 165–167 (1993)

NOTE

Wake-Induced Dust Cloud Formation Following Impact of Planetary Landers

RALPH D. LORENZ

Unit for Space Sciences, University of Kent, Canterbury, Kent CT2 7NR, United Kingdom

Received May 13, 1992; revised October 2, 1992

Measurements from landers on Venus have indicated dust clouds thrown up at impact. The possibility of similar phenomena occurring on planned Titan and Mars missions is assessed: it is found that the Huygens probe to Titan may observe such a cloud.

Introduction. Landers on planets with significant atmospheres wherever possible use aerodynamic forces to control their descent. Typically at impact they are descending at a terminal velocity, where the aerodynamic drag equals their weight. Thus momentum is continuously being transferred to the atmosphere; this momentum transfer manifests itself as a wake behind the descending craft.

During the landing of the Soviet Venera 9 and 10 spacecraft on Venus, sudden drops in the light intensity measured by up- and down-looking photometers (Moshkin *et al.* 1979) were observed. The light levels subsequently returned to their original preimpact values. These observations have been interpreted (Moshkin *et al.* 1979) as light being blocked by clouds of dust being stirred up by the wake of the landers.

Similarly, the Pioneer Venus Day Probe (Ragent and Blamont 1979) detected a sudden increase in its nephelometer reading at impact (the nephelometer emits light and measures how much is backscattered from cloud droplets or dust in the atmosphere). Again, this measurement decayed afterward to its preimpact level and was interpreted as being due to the lander-induced agitation of surface particulates.

A number of other missions are planned to bodies with atmospheres, and it is appropriate to consider whether a similar phenomenon is likely on these missions. In particular, while most Mars landers plan to use Radioisotope Thermoelectric Generators (RTGs) to provide power (Hubbard *et al.* 1991), the baseline concept for the ESA MARSNET mission (Chicarro *et al.* 1991) is to use a solar array. The deposition of dust on this array could reduce the available power.

Also, the European Space Agency Huygens probe to Titan, while not strictly a lander, may well survive impact and return data from the surface (Lorenz 1991). Further, it carries a Descent Imager/Spectral Radiometer (DISR) (Tomasko *et al.* 1990) which, as well as performing imaging and spectral measurements, also includes photometric channels which could detect a dust cloud raised following impact. Such a dust cloud could degrade surface imaging immediately following touchdown.

Method. First it is necessary to consider the wake velocities required to agitate surface particles. It will be assumed that the terminal velocity of particles is a representative figure for the atmospheric motions required to generate and sustain a dust cloud. Terminal velocities are calculated by equating drag to weight, i.e., for spherical particles

$$4\pi r^3 \rho_P g/3 = \rho_a \pi r^2 C_d V^2/2, \quad (1)$$

with ρ_P being the particle density, r the particle radius, g the local acceleration due to gravity, ρ_a the atmospheric density, C_d the drag coefficient, and V the terminal velocity. These parameters for the various planetary bodies in question are listed in Table I. The drag coefficient is assumed to be that of a smooth sphere, varying with Reynolds number $\mathrm{Re} = (2\rho_a r V/\mu)$, where μ is the viscosity of the atmosphere, with the relation (Massey 1975, p. 311)

$$C_d = (24/\mathrm{Re})(1 + 3\mathrm{Re}/16)^{1/2}. \quad (2)$$

Note that Stokes' Law, used in some studies (e.g., see Ragent and Blamont 1980) is inappropriate for larger particles, which fall at Reynolds numbers too high for Stokes' Law to be valid.

The above system of equations is iterated several times to achieve convergence. (Note that while surface particulates are unlikely to be perfectly smooth spheres, the method gives representative values for the full Reynolds numbers range.) The results are illustrated in Fig. 1. For small particles (low Reynolds numbers), the descent velocities are affected by the particle weight and the gas viscosity: larger particles fall at higher speeds and Reynolds numbers, where viscosity is unimportant, and the velocity is controlled by weight and atmospheric density. The differing parameters for the various bodies for these two different flow regimes lead to the (perhaps unexpected) crossover of the terminal velocity curves for Earth and Mars (and the hint thereof for Venus and Titan). For small sizes (the low Reynolds number Stokes' flow regime) all the descent velocities are within an order of magnitude of each other, whereas for large particles the speeds differ significantly. The low gravity and thick atmosphere of Titan give terminal velocities similar to Venus with its very thick atmosphere. These values contrast with the very thin atmosphere of Mars where particles fall rapidly. Values for Earth are intermediate.

Having considered the flow velocities necessary to levitate a particle, it is now appropriate to consider the flow velocities in the wake of landing spacecraft.

Velocities in the wake of a body in a flow clearly vary from zero (the undisturbed condition at infinity) to the velocity of the body itself (the

0019-1035/93 $5.00

TABLE I
Planetary Parameters for Aeolian Dust Pickup

Body	Venus	Mars	Titan	Earth
Surface atmospheric pressure (bar)	90	7E-3	1.5	1
Surface atmospheric temperature (K)	740	200	95	283
Dominant species	CO_2	CO_2	N_2	N_2
Atmospheric density (kg m^{-3})	64	0.02	5.3	1.23
Atmospheric viscosity (10^{-6} Pa-sec)	35[a]	13	6	17
Surface gravitational acceleration ($msec^{-2}$)	8.9	3.7	1.35	9.8
Particle composition	Rock	Rock	Water ice	Rock
Particle density (kg m^{-3})	2800	2800	1000	2800

[a] Value for CO_2 at 770 K and 1-bar pressure. Higher pressure may substantially increase this value.

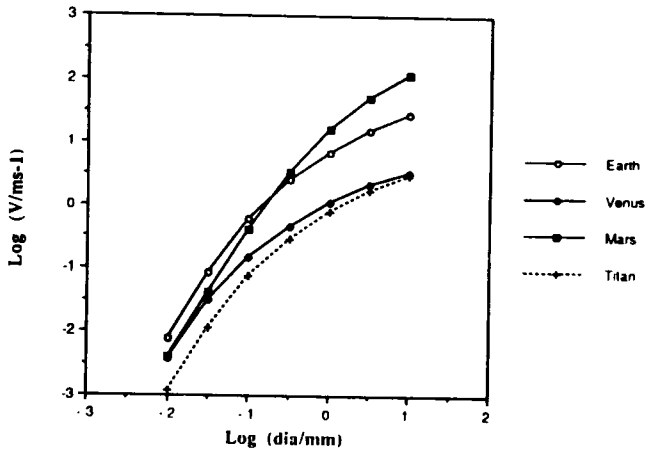

FIG. 1. Terminal descent velocities of particles from submillimeter to centimeter sizes: Large particles fall far slower on Venus and Titan than on Mars or Earth.

"no-slip" condition). Here the method of Moshkin *et al.* (1979) is used to estimate wake dimensions and velocities.

The width of the wake B at a distance x downstream is taken as

$$B \approx (\beta C_x S x)^{1/3}, \tag{3}$$

where the C_x is the drag coefficient of the spacecraft and S is its reference area; dimensionless parameter β is assumed to be 0.2. The wake velocity U compared to the descent velocity U_{dv} is given as

$$U/U_{dv} = (C_x S/\beta^2 x^2)^{1/3}. \tag{4}$$

For the purpose of this paper, we assume the cloud-generating wake to be that with a velocity of half or more of the descent velocity, i.e., that in the range $0 < x < x_{1/2}$, where

$$x_{1/2} = \sqrt{8 C_x S/\beta^2}. \tag{5}$$

Thus the mass of this wake is given by

$$M_W = (\rho_a \pi/4) \int_0^{x_{1/2}} B^2(x) dx \approx 2.7 \rho_a (C_x S)^{3/2}/\beta. \tag{6}$$

Conservation of momentum dictates that the mass of particular material in any dust cloud formed by the wake must be significantly lower than this.

The relevant parameters and results are listed in Table II. Also listed is the ratio $x_{1/2}/U_{dv}$, which gives an indication of how quickly the wake reaches the surface. It is seen that the Huygens and Venus probes have broadly similar characteristics, with wakes of 80 kg or more which deposit themselves on the surface over a couple of seconds. On the other hand, Mars landers have much less massive wakes which "splash" onto the surface much more quickly. The descent velocities quoted in the table give an upper limit for wake velocity and can be compared with the terminal velocities in Fig. 1 to derive an upper limit for the size of particle which can be supported by the atmospheric motions induced by the wake.

Conclusions. The terminal descent velocities for particles of surface material for various bodies have been calculated and compared with the wake velocities of various landers. The wake dimensions and a characteristic wake mass have also been evaluated. It is seen that, on Mars, wake masses are so low that minimal disturbance of surface material due to lander wakes is expected, although it should be noted that the high landing velocities may cause some surface material to be (briefly) disturbed as impact ejecta. On the other hand, the wake characteristics for the Huygens probe are similar to those of the Venus landers, and the terminal velocities of particles on Titan are similar to those on Venus, so that should there be fine (or even millimeter-size) particles at the Huygens landing site, an optically thick cloud may be formed for some seconds, as on the Venus missions. The nature of Titan's surface remains a matter of considerable debate at present, but the possibility of fine particulates certainly cannot be eliminated: indeed some models (Raulin *et al.* 1992) suggest "fluffy" organic deposits on

TABLE II
Planetary Landers and Wake Characteristics

Lander	Diameter (m)	Descent velocity U_{dv} ($msec^{-1}$)	Drag area S (m^2)	$C_x S$ (m^2)	Wake length $x_{1/2}$ (m)	Wake mass (kg)	Wake time $x_{1/2}/U_{dv}$ (sec)
Venera, 9,10	2.1	7	3.5	3.2	25	5000	3.5
Pioneer Venus Day Probe	0.8	9	0.45	0.4	9	220	1
Huygens	1.3	7	1.23	1.1	15	85	2.1
Mesur	1.0	30	0.8	0.7	12	0.16	0.3
Marsnet	0.9	30	0.6	0.6	11	0.12	0.3
Mars 94 Penetrator	0.7	100	0.38	0.35	8	0.05	0.1

Titan's surface which might be susceptible to aeolian pickup. If such particulate deposits exist and are agitated into a cloud by the Huygens probe wake, the cloud may be detectable by the DISR instrument.

The method used in this paper has been approximate. It might be instructive to characterize the wake of spacecraft models by means of simple wake traverse measurements in a wind tunnel, or perhaps by computational fluid dynamics. Drop tests of models onto particle beds might also be interesting, in particular to understand how the wake dumps itself onto the surface and picks up particulates.

ACKNOWLEDGMENT

The author acknowledges the support of a postgraduate research grant from the Science and Engineering Research Council of the U.K.

REFERENCES

CHICARRO A. F., M. CORADINI, M. FULCHIGNONI, I. LEIDE, P. LOGNONNE, J. M. KNUSDEN, G. E. N. SCOON, AND H. WANKE 1991. *MARSNET—Assessment Study Report*. ESA SCI (91)6.

HUBBARD, G. S., P. F. WERCINSKI, G. L. SARVER, R. P. HANEL, AND R. RAMOS 1991. *A Mars Environmental Survey (MESUR)—Feasibility of a Low Cost Global Approach*. IAF-91-432

LORENZ, R. D. 1991. Huygens Probe—The surface mission. *Proceedings of the Conference on Titan, Toulouse, France, September 1991 (ESA SP-338)*.

MASSEY, B. 1979. *Mechanics of Fluids*, 4th ed. Van Nostrand Reinhold, Wokingham.

MOSHKIN, B. E., A. P. EKONOMOV, AND YU. M. GOLOVIN 1979. Dust on the surface of Venus. *Kosm. Issled.* 17(2), 280–285.

RAGENT, B., AND J. BLAMONT 1979. Preliminary results of the Pioneer Venus nephelometer experiment. *Science* 203, 790–792.

RAGENT, B., AND J. BLAMONT 1980. Structure of the clouds of Venus: Results of Pioneer Venus nephelometer experiment. *J. Geophys. Res.* 85(A13), 8089–8105.

RAULIN, F., C. FRERE, P. RAILLOUS, E. DE VANSSAY, L. DO, AND M. KHLIFI 1992. Titan and the exobiological aspects of the Cassini/Huygens Mission. *J. Br. Interplanet. Soc.* 45, 257–271.

TOMASKO, M., L. R. DOOSE, P. H. SMITH, R. A. WEST, L. SODERBLOM, M. COMBES, B. BEZARD, A. COUSTENIS, O. SAINT-PE, C. DE BERGH, E. LELLOUCH, H. U. KELLER, N. THOMAS, AND F. GLIEM 1990. *Descent Imager/Spectral Radiometer Instrument Proposal to ESA*. Vol. 1, *Scientific/Technical Plan*.

Appendix 4

Planet. Space Sci., Vol. 41, No. 9, pp. 647–655, 1993
Printed in Great Britain.

0032–0633/93 $6.00 + 0.00

The life, death and afterlife of a raindrop on Titan

Ralph D. Lorenz

Unit for Space Sciences, University of Kent, Canterbury CT2 7NR, U.K.

Received 26 April 1993; revised 27 August 1993; accepted 30 August 1993

Abstract. A model is presented which describes the descent rate and evaporation rate of methane raindrops on Titan. The model, using conventional aerodynamics, with raindrop distortion parameterized by the Weber number, gives excellent agreement with terrestrial raindrop data. Terminal descent velocities for drops of various sizes at different altitudes are presented, and it is found that the largest raindrops may be larger than those on Earth (9.5 mm diameter vs 6.5 mm diameter) yet fall much more slowly (1.6 m s^{-1} vs 9.2 m s^{-1}. Under standard conditions on Titan, raindrops evaporate before they reach the ground: profiles showing the shrinking of drops due to evaporation during their descent are shown for various values of relative humidity. A 500 m increase in elevation can lead to a tenfold increase in rain mass flux, leading to increased "washing" of highland terrain. It is pointed out that evaporating raindrops will leave behind their condensation nuclei: fall times for these are presented, and it is noted that they may significantly affect visibility in the troposphere. The effects of additional factors on raindrop behaviour, such as the nonideal solubility of nitrogen in methane, are briefly considered.

Nomenclature

a	Semi-major axis (half-"width") of flattened droplet
a_0	Equivalent spherical radius of droplet
b	Semi-minor axis (half-"height") of flattened droplet
B	Bond number ($=\rho a_0^2 g/\gamma$)
C_d	Drag coefficient
C_{d0}	Drag coefficient of undistorted sphere
D	Coefficient of diffusivity
D_0	Diffusivity coefficient at standard conditions
Eo	Eotvos number (= Bond number)
f_v	Ventilation coefficient
g	Acceleration due to gravity
k	Flattening ratio
L	Specific heat of evaporation
M	Mass of droplet
m_a	Relative molecular mass of atmosphere
m_d	Relative molecular mass of volatile droplet component
m_i	Relative molecular mass of involatile droplet component
N_{Re}	Reynolds number ($=2a_0\rho V/\mu$)
N_{Sc}	Schmidt number ($=\mu/\rho_a D$)
N_{We}	Weber number ($=\rho_a V^2 a/\gamma$)
P	Atmospheric pressure
P_0	Standard pressure (101,325 Pa)
q	Fraction of surface area where convective updraughts occur
R_0	Universal gas constant
RH	Relative humidity
S	Drag area
S_0	Drag area of undistorted sphere
T	Temperature
T_0	Standard temperature (273K)
U	Updraught velocity
V	Terminal velocity of raindrop
X	Parameter
Y_a	Mole fraction of volatile raindrop component in atmosphere
Y_d	Mole fraction of volatile raindrop component in droplet
γ	Surface tension
μ	Coefficient of dynamic viscosity
ρ_a	Density of atmosphere
ρ_l	Density of liquid

Correspondence to: R. D. Lorenz

Introduction

Titan is perhaps one of the most fascinating bodies of the solar system and has attracted particular interest recently in connection with the preparations for the joint NASA/ESA *Cassini/Huygens* mission (Lebreton, 1992; Lebreton and Matson, 1992). One of the most exciting aspects is the possibility of seas of liquid hydrocarbons on the surface (Lunine *et al.*, 1983; Flasar, 1983) and of methane rainfall (Eshleman *et al.*, 1983; Flasar, 1983; Thompson and Sagan, 1984; Toon *et al.*, 1988; Lorenz, 1993).

In this paper, I present a model of the behaviour of individual raindrops on Titan, and consider the fate of raindrops as they descend towards the ground. Previous

treatments of rain on Titan (e.g. Toon *et al.*, 1988) have suffered from poor estimates of fall velocities of raindrops: an accurate model and results are presented here.

The scope of this paper is limited to near-surface conditions and large methane drops and the evolution and behaviour of such drops as they approach or reach the surface of Titan (the "life and death" of the raindrops). The processes associated with the "birth" of raindrops, namely cloud microphysics and convection, are not treated here, nor is the high-altitude formation of the photochemical aerosols (Scattergood *et al.*, 1992; Cabane *et al.*, 1992; Toon *et al.*, 1992) that may act as the condensation nuclei for such raindrops.

Nature of rain on Titan

The *Voyager* 1 radio-occultation experiment indicates that the lower atmosphere of Titan may have appreciable methane "humidity", and therefore clouds and rain have long been suspected. Attempts to constrain the extent and type of clouds (Thompson and Sagan, 1984; Toon *et al.*, 1988; Griffith *et al.*, 1991) from ground-based and *Voyager* measurements have not yet been conclusive, although the best indications are (Toon *et al.*, 1988; Griffith *et al.*, 1991) that if clouds exist, they are either patchy, occupying only a fraction of Titan's disc, or are optically thin.

Vertical atmospheric motions associated with rainfall could be triggered by the interaction of Titan's zonal winds (Flasar *et al.*, 1981) with topography (i.e. orographic rain), or by convection: in the lower atmosphere about 1% of the solar flux may be transported upwards by convection (McKay *et al.*, 1991).

An alternative scenario is that individual aerosol particles may simply accrete methane and rain out when they pass through supersaturated regions of the troposphere. This scenario ["rain without clouds", Toon *et al.* (1988)] is plausible due to the relatively low number density of aerosols able to act as condensation nuclei.

However raindrops may form, the purpose of this paper is to consider their behaviour and fate near the surface.

Raindrop model

A problem with rain studies is that, to date, they have been almost exclusively devoted (perhaps not unnaturally) to terrestrial rain, so many results and expressions are empirical in nature, and inapplicable to rain in other planetary environments.

The model used here to predict sizes and descent rates of methane drops in the Titan atmosphere was first developed in studies (Lorenz and Zarnecki, 1992) prompted by the concerns (now largely allayed) that supercooled methane drops could freeze on the *Huygens* probe during its descent. The model includes the variation of drag coefficient with Reynolds number and models the deformation of drops due to aerodynamic forces.

Descent velocity for spheres

The steady-state descent velocity V of a sphere moving under the action of aerodynamic drag and gravity (i.e. falling at its terminal velocity) is straightforward to compute:

$$Mg = (\tfrac{1}{2})\rho_a S C_d V^2. \quad (1)$$

where the mass of the drop is simply:

$$M = (\tfrac{4}{3})\pi\rho_l a_0^3 \quad (2)$$

and for a spherical droplet the drag reference area is:

$$S = S_0 = \pi a_0^2. \quad (3)$$

The most awkward element in the equation is the drag coefficient of a sphere. There are various empirical relations for this quantity as a function of Reynolds number [e.g. see Davies (1945): for a detailed review, see also Clift *et al.* (1978)]. Here, the relation:

$$C_d = (24/N_{Re})(1 + 0.197N_{Re}^{0.63} + 2.6\times10^{-4}N_{Re}^{1.38}) \quad (4)$$

is used for convenience. The Reynolds number (the ratio of inertial to viscous forces) is given as:

$$N_{Re} = 2a_0\rho_a V/\mu. \quad (5)$$

For low Reynolds numbers ($N_{Re} < 1$) the viscous effects dominate and the expression above reduces to Stokes' law ($C_d = 24/N_{Re}$). For higher Reynolds number, the drag coefficient tends to lie between 0.6 and 1.0. The relation does not predict the drop in drag coefficient associated with the transition from laminar to turbulent flow, but this never happens in raindrops, since drops break up before reaching such high Reynolds numbers.

The above method (and, for that matter, the unmodified Stokes' law) breaks down for very rarified atmospheres and very small droplets, where the frequency of collision of gas molecules with the droplet is so low that a correction factor for the slip flow regime must be applied. However, this occurs only for droplets so small (typically submicron) that we would consider them aerosol particles, rather than drops, and they are therefore beyond the scope of this paper.

Deformation of drops

It is found that the above method, while effective in predicting fall velocities of rigid spheres and small droplets, breaks down for large drops, which are deformed by aerodynamic forces.

To model this deformation, we modify the drag area and the drag coefficient by factors related to the flattening ratio ($k = b/a$) of the drop.

$$S = Sk_0^{-2/3}, \quad (6)$$

$$C_d = C_{d0}/k, \quad (7)$$

where we assume that the drop is deformed into an oblate spheroid (typically in free air the drop will be oscillating—jelly-like—about a mean, oblate shape, possibly becoming momentarily prolate: here it is assumed that it suffices simply to model the average shape).

Pruppacher and Beard (1970) found that drops smaller than 0.5 mm in radius have their deformations given as:

$$k = [1-(9/16)a_0\rho_a V/\gamma]^{0.5}, \quad (8)$$

as suggested by Imai (1950), while for the size range 0.5 mm $< a_0 <$ 4.5 mm the deformation is linearly related to drop radius:

$$k = 1.030-0.124a_0 \ (a_0 \text{ in mm}). \quad (9)$$

Note that strictly speaking for large droplets the shape is not an oblate spheroid, but has a flattened bottom—for a fuller discussion see Pruppacher and Beard (1970) and Clift *et al.* (1978). Green (1975) suggests that an oblate spheroid is an adequate approximation for most purposes.

The linear relation with diameter, though, is of little use in this application. The linearity may be fortuitous for the terrestrial parameter regime, and in any case, the constant of proportionality will be different for other planets. Since the deformation is due to a balance between aerodynamic and surface tension, the ratio between these forces, the Weber number:

$$N_{We} = a_0 V^2 \rho_a/\gamma, \quad (10)$$

seems a more appropriate parameter on which to derive a general relation for deformation. It can be seen (Fig. 1) that, for terrestrial raindrops at least, deformation is a reasonably linear function of Weber number. Thus for Weber numbers $N_{We} > 0.1$:

$$k = 0.97-0.072N_{We}, \quad (11)$$

while for the smaller drops with $N_{We} < 0.1$, the relation derived by Imai (1950) is used, which can be expressed as:

$$k = [1-(9N_{We}/16)]^{1/2} \quad (12)$$

[Green (1975) gives an alternative fit for flattening ratio as a function of Bond number $B = \rho a_0^2 g/\gamma$ (the ratio of gravity to surface tension forces, also known as the Eotvos number *Eo*)]. His relation:

$$k = [(4/17)(17B/4+1)^{1/2}+13/17]^{-3/2}, \quad (13)$$

also fits terrestrial drop data quite well, and since for a drop falling at terminal velocity weight and aerodynamic forces are balanced, the Bond number and Weber number are related. For the results presented here, however, the Weber number formulae above have been used: using the Weber number formulation is more closely related to physical reality, and allows the model to be applied to unsteady cases, e.g. for accelerating or unsteady drops.

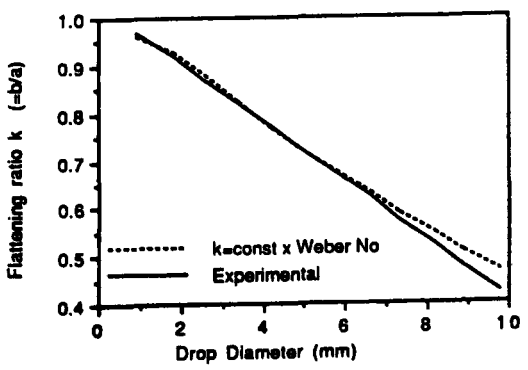

Fig. 1. Deformation ratio of terrestrial k ($=b/a$) as a function of the diameter of the (undeformed) drop. The k = constant $\times N_{We}$ agrees well with the linear relation of k with diameter found by Pruppacher and Beard (1967)

Figure 2a and b compares experimental measurements of terminal velocities with those predicted by the method described above, by approximating drops as spheres, and using Stokes' law. It is seen that Stokes' law breaks down for terrestrial raindrops of 0.1 mm diameter or larger. The rigid sphere approximation works well up to diameters of about 3 mm, above which the deformation of the drops becomes significant. Indeed, for drops larger than 4 mm the terminal velocity is virtually constant, with the increase in flattening of the droplet almost completely compensating for the increase in mass.

Note that the equations for descent rate, Reynolds number and deformation are all coupled, so to solve them a "first guess" terminal velocity must be input to derive N_{Re} and k, which must be folded back into the equations. For large drops, several iterations are usually required before convergence can be achieved.

Figure 3 gives a plot of descent rates for raindrops of various sizes at two altitudes on Titan, and on Earth for comparison. It is seen, as might be expected from the dense atmosphere and low gravity, Titan raindrops fall considerably slower than their terrestrial counterparts, with the maximum velocity for the largest drops (see next section) of 1.6 m s^{-1}. Toon *et al.* (1988) state that a 1 mm drop on Titan would fall 10 km in 1 hr, an estimate, based presumably on Stokes' law, that overestimates the fall rate by a factor of 2–3.

Clift *et al.* (1978, p. 179) give the relation $V_{max} = 2(\rho_l g\gamma/\rho_a^2)^{0.25}$ to predict the maximum velocity attainable by a large free-falling drop—independent of size or atmosphere viscosity—which yields 1.65 m s^{-1}, in excellent agreement with the result of the present model.

For the convenience of use by other workers, the descent rates of drops for various sizes and various altitudes are tabulated in Table 1. Note, however, that above 14 km, the equilibrium state (Kouvaris and Flasar, 1991; Thompson *et al.*, 1992) of the methane–nitrogen mix is solid: metastable supercooled drops will have descent velocities as in the table, but particles of ice (i.e. hailstones) will fall rather faster than drops of the same size.

Maximum drop size

An important parameter for work on raindrops is the maximum size a drop can attain. This is dictated (as is the drop shape) by the balance between surface tension holding the drop together and the aerodynamic forces which threaten to disrupt the drop. Photographic work by Matthews and Mason (1964) and references therein show that the disruption mechanism is as follows: for increasing drop sizes and descent rates, the drop becomes more and more flattened, until ultimately the centre of the

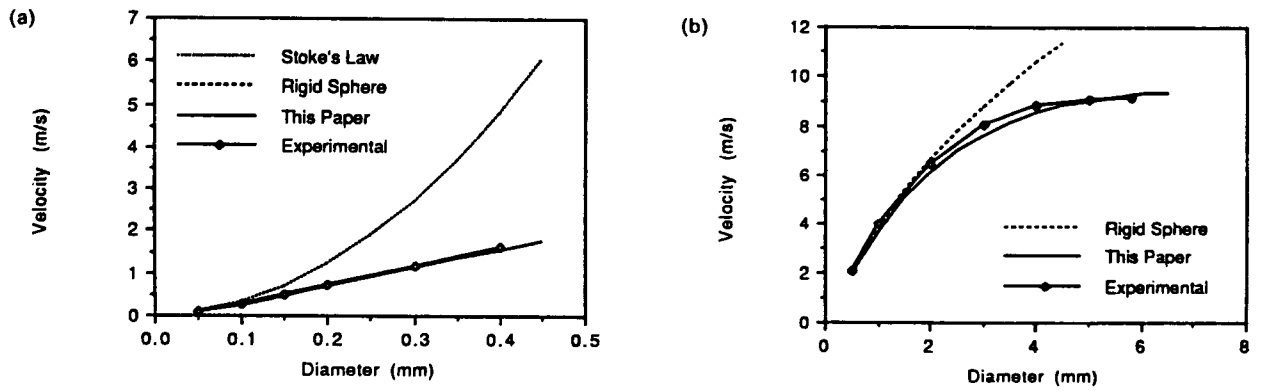

Fig. 2. Terminal descent velocities for terrestrial drops, showing results for Stokes' law, rigid sphere [equation (4)], the model used in this paper (with k = constant $\times N_{We}$) and experimental data from Mason (1971). Panel (a) shows small drops: since drop deformation is small, the rigid sphere curve is identical to, and hidden by, the "this paper" curve. Panel (b) shows large drops - Stokes' law is so inaccurate that it is not shown

drop becomes so thin that it is blown upwards, forming a sac, which quickly bursts.

Naturally, there is strictly no such thing as a hard limit on drop size, since disruption is not instantaneous, and depends on ambient conditions, such as the turbulence of the atmosphere. Thus the maximum drop size is something of a statistical concept. However, it is known that drops much larger than about 6 mm diameter are rarely found in terrestrial rain. Further, studies by Komabayasi *et al.* (1964) showed that while 50% of drops of diameter 7 mm broke up within 20 s, the same fraction of drops of diameter 6 mm took 100 s to break up.

Matthews and Mason (1964) give the relation:

$$V^2 d = 8\gamma/n\rho C_d, \tag{14}$$

as defining the upper limit of drop size, with n a factor between 1 and 2, and $d = 2a$. This can be rewritten using the Weber number definition above, and assuming the nC_d product equal to 1, as:

$$N_{We} = 4. \tag{15}$$

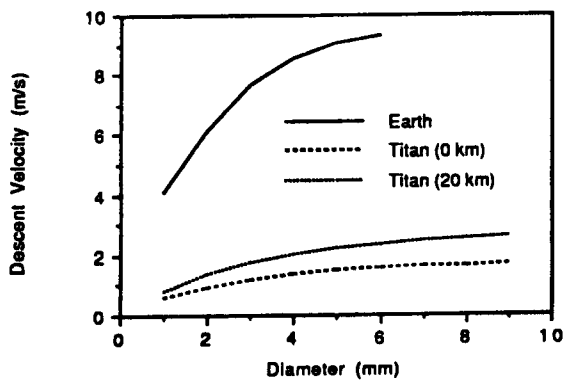

Fig. 3. Terminal descent velocities for Earth and Titan. The terminal velocities for raindrops on Earth and Titan are shown: clearly drops on Titan fall rather slower. In the thinner air at 20 km altitude on Titan, drops fall 50% or so faster than at ground level

Applying the parameters for water gives a limit size for terrestrial drops of 6.5 mm, which compares well with the experimental data cited above. For Titan conditions, the result is 9.5 mm.

[Note: Clift *et al.* (1978) give a formula, $d_{max} = 4(\gamma/g\rho_l)^{0.5}$ which suggests that the maximum size of a drop is given by the relation $Eo = 16$, suggesting the largest drop has a diameter of 10 mm on Earth, or 18 mm on Titan: this relation may be appropriate for controlled laboratory conditions—Clift *et al.* (1978) is primarily a chemical engineering book—but in the turbulent "real world", such large drops do not occur, and so this formula is inappropriate to describe natural raindrops.]

Evaporation of raindrops

The usual method of computing the evaporation rate is to assume first that the drop is at rest, and compute the mass flux diffusing from it, then to modify this mass flux by an empirical coefficient f_v to take into account the ventilation of the drop by the airflow around it (which for large terrestrial drops can increase the flux by a factor of 15).

Thus:

$$\frac{dM}{dt} = \frac{f_v 4\pi a_0 D m_d}{R_0 T}(P_v - P_d), \tag{16}$$

where D is the molecular diffusivity of the raindrop material, P_v is the ambient vapour pressure of the raindrop material [equals the saturation vapour pressure P_{sat} of the drop fluid multiplied by the ambient relative humidity (RH), or the ambient atmospheric pressure P multiplied by the ambient mole fraction Y_a of the vapour]. Thus:

$$P_v = (RH)P_{sat} = PY_a. \tag{17}$$

P_d is the vapour pressure of the raindrop fluid. Since (as on Earth) there may be involatile solutes in the raindrop (in Titan's case, the most likely candidate is ethane), these will depress the vapour pressure of the volatile component from the saturation level. Applying Raoult's law, this is

Table 1. Terminal descent velocities for methane drops on Titan at various altitudes. Terminal velocities of water drops on Earth are shown for comparison. N.B. terrestrial drops are not larger than about 6 mm

Diameter (mm)	Descent velocity of drops (m s^{-1})					
	Titan (0 km)	Titan (10 km)	Titan (20 km)	Titan (30 km)	Titan (40 km)	Earth (0 km)
0.1	0.04	0.044	0.048	0.052	0.055	0.236
0.2	0.107	0.121	0.138	0.156	0.174	0.668
0.3	0.173	0.198	0.231	0.269	0.311	1.11
0.4	0.236	0.271	0.32	0.38	0.448	1.538
0.5	0.295	0.341	0.406	0.487	0.583	1.942
0.75	0.431	0.499	0.602	0.735	0.9	2.854
1	0.547	0.638	0.776	0.958	1.188	3.606
1.25	0.65	0.761	0.931	1.159	1.451	4.339
1.5	0.737	0.865	1.062	1.331	1.689	4.993
2	0.904	1.065	1.317	1.661	2.113	6.098
2.5	1.042	1.232	1.533	1.948	2.5	6.965
3	1.157	1.372	1.715	2.194	2.836	7.636
4	1.33	1.587	1.999	2.581	3.375	8.53
5	1.454	1.737	2.198	2.859	3.77	9.02
6	1.538	1.84	2.338	3.055	4.054	9.2
7	1.594	1.91	2.43	3.191	4.254	—
8	1.632	1.957	2.498	3.284	4.393	—
9	1.655	1.987	2.539	3.346	4.487	—

equal to the saturation vapour pressure of the raindrop fluid, multiplied by its mole fraction in the droplet:

$$P_d = P_{sat} Y_d. \tag{18}$$

As the volatile component evaporates, this mole fraction, Y_d, and hence the vapour pressure and evaporation rate will decrease. The saturation vapour pressure is a function of temperature (see the Appendix).

Pruppacher and Rasmussen (1978) found that the ventilation coefficient could be calculated as a function of Reynolds number and Schmidt number (the ratio of viscosity to diffusivity of the atmosphere) as follows:

$$f_v = 1+0.108X^2 \quad \text{for} \quad 0 < X < 1.4 \tag{19}$$

and:

$$f_v = 0.78+0.308X \quad \text{for} \quad 1.4 < X < 51.4, \tag{20}$$

with:

$$X = N_{Re}^{0.5} N_{Sc}^{0.33}, \tag{21}$$

where N_{Sc} is the Schmidt number ($\mu/\rho_a D$).

The temperature T_a is assumed to be the temperature of both the droplet and the atmosphere. Strictly, the droplet should be cooled slightly with respect to the atmosphere by virtue of the loss of energy due to the evaporation of the volatile component of the droplet. A more refined model could include this factor, and suitable expressions are given in Pruppacher and Rasmussen (1978).

Evaporation (or growth) of droplets can be computed for a given altitude range Δh (100 m, for example), using the method above to obtain the rate of change of mass, noting that the time interval Δt to descend through Δh is given by:

$$\Delta t = \Delta h/(V-U), \tag{22}$$

where V is the terminal velocity of the drop relative to the atmosphere, and U the velocity (positive upwards) of the ambient air. In an updraught, a drop will take longer to traverse a given altitude range, allowing more time for evaporation or condensation.

Collision and growth of raindrops

The growth of drops by direct condensation onto an existing drop or a nucleation centre can be computed directly using the evaporation relation described above, with a relative humidity greater than 100%. This is the dominant process where nucleation centres are limited (which may be the case on Titan, which may even have rainfall without clouds). However, a significant process in terrestrial clouds is the growth of drops by collision. In a cloud, droplets of different sizes will have different terminal velocities and so move relative to one another. When droplets collide, they may coalesce to form one larger droplet. Very small droplets are inefficient at colliding, since, having low inertia, they follow the streamlines around a larger drop, rather than impacting upon it. Thus, there is an efficiency parameter associated with a given pair of drops, defining the likelihood of coalescence, although for most drops (above a size of a few microns) the efficiency is virtually unity.

By following the trajectories of individual drops in a cloud with an "ambient" drop population, the evolution of the population may be investigated. Typically, "medium-sized" drops will be scavenged rapidly by collisions, leaving behind small droplets which are inefficient at colliding, and large drops which have terminal velocities high enough that their residence time in the cloud is short. However, such a rigorous and computationally intensive simulation is not considered further in this paper.

Results of evaporation model

The results of the evaporation/descent model described in the earlier sections indicate that, for the 70% maximum relative humidity indicated by the *Voyager* data (Flasar, 1983) and a 3 km cloudbase, rain (assuming pure methane rain, and ignoring the effect of nitrogen solubility) evaporates before it reaches the ground (see Fig. 4).

Addition of the effects of nitrogen solubility (Kouvaris and Flasar, 1991; Thompson *et al.*, 1992) is a significant complication to the model, and has not yet been attempted. It is believed that the current approach of assuming pure methane drops is qualitatively accurate (the maximum droplet nitrogen concentration below 3 km altitude is only 20%, and due to the slightly nonideal behaviour of the nitrogen–methane mix, the vapour pressure of methane is only reduced by 10% (Kouvaris and Flasar, 1991, Fig. 7). Thus, since the evaporation of the drop is in any case controlled by the methane in the drop [atmospheric nitrogen will quickly (Hibbard and Evans, 1968) be dissolved into or exsolved from the drop to attain equilibrium with whatever methane is in the drop] the present model should overestimate evaporation by only 10% or so [as a very crude estimate, using the curves on Fig. 4, the effect of nonideality may be seen by following a curve for a higher ambient humidity (e.g. 80% instead of 70%)].

Whether or not nitrogen is included, evaporation will be slower (and therefore the probability of reaching the surface higher) for colder or more humid regions, such as the perhaps cooler polar regions. Stevenson and Potter (1986) have argued that the observed temperature distribution on Titan suggests polar temperatures may be "pinned" by liquid polar caps of methane. The growth of such caps can be imagined if methane rain occurs globally and is unable to reach the ground in the warmer equatorial regions, yet may do so at the poles. However, the temperature estimates used by Stevenson and Potter were based on observations of the 530 cm^{-1} emission temperature, which may have a significant stratospheric contribution (Toon *et al.*, 1988), so the inferred surface temperature difference may not be real, although this point remains contentious (Flasar and Conrath, 1992).

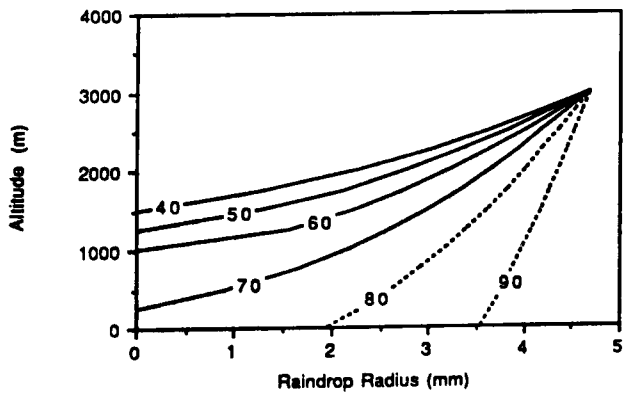

Fig. 4. Evaporation of drops on Titan. A 4.5 mm radius drop (approximately the largest possible) is released from the estimated cloudbase of 3 km and allowed to fall and evaporate in air of given relative humidity. It is seen that for humidities of 70% and lower (70% is the limit on surface humidity imposed by *Voyager* 1 data), the drop completely evaporates

Perhaps the most likely locations for rainfall to actually reach the surface are on mountains, where the surface is elevated with respect to the reference sphere of radius 2575 km on which the atmosphere profile is based: here the raindrops have a shorter distance to travel to reach the surface, and the atmosphere is slightly cooler.

As seen from Fig. 4, assuming drops start with a radius of 4.5 mm, the radius of the residual drops reaching topography elevated by 1000 m above the reference surface is about double those reaching topography at 500 m. The mass flux is therefore about an order of magnitude higher: this has intriguing implications (see later) for the appearance of mountains on Titan.

Ethane mists: "rain-ghosts"

The raindrops may have originally condensed on aerosol particles or tiny ethane droplets: indeed aerosol modellers (Toon *et al.*, 1992) assume "rainout" as the sink process for the flux of photochemical products. It is conventionally assumed that the aerosol number density in the lower troposphere is small as, sooner or later [Toon *et al.* (1991) assume within 1 year] drops are washed out and deposited on the surface. However, if, as is argued here, the rain cannot reach the ground, the aerosols will be redeposited in the atmosphere above the surface.

The aerosol particles are so small that they have very low sedimentation velocities, and hence long residence times in the atmosphere. While they are trapped inside a raindrop, however, they will be transported by it at the raindrop's much higher fall speed.

If there is convective activity in the lower levels of the atmosphere, then the aerosols will be unable to simply fall through, but may accumulate until rainout occurs. If raindrops grow by collision, the aerosols that formed the nucleation centres for the original smaller drops will be collected together. If the raindrop subsequently evaporates during its descent to the ground, the aerosol material (tholin or ethane or both) will be released (although it will be slightly diluted by some residual methane which is allowed to stay unevaporated because its vapour pressure is lowered by dissolution in the ethane). The aerosol will slowly descend—see Fig. 5 which shows (long) fall times for droplets released at 1 km altitude.

Thus, beneath an active raincloud there will be a zone where there are some aerosols and raindrops, then below this a region where all the raindrops have evaporated and there are only aerosols. Thus, after the rain ceases, there will be a cloud of aerosol particles left—a "ghost" of the raincloud. If rainfall is a rare occurrence, then this "ghost" cloud may contain a large number of aerosol droplets, accumulated in the convective cloud layers over weeks or months. Such a ghost cloud may have sufficient optical depth (see below) to be detectable with instrumentation on the *Huygens* probe.

If we take the ethane production rate of 1.5×10^9 cm^{-2} s^{-1} [Lara *et al.* (1992), although note that Yung *et al.*

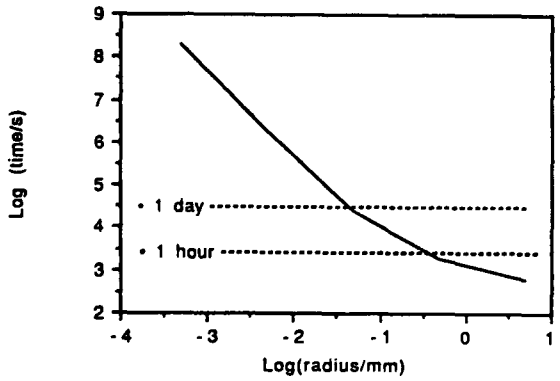

Fig. 5. Fall times for droplets on Titan from 1 km. While raindrops take about $\frac{1}{2}$ h to reach the surface, small aerosol particles may take days

(1984) give a rather higher value of ethane production rate of 5.8×10^9 cm^{-2} s^{-1}) and assume it is deposited in the troposphere near the surface as 1 μm radius drops, these will fall at about 0.02 mm s^{-1} and will have a number density of about 1.6×10^8 m^{-2}, giving an extinction of about 4.8×10^{-4} m^{-1} or 0.5 km^{-1} (compare this with about 20 km^{-1} for thick terrestrial fog). This type of haze should be easily detectable with the optical instrumentation on the *Huygens* probe (e.g. a 100 m thick layer of such a haze above a surface of albedo 0.2, seen from the probe 500 m above it and about 1 km away, would cause a 50% change in brightness: such contrasts will be easily observed). On the other hand, if aerosols are accumulated in the cloud layer, they may be more likely to be gathered into larger particles: if the ethane flux above is deposited as 10 μm radius particles instead of 1 μm, the extinction is a factor of 10^4 less (as well as having a lower number density for a given ethane deposition rate, such drops also fall much faster).

The existence of a near-surface ethane mist was proposed by Lunine *et al.* (1983) and has been investigated using near-i.r. observations (inconclusively) by Griffith *et al.* (1991). It will be an interesting challenge to determine whether any mists detected by *Huygens* are due to the condensation of ethane vapour near the surface, aerosol generation above an ocean (bubble-bursting and spin-drift), or are the ghosts of past rainstorms.

The size (and sedimentation time) of the aerosols will depend first on the size of the particles that are delivered to the troposphere from above, and then on how much convective activity there is (how long the aerosol is "detained" in the troposphere) before rainout occurs. As to whether (or to what extent) aerosol particles are accumulated together by collision-induced droplet growth, this will depend on many parameters, such as cloud droplet number density, updraught strength and so on.

The fate of raindrops that reach the surface

Some rain may reach the surface, whether due to elevated ground, a low cloudbase, or reduced evaporation during descent.

If the "ground" is liquid, for example a methane-ethane lake, the drop will be absorbed. Such lakes or seas will be in equilibrium with the atmosphere—implications of this equilibrium on the allowable compositions are discussed by Dubouloz *et al.* (1989). If a large amount of rain is deposited in the sea, the sea composition will become methane-rich and will attempt to eventually lose methane by evaporation. However, the rate at which it can lose methane to re-attain equilibrium depends on the efficiency of ocean/atmosphere exchange processes (which are poorly understood, even on Earth).

If a drop lands on porous ground (as might be expected from impact-tilled icy regolith) the drop may be absorbed, percolating downwards into the soil. The area of liquid exposed to the atmosphere will be small, and vapour transport in the intergranular spaces will be relatively slow, so evaporation may be substantially reduced. If the regolith contains nonvolatile materials soluble in methane (such as photochemical aerosol) these materials may be dissolved, and will reduce evaporation further by lowering the methane vapour pressure. As the methane trickles down through the regolith, it may carry the material with it: rain could wash the surface clear of dark photochemical material. This scenario has been proposed by Griffith *et al.* (1991) to account for the "dirty ice" near-i.r. albedo of Titan: some regions have the bright icy bedrock or regolith exposed by rain, while other areas are dark, either (dirty) seas/lakes, or surface regions which have not been washed clean.

On Earth, mountain peaks are often covered with brilliant white caps of snow. Similarly, undersea mountains often have their upper regions covered with white deposits of calcium carbonate (from the skeletons of dead sea-creatures), while lower slopes are clear of such deposits (at the higher pressures at depth, the solubility of calcium is increased, and the deposits are dissolved away). This brings to mind the intriguing notion that mountains on Titan, since they are more likely to have their surfaces washed clean of organics by rainfall, may also have white peaks: whitecapped mountains can be found in a variety of environments in the solar system, albeit for a diverse range of reasons.

If a drop lands on a smooth, impermeable ice surface, it will probably evaporate: the low surface tension of methane (0.017 N m^{-1}, rather than 0.070 N m^{-1} for water) implies it should spread into a relatively large, flat drop, with a large surface area for evaporation. Similarly, the low surface tension suggests the drop is more likely to break into small droplets (again with a large surface area) on impact. If the drop does not evaporate immediately, it will flow along the local downhill until it either evaporates, meets porous ground, or a more substantial volume of liquid (like a lake). The high evaporation rate of drops, however, suggests that the first possibility is more likely, and that methane rivers require exceptionally (improbably?) wet conditions.

The low impact velocity (and hence low impact pressure), and the low solubility of water and other ices in cryogens (Rest *et al.*, 1990) suggests that erosion due to rainfall should be minimal (unless rain is an extremely frequent occurrence on Titan).

Conclusions and directions for further work

The question of rain on Titan remains open at present, but the properties of the atmosphere and environment on Titan suggest that, if it occurs, rainfall and its effects will be rather different from the rain we observe on the Earth. Rainfall on Titan is probably not a significant agent of erosion, but may cause variations in albedo over the surface by washing away dark photochemical material from some areas. There may also be near-surface "ghost" clouds of aerosol left behind by rainfall that has evaporated before it reaches the ground.

Directions for further work include:

(1) incorporate the effects of droplet cooling by evaporation, and the (nonideal) effects of nitrogen solubility in methane, to refine estimates of the drop evaporation rate;

(2) set up a 1-D convection model of a raincloud, using the descent and evaporation/growth model presented here for individual drops, to investigate the heat and mass transport processes within a "storm" on Titan. A possible result of such a model may be that a "rain shaft" may form—a region of air below the cloud the humidity of which has been increased by evaporating drops to the point where subsequent drops are able to reach the surface; and

(3) consider the effect on rainfall on the near-surface aerosol distribution.

Acknowledgements. The author acknowledges the support of a postgraduate research grant from the U.K. Science and Engineering Research Council (SERC). Some of this work was carried out in collaboration with Dr Athena Coustenis at Observatoire de Paris (Meudon) with the support of Centre National des Recherches Scientifiques. The author thanks Dr Chris McKay of Ames for a detailed and thoughtful review of this paper, and an anonymous referee for helpful comments.

References

Cabane, M., Chassefiere, E. and Israel, G., Formation and growth of photochemical aerosols in Titan's atmosphere. *Icarus* **96**, 176–189, 1992.

Clift, R., Grace, J. R. and Weber, M. E., *Bubbles, Drops and Particles*. Academic Press, New York, 1978.

Davies, C. N., Definitive equations for the fluid resistance of spheres. *Proc. Phys. Soc.* **57**, Part 4, No. 322, p. 4, 1945.

Dubouloz, N., Raulin, F., Lellouch, E. and Gautier, D., Titan's hypothesized ocean properties: the influence of temperature and atmospheric composition uncertainties. *Icarus* **82**, 81–96, 1989.

Eshleman, V. R., Lindal, G. F. and Tyler, G. L., Is Titan wet or dry? *Science* **221**, 53–55, 1983.

Flasar, F. M., Oceans on Titan? *Science* **201**, 55–57, 1983.

Flasar, F. M. and Conrath, B. J., The meteorology of Titan. ESA SP-338, pp. 89–99, 1992.

Flasar, F. M., Samuelson, R. E. and Conrath, B. J., Titan's atmosphere: temperature and dynamics. *Nature, Lond.* **292**, 693–698, 1981.

Green, A. W., An approximation for the shapes of large raindrops. *J. appl. Meteorol.* **14**, 1578–1583, 1975.

Griffith, C. A., Owen, T. and Wagener, R., Titan's surface and troposphere, investigated with ground-based, near-infrared observations. *Icarus* **93**, 362–378, 1991.

Hibbard, R. R. and Evans, A. Jr, On the solubilities and rates of solution of gases in liquid methane. NASA TN D-4701, 1968.

Imai, I., On the velocity of falling raindrops. *Geophysical Magazine (Tokyo)* **21**, 244–249, 1950.

Kinzer, G. D. and Gunn, R., The evaporation, temperature and thermal relaxation-time of freely falling waterdrops. *J. Meteorol.* **8**, 71–83, 1951.

Komabayasi, M., Gonda, T. and Isono, K., Lifetime of water drops before breaking and size distribution of fragment droplets. *J. Meteorol. Soc. Jpn* **42**, 330–340, 1964.

Kouvaris, L. C. and Flasar, F. M., Phase equilibrium of methane and nitrogen at low temperatures: application to Titan. *Icarus* **91**, 112–124, 1991.

Lara, L. M., Rodrigo, R., Coustenis, A., Lopes-Moreno, J. J. and Chassefiere, E., Neutral composition of Titan's atmosphere: a theoretical model. *Proc. Symp. on Titan*, Toulouse. ESA SP-338, pp. 137–146, 1992.

Lebreton, J. P., The *Huygens* Probe. *Proc. Symp. on Titan*, Toulouse. ESA SP-338, pp. 287–292, 1992.

Lebreton, J. P. and Matson, D. L., An overview of the *Cassini* mission. *Nuovo Cim.* **15C**, No. 6, 1992.

Lellouch, E., Coustenis, A., Gautier, D., Raulin, F., Dubouloz, N. and Frere, C., Titan's atmosphere and hypothesized ocean: a reanalysis of the *Voyager* 1 radio-occultation and IRIS 7.7 μm data. *Icarus* **79**, 328–349, 1989.

Lindal, G. F., Wood, G. E., Hotz, H. B., Sweetnam, D. N., Eshleman, V. R. and Tyler, G. L., The atmosphere of Titan: an analysis of the *Voyager* 1 radio occultation measurements. *Icarus* **53**, 348–363, 1983.

Lorenz, R. D., Raindrops on Titan. *Adv. Space Res.*, in press, 1993.

Lorenz, R. and Zarnecki, J. C., Precipitation on Titan and the methane icing hazard to the *Huygens* probe. Paper presented at Session PS.13 of the EGS Meeting 1992, Edinburgh (Abstract in *Ann. Geophys.*, Vol. 10, Supplement 3, p. C 487), 1992.

Lunine, J. I., Stevenson, D. J. and Yung, Y. L., Ethane ocean on Titan. *Science* **222**, 1229–1230, 1983.

Mason, B. J., *The Physics of Clouds*, 2nd Edn, pp. 592–613. Clarendon Press, Oxford, 1971.

Matthews, J. B. and Mason, B. J., Electrification produced by the rupture of large water drops in an electric field. *Q. J. Roy. Meteorol. Soc.* **90**, 275–286, 1964.

McKay, C. P., Pollack, J. B. and Courtin, R., The greenhouse and antigreenhouse effects on Titan. *Science* **253**, 1118–1121, 1991.

Pruppacher, H. R. and Beard, K. V., A wind tunnel investigation of the internal circulation and shape of water drops falling at terminal velocity in air. *Q. J. R. Meteorol. Soc.* **96**, 247–256, 1970.

Pruppacher, H. R. and Rasmussen, R., A wind tunnel investigation of the rate of evaporation of large water drops falling at terminal velocity in air. *J. atmos. Sci.* **36**, 1255–1260, 1978.

Rest, A. J., Scurlock, R. G. and Wu, M. F., The solubilities of nitrous oxide, carbon dioxide, aliphatic ethers and alcohols and water in cryogenic liquids. *Chem. Engng J.* **43**, 25–31, 1990.

Scattergood, T. W., Yau, E. Y. and Stone, B. M., Titan's aerosols. *Icarus* **99**, 98–105, 1992.

Stevenson, D. J. and Potter, B. E., Titan's latitudinal temperature distribution and seasonal cycle. *Geophys. Res. Lett.* **17**, 93–96, 1986.

Thompson, W. R. and Sagan, C., Titan: far-infrared and microwave remote sensing of methane clouds and organic haze. *Icarus* **60**, 236–259, 1984.

Thompson, W. R., Zollweg, J. A. and Gabis, D. H., Vapor-liquid equilibrium thermodynamics of N_2+CH_4: model and Titan applications. *Icarus* **97**, 187–199, 1992.

Toon, O. B., McKay, C. P., Courtin, R. and Ackerman, T. P., Methane rain on Titan. *Icarus* **75**, 255–284, 1988.

Toon, O. B., McKay, C. P., Griffith, C. A. and Turco, R. P., A physical model of Titan's aerosols. *Icarus* **95**, 24–53, 1992.

Yung, Y. L., Allen, M. and Pinto, J. P., Photochemistry of the atmosphere of Titan: comparison between models and observations. *Astrophys. J.* **55**, 465–506, 1984.

Appendix: physical properties

The viscosity of nitrogen is assumed to be well represented by the following equation

$$\mu = 1.718 \times 10^{-5} + [5.1 \times 10^{-8}(T-273)], \quad \text{(A1)}$$

where T is the atmosphere temperature in kelvin.

The diffusivity is assumed to be represented as follows:

$$D_v = D_0(T/T_0)^{1.75}(P/P_0), \quad \text{(A2)}$$

where the ambient pressure and temperature are in the same units as standard conditions (i.e. $T_0 = 273$K, $P_0 = 101{,}325$ Pa). Diffusivity at standard conditions D_0 for H_2O is 2.2×10^{-5} m^2 s, while for CH_4, $D_0 = 1.96 \times 10^{-5}$ m^2 s.

For atmospheric models which do not list all the relevant properties (e.g. the Lellouch–Hunten Titan atmosphere model lists only density and temperature), the other required properties can be obtained using the equation of state:

$$P = \rho_a R_0 T/m_a. \quad \text{(A3)}$$

For the saturation vapour pressure of methane over the temperature range of interest, the following relation has been used [although see Kouvaris and Flasar (1991) and Thompson *et al.* (1992) for the partial pressure of methane above mixtures of nitrogen and methane]:

$$\log_{10}(P_{sat}) = 0.06T - 1.66 \quad \text{(A4)}$$

(T in kelvin, P_{sat} the saturation vapour pressure in pascals).

The density of liquid methane is about 450 kg m^{-3}, but to account for the presence of heavier hydrocarbons in drops (e.g. ethane, density 650 kg m^{-3}) and the dissolution of nitrogen (density 800 kg m^{-3}), a value of 600 kg m^{-3} has been used in this work.

The surface tension of liquid methane, like that of many hydrocarbons, is about 0.017 N m^{-1}.

The atmosphere model used for the studies here is the engineering model used for mission design purposes for the *Huygens* probe, due to Lellouch and Hunten (European Space Agency, Space Science Department Report ESLAB 87/199). Other models are given by Lindal *et al.* (1983) and Lellouch *et al.* (1989). A measure of the uncertainty of the model is given by the temperature uncertainty at the surface: 92.5–101K.

The nominal values from the model in the troposphere are given in Table A1.

Table A1. Titan atmosphere properties from ESLAB 87/199, used in the raindrop studies. The scale height near the surface is about 20 km, about 3 times that of Earth (i.e. Titan's atmosphere is not only dense, it is "thick")

Altitude (km)	Density (kg m^{-3})	Temperature (K)
0	5.3	97.2
1	5.14	95.9
2	4.99	94.4
3	4.83	93.0
4	4.65	92.0
5	4.45	91.4
10	3.67	85.8
20	2.24	78.6
30	1.28	74.4
40	0.7	72.7
50	0.37	73.3

Appendix 5

R.D. Lorenz
Unit for Space Sciences, University of Kent, Canterbury, UK

The Surface of Titan in the Context of ESA's Huygens Probe

Abstract The ESA Huygens Probe is scheduled for launch as part of the NASA/ESA Cassini mission to the Saturnian system in 1997, due to arrive at Titan in late 2004, to make a 2.25 h exploratory descent to the surface. However, the state of Titan's surface is completely unknown and the moon may be at least partially covered in liquid hydrocarbons. This paper reviews the current theories and observations relating to Titan's surface and suggests that a heterogenous surface composed of ice and organic compounds (some of them liquids, accumulating in seas and lakes) is the most plausible. Geological and meteorological processes that may be occurring on Titan are considered from a comparative planetological viewpoint, in order to make predictions about features that may exist on Titan's surface. Several 'model' surfaces are presented for the future estimation of the Huygens Probe's survivability on the Titan surface.

1. Introduction

Saturn's mysterious satellite Titan[1-4] is the only body in the Solar System, apart from the Earth, to have a thick atmosphere dominated by nitrogen. Complex photochemistry in the atmosphere, which also contains methane, produces organic compounds, perhaps resembling the first steps in the origins of life. Consequently, Titan is an object of great scientific interest. However, very little is known about the surface of this world, hidden from view by the organic haze.

The ESA Huygens Probe, as part of the joint NASA/ESA Cassini[5-10] mission, due to be launched in 1997, will descend through Titan's atmosphere down to the surface in late 2004: it will carry instruments to make accurate measurements of the composition of gas and aerosols in the atmosphere, measure atmospheric structure and dynamics, and take images of and determine the physical characteristics of the surface.

This paper attempts to review the current knowledge of the surface of Titan, with several goals:

- to summarise the latest information, in what has recently become an area of intense scientific activity
- to identify the likely nature of the Huygens landing site, to assist evaluation of landing survivability and the planning of post-impact operation of the Probe
- to suggest topics that would benefit from further work.

The paper takes a comparative planetological perspective, attempting to note similarities and differences with other, better-known, solar system bodies in order to make some predictions about the nature of Titan's surface. Some of Titan's general characteristics are summarised in Table 1.

Table 1. Properties of Titan

Radius	2575 km
Mass	1.35×10^{23} kg
Surface gravity	1.35 ms^{-1}
Mean density	1880 kgm^{-3}
Surface pressure	1.5 bar
Surface temperature	94 K
Atmosphere constituents	N_2, CH_4, Ar(?)
Solar flux	15 Wm^{-2}
Orbital period	15.95 days
Orbital eccentricity	0.029
Mean distance from Saturn	1.22×10^{6} km

2. Clues to the nature of Titan's surface

The Voyager-1 encounter with Titan was something of a disappointment for planetary geologists, because its surface was obscured from Voyager's cameras[11] by the optically thick organic haze that gives the moon its characteristic orange colour (Fig. 1). No features observed elsewhere in the Solar System, such as volcanoes, grooved terrain, or craters could be seen. However, analysis of infrared spectra[12,13] detected large amounts of organic molecules in the atmosphere. Condensation of these organic compounds forms an orange haze which makes Titan's atmosphere opaque at visible wavelengths. Scientific interest therefore focused on the complex atmospheric chemistry, which begins with the photolysis of methane, which has a mixing ratio in the stratosphere of between 0.5 and 3.5%. The fact that this amount of methane should have been depleted photolytically within approximately 10 million years, coupled with Titan's surface temperature which is close to the triple point of methane, suggested the possibility of reservoirs of (liquid) methane on the surface, or that methane was being resupplied from the interior[14,15].

Subsequent work[16] was able to reconcile the near-surface under-saturation of methane (70% max., inferred from Voyager-1 radio-occultation measurements) with such a reservoir, noting that the dissolution of the less-volatile ethane (the dominant photochemical product) in methane seas would lower the methane vapour pressure. A global ocean was therefore a widely-accepted model of Titan's surface, considering that early photochemical models[17] (see later) predicted a 600 m global depth of ethane, forming (with methane and nitrogen[18]) an ocean with an average depth of between 700 m and 9 km. Such a model was aesthetically attractive and agreed with the photochemical models and Voyager observations. Additionally, Sagan & Dermott[19] introduced a theoretical argument (see below) that if oceans exist on Titan, they must be deep.

However, since the time when this idea came into vogue, observations have become available which suggest that Titan is not covered by a global ocean. The various observations and theories pertinent to the surface of Titan are summarised in the following subsections. For further details, see the references mentioned in each section. Several earlier review papers[20-23] are also of interest, and a recent review by Lunine[24] is essential reading.

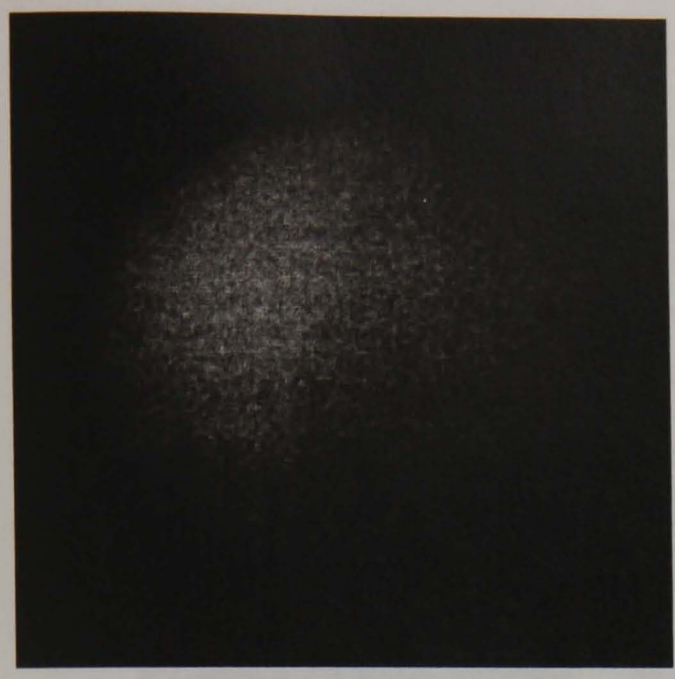

Figure 1. Titan's surface hidden by the thick haze-laden atmosphere. Note the hemispherical asymmetry

Figure 2. Ganymede, Jupiter's and the Solar System's largest satellite, which is only marginally larger than Titan

2.1. Radar observations

Direct radar sensing of Titan's surface[25] was first achieved in 1989. The radar reflectivity of the surface was successfully measured, albeit with a low signal-to-noise ratio, on three nights at 0.38, 0.78 and 0.25; i.e. extremely variable, but quite high (much higher than the reflectivity of a global hydrocarbon ocean). Subsequent measurements[26] have confirmed these results, noting that there is a 'bright spot' of high radar reflectivity and that the radar reflectivity resembles (although is generally somewhat lower than) those of the icy Galilean satellites.

The high reflectivity is believed to be due to a backscattering mechanism caused by multiple reflections between cracks in the ice. The interpretation of the radar data is complex (see Refs. 24 for 25 for a fuller discussion).

2.2. Microwave radiometry

Microwave radiometry[25,27] suggests that the surface emission temperature is about 82 K, indicating an emissivity of about 0.88, which is consistent with an icy surface, but not with a global ocean.

Such a high emissivity – higher than those of the Galilean satellites Europa and Ganymede (Fig. 2), but similar to that of Callisto – is difficult to reconcile with a high reflectivity: it suggests that the surface is solid, but is not 'clean' ice, ice contaminated with organic compounds seeming to be the most plausible answer.

2.3. Near-infrared studies

While the atmosphere is opaque at most optical and infrared wavelengths, due to absorption and scattering by the haze and gases, there are some near-infrared 'window' regions (0.94, 1.08, 1.28, 1.58, 2 and 5 microns) between the methane absorption bands, where it may be possible to sense the surface[28,29,30]. Recent observations[31,32] have noted a variation in albedo at these window wavelengths which is correlated with the orbital period, suggesting that it is possible to sense the surface (or at least the lower troposphere) in these regions.

Observations by Griffith et al.[28,29] at 1.28, 1.6 and 2.0 microns suggested a 'dirty ice' surface – neither completely dark, such as would be expected for a surface covered in organic material, nor completely bright – the analogue suggested by Griffith et al. is '⅓ Ganymede + ⅔ Phoebe' (Phoebe is the dark outermost satellite of Saturn). One scenario is a surface of organics (solid and liquid) mixed with ice,

191

Figure 3. Callisto, the optically darkest of Jupiter's satellites, which has an albedo that seems to resemble Titan's surface at radar and mid-infrared wavelengths. It also has the oldest surface of the Galilean satellites, as evidenced by the heavy cratering

although it is impossible to discriminate with the data currently available whether this is an intimate mixture (dirty ice everywhere), an icy surface with lakes and seas present, or a dark organic/ice surface with some bright regions of ice exposed.

Observations at 5 microns[33] also suggest, if the atmosphere is relatively transparent, that the surface albedo is too high for a global hydrocarbon covering, and resembles that of Callisto (Fig. 3).

P. Smith (priv. comm.) has obtained an image of Titan (some 20 pixels across) with the Hubble Space Telescope Wide-Field and Planetary Camera (WFPC) which appears to show surface features or clouds: more observations are planned with WFPC-2. Additionally, there has been recent progress in ground-based infrared imaging using adaptive optics (see O. Saint-Pe et al., *Icarus*, Vol. 105, pp. 263–270), again indicative of surface or deep atmospheric features.

2.4. Photochemical models

Because the atmosphere of Titan is so thick (the column mass of gas per unit area is about 10 times that of the Earth), it has probably played a major role in the evolution of the surface. It has long been realised[34] also that the products of methane photochemistry must accumulate in large quantities on the surface, although it is only in the last decade that the nature and quantity of these products have been assessed with any confidence.

In particular, a model proposed by Yung et al.[17] has guided much of the work to date. Most notably, it suggested that 600 m of ethane should have been deposited over the age of the Solar System, hence focusing attention on the concept of a global ocean, since 600 m (and for that matter 9 km) is much greater than the expected surface-topography height.

However, the photochemistry is complex, and many uncertainties in reaction coefficients and transport processes exist. (Photochemical modelling of outer-planet atmospheres has had to be revised following the recent discovery that methyl radicals (CH_3) may be the dominant product of methane photolysis by ultraviolet light (see Mordaunt et al. 1993, *J. Chem. Phys.*, Vol. 98, pp. 2054–2065); previously it was thought that only CH_2 was produced.) Additionally, some exotic processes such as impact[35] or lightning[36] shock chemistry, and the influence of magnetospheric electrons and cosmic rays have to be invoked to explain the abundance of some nitrogen compounds, for example. Recently, a new model has been developed[37], which includes 130 reactions, many updated reaction coefficients, and an improved treatment of transport and condensation processes. This model yields atmospheric mixing ratios for most constituents in excellent agreement with those determined from Voyager[13] and ground-based measurements.

In particular, the new model predicts[38] a rather lower ethane production rate than the Yung et al. model, leading to 100–300 m of ethane on the surface, a value that is much easier to reconcile with observations, since ~200 m of ethane is much easier to 'hide' in the porous regolith[23,24,38]

Production/deposition rates computed for the two models are compared in Table 2. Some of the processes linking the photochemical products with the surface are shown in Figure 4.

2.5. Tides

Sagan & Dermott[19] have argued that tidal dissipation in shallow seas on Titan should have damped the significant (0.029) free eccentricity of Titan's orbit to low values over the age of the Solar System: they suggested that oceans should either be deep (>400 m) or non-existent.

However, the preservation of such a large eccentricity over the age of the solar system is difficult to account for[39], even if Titan is a completely rigid body with no dissipative oceans.

Lunine[24] has reviewed the tidal argument and notes that it relies heavily on analogy with the Earth–Moon system, which is perhaps inappropriate. Thus, although the argument is interesting, it is no longer felt to be a significant constraint against shallow seas on the surface of Titan.

192

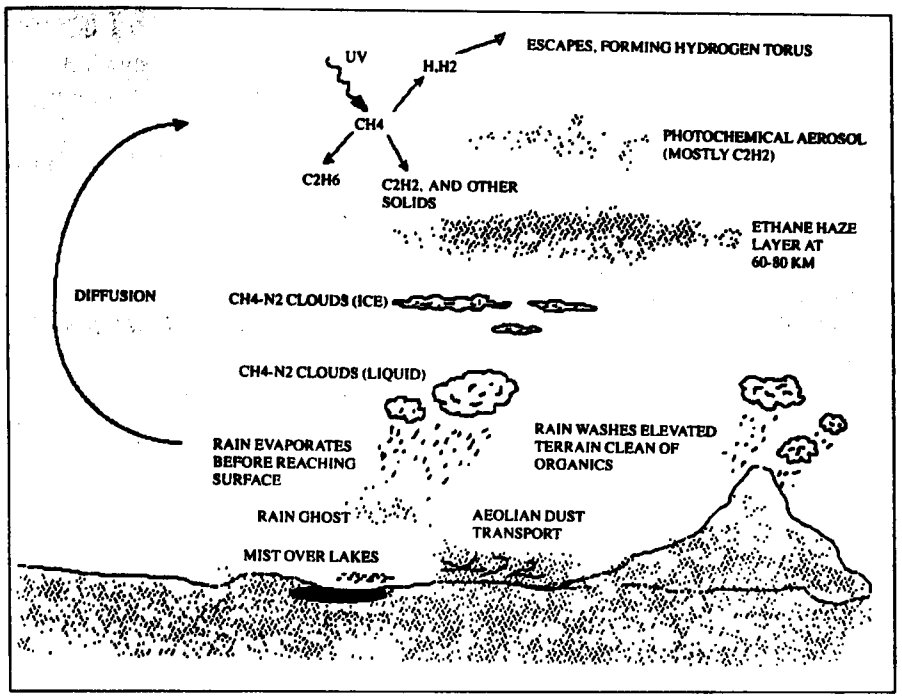

Figure 4. Sketch illustrating some of the processes occurring near Titan's surface related to the processing of hydrocarbons

3. Reconciliation of theories and observations

We are in a far better position to understand Titan's surface than we were even two years ago: the trickle of new data has grown into a flood, and theories and models are being refined continually. While the ultimate resolution of the scientific debate (and, for that matter, the satisfaction of our simple curiosity) must await the arrival of Cassini/Huygens, we can predict with moderate confidence that Titan's surface is heterogenous, mostly solid, consisting of a mixture of ice and solid hydrocarbons, probably with some lakes or seas of liquid hydrocarbons present.

The notion of the global ocean (at least in the classic sense of a thick, global covering of liquid) is ruled out by all the observational data, and even the more exotic models, such as oceans rendered radar-reflective by suspended particles[22], developed to satisfy simultaneously the tidal constraint, radar data and photochemical production, struggle to agree with the infrared data.

Note that the considerations and observations described above describe Titan as it is now: studies of long-term atmosphere/climate evolution[40] on Titan suggest there may have been a colder epoch 3 Gyr ago when most of the atmosphere was condensed on the surface. Additionally, while the lower atmosphere is not currently saturated with methane, depending on the rate at which methane was delivered to the surface it may have been saturated – possibly with a global ocean – at some time in Titan's history.

4. Surface heterogeneity and rotation period

Monitoring of Titan's albedo in the near-infrared windows has indicated a substantial (~20%) variability[31,32], correlated with the rotation period, suggesting that we are sensing the surface. Thus it is possible we are sensing near-surface clouds, perhaps associated with topography (i.e. orographic clouds, or clouds above seas), although this in itself is indicative of heterogeneity and topography.

Further evidence of heterogeneity is provided by the strong variability of Titan's radar cross-section[25,26]. Several observations indicate a 'bright spot' of reflectivity 0.73, as against the average of other measurements at 0.21.

Interestingly, the 'bright spot' appears slightly earlier from year to year than would be expected from synchronous rotation (15.945 days). Tracking of this bright spot suggests a rotation period of 15.911 days, 0.82 h shorter than the orbital period[26]. (Alternatively, Titan could be rotating synchronously, but with a significant libration, although this seems less likely than non-synchronous rotation.)

Infrared tracking[32] of albedo variations has so far only constrained the rotation

period to within 2.7 h of synchronous. While synchronicity is expected for most Solar-System satellites[41], it should be noted that the equilibrium spin rate for spherical bodies in orbits with non-zero eccentricity[42], like Titan[43], is slightly faster than synchronous.

The rotation period is important for two main reasons. Firstly, tidal effects on the atmosphere and liquids on the surface are radically different for synchronous and non-synchronous cases (see later). Secondly, non-synchronicity implies that Titan is too soft to support a crustal bulge large enough to generate sufficient torque to achieve tidal lock. It has been calculated that a 'slab' 1 km thick and 100 km in diameter would be large enough to capture Titan into synchronous rotation[42]; thus, knowledge of the rotation state of Titan would allow us to place constraints on Titan topography. (Recently it has been suggested that a 'continent' up to 360 km in diameter, 'poking' through a near-global ocean would be compatible with non-synchronicity[43].)

5. Latitudinal temperature variations

It has been argued[44] that the latitudinal temperature distribution inferred from Voyager infrared measurements at 530 cm^{-1} (18.9 microns) suggests that the poles are 1−2 deg cooler than the equator (where temperatures are known more accurately from radio-occultation data). Furthermore, while the Voyager encounter took place in northern Titan spring, symmetry between north and south would not be expected (due to the long radiative time constant of Titan's atmosphere), yet this is what was observed. (Note: An asymmetry is apparent at visible wavelengths[11,45,46], which is due to compositional variations due to seasonal effects on chemistry and aerosol characteristics.)

The symmetry could be accounted for if the polar-surface temperatures were 'pinned' to fixed levels by the presence of polar caps of liquid CH_4-N_2. Such caps would float above an ethane ocean if present (although it is difficult to understand how a polar cap could be restrained from flooding all over Titan, especially in the face of significant equatorward tidal accelerations[47]).

Additionally, it has been argued[48] that the stratosphere contributes the major part of the observed 530 cm^{-1} flux, and therefore the measurements cannot be used to infer surface temperatures. If this is the case, then such polar caps may not exist. However, the interpretation of the 530 cm^{-1} data is still a matter of debate[49].

6. Surface modelling

Figure 5. Irregular Hyperion, the closest Saturnian satellite to Titan, which is probably the remnant of a catastrophic collision, the debris of which fell onto Titan

6.1. Impacts

If Titan's surface is old (4 Gyr), comparison with other satellite surfaces in the Saturnian system and then interpolating between Hyperion and Rhea[50] (the satellites adjacent to Titan) suggests there should be about 200 craters with a diameter of 20 km or more in every 10^6 km^2 of surface. Most of these will have been generated in the initial heavy bombardment following the formation of the Saturnian system. The 'steady state' production rate of >20 km craters[51] is 4×10^{-15} km^{-2} yr^{-1}.

Titan may, however, have suffered an additional bombardment event. Hyperion, the satellite next outward from Titan, is an irregular fragment-shaped body (Fig. 5), yet it is large enough to have gravitated into a sphere. This implies that it is the remnant of a larger body that was catastrophically disrupted by a collision. (Such a violent event would not be unique: Mimas, in the inner Saturnian system, has a large crater 'Herschel' whose diameter is one-third that of Mimas itself, close to the breakup threshold: Miranda, one of Uranus's satellites, shows evidence of having been completely broken up and re-assembled by gravity.) Due to the 3:4 orbital resonance between Titan and Hyperion, most of the cloud of debris generated by the fragmentation of Hyperion would quickly (within 100 years) have fallen onto Titan[52]. The cratering record on Hyperion suggests that this event happened early in the age of the Saturnian system.

Thus, for a range of probable sizes of Hyperion, the equivalent depth of infalling material on Titan may be between 100 m and 8 km − enough to completely alter the nature of the surface, saturating it with craters, so the crater population may be much

higher than suggested above. (It is interesting to note that at radar and infrared wavelengths, Titan appears to most closely resemble Callisto, which is the most heavily cratered of the Galileans.)

Unlike most bodies on which craters are observed, Titan has a thick atmosphere. In this respect, the planetary science community has learned much from recent studies of Magellan radar images of the surface of Venus, which has been protected from bombardment (and, for that matter, hidden from view) by an atmosphere even thicker than Titan's. This shielding has several effects, most notably that small impactors are screened out[51] so that few small craters exist. Additionally, breakup of impactors[53] may lead to the formation of crater clusters, as seen on Venus[54].

The aerodynamic wake of an impactor, or the shock wave associated with the explosion of an impactor in the atmosphere, can lead to 'scouring' – the clearing of particles of material around the impact site (or 'ground zero') – and even fragmentation of bedrock. Such a mechanism has been proposed to account for the radar-dark[55] regions on Venus, and is believed to describe the Tunguska event on Earth[56].

The constrained expansion of the ejecta cloud means that a significant ejecta fraction is in liquid form (i.e. water). This may mean that large breccia-like ejecta blankets exist around craters, perhaps about four times wider than the crater itself[51], as on Mars. The exposure of organic material on the surface to liquid water for short periods (impact melt pools in larger craters may take some centuries to freeze) may have interesting implications for pre-biotic chemistry. The atmosphere also affects the distribution of ejecta, such that 'rays' of material on a planet-wide scale are not seen, but (except in the case of extremely large impacts) ejecta are confined to the immediate vicinity of the crater[57]. Many craters on Titan may have central peaks[58].

The presence of liquids on the surface of Titan also suggests the occasional occurrence of impact-generated tsunamis ('tidal waves').

Impacts may have been instrumental in delivering an atmosphere to Titan[59]. Also, the shock wave associated with meteoric entry and impact may have been a major driver in atmospheric chemistry[35]. Even today, the steady influx of water (in the form of meteoric ices) plays a significant role, leading to the formation of trace amounts[60] of CO and CO_2. Meteor ablation in the 500–600 km range may also contribute to an ionised layer of the atmosphere[61].

Meteoric interactions with Titan are summarised in Figure 6.

6.2. Regolith compaction

The rate of annealing/sintering of ice particles is a function of temperature and pressure[62]. The low temperature of Titan's surface implies that consolidation of regolith grains is very slow, such that over the age of the solar system, regolith on Titan should remain porous to kilometre depths[38].

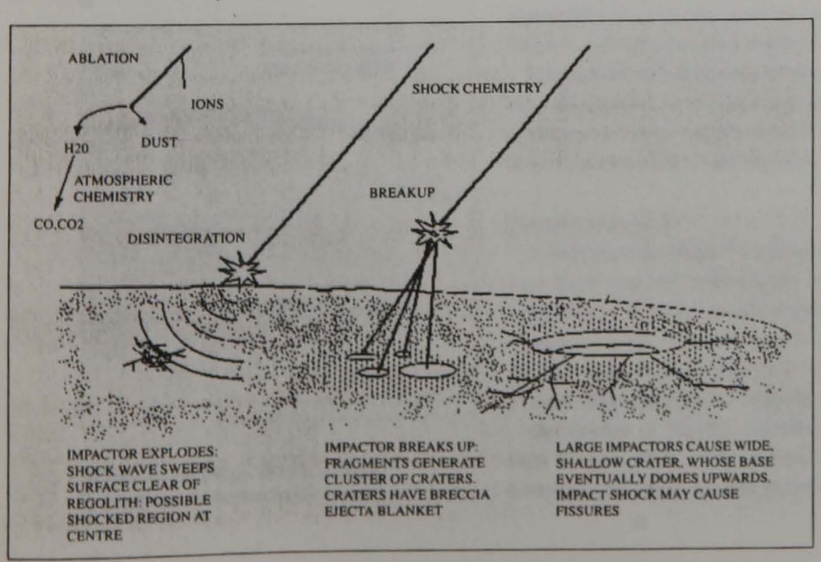

Figure 6. Sketch illustrating the influence of bombardment processes on the surface and atmosphere of Titan

This has many implications for the distribution of fluids on the surface – it may be possible to 'hide' several hundred metres' worth of liquid hydrocarbons in the pores between regolith particles[23,24,38].

Also, a deep porous regolith will affect the heat flow from Titan's interior. A thick porous regolith acts as an insulator, increasing the geothermal temperature gradient (until the regolith becomes sufficiently warm that it is annealed). Heat flow through the regolith may be strongly influenced by the presence of volatile liquids (ethane/methane) acting as a 'heat pipe', much like water in the Martian regolith[63] may have done (Fig. 7). Such a heat-transport mechanism may be instrumental in maintaining porosity to significant depths.

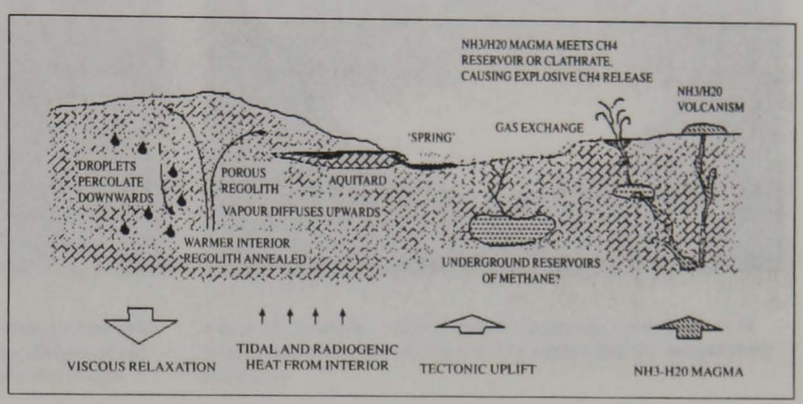

Figure 7. Sketch indicating the influence of the interior on the surface of Titan.

6.3. Tectonics/volcanism

We are, of course, as ignorant of the interior of Titan as of its surface, but knowing Titan's density, and making reasonable assumptions about Titan's thermal history, it is possible to devise models of the interior[23]. Figure 8 shows a currently-favoured model with a rock-ice core, a liquid mantle and a thick icy crust.

Whether, and to what extent, tectonic and volcanic effects have manifested themselves (and are occurring now) depends on many factors in Titan's thermal history[64], notably the volatile content of the interior, and the completeness of differentiation.

Key points are that, like the Galileans, accretional heating on Titan was likely to have been enough to melt most of the body, and its size is sufficient that conduction is inadequate to remove internal heat; convection of some sort must have played a role. Unlike the Galileans, however, Titan probably incorporated large amounts of volatiles.

Modelling of Titan's thermal history is complicated by uncertainties in the rheologies of high-pressure ice phases, and clathrate or ammonia-laden ices, and the impact and tidal heating history: there are many free parameters.

Estimation of radiogenic heating[64] from the interior yields about 4×10^{11} W, with tidal dissipation in a solid Titan about 8×10^{10} W, although perhaps rather larger for a slushy or liquid mantle. (Tidal heating may have been stronger in the past, when Titan's eccentricity was higher.)

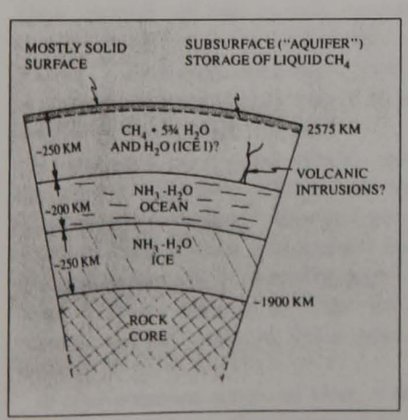

Figure 8. Model of Titan's interior, reproduced from Stevenson (1992)

Crater relaxation

Parmentier & Head[65] examined the relaxation of craters, noting that geothermal heat flow requires temperature to increase with depth, and thus viscosity decreases with depth. A larger crater is naturally deeper, and hence 'feels' warmer, with less-viscous crustal material which relaxes faster. They computed relaxation times of 30 Myr for 100 km-diameter craters (i.e. short) to 30 Gyr for 10 km-diameter craters. The bottoms of large craters tend to dome upwards (Fig. 9).

Parmentier & Head's calculations use a temperature of 120 K, somewhat higher than Titan's 94 K. The increased viscosity of ice at this lower temperature may, however, be offset by the possibly greater mobility[66] of NH_3-H_2O ice.

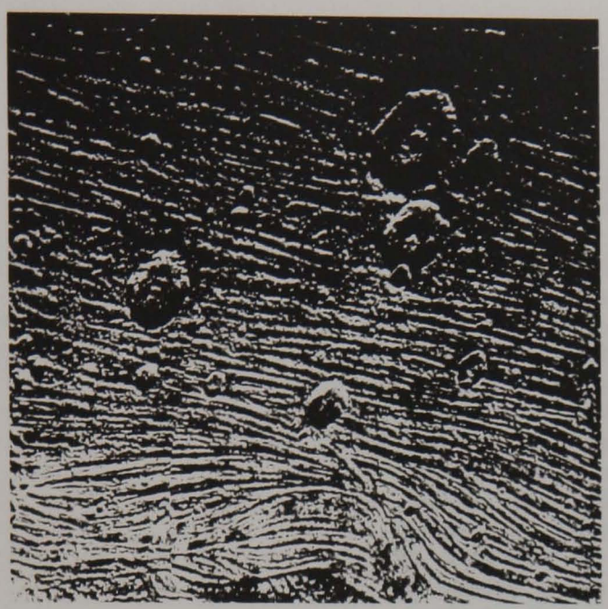

Figure 9. The best topographic data on large icy satellites comes from Ganymede, which was observed by Voyager-2 from a distance of only 59 500 km. Note the grooved terrain and the domed bottom to the impact crater, with central pit

Figure 10. Enceladus which, despite its small size, shows evidence of recent resurfacing: note the grooves and regions that are comparatively crater-free

Thus the crater population on Titan will be interesting. Large craters will be modified by relaxation processes, perhaps disappearing altogether in topographic terms[67], like the 'palimpsests' on Ganymede and Callisto (Figs. 2 & 3), while very small craters will be few (due to atmospheric shielding) and have their ejecta patterns modified by the atmosphere.

Cryovolcanism

Studies of Saturnian satellites have indicated recent resurfacing activity[68]. In particular, the small satellite Enceladus (Fig. 10) has bright, young terrain, and Saturn's E-ring shows a peak in particle concentration near Enceladus' orbit, suggesting that the satellite is a recent source of these particles. Such resurfacing would not be expected on a water-ice body: the key is the low-temperature mobility of fluids other than pure water, in particular the H_2O-NH_3 mixture, which melts at 176 K, thus requiring much less energy to activate volcanic activity[69].

Lunine & Stevenson[70], in considering the migration of CH_4 from the interior of Titan, pointed out that as CH_4 percolates upwards and passes its critical point (46 bar) it will vaporise explosively, yielding ejection velocities of the order of 300 ms^{-1}. Such explosive activity could lead to pit chains and 'blow-out' troughs[71]. Such features could also be caused by the devolatilisation of clathrates due to the intrusion of NH_3-H_2O magma[69].

On the other hand, gently effusive volcanism based on NH_3-H_2O could occur, if the crust is sufficiently dense for the magma to be buoyant. The mobility of lavas scales with a parameter[72] (density x gravity/viscosity): this parameter for ammonia-water on Titan is about 10 times less than for basalt on Earth: even less if the fluid is contaminated with methanol (a major volatile constituent of comets), or suspended solids[73]. Thus, features on Titan based on ammonia–water may resemble the volcanic domes[74] seen on Venus (also the result of viscous, perhaps rhyolitic[75], lavas).

If cryovolcanism occurs on Titan, it will be unique since no other icy satellite has a dense atmosphere. Convection of an eruption plume, distribution of tephra, the devolatilisation of magmas/lavas, and the cooling of lava will all be affected by the presence of the atmosphere. Submarine volcanoes could present an even more exotic scenario.

Faulting, grooves

Large groove structures[76] (Fig. 9) and rift-valleys appear on several icy satellites. Such structures could appear on Titan too, and might have interesting implications for the distribution of liquids on the surface.

Such features can be due to extensional and compressive stresses induced by ice phase changes, impacts and tidal forces. Thus, there are far too many uncertainties to attempt any predictions about such features on Titan.

6.4. Aeolian transportation

The presence of particulates (photo-chemical aerosols and impact ejecta) on the surface suggests the possibility that these materials could be transported by winds. Allison[77] computed the threshold velocity of 1.7 cm/s, and noted that the friction velocity at the surface was only slightly lower (~ 1 cm/s): he concluded that 'windblown dust may be an occasional feature of Titan meteorology'. The surface of Mars (Fig. 11) shows clear evidence of aeolian resurfacing.

It may even be possible to make predictions about the distribution of aeolian materials, similar to those made about Venus[78], on the basis of our knowledge about the circulation of Titan's atmosphere. The probable dominant transport direction is E−W (or W−E; the wind direction is not yet confirmed), due to the zonal winds, predicted by analogy with Venus and by Voyager measurements of atmospheric temperatures[79]. These winds (of order 100 ms^{-1} in the stratosphere, falling to near zero at the ground) are an important mission driver for the Probe[80], leading to an eastward drift of up to some 600 km. The existence of these zonal winds has been confirmed by circulation simulations[81,82], and by the oblateness in the atmosphere, determined from the fortuitous occultation[83,84] of a star by Titan in 1989.

Superimposed on the zonal winds may be tidal winds (associated with the gravitational effects of Saturn[85]; see also the section on lakes later) and slope winds, caused by local topography and its interaction with incident sunlight. (It is believed that such winds dominate transport on Venus[86], although since the amount of sunlight reaching the surface[87] of Titan is only about 1 Wm^{-2} – about 80 times less than on Venus – the effect on Titan may be much reduced.)

6.5. Weathering

Weathering of rocks[88] on the Earth occurs by a variety of mechanisms, among the most important being the combined action of carbon dioxide and water, temperature cycling, and the effects of salts. Analogous effects are difficult to imagine on an icy surface, since chemical weathering of ice bedrock seems improbable.

Lunine & Stevenson[89] computed the time by topographic obstacles to erode by solution in the presence of a hydrocarbon ocean, based on early measurements of ice

Figure 11. The immediate vicinity of the Viking-2 lander on Mars: a combination of rocks and wind-blown dust

solubility in methane. However, recent measurements of the solubility[90], and calculations using regular solution theory, indicate much lower solubility than that used in Reference 89, so erosion by this mechanism may be insignificant. Erosion of ammonia ice, however, would be much faster. Similarly, solution and removal of organic materials such as the dark photochemical aerosol, may be relatively efficient.

Abrasion by airborne particles, and possibly those suspended in lakes and seas, may therefore be relatively significant on Titan, although there is currently insufficient data to quantify this. Rainfall (see later) is unlikely to be a powerful erosion agent (except perhaps for removing dark material from the surface). Also, since the temperature variations over Titan's surface are believed to be small, temperature cycling is also likely to be a negligible weathering agent.

6.6. Rainfall

The possibility of methane rain on Titan has long been realised[14,15,48]. While the equilibrium state of methane-nitrogen above an altitude of 14 km is solid[91,92], below this level there may be clouds of methane droplets and hence rain (Fig. 4).

A model of raindrop behaviour[93] predicts that raindrops fall more slowly than on Earth. The largest terrestrial drops (6.5 mm diameter, dictated by a balance between surface tension and aerodynamic forces) fall at about 9.2 ms^{-1}. The largest drops on Titan (9.5 mm diameter) fall at only 1.6 ms^{-1}. Their low speed suggests that impact pressures are low, and therefore erosion by rainfall is very modest.

This slow descent rate also implies that drops have more time to evaporate as they fall from the cloud base (assumed to be 3 km, on the basis of Voyager-1 radio-occultation data) through undersaturated air. Models of evaporation[94] suggest that most drops evaporate before they reach the surface (for equatorial conditions). For the 3 km cloud base and 70% relative humidity, even the largest drops of methane would evaporate before reaching the surface. Rivers of methane therefore seem highly unlikely. When they evaporate, they may leave behind their condensation nuclei – the same aerosols seen in the stratosphere – which may form a 'rain-ghost', a near-surface mist cloud with a significant residence time.

The high, but non-ideal[91,92,95], solubility of nitrogen in liquid methane may retard the evaporation of drops somewhat[94], such that some rain may reach the surface, even near the equator, but this requires further study.

The mass flux on elevated terrain (1 km) could be an order of magnitude higher than it is 500 m lower, perhaps leading to increased removal of dark organic material: mountain peaks, as on Earth, may be white[94] (there are mountains up to 2 km high on Ganymede[76]).

It is possible that, if regions of Titan (like the poles) are cooler and therefore more humid (see Section 5), rainfall may more easily reach the surface. Rivers may also exist in these regions.

6.7. Liquids on the surface

Seas and lakes

Much of the inventory of liquids on Titan may be in subsurface[23] 'aquifers' of porous regolith[38], but the accumulation of at least some liquids in lakes seems likely, since the ethane is produced in the atmosphere. In particular, since craters and their immediate surroundings may be relatively impervious due to impact melting, hydrocarbons may accumulate therein, forming circular lakes.

Interestingly, if (as expected) the centres of large craters dome upwards due to viscous relaxation, the liquids will be pushed out to the crater rim, forming ring or horseshoe lakes[47].

Waves

Srokosz et al.[96] evaluated the likely characteristics of gravity waves on Titan's seas. For a fully-developed sea and a given wind speed, waves are larger on Titan than on Earth; e.g. for a 1 ms^{-1} surface wind, waves are 0.18 m high (compared with 0.025 m on Earth) and have much longer periods (5.7 s vs. 0.8 s) and wavelengths.

Spindrift (droplet formation at wave crests) may be significant, due to the lower

surface tension of hydrocarbons, and aerosol generation by bubble-bursting, similar to the generation of the sea-salt aerosol on Earth, may also be important. The long sedimentation times of droplets in Titan's thick atmosphere may mean, therefore, that an optically-thick mist may be associated with bodies of liquid on Titan.

Tides

Saturn is about three times further from Titan than the Earth is from the Moon, but it is also some 7730 times more massive than the Moon. Even taking Titan's smaller radius into account, it is clear that tidal accelerations on Titan are some 100 times larger than on Earth. Also, since gravitational acceleration is so much smaller, the importance of tidal effects is correspondingly larger: for example, the depth of the tidal bulge in a global ocean would be over 100 m[19]: the atmospheric tide (of about 1% of the surface pressure[84]) would be readily detectable with surface instrumentation, and may lead to significant surface winds.

Tides produce, in effect, a shift in the local vertical, up to 7×10^{-5} rad on Titan[47]. Liquid in lakes will respond to this, much like a spirit level. The difference in Titanocentric height of the two edges of a lake 100 km across will be 7 m, which is enough to turn a shallow ring-shaped lake into a horseshoe. Due to the 0.029 eccentricity of Titan's orbit, the magnitude of the tide varies by about 9% (= 3 e), and the sub-Saturn point oscillates along the equator with an amplitude of 3 deg (~ 100 km).

Since Titan's rotation may be slightly non-synchronous (superimposed on the oscillation will be a 0.05 deg/day drift of the sub-Saturn point), it has been conjectured that, assuming erosion is efficient enough (see earlier), the net effect of tides over geologic time may be to erode preferentially the equatorward margins of lakes, causing them to slowly creep anti-poleward[47].

Since, for mission-analysis reasons[80], the Huygens Probe is constrained to enter at about 200 E 20 N, and due to the zonal winds will land about 10 deg east of there (assuming the winds are prograde), we may expect Huygens to see any lakes 'pointing' in a southwesterly direction. If lakes or seas on Titan have beach slopes similar to those of tidal flats on Earth (10^{-3}), then the tidal range can be up to 0.07 times the lake diameter.

Sedimentation

In any body of liquid on the surface, solid material will also be deposited: impact ejecta, and photochemical aerosols which may be brought to the atmosphere-sea interface directly, by winds, or washed down by rainfall. Comparing the deposition rates (Table 2) of solid and liquid organics with the some 300 m of impact ejecta[51], it can be noted that the lakes or seas will be quite 'silty'. Lunine[21,22] calculated the settling velocity of particles and found that particulate matter will have long residence times, noting also that the upper layers of liquid will be constantly stirred by wind, tidal currents and temperature effects, and so may never clear. The suspension of large amounts of solid material may make the liquid more erosive than it might otherwise be.

Ultimately, some organic material will be deposited on the sea-bottom (Raulin[97] calculated the solubility of various organic materials in hydrocarbon oceans, and noted that saturation is exceeded for most or all of them: also, since the density of these solid materials is greater than that of the liquid, they will sink and there should

Table 2. Deposition rates of compounds on Titan's surface. Depth figure given is equivalent depth of deposit generated over 4.5×10^9 years for the Lara rate. Similar equivalent depths for Yung et al.'s production rates can be obtained by scaling

	Production/Deposition Rate (10^8 cm^{-2}s^{-1})			
Compound	Lara	Yung	Density (kg/m^3)	Depth (m)
C_2H_6 (l)	23	58	650	250
C_3H_8 (l)	0.014	1.4	730	0.2
C_2H_2 (s)	5.6	12	800	43
HCN (s)	0.05	2	675	0.5

be no floating 'icebergs'). Because the photo-chemical aerosols may have a fractal shape, they may be efficient at trapping bubbles, leading to floating 'mats' of entangled aerosol particles.

7. Engineering models of the surface

From the considerations presented in this paper, it is possible to suggest a number of surface types which describe the probable nature of the Huygens Probe's landing site. These models are listed in Table 3.

Naturally, combinations of these various surface types are also possible. The Viking lander sites on Mars, for example, are a combination of 'rock field' and 'fine particles'; the Venera 13 and 14 landing sites on Venus (Fig. 12) are geologically young, showing bedrock plus some fine particulates; lakes on Titan may have a constituency somewhere between 'lake/sea' and 'sludge', depending on their silt burden, and so on.

As more modelling is done, it may be possible to generate plausible topographic surfaces associated with each surface type: such modelling has recently been performed for Mars[98]. An evaluation of the landing loads and survivabilities corresponding to these surface types will be presented in a future paper.

Table 3. Surface types on Titan

Type	Formation	Composition
1. Sea/lake	Accumulation of liquids in basins	Liquid hydrocarbons and dissolved compounds
2. Sludge	Accumulation of liquids and solids. Shorelines of lakes or seas.	Solid organics, ices, silicates, moistened with liquid
3. Fine particles	Wind-blown regolith Deposition of solid aerosol particles	Fine dry particles of silicates, ices and organics: high porosity
4. Rock field	Weathering of bedrock Impact ejecta Regolith, with fines removed by aeolian or fluvial processes	Coarse lumps of ice
5. Bedrock	Crater bottom or ejecta blanket. Removal of regolith by erosion Fresh lava flow Solidification of sludge.	Ice, perhaps with some organics and silicates
6. Slope	Crater rim, edge of lava flow Faulting, tectonic uplift Erosion of bedrock	As bedrock or rock field

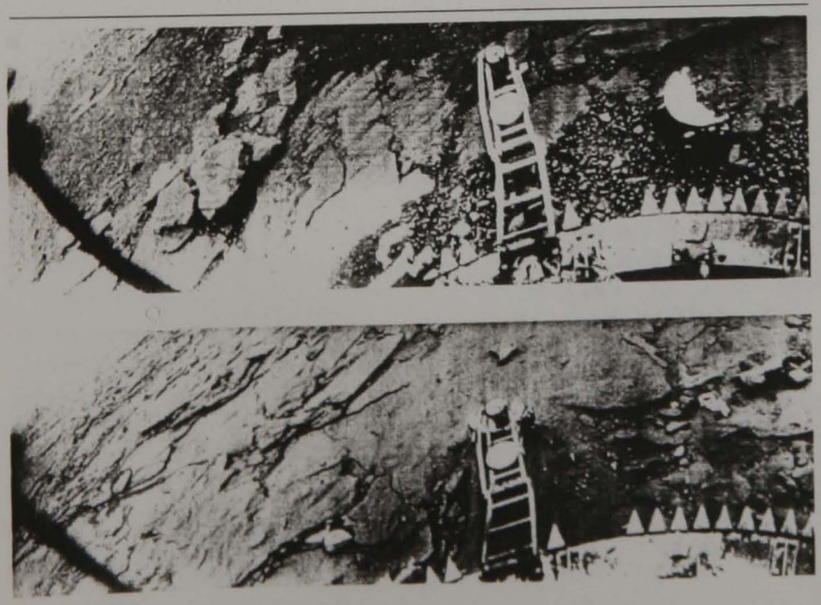

Figure 12. The landing sites of Veneras-13 and -14 show a fresh-bedrock surface, with a few aeolian deposits, an unpleasantly harsh surface on which to land

8. Conclusion

Consideration of both observations and theories suggests that Titan has a heterogenous surface with liquid hydrocarbons and icy regions present. Further, we are developing a picture of an exciting, active world with many interesting geological and meteorological phenomena occurring, in parameter regimes far different from those on Earth.

Among the more fanciful (although not necessarily improbable) features we may expect to see are ring- or horseshoe-shaped lakes, near-surface mists, giant waves and white-capped mountains. Weathering is probably weak on Titan, but atmospheric photo-chemistry, tidal effects and impacts have been strong drivers in the evolution of the moon's surface. A major unknown is the extent and nature of tectonic/volcanic activity.

Some broad classifications of surface types have been derived and will be used in a future paper to assess the survivability of the Huygens Probe landing, and to consider its possible mission on the surface. A working group has been set up within the Huygens Science Working Team (HSWT) to consider these aspects, and to plan the related scientific investigations.

It is clear that much work remains to be done on Titan even before Cassini/Huygens brings us more data to work with. Among areas that deserve close attention are the following:

- *Further Observations:* identification of surface materials and monitoring of the spatial and temporal variability of albedo at radar and infrared wavelengths, the determination of rotation period, and detection of weather systems.
- *Evaluation of Surface Impacts:* quantification of cratering density for representative impactor populations (heliocentric and Saturnocentric, especially proto-Hyperion).
- *Tides:* interaction of atmospheric tide with zonal wind field. Tidal dissipation in crust and effects on heat budget. Tidal dynamics in seas.
- *Interior:* modelling of internal structure and heat flow: tectonics and cryo-volcanism.
- *Liquids:* stratification of lakes/seas and sedimentation therein. Conditions required for rivers on surface. Transport of liquids and vapours through the regolith. Simulation of weather systems.

9. Acknowledgements

The author acknowledges the support of a postgraduate research grant from the UK Science and Engineering Research Council (SERC). The encouragement and review of an early version of the paper by J-P. Lebreton of ESA Space Science Department is gratefully acknowledged, as is the subsequent review by F. Raulin.

The author acknowledges many fruitful discussions with fellow workers: among these it is a pleasure to note the particular contributions of J. Lunine, W. Sears, M. Lemmon, A. Coustenis, L.M. Lara, D. Jewitt, P. Smith, D. Gautier and C. McKay.

References

1. Hunten D.M. et al. 1984, Titan, in 'Saturn' [Gehrels T. & Matthews M.S. (Eds)], University of Arizona Press.
2. Morrison D., Owen T. & Soderblom L.A. 1986, Titan, in 'Satellites' [Burns A.J. & Matthews M.S. (Eds)], University of Arizona Press.
3. Lunine J.I. 1990, Titan, *Advances in Space Research*, Vol. 10, pp. (1)137–(1)144.
4. Coustenis A. 1991, Titan: Recent Developments, *Vistas in Astronomy*, Vol. 34, Part 1.
5. Lebreton J.-P. & Scoon G.E. 1988, Cassini – A Mission to Saturn and Titan, *ESA Bulletin No. 55*, August 1988, pp. 24–30.
6. Lebreton J.-P. 1991, The Huygens Probe, Proceedings of the Symposium on Titan, Toulouse, 9–12 September 1991, ESA SP-338 (April 1992), pp. 287–292.

7. Mooij E. 1992, De Cassini-missie, *Ruimtevaart*, June 1992, pp. 2–8.
8. NASA/ESA Cassini Phase-A Study ESA/SCI 88(5).
9. Lebreton J.-P. & Matson D.L. 1992, An overview of the Cassini Mission, *Il Nuovo Cimento*, Vol. 15C, No. 6.
10. Lorenz R. 1992, Huygens Probe – The Surface Mission, Symposium on Titan, Toulouse, September 1991 ESA SP-338, pp. 359–364.
11. Smith B.A. et al. 1981, Encounter with Saturn: Voyager 1 Imaging Science Results, *Science*, Vol. 212, pp. 163–191.
12. Hanel R. et al. 1981, Infrared observations of the Saturnian system from Voyager 1, *Science*, Vol. 212, pp. 192–200.
13. Coustenis A.B., Bezard B. & Gautier D. 1989, Titan's Atmosphere from Voyager Infrared Observations. I. The gas composition of Titan's equatorial region, *Icarus*, Vol. 80, pp. 54–76.
14. Eshleman V.R., Lindal G.F. & Tyler G.L. 1983, Is Titan Wet or Dry? *Science*, Vol. 221, pp. 53–55.
15. Flasar F.M. 1983, Oceans on Titan, *Science*, Vol. 221, pp. 55–57.
16. Lunine J.I., Stevenson D.J. & Yung Y.L. 1983, Ethane Ocean on Titan, *Science*, Vol. 222, pp. 1229–1230.
17. Yung Y.L., Allen M. & Pinto J.P. 1984, Photochemistry of the Atmosphere of Titan: Comparison between model and observations, *Astrophysical Journal Supplement Series*, Vol. 55, pp. 465–506.
18. Dubouloz N, Raulin F, Lellouch E. & Gautier D. 1989, Titans Hypothesized Ocean Properties: The Influence of Surface Temperature and Atmospheric Composition Uncertainties, *Icarus*, Vol. 82, pp. 81–96.
19. Sagan C. & Dermott S.F. 1982, The Tide in the Seas of Titan, *Nature*, Vol. 300, pp. 731–733.
20. Lunine J.I. 1985, Titan's Surface: Nature and Implications for Cassini, in The Atmospheres of Saturn and Titan, ESA SP-241, pp. 83–88.
21. Lunine J.I. 1990, Evolution of the Atmosphere and Surface of Titan, in Formation of Stars and Planets, and the Evolution of the Solar System, ESA SP-315, pp. 159–165.
22. Lunine J.I. 1992, Plausible Surface Models of Titan, ESA SP-338, pp. 233–239.
23. Stevenson D.J. 1992, The Interior of Titan, ESA SP-338, pp. 29–33.
24. Lunine J.I. 1993, Does Titan Have an Ocean? A Review of Current Understanding of Titan's Surface, *Reviews of Geophysics*, Vol. 31, pp. 131–149.
25. Muhleman D.O., Grossman A.W., Butler B.J. & Slade M.A. 1990, Radar Reflectivity of Titan, *Science*, Vol. 248, pp. 975–980.
26. Muhleman D.O., Grossman A.W., Slade M.A. & Butler B.J. 1992, The Surface of Titan and Titans Rotation: What is Radar Telling Us? *Bull. Am. Astron. Soc.*, Vol. 24, No. 3.
27. Grossman A.W. & Muhleman D.O. 1992, Observations of Titan's Radio Light-Curve at 3.5 cm, *Bull. Am. Astron. Soc.*, Vol. 24, No. 3, p. 954.
28. Griffith C.A., Owen T. & Wagener R. 1991, Titan's Surface and Troposphere, Investigated with Ground-Based, Near-Infrared Observations, *Icarus*, Vol. 93, pp. 362–378.
29. Griffith C.A. & Owen T. 1992, Observing the Surface of Titan Through Near-Infrared Windows in Its Atmosphere, ESA SP-338, pp. 199–204.
30. Stammes P. 1992, The Detectability of Titan's Surface in the Near-Infrared, ESA SP-338, pp. 205–210.
31. Lemmon M.T., Karkoshka E. & Tomasko M. 1993, Titan's Rotation: Surface Feature Observed, *Icarus*, Vol. 103, pp. 329–332.
32. Griffith C.A. 1993, Evidence for surface heterogeneity on Titan, *Nature*, Vol. 364, pp. 511–514.
33. Noll K.S. & Knacke R.F. 1993, Titan: 1–5 micron photometry and spectrophotometry and a search for variability, *Icarus*, Vol. 101, pp. 272–281.
34. Hunten D.M. (Ed.) 1974, The Atmosphere of Titan, NASA SP-340.

35. Jones T. & Lewis J. 1987, Estimated impact shock production of N_2 and organic compounds on Early Titan, *Icarus*, Vol. 72, pp. 318–392.
36. Borucki W.J., McKay C.P. & Whitten R.C. 1984, Possible Production by Lightning of Aerosols and Trace Gases in Titan's Atmosphere, *Icarus*, Vol. 60, pp. 260–273.
37. Lara L.M. 1993, Estudio fotoquimico de los componentes neutros de la atmosfera de Titan, PhD Thesis, University of Granada, Spain.
38. Lara L.M., Lorenz R.D. & Rodrigo R. 1993, Liquid and Solids on the Surface of Titan: Results of a New Photochemical Model, submitted to *Planetary and Space Sciences*.
39. Peale S.J., Cassen P. & Reynolds R.T. 1980, Tidal Dissipation, Orbital Evolution & Nature of Saturn's Inner Satellites, *Icarus*, Vol. 43, pp. 65–72.
40. McKay C.P., Pollack J.B., Lunine J.I. & Courtin R. 1993, Coupled Ocean-Atmosphere models of Titan's Past, *Icarus*, Vol. 103, pp. 88–98.
41. Peale S.J. 1977, Rotation Histories of the Natural Satellites in J.A. Burns (Ed.) Planetary Satellites, University of Arizona Press, pp. 87–112.
42. Greenberg R. & Weidenschilling S.J. 1984, How Fast Do Galilean Satellites Spin? *Icarus*, Vol. 58, pp. 186–196.
43. Sears W., Lunine J.I. & Greenberg R. 1993, Equilibrium Non-Synchronous Rotation of Titan, *Icarus*, Vol. 105, pp. 259–262.
44. Stevenson D.J. & Potter B.E. 1986, Titan's Latitudinal Temperature Distribution and Seasonal Cycle, *Geophys. Res. Lett.*, 13, pp. 93–96.
45. Caldwell J. et al. 1992, Titan – Evidence for Seasonal Change: A Comparison of Hubble Space Telescope and Voyager Images, *Icarus*, Vol. 97, pp. 1–9.
46. Coustenis A. 1990, Spatial Variations of Temperature and Composition in Titan's Atmosphere: Recent Results, *Annales Geophysica*, Vol. 8, p. 645–652.
47. Lorenz R.D. 1993, Crater Lakes on Titan: Rings, Horseshoes and Bullseyes, *Planet. Space Sci.*, in press.
48. Toon O.B., McKay C.P., Courtin R. & Ackerman T.P. 1988, Methane Rain on Titan, *Icarus*, Vol. 75, pp. 255–284.
49. Flasar F.M. & Conrath B.J. 1992, The Meteorology of Titan, ESA SP-338, pp. 89–99.
50. Plescia J.B. & Boyce J.M. 1985, Impact Cratering History of the Saturnian Satellites, *J. Geophys. Res.*, Vol. 90, No. B2, pp. 2029–2037.
51. Thompson W.R. & Sagan C. 1992, Organic Chemistry on Titan – Surface Interactions, Proc. Symposium on Titan, Toulouse, September 1991, ESA SP-338, pp. 167–176.
52. Farinella P. et al. 1990, The Fate of Hyperions Fragments, *Icarus*, Vol. 83, pp. 186–204 (See also McKinnon W.B. 1990, The Hyperion Hypothesis, *Nature*, Vol. 346, pp. 414–415).
53. Hills J.G. & Goda M.P. 1993, The Fragmentation of Small Asteroids, *Atmos. Astron. J.*, Vol. 105, pp. 1114–1144.
54. Phillips R.J. et al. 1992, Impact Craters and Venus Resurfacing History, *J. Geophys. Res.*, Vol. 97, pp. 15923–15948.
55. Zahnle K.J. 1992, Airburst Origin of Dark Shadows on Venus, *J. Geophys. Res.*, Vol. 97, No. E10, pp. 10243–10255.
56. Chyba C.F., Thomas P.J. & Zahnle K.J. 1993, The 1908 Tunguska Explosion: Atmospheric disruption of a stony asteroid, *Nature*, Vol. 361, pp. 40–44.
57. Shultz P.H. 1992, Atmospheric Effects on Ejecta Emplacement, *J. Geophys. Res.*, Vol. 97, No. E7, pp. 11623–11662.
58. Schenck P.M. 1989, Crater Formation and Modification on the Icy Satellites of Uranus and Saturn: Depth/Diameter and Central Peak Occurrence, *J. Geophys. Res.*, Vol. 94, No. B4, pp. 3813–3832.
59. Zahnle K. & Dones L. 1992, Impact Origin of Titan's Atmosphere, ESA SP-338, pp. 19–25.
60. Samuelson R.E., Maguire W.C., Hanel R.A., Kunde V.G., Jennings D.E., Yung Y.L. & Aiken R.C. 1983, CO_2 on Titan, *J. Geophys. Res.*, Vol. 88, pp. 8709–8715.

61. Ip W.H. 1990, Meteoroid Ablation Processes in Titan's Atmosphere, *Nature*, Vol. 345, pp. 511–512.
62. Smoluchowski R. & McWilliam A. 1984, The structure of ices on satellites, *Icarus*, Vol. 58, pp. 282–287.
63. Clifford S.M. 1991, The Role of Thermal Vapour Diffusion in the Subsurface Hydrologic Evolution of Mars, *Geophys. Res. Lett.*, Vol. 18, pp. 2055–2058.
64. Schubert G., Spohn T. & Reynolds R.T. 1986, Thermal Histories, Compositions and Internal Structures of the Moons of the Solar System, in 'Satellites' (Burns J.A. & Matthews M.S., Eds.), University of Arizona Press.
65. Parmentier P.M. & Head J.W. 1981, Viscous Relaxation of Impact Craters on Icy Planetary Surfaces: Determination of Viscosity Variation with Depth, *Icarus*, Vol. 47, pp. 100–111.
66. Consolmagno G.J. 1983, Ice-Rich Moons and the Physical Properties of ICE, *J. Phys. Chem.*., Vol. 87, pp. 4204–4208.
67. Smith B.A. et al. 1979, The Jupiter System Through the Eyes of Voyager 1, *Science*, Vol. 204, pp. 951–972.
68. McKinnon W.B. 1985, Geology of Icy Satellites, Ices in the Solar System, (J. Klinger et al., Eds.), D. Reidel, pp. 829–856.
69. Stevenson D.J. 1982, Volcanism and Igneous Processes on Small Icy Satellites, *Nature*, Vol. 298, pp. 142–144.
70. Lunine J.I. & Stevenson D.J. 1987, Clathrate and Ammonia Hydrates at High Pressure: Application to the Origin of Methane on Titan, *Icarus*, Vol. 70, pp. 61–77.
71. Murchie S.L. 1990, Tectonics of Icy Satellites, *Advances in Space Research*, Vol. 10, No. 1, pp. (1)173–(1)182.
72. Kargel S.K., Croft S.K., Lunine J.I. & Lewis J.S. 1991, Rheological Properties of Ammonia-Water Liquids and Crystal-Liquid Slurries: Planetological Applications, *Icarus*, Vol. 89, pp. 93–112.
73. Friedson A.J. & Stevenson D.J. 1983, Viscosity of Rock-Ice Mixtures and Applications to the Evolution of Icy Satellites, *Icarus*, Vol. 56, pp. 1–14.
74. Garvin J.B. 1990, Small Domes on Venus: Probable Analogs of Icelandic Lava Shields, *Geophys. Res. Lett.*, Vol. 17, No. 9, pp. 1381–1384.
75. McKenzie D., Ford P.G., Liu F. & Pettengill G.H. 1992, Pancake-like Domes on Venus, *J. Geophys. Res.*, Vol. 97, No. E10, pp. 15967–15976.
76. Squyvres S.W. 1981, The Topography of Ganymedes Grooved Terrain, *Icarus*, Vol. 46, pp. 156–168.
77. Allison M. 1992, An Assessment of Titan's Boundary Layer, Proc. Symposium on Titan, Toulouse, September 1991, ESA SP-338, pp. 113–118.
78. Saunders R.S. et al. 1990, Large-Scale Patterns of Eolian Sediment Transport on Venus: Predictions for Magellan, *Geophys. Res. Lett.*, Vol. 17, No. 9, pp. 1365–1368.
79. Flasar F.M., Samuelson R.E. & Conrath B.J. 1981, Titan's Atmosphere: Temperature and Dynamics, *Nature*, Vol. 292, pp. 693–698.
80. Ott S. 1992, Cassini Mission: The Targetting of the Huygens Probe, IAF-92-0067 Presented at the World Space Congress, Washington DC.
81. Hourdin F. et al. 1992, Numerical Simulation of the Circulation of the Atmosphere of Titan, ESA SP-338, pp. 101–110.
82. Del Genio A.D., Zhou W. & Eichler T.P. 1993, Equatorial Super-rotation in a Slowly Rotating GCM: Implications for Titan and Venus, *Icarus*, Vol. 101, pp. 1–17.
83. Hubbard W.B. et al. 1990, Results for Titan's Atmosphere from its Occultation of 28 Sagitarii, *Nature*, Vol. 342, pp. 353–355.
84. Sicardy B. et al. 1990, Probing Titan's Atmosphere by Stellar Occultation, *Nature*, Vol. 343, pp. 350–353.
85. Lorenz R.D. 1992, Gravitational Tide in the Atmosphere of Titan, ESA SP-338, pp. 119–123.
86. Dobrovolskis A.R. 1993, Atmospheric Tides on Venus. IV. Topographic Winds and Sediment Transport, *Icarus*, Vol. 103, pp. 276–289.

87. McKay C.P. et al. 1991, The Greenhouse and Anti-greenhouse effects on Titan, *Science*, Vol. 253, pp. 1118–1121.
88. Ollier C. 1982, Weathering (2nd Edition), Longman Group Limited, Harlow, England.
89. Lunine J.I. & Stevenson D.J. 1984, Coupled Evolution of Titan's Ocean-Atmosphere System and interaction of Ocean with Bedrock, in 'Ices in the Solar System', pp. 741–757.
90. Rest A.J., Scurlock R.C. & Wu M.F. 1990, The Solubilities of Nitrous Oxide, Carbon Dioxide, Aliphatic Ethers and Alcohols, and Water in Cryogenic Liquids, *Chem. Eng. J.*, Vol. 43, pp. 25–31.
91. Kouvaris L.C. & Flasar F.M. 1991, Phase Equilibrium of Methane and Nitrogen at Low Temperatures: Application to Titan, *Icarus*, Vol. 91, pp. 112–124.
92. Thompson W.R., Zollweg J.A. & Gabis D.H. 1992, Vapour-Liquid Equilibrium Thermodynamics of N2+CH4: Model and Titan Applications, *Icarus*, Vol. 97, pp. 187–199.
93. Lorenz R. 1993, Raindrops on Titan, Presented at COSPAR Meeting, Washington DC, September 1992: *Advances in Space Research*, in press.
94. Lorenz R. 1993, The Life, Death and Afterlife of a Raindrop on Titan, *Planetary and Space Science*, Vol. 41, No. 9, pp. 647–655.
95. Thompson W.R. 1985, Phase Equilibria in N_2-Hydrocarbon Systems: Application to Titan, in 'The Atmospheres of Saturn and Titan', ESA SP-241, pp. 109–119.
96. Srokosz M.A., Challenor P.G., Zarnecki J.C. & Green S.F. 1992, Waves on Titan, ESA SP-338, pp. 321–323.
97. Raulin F. 1987, Organic Chemistry in the Oceans of Titan, *Advances in Space Research*, Vol. 7, No. 5, pp. (5)71–(5)81.
98. Gaskell R.W. 1993, Martian Surface Simulation, *J. Geophys. Res.*, Vol. 98, No. E6, pp. 11099–11103.

Manuscript received 27 September 1993

Pergamon

Planet. Space Sci., Vol. 42, No. 1, pp. 5–14, 1994

0032–0633/94 $7.00+0.00

0032–0633(93)E0039–F

Liquids and solids on the surface of Titan: results of a new photochemical model

L. M. Lara[1,*], R. D. Lorenz[2] and R. Rodrigo[1]

[1]Instituto de Astrofisica de Andalucia, CSIC, Apartado 3004, 18080 Granada, Spain
[2]Unit for Space Sciences, University of Kent, Canterbury, CT2 7NR, U.K.

Submitted July 1993; revised November 1993; received for publication 6 December 1993

Abstract. Recent radar, microwave and infrared observations of Titan suggest that a significant fraction of the surface may be covered by ice, in conflict with previous photochemical models which suggested a global ocean, 700 m deep, of ethane. We present here results of a new photochemical model, including updated reaction coefficients, and improved treatments of transport and condensation processes, which predict a lower ethane production (<285 m equivalent). We additionally consider the likely existence of a deep porous icy regolith on Titan's surface, which could "hide" the liquid hydrocarbons from observation, while permitting communication with the atmosphere to maintain the observed methane abundance against photolysis. This "shallow, buried ocean" model is compatible with current observational constraints on Titan's surface.

Introduction

The *Voyager* 1 encounter with Titan was something of a disappointment for planetary geologists, since the surface was obscured from *Voyager*'s cameras. No features such as volcanoes, grooved terrain or craters were observed, as seen elsewhere in the solar system. However, analysis of i.r. spectra (Hanel *et al.*, 1981) detected large amounts of organic molecules in the atmosphere. Polymerization of these organic compounds forms an orange haze which makes Titan's atmosphere opaque at visible wavelengths. Scientific interest therefore focused on the complex atmospheric chemistry, which begins with the photolysis of methane, which has a mixing ratio of about 2%. The fact that this amount of methane should have been depleted photolytically within approximately 10 million years, coupled with Titan's surface temperature, close to the triple point of methane, suggested the possibility of reservoirs of (liquid) methane on the surface (Eshleman *et al.*, 1983; Flasar, 1983), or that methane was being resupplied from the interior.

Subsequent work (Lunine *et al.*, 1983) was able to reconcile the near-surface undersaturation of methane (70% maximum, inferred from *Voyager* 1 radio-occultation measurements) with such a reservoir, noting that the dissolution of the less volatile ethane in methane seas would lower the methane vapour pressure. A global ocean was a widely-accepted model of Titan's surface, considering that early photochemical models (Yung *et al.*, 1984) predicted a 600 m global depth of ethane, forming (with methane and nitrogen) an ocean with an average depth of between 700 m and 9 km (Dubouloz *et al.*, 1989). Such a model was aesthetically attractive and agreed with the photochemical models and *Voyager* observations. Additionally, Sagan and Dermott (1982) introduced a theoretical argument (see later) that if oceans exist on Titan, they must be deep.

However, since the time this model came into vogue, observations have become available which suggest that Titan is not immersed in a global ocean. In this paper, after summarizing the observations, we present the results of a revised photochemical model which suggest a lower ethane production than before. In addition, arguments are presented which suggest regolith on Titan's surface may retain porosity to substantial depths, such that [as suggested by Stevenson (1992); for a detailed discussion on the surface of Titan, see Lunine (1993) and Lorenz

Correspondence to: L. M. Lara
*Present address: DESPA, Observatoire de Paris-Meudon, 92195 Meudon, France

(1993a)] large amounts of ethane and methane may be "buried".

Observations of Titan's surface

While it is not the purpose of this paper to provide a comprehensive review of observations of the surface of Titan, it is appropriate to summarize the available data to put our results into context.

Direct radar sensing of Titan's surface was achieved by Muhleman *et al.* (1990). Radar reflectivity of the surface, albeit at low signal-to-noise, was successfully measured on three nights at 0.38, 0.78 and 0.25—i.e. highly variable, but quite high (much higher than the reflectivity of a global hydrocarbon ocean). Subsequent measurements (Grossman *et al.*, 1991; Muhleman *et al.*, 1992) have confirmed the results, noting that there is a "bright spot" of high radar reflectivity, and that the radar reflectivity resembles those of the icy Galilean satellites, in particular Callisto.

Microwave radiometry (Grossman and Muhleman, 1992) suggests the surface emission temperature is about 82 K, suggesting an emissivity of about 0.88, consistent with an icy surface, but not with a global ocean.

While the atmosphere is opaque at most optical and i.r. wavelengths, due to absorption and scattering by the haze and gases, there are some near i.r. "window" regions (0.94, 1.08, 1.28, 1.58, 2 and 5 μm) between the methane absorption bands, where it may be possible to sense the surface. Recent observations (Lemmon *et al.*, 1993) have noted a variation in albedo at these window wavelengths that is correlated with the orbital period, suggesting that it is possible to sense the surface (or at least the lower troposphere) in these regions. These observations have since been confirmed by Griffith (1993).

Infrared observations by Griffith *et al.* (1991) at near-i.r. wavelengths (1.28, 1.68 and 2.0 μm) suggested a "dirty ice" surface—neither completely dark, such as would be expected for a surface covered in organic material, nor a completely bright icy surface. The analogue suggested by Griffith *et al.* is "1/3 Ganymede + 2/3 Phoebe".

Infrared observations (Noll and Knacke, 1993) at 5 μm suggest, if the atmosphere is relatively transparent at these wavelengths, that the surface albedo is too high for a global hydrocarbon covering, and resembles that of Callisto.

Thus, in summary, the observational evidence points to a (dirty) ice surface, although seas and lakes of liquid hydrocarbons are not ruled out. It is, in part, this observational evidence that has prompted us to re-examine the photochemical models suggesting that a deep global ocean should be present.

Theoretical model

Due to the complexity of organic chemistry (especially that involving nitrogen and oxygen compounds, as well as hydrocarbons), there are few comprehensive photochemical models which include a detailed treatment of condensation and dynamical processes.

A brief summary of the model (to be described in more detail in a forthcoming paper) is presented in this section. The solution of the continuity and momentum coupled equations for each constituent is computed, taking into account photochemical and dynamical processes: turbulent transport, parameterized by means of an eddy diffusion coefficient, $K(z)$, and molecular diffusion (coefficients calculated according to the Chapman–Enskog theory).

The model is applied to middle latitudes, with moderate solar activity, in the 40–1432 km altitude range. Modelled reactions include minor as well as major constituents.

Updated laboratory kinetics data and photodissociation cross-sections are used and a new eddy diffusion coefficient $K(z)$ is defined, in such a way that the theoretical profiles derived in this model are in good agreement with most recent analyses of *Voyager* data (Coustenis *et al.*, 1989a–c, 1991; Coustenis, 1990) and ground based observations (Tanguy *et al.*, 1990; Bézard *et al.*, 1992).

The temperature profile used is that obtained from *Voyager* 1 data below 250 km (Lellouch *et al.*, 1989). Above that altitude, profile J of Yelle's (1991) non-LTE model is used to represent the thermal structure at the upper atmosphere.

The main differences from the Yung *et al.* (1984) model are:

(1) The different thermal structure, showing a clearly marked stratopause and mesopause, while in previous photochemical models the temperature was an increasing function of height above 50 km. Since most of the reaction rates are temperature-dependent, it is to be expected that our results differ appreciably from Yung *et al.*'s predictions.

(2) Different $K(z)$. This is frequently the least known factor in the development of photochemical models. Depending on the main features of the atmosphere, it plays an important role on the distribution of the constituents. In the case of Titan, where many of the components are long-lived, the use of an adequate eddy diffusion coefficient is required to reproduce the available measurements. The re-analysis of *Voyager* i.r. data by Coustenis *et al.* (1989a) has obliged us to revise the modelling of photochemical and transport processes. Consequently, a new eddy diffusion coefficient has been used in an attempt to reproduce the stratospheric mixing ratios of minor constituents and thermospheric methane abundance. Comparing with Yung *et al.*'s profile, the most outstanding differences are seen at 150 km (3.2 mb) and at 700 km (7×10^{-5} mb), where two discontinuities in their profile are forced in an attempt to reproduce the stratospheric mixing ratios and C_2H_2 observations in the thermosphere. These latter measurements have been found very difficult to explain and must be regarded with caution (Strobel *et al.*, 1992).

(3) Updated rate coefficients and photoabsorption cross-sections, since a strong effort has been devoted to determine new reaction rates at low temperatures and involving the most controversial constituents in Titan's

atmosphere, namely, ethane and nitrogen compounds (Slagle *et al.*, 1988; Marston *et al.*, 1989a, b; Marston and Stief, 1989; Nesbitt *et al.*, 1990, 1991; Balla *et al.*, 1991). CH_3CN has also been included in the model and very recently discovered observationally.

(4) Oxygen chemistry. In order to reproduce the CO_2 abundance in the stratosphere, it is necessary to invoke an oxygen source (Samuelson *et al.*, 1983). The possible meteoroid ablation from Saturn's rings or interplanetary ices has been studied by Ip (1990). Thus, an incoming flux of water vapour or, equally, a deposition rate of water vapour molecules, is considered in the model. The magnitude is higher than that used by Samuelson *et al.* (1983) and by Yung *et al.* (1984), but still within theoretical predictions (Moses, 1992; Shemansky *et al.*, 1993; Johnson, 1993). The stratospheric H_2O mixing ratio is equal to $\sim 7 \times 10^{-9}$, a value in agreement with theoretical estimates (Coustenis *et al.*, 1993).

(5) A new treatment of condensation processes, similar to that developed by Romani and Atreya (1988, 1989) for Neptune's atmosphere. An aerosol distribution (Cabane *et al.*, 1992), consistent with albedo measurements, is taken into account to parameterize the loss due to the diffusive growth of the crystals. The radius and number of solid particles are functions of altitude.

(6) Dissociation of N_2 and CO by electron impact is exhaustively modelled. Incoming flux of primary saturnian magnetospheric electrons (Sagan and Thompson, 1984), energy degradation, energy deposition and secondary electron production are considered in order to reproduce the mixing ratio profiles of nitrogen compounds.

Photochemical processes: an overview

On Titan, most of the species are photochemically active, although many of them are removed from the vapour phase by condensation into various clouds (around 70 km) and hazes extending from 40 to 400 km. We have considered similar photochemical schemes to those in Yung *et al.*'s model. The photolysis processes are considered in the wavelength range 1150–2780 Å, integrals made every 2 Å, since most of the absorption cross-sections show very strong variations in a small range (integration intervals of 5–10 Å are inaccurate). Solar flux corresponding to moderate solar activity (Mount and Rottman, 1983) and modified to take into account the distance between Sun and Titan has been used. The aerosol distribution was considered to attenuate the incoming solar flux from 40 to 400 km, by means of a transmission factor consistent with the measurement of 0.03 for the u.v. albedo of Titan (Caldwell *et al.*, 1981). The effect of this additional opacity is relevant when studying the u.v. solar flux below 200 km. For $\lambda \leqslant 3000$ Å, the absorption of solar radiation is only 4% at 250 km (where aerosols are not present according to the distribution we have assumed); this absorption increases as the altitude decreases, reaching values of 90% at 130 km and 98% at the tropopause.

The removal of gas phase molecules by condensing processes is modelled by the diffusive growth rate for ice crystals, i.e. vapour phase molecules hit an ice crystal and stick to it. The diffusive mass growth rate (g s^{-1} per crystal) is taken from Pruppacher and Klett (1980):

$$\frac{dM}{dt} = \frac{4\pi C S V_p D M}{RT}, \qquad (1)$$

where C is proportional to the crystal size and is a function of the crystal geometry, S is the supersaturation, T is the absolute temperature, R is the universal gas constant, V_p and M are, respectively, the vapour pressure and the molecular weight of the condensing species, and D is the molecular diffusion coefficient of the condensing species. For simplicity in our calculations, we assume the crystals to be spherical, in which case C equals the radius, and that each species condenses only on its own ice particle. Three parameter saturation laws were used for each constituent, derived using the three coldest points given in the *CRC Handbook of Chemistry and Physics* (Weast, 1988), together with information in Sagan and Thompson (1984), Reid *et al.* (1988), and in the paper by Moses *et al.* (1992), which performs similar calculations for Neptune's atmosphere.

Since the above vapour phase loss process is per crystal, we require a number density profile of the hydrocarbon ice crystals. We have used that given by Cabane *et al.* (1992). The model calculates the number densities as a function of altitude, and where the obtained mixing ratio is greater than that allowed by saturation laws, the loss due to condensing processes is taken into account.

General results

We present here a brief summary of the main results of the dynamical–photochemical model:

(1) The atmosphere is well mixed up to very high levels ($\sim$900 km), and above that altitude, diffusive equilibrium is reached for most of the constituents.
(2) Stratospheric mixing ratios of all the minor constituents are in broad agreement with latest analysis (*Voyager* i.r. data and ground based) for simple hydrocarbons (see Fig. 1a–c).

These results are reassuring, indicating that the photochemical schemes considered and transport phenomena [mostly $K(z)$] developed in this model are adequate for Titan's atmosphere.

Ethane production

Sensitivity to reaction rate constants

The most important chemical reaction producing ethane in Titan's atmosphere is:

$$CH_3 + CH_3 + M \rightarrow C_2H_6 + M,$$

although there are small contributions at high and low atmospheric levels coming from propane photolysis, self-

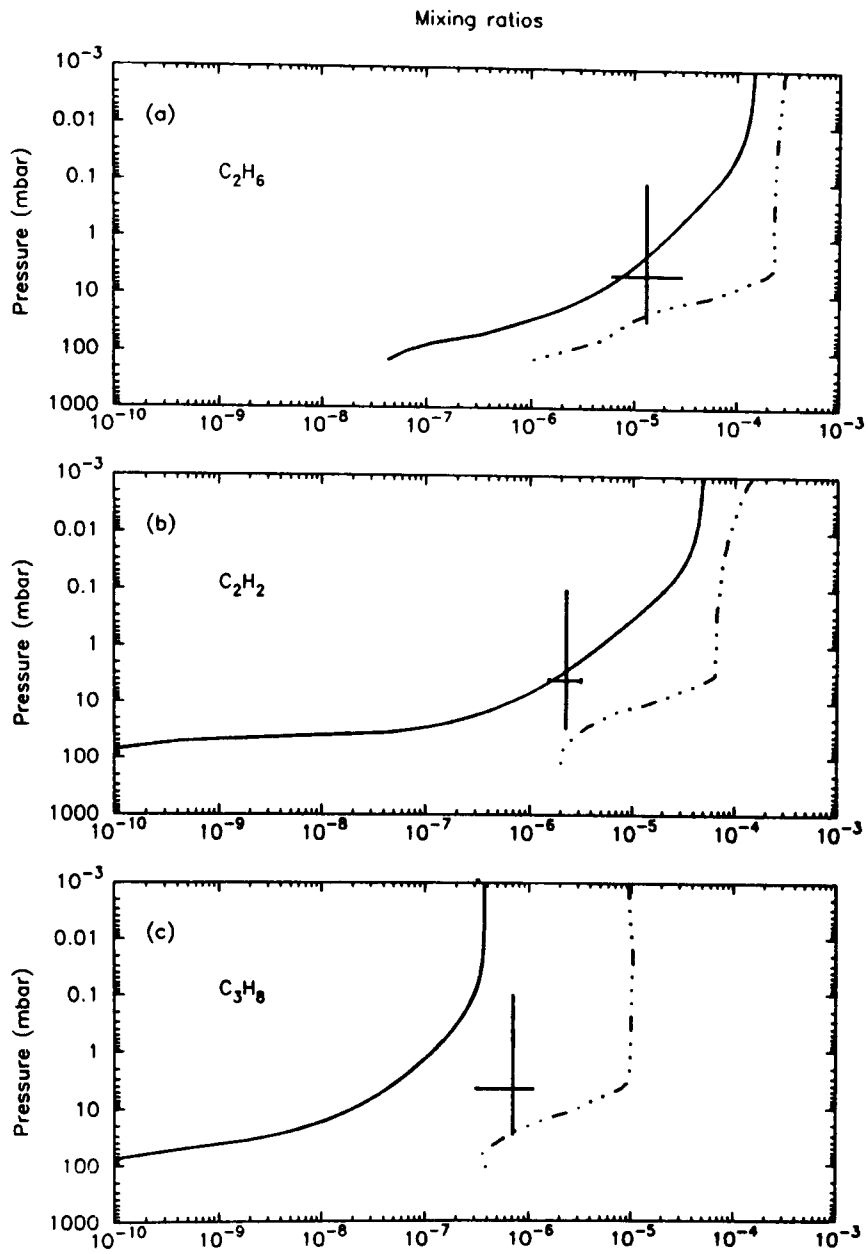

Fig. 1. Mixing ratio profiles of compounds important for understanding the nature of the surface: (a) ethane; (b) acetylene; (c) propane. Solid curves are those generated by our model, dashed curves are due to Yung *et al.* (1984) and crosses are observational values of Coustenis *et al.* (1989a)

reaction of C_2H_5 and reaction of C_2H_5 with C_2H_3, respectively.

The main difficulty is that there is little information about the rate coefficient at low temperatures. Accordingly, in this work, we have considered two different reaction rates given by: (1) Slagle *et al.* (1988) and (2) Laufer *et al.* (1983).

The results are referenced in the text as (1) and (2), respectively. The corresponding production profiles for the two rate coefficients are shown in Fig. 2. The stratospheric abundance is well-reproduced (within the error bars) with (1) and (2), although by using the reaction rate given by Laufer *et al.* (1983), we obtain an ethane stratospheric mixing ratio equal to the lower limit given by Coustenis *et al.* (1989a).

In order to calculate the depth of the liquid surface existing on Titan, if any, several methods have been used. Some authors consider that all the gaseous ethane produced by methyl radical self-reaction in Titan's atmosphere is lost by condensation at the cold trap. The photochemical loss is negligible when compared with that due to condensation, which is the case by considering both rates ($\sim 10^7$ cm $^{-2}$ s $^{-1}$ compared with 10^9 cm $^{-2}$ s $^{-1}$).

Now, if we assume instead of "instantaneous" loss at the cold trap, that the amount of ethane deposited on the surface is that which condenses according to the condensation equation (1) above, we obtain the following results:

(1) The loss due to ethane condensation at 52 km is 4.98×10^3 cm $^{-1}$ s $^{-1}$ and at 40 km is negligible, 1.2×10^{-7}

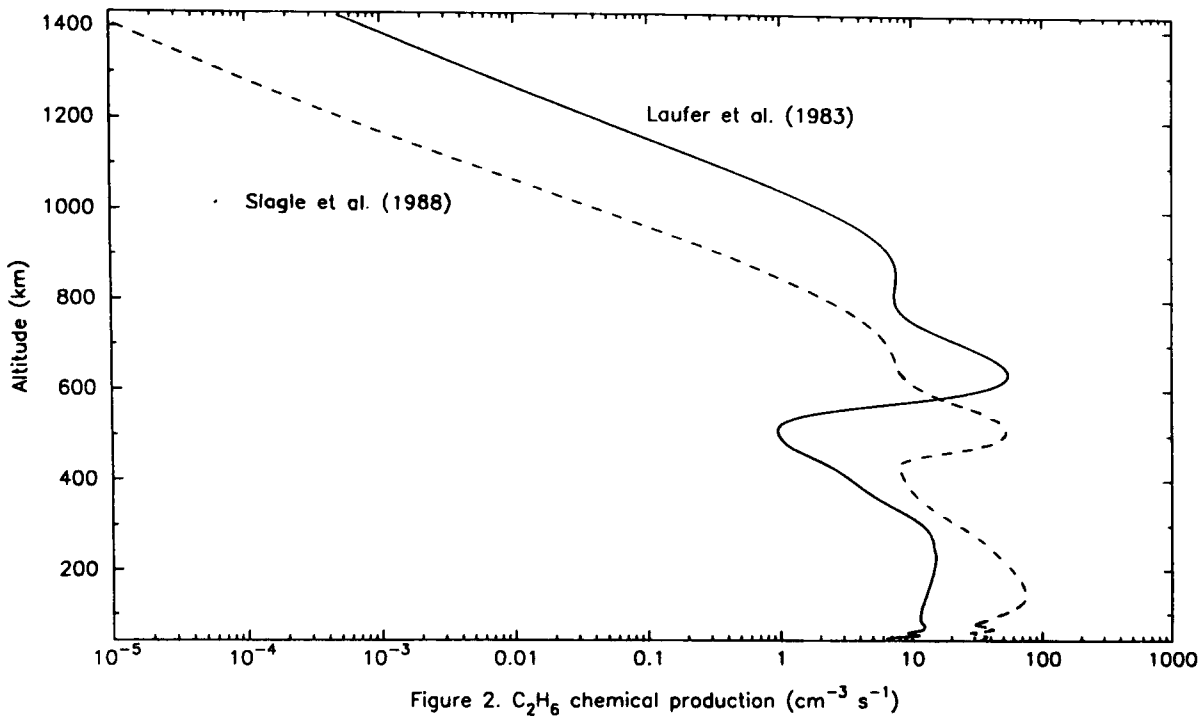

Fig. 2. Production rate profiles generated by our model, using two different reaction rates (see text)

cm^{-3} s^{-1} (because the boundary condition at 40 km is exactly the mixing ratio given by the saturation law and it cannot condense any further). Given the pronounced slope, we interpolate between 40 and 52 km and integrate the total loss in that altitude range, obtaining 2.27×10^9 cm^{-2} s^{-1}, multiplying by the age of Titan and dividing by the density, we obtain 250 m depth for the ocean.

(2) Similarly, for rate coefficient (2), we obtain that ethane saturates at 52 km, with a total loss equal to 4.39×10^3 cm^{-3} s^{-1}, giving a deposition rate of condensate of 2.06×10^9 cm^{-2} s^{-1}. In this case, the ocean would be 226 m deep.

Condensation of other compounds

Using our model, it is possible to compute the production rates of other organic materials, to compare the likely ratio of solid and liquid materials produced. The production rates for the most important compounds are given in Table 1. Making use of the density of the various organic compounds, the equivalent depth of deposit of them may be scaled in the same way as the ethane production (i.e. depth in metres = production rate × scaling factor). These scaling factors are also listed in Table 1. Dealing with the photochemical aerosols, we have deduced an integrated production rate of $\sim 1.7 \times 10^{-14}$ g cm^{-2} s^{-1}, to be compared with $\sim 1.2 \times 10^{-14}$ g cm^{-2} s^{-1} given by McKay *et al.* (1989), a value which provides the best theoretical results to explain the thermal structure of Titan's atmosphere.

It may be seen in Table 1 that the ethane production (deposition) rate is of the order of four times the acetylene production. All the other solid materials are produced in much smaller quantities. Propane is a liquid at Titan surface temperatures, and therefore contributes a small amount (of the order of 2 m) to ocean depth. Thus, the net production of liquids (2.3×10^9 cm^{-2} s^{-1} for C_2H_6 and a negligible amount for C_3H_8) exceeds the production of solid organics (C_2H_2, HCN and CO_2), but by a factor of about 4. Bodies of exposed liquid on the surface of Titan are likely to contain large amounts of suspended organic material, and will probably therefore be "dark".

If the particles of solid hydrocarbons or ice regolith are exposed on the surface and are non-cohesive (although if moistened by ethane/propane, they will presumably be

Table 1. Integrated production (deposition) rates (cm^{-2} s^{-1}) of liquid (C_2H_6 and C_3H_8) and solid (others) materials on the surface of Titan

	Integrated production	Scaling factor	Depth (m)
C_2H_6	2.3×10^9	1.1×10^{-7}	250
C_3H_8	4.3×10^6	1.4×10^{-7}	0.6
C_2H_2*	5.6×10^8	7.7×10^{-8}	43
CO_2	6.5×10^5	7.1×10^{-8}	0.05
HCN	5.0×10^6	9.5×10^{-8}	0.5

*Deposited as a stable polymer.

somewhat sticky), they may be kicked up into a dust cloud of measurable opacity by the aerodynamic wake of the *Huygens* probe when it lands (Lorenz, 1993b). Detection of such a dust cloud would imply that the surface deposits are non-cohesive, and that any binding agent (like ethane) has evaporated or drained away.

Sensitivity to the aerosol distribution and eddy diffusion coefficient

To test the sensitivity of the model to the assumed aerosol distribution, we have considered two different ones corresponding to the mass production rates 3.5×10^{-14} and 3.5×10^{-12} kg cm^{-2} s^{-1} (Cabane *et al.*, 1992), respectively. The results concerning the amount of solid and liquid material formed under such conditions are identical. This behaviour is explained because photochemistry acts in such a way that supersaturation, after a certain number of iterations, balances the loss due to condensation since all the other terms in formula (1) depend explicitly on the physical parameters of the aerosol distribution, i.e. radius and number density of crystals.

Dealing with $K(z)$, and since this free parameter may not be unique, we also computed the mixing ratio profiles and the removal by condensation when using $K(z)/5$, $K(z) \times 5$ and that given by Steiner and Bauer (1990).

In the case of $K(z)$ higher by a factor of 5, the outstanding disagreement between observations (IRIS and ground based) and the theoretical predictions of the model makes any study of Titan's inferred surface properties invalid.

However, when using $K(z)/5$, the results can be considered as acceptable for C_2H_6, C_2H_2, C_3H_8 and CO_2 mixing ratios, these being within either the observational values or 2σ, depending on the species, with σ the uncertainty associated with the observational measurements. The disagreement between available data and theoretical profiles is noticeable for the other species. The production of condensate is lower, and the total ocean depth is decreased by a factor of 10, while that of the solid substrate is four times lower.

In the case of taking $K(z)$ into account (Steiner and Bauer, 1990), the stratospheric mixing ratios are not fully compatible with IRIS data. Ethane, acetylene and methyl acetylene are below the lower limit, but are within 2σ. The amount of solid and liquid material produced by condensation is also diminished. More concisely, solid acetylene formation decreases by a factor of 5, while CO_2 formation is 14 times lower. Ethane is not saturated in the stratosphere, while propane only gives rise to 0.2 m of liquid material deposited on Titan's surface.

Sensitivity to CH_4 stratospheric mixing ratio

As Lellouch *et al.* (1989) noted, there is no unambiguous determination of the methane mixing ratio in the stratosphere, although it is well constrained between 0.005 and 0.034, and between 0.01 and 0.017 when argon in absent. According to Strobel *et al.*'s (1992) results, retrieved from u.v.s. data analysis, in order to obtain a better fit of the inferred optical depths, the CH_4 mixing ratio at the tropopause must be higher than 0.017. Our nominal values are referred to methane and argon relative abundances of 0.026 and 0.014, respectively.

In the case of methane and argon relative abundances at the tropopause, equal to 3.4×10^{-2} and 13.6×10^{-2}, respectively, we obtain stratospheric mixing ratios in accordance with IRIS observations. Solids are deposited in slightly larger amounts. Actually, CO_2 is modified with respect to the nominal value by a factor of 1.22 lower, while C_2H_2 is 3% higher. In the case of ethane and propane, liquids at the physical conditions of Titan's surface, the difference is negligible, and C_2H_6 and C_3H_8 would yield an ocean 0.12% deeper.

On the other hand, when argon is not present in Titan's atmosphere and we assume the highest CH_4 stratospheric mixing ratio (1.7%), deposits on Titan are lowered. Solids, mainly C_2H_2, decrease by 2.8%, and CO_2 increases by a factor of 1.4, while, as in the previous case, the amounts of ethane and propane diminish by 0.4% and 3.5%, respectively.

Sensitivity to CH_4 photolysis at Ly-α

Mordaunt *et al.* (1993) have very recently found that C–H bond fission is the dominant primary process following CH_4 excitation at 1216 Å. They note that the methane photodissociation at Ly-α yields CH_3 (and H) fragments, rather than methylene radical ($^{1,3}CH_2$). As they also point out, current models of the hydrocarbon photochemistry prevailing in the atmospheres of the outer planets and some of their moons, especially Titan, will need some revision.

Since these authors do not give a unique interpretation of their results, as can be seen from Table II in their paper, we have computed the theoretical mixing ratio profiles when considering both models separately.

Model 1, which would not produce CH, gives rise to excellent agreement between observations and stratospheric results, for hydrocarbon as well as for nitrogen compounds [for a more detailed study, see Lara *et al.* (1993a)]. The production of solid and liquid material is slightly modified with respect to the nominal values. More concisely, acetylene solid deposition decreases by a factor of 2, while that of carbon dioxide is 1.6 times higher. Most of the liquid production does not change with respect to the values we assume as nominal. The ocean is 3.3% deeper because of the increase in the propane deposition rate, but not due to that of ethane.

When we consider Model 2, in which $^{1,3}CH_2$ is not produced by methane photolysis, the stratospheric mixing ratio profiles are in accordance with available data, excepting ethylene, which is two orders of magnitude higher than the value reported by Coustenis *et al.* (1989a). In this case, deposits on Titan are quite different from those obtained in the previous cases. The equivalent ocean depth is diminished by a factor of 1.08, adding the contributions from ethane, which decrease by a factor of 1.13, and propane, which increases by a factor of 13. Dealing with the solid

substrate, there is also an enhancement coming from C_2H_2, which leads to a deposition rate 1.6 times greater. On the other hand, CO_2 is diminished by a factor of 7.

In conclusion, and considering those cases where the agreement between IRIS and ground based data is broader, we estimate the accumulated depth of ethane on the surface as between about 250 and 258 m, where the theoretical predictions derived with Model 2 by Mordaunt *et al.* (1993) have been excluded. Thus, these limits are generated by means of the nominal results and those obtained making use of Model 1 in Mordaunt *et al.* (1993). It is possible, by constraining surface temperature and atmospheric composition with the *Voyager* 1 results, and by assuming that the ocean and atmosphere are in thermodynamic equilibrium, to deduce a range of allowable ocean compositions (Dubouloz *et al.*, 1989). The ocean, comprising methane, ethane and nitrogen, can have an ethane content of between 5% and 90%. Thus, for our 240 m depth of ethane, the total ocean depth may be between 250 m and 5 km [compared with 700 m and 10 km for the ethane deposition and methane chemical loss predicted by Yung *et al.* (1984)].

We note, in passing, that on the basis of a simple photolysis experiment, Bar-Nun and Podolak (1979) deduced an ethane production rate of 5.1×10^8 cm^{-2} s^{-1}, corresponding to an integrated depth of ethane of 56 m.

Tidal considerations

Sagan and Dermott (1982) introduced a theoretical argument that oceans on Titan should either be deep or non-existent, since shallow oceans would have strong tidal dissipation (the tidal potential due to Saturn's gravitational field is approximately 200 times that of the Moon on the Earth), such that Titan's orbit would have been quickly circularized, a situation inconsistent with Titan's observed high eccentricity (0.029). They argued for global oceans of at least 400 m depth.

This argument was consistent with the Yung *et al.* (1984) photochemical model, which suggested about 600-m-deep oceans, so until the late 1980s (when observational data became available), a widely-accepted model of Titan's surface was the deep, global ocean.

When the radar observations became available in the early 1990s, some imaginative (yet suspiciously exotic) models were formulated to account for the high radar reflectivity that was inconsistent with a global liquid covering. These included radar-reflective particles suspended in the ocean, bubbly or frothy ocean (Lunine, 1993), and an "ocean" hidden in subsurface "aquifers" (Stevenson, 1992).

While Sagan and Dermott's argument is essentially correct, it ignores the dissipation in Titan's interior. Pre-*Voyager* assessments (Peale *et al.*, 1980) of the tidal dissipation in the Saturnian satellites (made before there were thoughts of oceans on Titan) found Titan's current high orbital eccentricity hard to explain. Solid body dissipation should have damped the eccentricity to small values in any case.

The presence of liquids on the surface [whether ethane/methane oceans, or a hypothesized liquid water–ammonia mantle (Stevenson, 1992), some hundreds of kilometres below the surface] only makes the eccentricity somewhat harder to explain than it is anyway for a completely solid Titan. We therefore do not consider the Sagan and Dermott limit to be a valid constraint on permitted ocean depth.

Timescale

The timescale assumed for both the formation/deposition of ethane on Titan and for the tidal circularization of the orbit have been assumed to be the age of the solar system, namely 4.5 Gy. However, recent work by McKay *et al.* (1993) suggests that Titan's atmosphere may have been frozen on the surface for a large part of Titan's history, the current atmosphere having been liberated as recently as 3 Gy ago [see Fig. 5 of McKay *et al.* (1993)].

This reduced timescale further erodes the significance of the alleged tidal constraint on ocean depth, and reduces the time available for chemistry. Thus, we may further reduce the ethane inventory on the surface by a factor of about 1.5, making the globally-averaged "ocean" depth between 167 and 172 m.

Impacts and regolith

In addition to the ethane and solid organic deposition on the surface, there is also deposition of meteoric material, we assume mostly water ice. Additionally, larger impactors will penetrate the atmosphere to form craters on the surface, producing large amounts of impact ejecta, which will form a regolith on the surface. Large impactors will form craters deeper than several hundred metres, i.e. they will excave crustal material from below the thin veneer of photochemical products. Consideration of planetary formation processes, and comparison with the other moons of Saturn, suggests that this crustal material should be dominated by water ice. Thus, most of the ejecta from large impacts, and hence much of the regolith, should be water ice, with perhaps some silicates.

On Earth, water ice particles (deposited as snow) stick together, and over time (and with increasing depth) fuse with one another to form impermeable ice. In cold, dry conditions (e.g. Greenland), the close-off depth (at which the pores between particles become sealed) is 80 m, while under warmer, wetter conditions (e.g. Seward Glacier in the Yukon), close-off is at about 13 m. These figures, taken from Patterson (1972), correspond to close-off times of 100 and 4 y, respectively.

At the extremely cold temperatures on Titan (94 K), annealing of ice particles will be considerably slower. Smoluchowski and McWilliam (1984) evaluated the densification of ices on outer planet satellites: application of their results to Titan suggests that water ice should remain porous to depths of the order of several kilometres.

There will be some localized impact melting—additionally, Thompson and Sagan (1992) have suggested that liquid ejecta blankets of the order of 4*D* diameter may

exist around craters of diameter D, as on Mars—and some compaction by impact shock will also occur. However, since these are localized processes, they do not affect the ability of the surface as a whole to absorb liquids. Impact shock may, in any case, fracture "bedrock" to substantial depths.

It is conceded that more volatile or motile ices such as water—ammonia will undergo annealing or compaction much quicker than water ice, but water ice remains an excellent candidate for the major surface constituent, based on comparisons with other outer solar system satellites.

The post-heavy bombardment calculations of Sagan and Thompson suggest an ejecta deposition rate of about 8 cm every 1 million years. This corresponds, over 4.5 billion years, to a regolith depth of 360 m. However, note that much of this will be "recycled" ejecta, so this may be taken as an upper limit.

Thompson and Sagan consider only impactors of diameter greater than 2 m: smaller impactors may ablate completely, or at least be disrupted, before reaching the surface. Such impactors will provide a source of meteoric "dust", as well as providing H_2O for atmospheric chemistry. However, we leave, estimation of the "dust" production rate to future work.

In addition to the "steady-state" population of impactor, there may have been a dramatic bombardment episode (Jones and Lewis, 1987) in Titan's history, following the collisional disruption of the parent of Hyperion (Hyperion's size and irregular shape suggest that it is the fragment of a once larger body that was fragmented by an impact). Calculations indicate that most (>90%) of proto-Hyperion's debris (i.e. between 1.9×10^{22} and 7.0×10^{23} g) will have fallen on Titan's surface within 100 y of the collision event (Farinella *et al.*, 1990). This corresponds to a depth of impacting material of between 300 m and 8.4 km. Jones and Lewis note that there would have been a substantial deposition of organic (and nitrogenous) material produced by atmospheric shock chemistry at this time.

Thus, it seems likely that above any solid "bedrock" on Titan, there is a largely porous icy regolith of at least several hundred metres thickness. Such a regolith could conceal a few hundred metres worth of liquid hydrocarbons from remote observation, yet remain in communication with the atmosphere to maintain the observed methane abundance.

Lunine (1993) suggests that a 1 km regolith could conceal an ocean of 300 m depth, noting Hartmann's (1973) estimate of a 2 km depth regolith in the Lunar terrae regions: the 300 m+regolith postulated here could, by the same argument, completely conceal a 100 m ocean, and would, even for the 200 m+ethane production suggested by our model, resemble an icy surface to ground based observations.

Conclusions

We have presented the results of a revised photochemical model of Titan's atmosphere, which predict a lower ethane production rate than previous models. We deduce a global-equivalent depth of the ethane "ocean" of between 250 and 258 m, and between 167 and 172 m in the case of considering the frozen epoch of Titan's atmosphere. This suggests a maximum total ocean ($C_2H_6+N_2+CH_4$) depth of about 5 km. We note that the regolith depth on Titan may be from 300 m to around 10 km. Globally speaking, then, much of Titan's ocean may be "buried", although some lakes and seas may be present at the surface (e.g. in crater basins).

Such a heterogeneous "dirty ice" surface, with possibly exposed lakes/seas of ethane, is consistent with all the available near-i.r., microwave radiometry and radar data.

The mystery of Titan's surface will not be conclusively resolved, however, until the middle of the next decade, when the *Cassini* mission begins a detailed exploration of the Saturnian system, including the release of the *Huygens* probe (Lebreton, 1992), which will descend by parachute to Titan's surface.

Acknowledgements. R. Lorenz acknowledges the support of a postgraduate research grant from the U.K. Science and Engineering Research Council. L. M. Lara and R. Rodrigo are supported by the Spanish Commisión Interministerial de Ciencia y Tecnologia under contracts ESP91-1290-CO2-01 and ESP93-0338.

References

Balla, R. J., Casleton, K. H., Adams, J. S. and Pasternack, L., Absolute rate constants for the reaction of CN with CH_4, C_2H_6 and C_3H_8 from 298 to 1500 K using high temperature photochemistry and diode laser absorption. *J. phys. Chem.* **95**, 8694–8701, 1991.

Bar-Nun, A. and Podolak, M., The photochemistry of hydrocarbons in Titan's atmosphere. *Icarus* **38**, 115–122, 1979.

Bézard, B., Marten, A. and Paubert, G., First ground-based detection of cyanoacetylene on Titan. *Bull. Am. astron. Soc.* **24**, 953, 1992.

Cabane, M., Chassefière, E. and Israel, G., Formation and growth of photochemical aerosols in Titan's atmosphere. *Icarus* **96**, 176–189, 1992.

Caldwell, J., Owen, T., Rivolo, A. R., Moore, V., Hunt, G. E. and Butterworth, P.S., Observations of Uranus, Neptune and Titan by the International Ultraviolet Explorer. *Astrophys. J.* **86**, 298–305, 1981.

Coustenis, A., Spatial variations of temperature and composition in Titan's atmosphere: recent results. *Ann. Geophys.* **8**, 645–652, 1990.

Coustenis, A., Bézard, B. and Gautier, D., Titan's atmosphere from Voyager infrared observations. I. The gas composition of Titan's equatorial region. *Icarus* **80**, 54–76, 1989a.

Coustenis, A., Bézard, B. and Gautier, D., Titan's atmosphere from Voyager infrared observations. II. The CH_3D abundance and D/H ratio from the 900–1200 cm^{-1} spectral region. *Icarus* **82**, 67–80, 1989b.

Coustenis A., Bézard, B. and Gautier, D., Titan's atmosphere from Voyager infrared observations: latitudinal variations of temperature and composition. *Bull. Am. astron. Soc.* **21**, 958, 1989c.

Coustenis, A., Bézard, B., Gautier, D. and Marten, A., Titan's atmosphere from Voyager infrared observations. III. Vertical distributions of hydrocarbons and nitriles near Titan's north pole. *Icarus* **89**, 152–167, 1991.

Coustenis, A., Encrenaz, Th., Bézard, B., Bjoraker, G., Graner,

G., Dang-Nhu and Arie, E., Modelling Titan's thermal infrared spectrum for high resolution space observations. *Icarus* **102,** 240–260, 1993.

Dubouloz, N., Raulin, F., Lellouch, E. and Gautier, D., Titan's hypothesized ocean properties: the influence of surface temperature and atmospheric composition uncertainties. *Icarus* **82,** 81–106, 1989.

Eshleman, V. R., Lindal, G. F. and Tyler, G. L., Is Titan wet or dry? *Science* **221,** 53–55, 1983.

Farinella, P., Paolicchi, P., Strom, R. G., Kargel, J. S. and Zappala, V., The fate of Hyperion's fragments. *Icarus* **83,** 186–204, 1990.

Flasar, F.M., Oceans on Titan. *Science* **221,** 55–57, 1983.

Griffith, C. A., Evidence for surface heterogeneity on Titan. *Nature* **364,** 511–514, 1993.

Griffith, C. A., Owen, T. and Wagener, R., Titan's surface and troposphere, investigated with ground-based, near-infrared observations. *Icarus* **93,** 362–378, 1991.

Grossman, A. W. and Muhleman, D. O., Observations of Titan's radio light-curve at 3.5 cm. *Bull. Am. astron. Soc.* **24,** 954, 1992.

Grossman, A. W., Muhleman, D. O., Slade, M. A. and Butler, B. J., VLA/Goldstone planetary radar results, in *Proc. Int. Symp. on Radars and Lidars in Earth and Planetary Sciences*, Cannes (2–4 September 1991), ESA SP-328, pp. 19–22, 1991.

Hanel, R., Conrath, B., Flasar, F. M., Kunde, V., Maguire, W., Pearl, J., Pirraglia, J., Samuelson, B., Herath, L., Allison, M., Cruikshank, D., Gautier, D., Gierasch, P., Horn, L., Koppany, P. and Ponnamperuma, C., Infrared observations of the saturnian system from Voyager 1. *Science* **212,** 192–200, 1981.

Hartmann, W. H., Ancient lunar mega-regolith and subsurface structure. *Icarus* **18,** 634–636, 1973.

Ip, W. H., Meteoroid ablation processes in Titan's atmosphere. *Nature* **345,** 511–512, 1990.

Johnson, R. E., Rough stuff at Saturn. *Nature* **363,** 300–301, 1993.

Jones, T. D. and Lewis, J. S., Estimated impact shock production of N_2 and organic compounds on early Titan. *Icarus* **72,** 381–393, 1987.

Laufer, A. H., Gardner, E. P., Kwok, T. L. and Yung, Y. L., Computations and estimates of rate coefficients for hydrocarbon reactions of interest in the atmospheres of the outer solar system. *Icarus* **56,** 566–567, 1983.

Lebreton, J.-P., The Huygens probe, in *Proc. Symp. on Titan*, Toulouse (9–12 September 1991), ESA SP-338, pp. 287–292, 1992.

Lellouch, E., Coustenis, A., Gautier, D., Raulin, F., Dubouloz, N., and Frere, C., Titan's atmosphere and hypothesized ocean: a reanalysis of the Voyager 1 radio-occultation and IRIS 7.7 mm data. *Icarus* **79,** 328–349, 1989.

Lemmon, M. T., Karkoshka, E. and Tomasko, M., Titan's rotation: surface feature observed. *Icarus* **103,** 329–332, 1993.

Lorenz, R., The surface of Titan. *ESA J.* **17,** 275–292, 1993.

Lorenz, R., Wake-induced dust cloud formation following impact of planetary landers. *Icarus* **101,** 165–167, 1993b.

Lunine, J. I., Does Titan have an ocean? A review of current understanding of Titan's surface. *Rev. Geophys.* **31,** 131–149, 1993.

Lunine, J. I., Stevenson, D. J. and Yung, Y. L., Ethane ocean on Titan. *Science* **222,** 1229–1230, 1983.

Marston, G. and Stief, L. J., Structure, spectroscopy and kinetics of the methylene amidogen (H_2CN) radical. *Res. chem. Intermediates* **12,** 161–186, 1989.

Marston, G., Nesbitt, F. L. and Stief, L. J., Branching ratios in the $N+CH_3$ reaction: formation of methylene amidogen (H_2CN) radical. *J. phys. Chem.* **91,** 3483–3491, 1989a.

Marston, G., Nesbitt, F. L., Nava, D. F., Payne, W. A. and Stief, L. J., Temperature dependence of the reaction of nitrogen atoms with methyl radicals. *J. phys. Chem.* **93,** 5769–5774, 1989b.

McKay, C. P., Pollack, J. B. and Courtin, R., The thermal structure of Titan's atmosphere. *Icarus* **80,** 23–53, 1989.

McKay, C. P., Pollack, J. B., Lunine, J. I. and Courtin, R., Coupled atmosphere–ocean models of Titan's past. *Icarus* **102,** 88–98, 1993.

Mordaunt, D. H., Lamber, I. R., Morley, G. P., Ashfold, M. N. R., Dixon, R. N., Western, C. M., Schneider, L. and Welge, K. H., Primary product channels in the photodissociation of methane at 121.6 nm. *J. Chem. Phys.* **98,** 2054–2065, 1993.

Moses, J. I., Meteoroid ablation in Neptune's atmosphere. *Icarus* **99,** 368–383, 1992.

Moses, J. I., Allen, M. and Yung, Y. L., Hydrocarbon nucleation and aerosol formation in Neptune's atmosphere. *Icarus* **99,** 318–346, 1992.

Mount, G. H. and Rottman, G. J., The solar absolute spectral irradiance 1150–3173 Å: May 17, 1982. *J. geophys. Res.* **88,** 5403–5410, 1983.

Muhleman, D. O., Grossman, A. W., Butler, B. J. and Slade, M. A., Radar reflectivity of Titan. *Science* **248,** 975–980, 1990.

Muhleman, D. O., Grossman, A. W., Slade, M. A. and Butler, B. J., The surface of Titan and Titan's rotation: what is radar telling us? *Bull. Am. astron. Soc.* **24,** 954–955, 1992.

Nesbitt, F. L., Marston, G. and Stief, L. J., Kinetics studies of the reactions of H_2CN and D_2CN radicals with N and H. *J. phys. Chem.* **94,** 4946–4951, 1990.

Nesbitt, F. L., Marston, G., Stieff, L. J., Wickramaartchi, M. A., Tao, W. and Klem, R. B., Measurement of the photoionization spectra and ionization thresholds of the H_2CN and D_2CN radical. *J. Phys. Chem.* **95,** 7613–7617, 1991.

Noll, K. S. and Knacke, R. F., Titan: 1–5 μm photometry and spectrophotometry and a search for variability. *Icarus* **101,** 272–281, 1993.

Patterson, S., *Physics of Glaciers*. Pergamon Press, Oxford, 1972.

Peale, S. J., Cassen, P. and Reynolds, R. T., Tidal dissipation, orbital evolution and the nature of Titan's inner satellites. *Icarus* **43,** 65–72, 1980.

Pruppacher, H. R. and Klett, J. D., *Microphysics of Clouds and Precipitation*. D. Reidel, Dordrecht, 1980.

Reid, R. C., Prausnitz, J. M. and Poling, B. E., *The Properties of Gases and Liquids*, 4th Ed. McGraw Hill, New York, 1988.

Romani, P. N. and Atreya, S. K., Methane photochemistry and haze production on Neptune. *Icarus* **74,** 424–445, 1988.

Romani, P. N. and Atreya, S. K., Stratospheric aerosols from CH_4 photochemistry. *Geophys. Res. Lett.* **16,** 941–944, 1989.

Sagan, C. and Dermott, S. F., The tide in the seas of Titan. *Nature* **300,** 731–733, 1982.

Sagan, C. and Thompson, W. R., Production and condensation of organic gases in the atmosphere of Titan. *Icarus* **54,** 133–161, 1984.

Samuelson, R. E., Maguire, W. C., Hanel, R. A., Kunde, V. G., Jennings, D. E., Yung, Y. L. and Aikin, R. C., CO_2 on Titan. *J. geophys. Res.* **88,** 8709–8715, 1983.

Shemansky, D. E., Matheson, P., Hall, D. T., Hu, H.-Y. and Tripp, T. M., Detection of the hydroxyl radical in the Saturn magnetosphere. *Nature* **363,** 329–331, 1993.

Slagle, I. R., Gutman, D., Davies, J. W. and Pilling, M., Study of the recombination reaction CH_3+CH_3. 1. Experiment. *J. phys. Chem.* **92,** 2455–2462, 1988.

Smoluchowski, R. and McWilliam, A., The structure of ices on satellites. *Icarus* **58,** 282–287, 1984.

Steiner, G. and Bauer, S. J., Molecular and eddy diffusion in the atmosphere of Titan. *Ann. Geophys.* **8,** 473–476, 1990.

Stevenson, D. J., The interior of Titan, in *Proc. Symp. on Titan*, Toulouse (9–12 September 1991), ESA SP-338, pp. 29–33, 1992.

Strobel, D. F., Summers, M. E. and Zhu, X., Titan's upper atmosphere: structure and ultraviolet emissions. *Icarus* **100**, 512–526, 1992.

Tanguy, L., Bézard, B., Marten, A., Gautier, D., Gérard, E., Paubert, G. and Lecacheux, A., Stratospheric profiles of HCN on Titan from millimeter observations. *Icarus* **85**, 43–57, 1990.

Thompson, W. R. and Sagan, C., Organic chemistry on Titan—Surface interactions, in *Proc. symp. on Titan*, Toulouse (9 12 September 1991), ESA SP-338, pp. 167–176, 1992.

Weast, R. C. (Ed.), *Handbook of Chemistry and Physics*, 68th Ed., 1987–1988. CRC Press, Boca Raton, FL, 1988.

Yelle, R. V., Non-LTE models of Titan's upper atmosphere. *Astrophys. J.* **383**, 380–400, 1991.

Yung, Y. L., Allen, M. and Pinto, J. P., Photochemistry of the atmosphere of Titan: comparison between model and observations. *Astrophys. J.* **55**, 465–506, 1984.

Meas. Sci. Technol. 5 (1994) 1033–1041. Printed in the UK

An impact penetrometer for a landing spacecraft

R D Lorenz†, M Bannister‡, P M Daniell†, Z Krysinski§, M R Leese†, R J Miller,†, G Newton||, P Rabbetts‡, D M Willett|| and J C Zarnecki†

† Unit for Space Sciences, University of Kent, Canterbury CT2 7NR, UK
‡ Rutherford Appleton Laboratory, Chilton OX11 0QX, UK
§ Space Research Institute, 00-716 Warsaw, Poland
|| Physics Laboratory, University of Kent, Canterbury CT2 7NR, UK

Received 5 April 1994, in final form 12 May 1994, accepted for publication 27 May 1994

Abstract. The design, development and calibration of an impact force transducer or penetrometer, for use on the Huygens spacecraft scheduled to land on the surface of Saturn's moon Titan, is described, The thumb-sized transducer employs a piezoelectric sensing element and is capable of working at cryogenic temperatures. Use of the sensor on a spacecraft imposes several reliability and safety constraints, as well as the desire to minimize mass (the sensor mass is 15 g). The impact force profile, measured at 10 kHz by the sensor, allows estimation of the density and cohesion of the surface material, and its particle size distribution. Sample profiles for terrestrial materials (sand, gravel and clay) are given.

1. Introduction

Saturn's giant satellite Titan is currently an object of intense scientific interest and will be the focus of attention of the joint NASA/ESA Cassini mission, which will arrive in the Saturnian system in 2004 [1, 2].

The mission includes a European-built probe, named Huygens, which will descend by parachute to the surface of Titan. The nature of Titan's surface [3] is largely unknown at present, with only hints from ground-based radar and telescope observations, and the results of the 1980 encounter with the Voyager 1 spacecraft. Possible surface candidates [4] are a hydrocarbon (liquid methane/ethane) ocean, fluffy deposits of organic aerosols and ice or rocky regolith.

The Huygens probe includes an instrument suite, the Surface Science Package (SSP, [5, 6]), which will determine the nature of the surface of Titan at the Huygens impact site (the spacecraft's survival after impact is not guaranteed [7]) with a variety of sensors. Among these, the ACC-E subsystem, or penetrometer, will measure the mechanical properties of the surface material, and is the subject of the present paper. These measurements will help identify the surface material and the geological processes that have formed it.

2. A brief overview of penetrometry

Soil mechanical properties are measured on Earth for a variety of civil engineering and exploration purposes,

0957-0233/94/091033+09$19.50

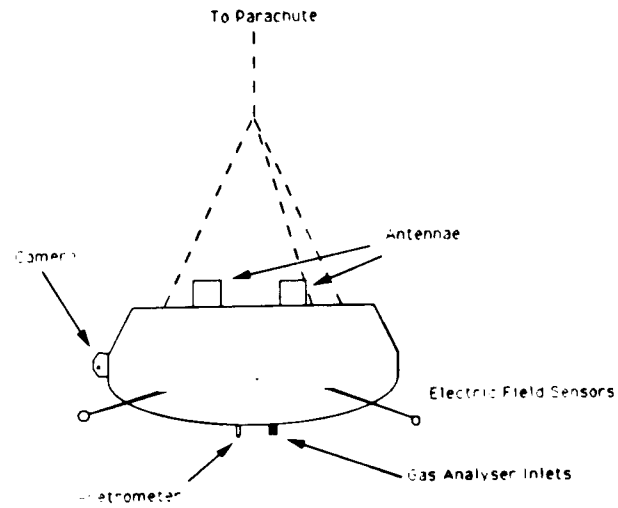

Figure 1. The Huygens probe, showing location of the penetrometer.

principally for assessing the suitability of soils for buildings or roads and for estimating the trafficability of soils or snows for aircraft landings or vehicle movement. The methods and techniques used to measure terrestrial soil strength vary widely [8]. Table 1 summarizes the various types of measurement. In addition to the two space missions mentioned in table 1 impact accelerometry on penetrators has been proposed for a number of space missions and was a favoured concept for early Moon exploration [19, 20].

Table 1. Penetrometer types.

Type	Penetration driver	Measurement	Application	Reference
Ram penetrometer	Hammered	Depth of penetration	Snow hardness/avalanche safety	[9]
Ram penetrometer	Inertia of 'penetrator' dropped from a frame	Depth of penetration	Coastal sediments	[10]
Dutch cone	Hydraulic ram	Force (strain gauge)	Civil engineering	[8, 11]
Field penetrometer	Electric motor/screw	Force (strain gauge)	Agricultural soil evaluation	[12]
Acoustic penetrometer	Hydraulic ram	Force plus microphone	Civil engineering	[8, 13]
Apollo penetrometer	Weight of astronaut	Force (mechanically recorded)	Lunar soil evaluation	[14]
Aerial penetrometer	Inertia of heavy rod inside light bomb case (air-dropped)	Depth of penetration (via optical encoder on rod)	Assessment of terrain for aircraft landing	[15]
Sea-ice penetrometer	Inertia of 'penetrator' (air-dropped)	Accelerometer	Measurement of sea-ice thickness	[16]
Luna-13 penetrometer	Rocket-powered cone (mounted on arm)	Depth of penetration (by arm joint position)	Lunar surface evaluation	[17]
Venera-13 penetrometer	Dropped cone (mounted on arm)	Depth of penetration (by arm joint position)	Venus surface evaluation	[18]

Typically these measurements allow determination of the bearing strength of the soil material as a function of depth. However, additional information may be obtained. An interesting variant of the standard cone penetrometer is the acoustic penetrometer: as well as a force transducer, the penetrometer incorporates a microphone to measure the noise generated by the soil as the penetrometer is driven slowly at a few centimetres per second into it. Noise emission typically peaks in the 2–5 kHz frequency range and the intensity correlates with the soil particle size [8, 13].

3. Measurements on the Huygens probe

The probe is a 210 kg instrument capsule, of about 1.3 m diameter (figure 1), which will spend 2–2.5 h descending by parachute through the atmosphere of Titan. It is equipped with instruments to sample the atmosphere and the organic aerosols, measure atmospheric properties and winds, and image the surface. The prime objectives of the probe are to study the atmosphere and surface during descent; survival of impact is not guaranteed (which is unsurprising, given our ignorance of the nature of the surface). However, since, in the thick atmosphere and low gravity of Titan, the impact velocity is only about 5 m s^{-1}, prospects for survival seem moderately good.

If the probe does survive, imaging and measurements of physical properties will continue. Additionally the gas analyser is equipped with heated inlets to vapourize any volatile components (such as ices) of the surface material and determine their chemical composition.

The probe is equipped with accelerometers for measuring the atmospheric density at high altitude during the hypersonic entry phase, and with an internal impact accelerometer (ACC-I), which is part of the Surface Science Package. These accelerometers will characterize the mechanical properties of the surface if it is a liquid or a soft solid, see [21] for details. It is, however, extremely difficult to measure the strength of surface material that is more rigid than the probe itself (which, not being designed explicitly for impact, has a flexible outer shell). In this 'hard' surface case, the force–acceleration coupling that is so straightforward for penetrators no longer applies. It was realized therefore that an accelerometer measurement was not appropriate, but rather a force measurement. As the sensor was originally envisaged to be an accelerometer [5], it bears the historical designation ACC-E (Accelerometer-External), but it is, in fact, a force transducer.

4. Transducer mechanical design

To transmit the force exerted by the surface material to the sensing element in a reliable fashion, the ACC-E subsystem has a rigid hemispherical penetrator head, directly behind which is mounted the transducer (figure 2). These are attached to a short rigid pylon on the SSP 'Top Hat' sensor accommodation structure (figure 3), which holds it at the front of the probe. A hemispherical head was chosen over the conical head used in some previous applications for the following reasons:

(i) it has a simpler mechanical impulse response (fewer and higher-frequency 'ringing' modes),

(ii) it has a faster initial rise of impact signal, allowing faster detection of impact,

(iii) it is safer during probe integration (won't poke anyone's eye out), and

(iv) it is less sensitive to errors in impact angle.

After initial experiments with steel and aluminium penetrator heads, titanium (appropriate, perhaps!) was selected for the penetrometer head: steel is heavy and could present magnetic cleanliness problems; aluminium, while lighter, is too soft (it is hard enough for most impacts that are survivable by the probe, but during testing when the penetrometer is struck with metal objects, an aluminium head would be damaged.)

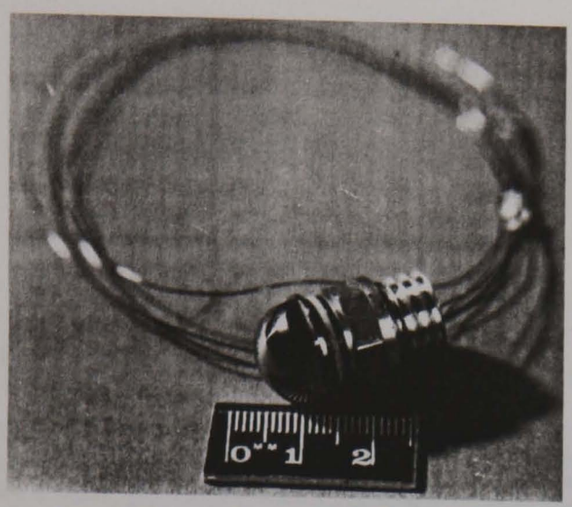

Figure 2. A photograph of the penetrometer sensor head.

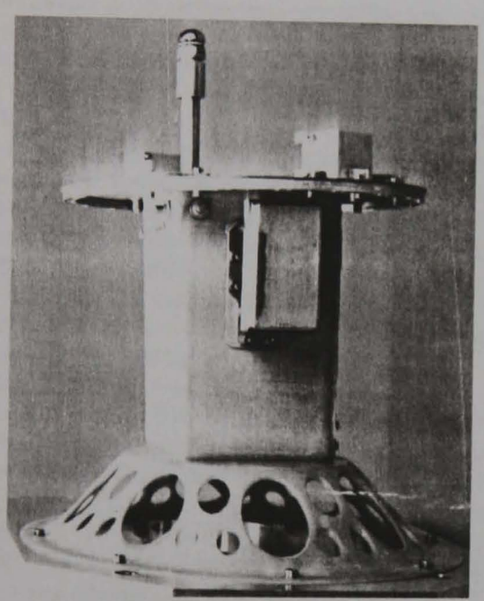

Figure 3. The penetrometer mounted on the mast of the structural/thermal model of the Surface Science Package, in preparation for a vibration test.

Following a suggestion by Al Sieff, a penetrometer with rim around the transducer was investigated, such that the penetrometer head could only move vertically (that is, it acted as a piston pressing on the transducer). However, this sensor design proved very difficult to manufacture and assemble, and gave results no better than the configuration currently adopted, and so was rejected.

The transducer was made as small as possible, to minimize weight. A diameter of 14 mm was felt to be the smallest size for which assembly would be straightforward.

The transducer is a simple 'washer' of PZT-5A (A donor-doped lead zirconate titanate piezoelectric ceramic), which generates a charge proportional to the stress on it. For background information on piezoelectric

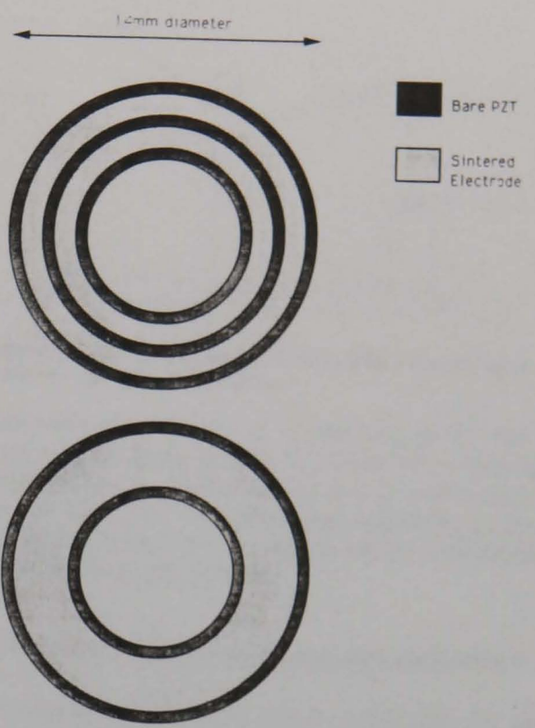

Figure 4. The piezoelectric sensing element, showing the electrode pattern. The disc is 1 mm thick.

materials, see [22, 23]. The material PZT-5A was selected for its high sensitivity and good temperature and age stability. The disc of PZT is held on to its electrical connections and the penetrator head by means of a central bolt, which holds the assembly under compression. An additional electrode allows the transducer to be stimulated in-flight for health and sensitivity drift checks during the long cruising phase.

The configuration of the piezoelectric washer is illustrated in figure 4. The common electrode is one side of the disc, while the sense and stimulus electrodes are 1 mm wide rings arranged concentrically around the the central whole, through which the bolt passes. The electrodes are as large as practicable, allowing a suitable gap between them and the bolt. The electrodes are ring-shaped (radially symmetric) in order to simplify assembly and to allow at least partial operation in the event of a crack in the washer.

Electrodes are formed on the transducer by silk-screen printing: a paste of ground glass and silver is deposited onto the PZT and sintered on. Care must be taken when soldering to these as (i) high temperature could locally de-pole the PZT and (ii) the silver electrodes can alloy with the solder and be accidentally removed.

The PZT element is sandwiched between two insulating washers made of the polyimide Vespel SP-1 (Vespel is a trademark of Du Pont): the washers have grooves cut in them to allow a small gap for the wires to pass through to reach the electrode, while keeping the PZT mechanically intimate with (but electrically isolated from) the titanium head and aluminium mounting collar. Vespel was selected for

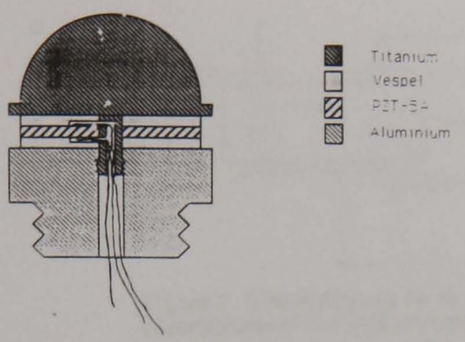

Figure 5. Section of the transducer, showing the individual components.

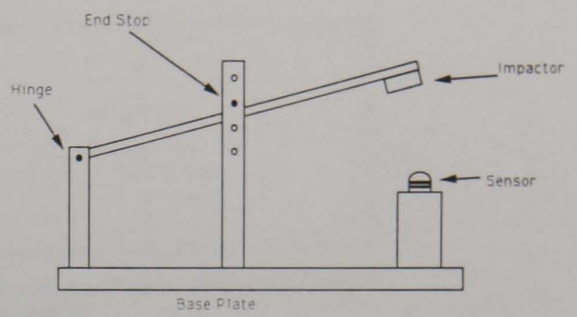

Figure 6. The pendulum jig for providing a known force pulse for instrument calibration.

its hardness, machinability, space qualification (such as low outgassing) and creep resistance (under compression for 8 years, polytetrafluoroethylene (PTFE) would creep, reducing the effectiveness of the mechanical connection between plastic and PZT).

To ensure good mechanical contact between the head and the PZT, the sandwich is held under compression (a pre-load) by the titanium bolt down the centre (figure 5). The wires to the electrodes pass down the centre of this bolt. While this design makes assembly awkward, it is robust. (Early experiments used sandwiches held together with epoxy adhesive, which had a tendency to crack after a few trials. Further, spacecraft safety requirements dictated that the head could not be held on by adhesive.) By having the bolt down the centre (rather than fixing on the outside) the bolt mass is minimized, and it is possible to inspect the PZT for cracks without dismantling the transducer.

The pylon on which the sensor is mounted is an aluminium tube. The transducer should be able to measure forces as low as a few newtons, while the upper limit of about 2000 N used as a working maximum figure is driven by the failure load of the support structure. For the about 1 cm^2 frontal area this corresponds to a soil bearing stress of 2000 N cm^{-2}, a value comparable with the bearing strength of some rocks and polymers. In practical terms, the 2000 N figures can be attained by a light blow with a wooden mallet, for example, see also the following section. Designing the measurement system (structure plus transducer) for loads much higher than 2000 N would be futile, since surfaces likely to generate these loads would probably cause the probe to fail in any case.

Clearly it is desirable to mount the transducer as far forward of the probe base as possible, to minimize probe structural effects on the transducer dynamics and to maximize the possible depth of penetration. However, there are clear limits to how far the transducer may project: an extendable or deployable boom (or, indeed, an ejectable penetrometer) was ruled out on cost and complexity grounds. The transducer is mounted as near as possible to the apex of the probe (also nearby are the inlets of the gas-sampling instrument) and as far forward as could be permitted, bearing in mind that the heat shield of the probe is mounted just in front. The outside of the heat shield reaches 900 °C during the hypersonic entry phase: it is jettisoned at the end of entry, at an altitude of 170 km, about 135 min before the probe reaches the surface. In fact, a small cut-out in the rear part of the heat shield was negotiated, to allow the penetrometer to project slightly further forward than would otherwise be possible.

5. Sensor electrical response and calibration

The calibration of the sensor is non-trivial, for two reasons. First, the robust construction necessitated for this application means that only a part of the impact force passes through the piezoelectric sensing element, and second, the device is not DC-sensitive, so calibration loads cannot be static. In other words, it is not possible simply to place a weight on the sensor: a known dynamic load must be used.

To generate a known force over a short period, masses were dropped using a swinging arm (pendulum) onto the sensor (see figure 6), with the sensor head impacting onto a plane surface of an elastic material. The impact of a spherical nose onto a plane semi-infinite surface can be modelled numerically (and indeed, analytically [19]). The force pulse has an approximately sinusoidal shape, with a peak magnitude proportional to $m^{0.6}E^{0.4}V^{1.2}$, where m is the mass of the impactor, E is Young's modulus of the impactor and V is the impact velocity.

The mass of the impactor could be determined by weighing; the impact velocity is determined from energy considerations, knowing the height over which the mass has been dropped. Two impactors were used, one made of PTFE, the other using a standard pencil eraser (synthetic rubber).

The impact forces ranged from about 30 N to 115 N for the rubber impactor and from 209 N to 585 N for the PTFE impactor. There is an uncertainty of order 40% in the absolute value of these forces, due mostly to an uncertainty of a factor of two in Young's modulus of the impactors. Work is underway to improve this uncertainty by *a posteriori* analysis of the duration of the force pulse.

Some description of the theoretical derivation of the transducer response is appropriate here, since the electrode areas of the transducer are not the same as the load-bearing area, so standard relations (such as in [23]) do not apply.

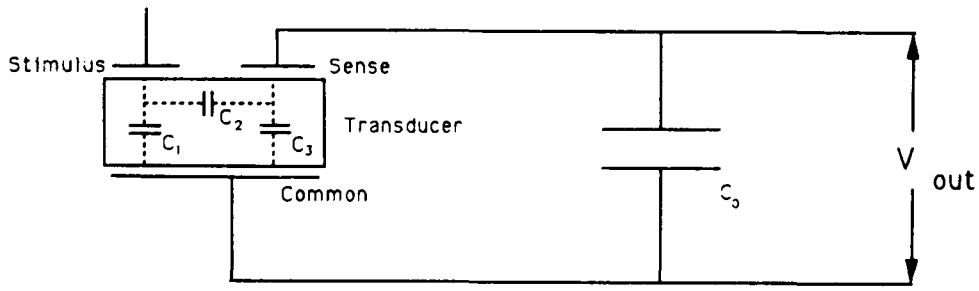

Figure 7. Circuit diagram for sensor calibration measurements, showing the internal capacitances of the lead zirconate titanate transducer.

Applying a capacitance meter across the sense and common electrodes yields (at room temperature) a value of about 590 pF. This is because what is being measured, C_s, is the sum of C_1 and the series combination of C_2 and C_3 (see figure 7). Measuring capacitance across the other pairs of electrodes allows the three capacitances to be determined: $C_1 \simeq 520$ pF, $C_2 \simeq 90$ pF and $C_3 \simeq 720$ pF. C_1 and C_3 are rather higher than might be expected from the electrode areas alone, due to edge effects. At liquid nitrogen temperatures, measurements yielded capacitances 3–3.5 times lower (manufacturer's data [23]) suggest capacitance should be about 2.5 times lower.)

The open-circuit voltage yielded by the transducer (area A, thickness t) when compressed with an effective force F_e is $g_{33}F_e t/A$, where g_{33} is the piezoelectric voltage constant, 24.8×10^{-3} V m N^{-1} at room temperature, but somewhat larger (by a factor of about 1.5, according to manufacturer's data) at liquid nitrogen temperature [23]). The effective force F_e may be lower than the applied force F by a factor k due to some of the applied force passing through the central bolt. An equal-deformation argument suggests that k is 2.5 at room temperature, or 2.1 at 80 K (lower due to the Vespel washers becoming stiffer): in practice k may be much lower (about 1) since the bolt is under tension and hence appears 'slack' to an applied compressive force.

The voltage actually measured will depend on how large a capacitance C_0 is loaded onto the circuit, since the charge generated by the transducer, $V_{oc}(C_1 + C_3)$ must be shared between C_0 and C_s.

Thus

$$V_{out} = \frac{F g_{33} t (C_1 + C_3)}{kA(C_s + C_0)} \qquad (1)$$

For this transducer ($t = 1$ mm, $A = 104$ mm^2), and $C_0 = 15$ nF, at room temperature we may predict $V_{out}/F = 0.0073$ V N^{-1} for $k = 2.5$, or 0.018 V N^{-1} for $k = 1$. At liquid nitrogen temperatures, the relation is more like $V_{out}/F = 0.0038$ V N^{-1} for $k = 2.1$, or 0.007 V N^{-1} for $k = 1$. Thus the drop in sensitivity at low temperature is by a factor of about 1.9.

Experimental results are given in figure 8 for room temperature and liquid nitrogen temperature. It is seen that the transducer appears linear for the force range investigated to date for both room temperature and liquid nitrogen temperature tests. The constants

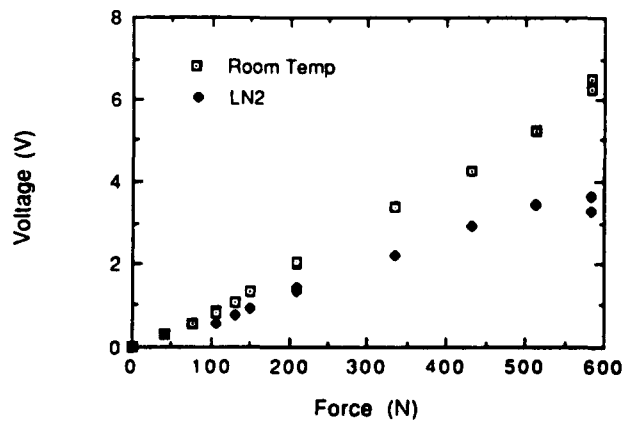

Figure 8. Transducer output for various force pulses at liquid nitrogen and room temperatures.

of proportionality are about 0.011 V N^{-1} for room temperature and 0.006 V N^{-1} for liquid nitrogen. These values are within the range suggested above. The drop in sensitivity at low temperatures is also in good agreement with predictions, at a factor of about 1.8.

6. Radiation effects

Piezoelectric materials are relatively insensitive to radiation effects and are routinely used to monitor vibration levels in nuclear reactors. However, to satisfy ESA product assurance requirements, a radiation test was performed.

During the long transit to the Saturnian system, equipment on the probe may receive a radiation dose of about 10 kRad from the on-board radio-isotope thermoelectric generators and radio-isotope heater units (used to generate power on the orbiter, and keep the probe warm respectively), Saturn, Jupiter magnetospheric particles, solar wind and galactic cosmic rays. Therefore, allowing a safety of 2, operation of all probe systems must be demonstrated after a dose of 20 kRad.

Samples of the piezoelectric discs were irradiated to 20 k Rad using a cobalt-60 γ-source at the National Physical Laboratory: no noticeable change in response was noted when these discs were checked against control samples kept in the laboratory.

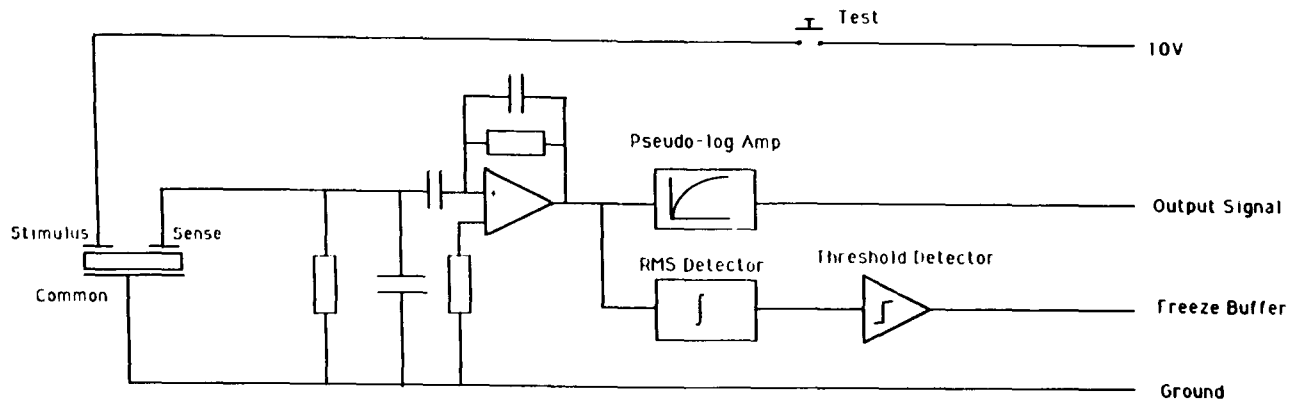

Figure 9. Schematic diagram or the sensor circuit in flight configuration.

7. Signal conditioning

In order to cope with the large dynamic range of expected signals while keeping the data volume low, the signal is amplified by a pseudo-logarithmic amplifier. The amplifier used has three linear segments in its input/output characteristic, but approximates closely a logarithmic response. The characteristic used in the development unit has the form $V_{out} = 0.7+2.5 \log_{10}(V_{in})$ for signals in the range of interest, but the exact characteristic may be 'tuned' prior to launch to optimize the science return.

While the low-end sensitivity is dictated by the lower response of the transducer at low temperature, and the required sensitivity of the measurement system as a whole, the high-end amplification (or, in fact, attenuation) is dictated by the maximum allowable impact at room temperature.

In worst-case scenarios, such as careless treatment with a hammer during ground test, the voltage generated by the transducer could be high enough to damage the amplifier. Thus, there is a 'charge attenuator', namely a capacitance in parallel with the transducer, to absorb excess charge to protect the circuitry. This capacitance C_0 dictates the sensitivity of the transducer (see section 6).

The amplifier output is passed to an A–D converter (8 bits) for digitization and storage, and also to an integrator/filter (based on a root-mean-squared converter chip). When sufficient energy is deposited in this device over a short interval of time, a voltage threshold is reached and the 'impact' flag is raised. This impact signal is used to freeze the sampling buffer.

Figure 9 shows a schematic diagram of the sensor circuit in its 'flight' configuration.

8. Sampling strategy

For the anticipated probe terminal velocity at the surface of 5 m s^{-1}, the sampling rate of ACC-E has been chosen to be 10 kHz, giving a depth resolution (applying the Nyquist theorem) of the order of 1 mm. Thus, in addition to estimating the density and bearing strength of the surface material, it may be possible to identify any layers in the surface (such as a 'crust' over a softer material) or particle size, if the surface is not a uniform solid.

Note that after about 5 cm penetration (about 10 ms after first contact) the fore dome (outer shell) will have begun to deform significantly, and equipments and experiments on the probe will begin to transmit loads to the experiment platform, slowing the probe down. From this point on, ACC-E measurements become slightly degraded, but will still contain some useful information.

To minimize load on the SSP processor at the high sampling rate, the data is stored continuously in a FIFO (first in–first out) buffer, with impact detection implemented in hardware (see section 7).

The buffer is 512 words long, and samples and stores data continuously until 448 samples have been taken after the 'impact' flag has been raised. The first 64 samples contain readings prior to detection of impact, and will contain therefore zero-force samples, plus the onset of impact (before the flag was raised.) The buffer length corresponds to about 25 cm penetration, which is about the maximum expected.

After impact, a 'quick-look' data set is transmitted, comprising the peak value of the impact profile, the time to reach the peak, and the time of the rising and falling half-peak values. If transmission should fail suddenly soon after impact, this data set will allow at least an estimation of the surface type. Subsequently the full 512 words are transmitted to allow detailed examination of the force profile.

9. In-flight testing

It was required that all probe sensors be capable, to the maximum extent possible, of being tested during the long (7 year) interplanetary cruise to Titan. Direct mechanical stimulation of the ACC-E sensor is clearly impracticable, but by including an additional electrode on the PZT washer, a stimulation signal can be injected into the sensor right at the start of the measurement chain. This test signal (nominally a short pulse) is coupled to the sense electrode of the sensor by its piezoelectric response and by the capacitance between these two electrodes.

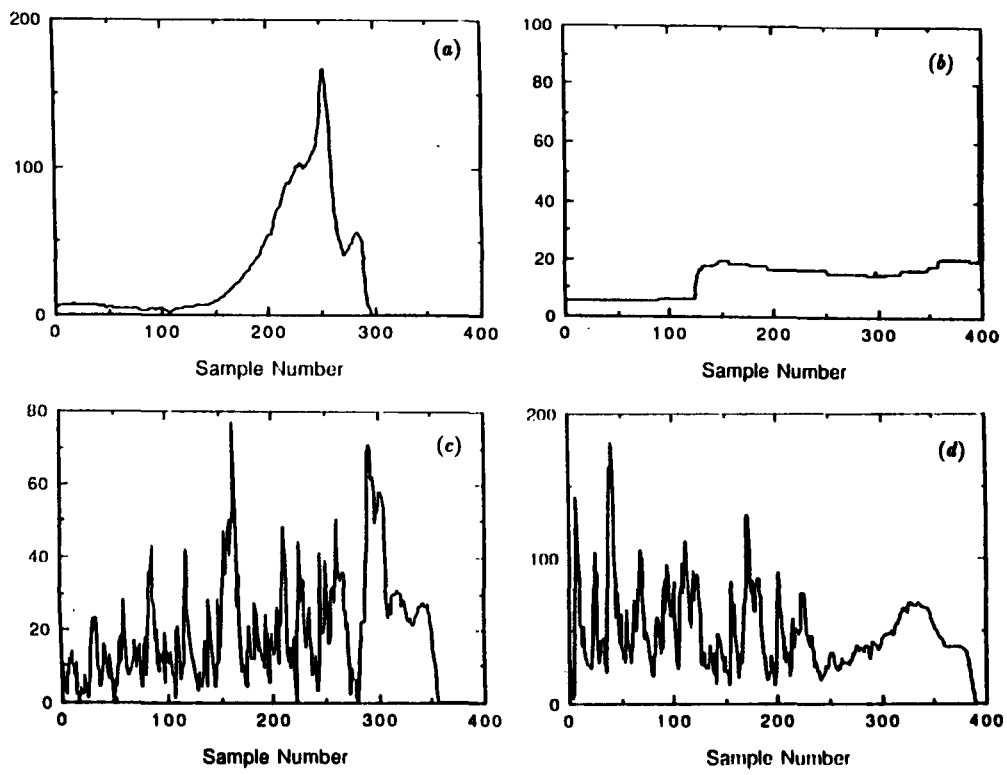

Figure 10. Sensor output (after pseudo-log amplification; units are arbitrary) for transducer drops at 5 m s^{-1} into various materials. Samples are at 10 kHz, so sample number 200 corresponds to 20 m s, or 10 cm depth. Materials are (*a*) sand, (*b*) clay, (*c*) fine gravel (particle size about 8 mm) and (*d*) medium grade gravel (particle size about 15 mm).

This allows the gain of the amplifier and the health of the transducer to be verified after the rigours of launch. For example, a cracked (but still functional) transducer would be indicated by a drop in its response.

10. Laboratory and field testing

The ACC-E subsystem on the probe has its data read by the SSP computer, formatted into telemetry packets with other SSP data, and sent to the probe on-board data handling system, which in turn puts these data, with those from other experiments, into telemetry frames and broadcasts these via a dual-redundant S-band uplink to the orbiter spacecraft, which eventually re-broadcasts the data to Earth for analysis.

For laboratory testing, the amplifier output is passed to the stimulus and monitoring unit (SMU): this is a desk-top PC equipped with A/D interfaces and software to permit inspection and archiving of test and calibration data.

It is clearly impracticable (desirable as it might be) to drop an entire 200 kg probe model with the sensor attached to obtain test data in a variety of materials. However, it was realized that, as long as the transducer velocity did not vary appreciably during the impact event, the force on the transducer would be representative of that encountered during probe impact at the same speed. Thus the transducer was attached, by means of a screw fitting attached to its support, to a set of steel discs, forming a mass of 3–8 kg, giving it enough inertia to maintain its velocity for the about 20 ms impact event. A guard structure was also attached to prevent the transducer burying itself too deeply.

A portable data-acquisition system was set up to enable field tests to be performed; it is easier to take a small sensor to locations of interest, rather than bringing large amounts of heavy samples into the laboratory. A Zenith notebook PC was procured, together with a Pico Electronics ADC-10 analogue-to-digital converter (able to sample at up to 13 kHz with 8 bit resolution). The amplifier circuit was powered by two 9 V batteries. The entire electronic equipment fits in a small briefcase and weighs only about 3 kg.

11. Results and data analysis strategy

In order to investigate what may be learned from the impact signature, the penetrometer was dropped onto a variety of terrestrial surface materials. The penetrometer was held vertical during impact by dropping it down a perforated drainpipe, which had only a small clearance. The speed of impact was controlled by dropping the penetrometer from a predetermined height: for 5 m s^{-1} impact velocity and terrestrial gravity, the drop height is about 135 cm. To compensate for drag and air resistance caused by dropping in the tube, the actual height used to achieve 5 m s^{-1} was about 190 cm, the speed being verified using standard laboratory 'ticker

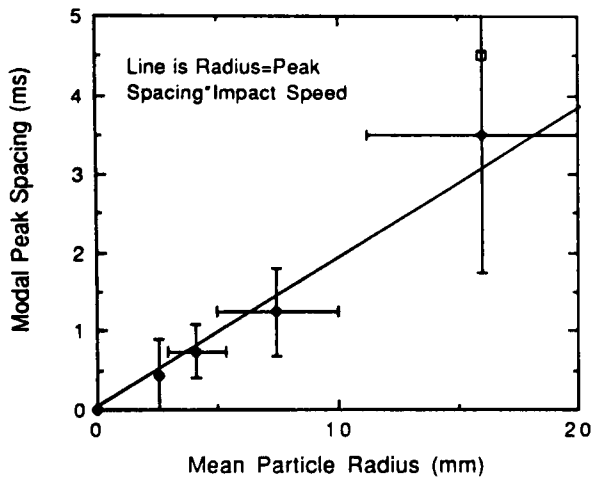

Figure 11. Correlation of peak spacing with particle size. A moving average is subtracted from the impact signature, and the spacings between positive-going crossings of the 3σ levels are placed into bins 0.5 m s wide. The location of the most popular (modal) bin is plotted again particle size.

tape'. The impact signatures were found to be only modestly sensitive to variations of order 10–20° impact attitude or 20% in impact velocity.

The sample results are shown in figure 10. Sand ramps up approximately quadratically, while clay has a fairly constant resistance throughout the impact event. After 200 samples (corresponding to 20 m s, or about 10 cm of penetration), the plate and weights hit the surface, and the data become corrupted; the characteristic 'bound' due to plate impact is clearly seen in the sand data, and to a lesser extent in the other figures.

While sand and clay have fairly smooth profiles, impacts on granular materials are very spikey. There appears to be a correlation between the height of the spikes for impacts onto gravel material, and the size of the gravel lumps (compare with the results of acoustic penetrometers, where the magnitude of the acoustic noise correlates with particle size [13]). Additionally, there is a correlation between the spacing of peaks and particle size (see figure 11). Since peak height is probably correlated somehow with the mass of the lumps, it may perhaps be possible to constrain both particle size and the density of the particle material.

It is clear that much can be learned from the impact signature. Additional experiments will investigate these potential results and will examine more rigourously the instrument's sensitivity to impact angle and velocity.

12. Conclusions

An impact penetrometer using a piezoelectric transducer has been developed for the ESA Huygens probe to Titan. This instrument, complying with rigourous spacecraft standards, will operate at about 94 K after a 7 year cruise in space. It will provide data on the surface material at the Huygens landing site, thereby constraining the nature and origin of that material. Penetrometers of this type may find application on other space missions, such as the forthcoming Rosetta mission to deposit a small lander on a comet.

Acknowledgments

Ralph Lorenz acknowledges receipt of a postgraduate research award from the UK SERC, now PPARC. The authors thank the mechanical workshops of the Physics Laboratory, University of Kent, and John Howes in particular for excellent workmanship. Trevor Rees of the electronics laboratory is to be thanked for his careful and patient assistance in the assembly of the transducer. Neil Young of Morgan Matroc (Vernitron Division) Southampton gave useful advice in the specification of the transducer material and electrode pattern. Don McCoy, the Huygens SSP payload engineer at ESTEC, and Michel Brisson, the Huygens payload engineer at Aerospatiale are to be thanked for their cooperation, notably in negotiating the cut-out in the entry shield to allow the sensor to project as far forward as possible. Lilian Valentin of the ESTEC library and Erwin Mooij of TU Delft helped by providing some useful, but difficult-to-obtain, references. Alvin Seiff of NASA Ames Research Center is thanked for useful comments in the early development of the transducer. Harjinder Jolly of the University of Kent assisted by performing the radiation test and Malcolm Wright is thanked for his efforts in procurement and documentation.

References

[1] Lebreton J-P and Matson D L 1992 An overview of the Cassini mission *Nuovo Cimento* **15** 1137–47

[2] Kohlhase C 1993 Meeting with a majestic giant: the Cassini mission to Saturn *Planetary Rep.* **13** 5–10

[3] Lunine J I 1993 Does Titan have an ocean? A review of the current understanding of Titan's surface *Rev. Geophys.* **81** 131–49

[4] Lorenz R D 1993 The surface of Titan in the context of the ESA Huygens probe *ESA J.* **17** 275–92

[5] Zarnecki J C *et al* (23 co-authors) 1992 A surface science package for the Huygens Titan probe *Proc. Symp. on Titan Toulouse September 1991* (ESA) pp 407–9

[6] Zarnecki J C 1992 Surface science package for the Huygens Titan probe *J. Br. Interplanetary Soc.* **45** 365–70

[7] Lorenz R 1992 Huygens probe – The surface mission *Proc. Conf. on Titan, Toulouse, September 1991* (ESA) pp 359–64

[8] Mitchell J K 1987 New developments in penetration tests *Int. Symp. on Penetration Testing, Balkema, Rotterdam, 1987* ed J De Ruiter pp 245–61

[9] Perle R and Martinelli M 1975 *Avalanche Handbook* (USA Agriculture and Forestry Service)

[10] Nikalchtar B 1987 Classification of ocean bottom sediments by dynamic penetrators *MSc Thesis* Louisiana State University

[11] De Ruiter J 1971 Electric penetrometer for site investigations *J. Soil Mech. Foundations Div. Am. Soc. Civil Eng.* **97** 457–72

[12] Olsen H J 1990 Construction of an electronic penetrometer for use in the field *Computers Electron. Agriculture* **5** May 65–75

[13] Tringale P T and Mitchell J K 1982 An acoustic penetrometer for site investigations *Proc. 2nd European Symp. on Penetration Testing, Amsterdam, May 1982* pp 909–14

[14] Mitchell J K, Bromwell L G, Carrier III W D, Costes N C, Houston W N and Scott R F 1971 Soil mechanics

experiment *NASA SP-289 'Apollo 15 Preliminary Science Report'* (NASA)

[15] Marten V R and Hansen V 1976 *An Inexpensive Aerial Penetrometer* AFWL-TR-74-56 (Albuquerque: Sandia Labs)

[16] Young C W and Keck L 1971 *An air-dropped Sea-Ice Penetrometer* SC-DR-71 0729 (AD-731 991) (Albuquerque: Sandia Labs)

[17] Cherkasov I I, Gromov V V, Zobachev N M, Musatov A A, Mikheyev V V, Petrukhin V P and Shvarev V V 1968 Groundmeter/penetrometer used on the automatic lunar station 'Luna-13' *Nauka* **179** 829–31 (translation NASA CR-94587)

[18] Kemurdzan A L *et al* 1983 Preliminary results of the determination of physico-mechanical properties of the Venusian ground by Soviet automatic stations Venera-13 and Venera-14 *Kosmicheskii Issledovania* **21** 323–30 (in Russian)

[19] McCarty J L and Carden H D 1962 *Impact Characteristics of Various Materials Obtained by an Acceleration-Time-History Technique Applicable to Evaluating Remote Targets*

[20] McCarty J L, Beswick A G and Brooks G W 1964 *Application of Penetrometers to the Study of Physical Properties of Lunar and Planetary Surfaces* NASA TN-D-2413

[21] Lorenz R 1994 Huygens probe impact dynamics *ESA J.* at press

[22] Van Randeraat J and Setterington R E 1974 *Piezoelectric Ceramics* (London: Mullard)

[23] Vernitron Ltd 1991 *Piezoelectric Ceramics* (Southampton: Morgan Matroc, Vernitron Division)

R.D. Lorenz
Unit for Space Sciences, University of Kent, Canterbury, UK

Huygens Probe Impact Dynamics

Abstract The ESA Huygens Probe is due for launch as part of the NASA/ESA Cassini mission in 1997, to arrive at Titan in late 2004, and will make a 2–2.5 h exploratory descent to the surface. However, the state of Titan's surface is largely unknown and it may be at least partially covered in liquid hydrocarbons. With such ignorance of the surface state, and the limited financial envelope of the project, it is not practicable to design the Probe to 'soft-land'. Survival may, nevertheless, be possible and this paper presents various impact-dynamics analysis methods and assesses the likely impact scenarios and their survivability.

It is concluded that the Probe has a good chance of surviving to continue its scientific mission from the surface. The scientific information about the surface that could be gathered from impact-dynamics measurements is also discussed.

1. Introduction

The Huygens Probe[1-5] will make a 2.25 h (nominal) descent to the surface of Saturn's enigmatic moon Titan (Fig. 1), which it will hit with a vertical velocity of about 5 m/s. Although for cost and complexity reasons post-impact survival has never been a design driver for the Probe, it has long been realised that survival is possible[6,7], and at the current stage in Probe development (early Phase-C/D; i.e. main development phase) prospects for a productive surface mission look relatively good, with a modest impact velocity and healthy energy and link margins. In the event of Probe survival, a surface mission lasting of the order of 30 min should be possible.

Thus a major factor in the surface mission becomes the load sustained by the Probe at impact. Both the energy and momentum of the descent must be dissipated: where they are dissipated depends largely on the relative hardnesses or strengths of the Probe and the surface. Ideally, dissipation would occur in the material on which the Probe must land, which will happen in the event of a soft surface material.

An earlier paper[8] has reviewed the likely surface types to be encountered on Titan. Here I examine the range of expected impact parameters and loads, and the likely effects on the Probe and its payload. The most up-to-date and comprehensive descriptions of the Probe and its payload are to be found in two recent articles in ESA Bulletin No. 77, February 1994 [9,10].

The aims of the present paper are to:

- summarise work on spacecraft impact dynamics, on which the literature is sparse and scattered
- investigate the impact dynamics of the Huygens Probe, in order to assess the likelihood of its survival on the surface of Titan
- examine the variation in impact deceleration with surface mechanical properties to see how acceleration measurements on the Probe can be used to measure these properties.

Figure 1. Huygens mission profile. The Probe makes measurements from an altitude of 170 km down to the surface, the descent taking between 2.0 and 2.5 h. Mission energy and link budgets are sized for a minimum of 3 min operation post-impact, although an extended surface mission of 30 additional minutes may be possible (Figure from Reference 2)

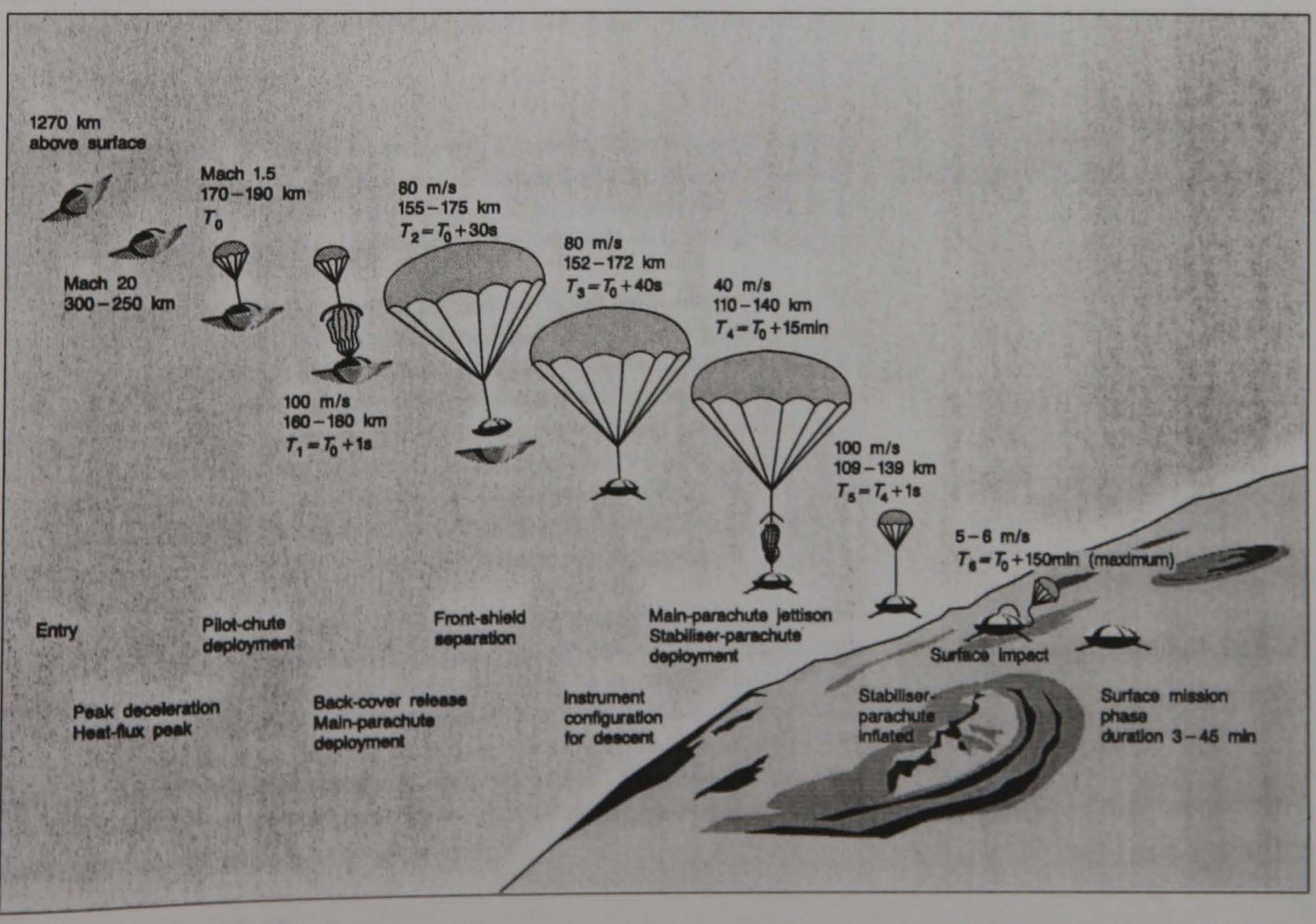

227

2. Comparisons with previous missions

Some useful comparisons may be drawn with previous planetary missions to put the Huygens landing scenario in context. A convenient summary of planetary missions is that by Wilson[11].

Luna 9, the first man-made object to have survived on the lunar surface, hit at approx. 6 ms^{-1}. Its internal equipment was 'protected by shock-absorbers'. It had a mass of about 100 kg. Luna 16 (an automatic sample return) and its successors were considerably larger, and soft-landed at about 2.5 ms^{-1}.

The Surveyor spacecraft had shock-absorbing legs and a propulsion system for soft-landing on the Moon; at touchdown they weighed just under 300 kg, and had vertical velocities of the order of 3 ms^{-1}. The main-structure loads were 8–20 g, although load-amplification effects on the spidery lander led to loads on the antenna and solar array (mounted on a mast) of the order of 90 g. The Viking landers on Mars (equipped with a throttlable hydrazine retro-rocket system, and shock-absorbing legs for soft-landing) touched down at about 2.5 ms^{-1}.

The Pioneer Venus (PV) probes have many similarities with the Huygens Probe, and a detailed comparison is given in a following section. They, and the Russian Venera probes, hit the surface of Venus at about 9 ms^{-1}, relying only on aerodynamic drag to brake their descent, and weighed between 93 kg (PV small probes) and 700 kg (Venera). The pictures sent back by the Veneras suggest they landed on rock slabs (possibly covered with some dust); these probes recorded landing loads[12] of up to 75 g.

Of the 30 or so missions described above, only Luna 18, Mars 2, and three of the four Pioneer Venus probes failed completely at impact (Table 1). Veneras 11 and 12 appear to have suffered extensive instrument failures on landing; Mars 3 sent back 20 s of (blank) TV signals before failing, and the sampler of Luna 23 was damaged by a rough landing. It is noteworthy that if spacecraft survived for a few seconds on the surface, they generally continued to function up to and often beyond their design life, with some missions being terminated either by command from Earth, or by relay spacecraft passing out of sight.

The impact velocity of the Huygens Probe is only slightly higher than that of 'true' soft-landers, and rather less than for several previous 'hard' or 'semi-hard' landers on the Moon and Venus. Thus, in relative terms, prospects for Huygens survival seem quite good, even though it has not been designed with impact survival in mind.

3. Comparions with Pioneer Venus

The NASA Pioneer Venus multi-probe mission is perhaps the most useful analogue for the Huygens impact: in part because the masses and velocities are comparable (Pioneer Venus, though robust, was not designed to survive impact), and because (unlike the Russian Mars and Venus missions) it is relatively well-documented in the open literature[13–15].

Four Pioneer Venus probes (three small and one large) were sent to Venus. The large probe was spherical (73 cm diameter) and had a mass of 310 kg (including its 1.4 m diameter heat shield, which it released after deploying a parachute). The small probes (50 cm diameter; 90 kg) descended without parachutes and kept their 76 cm-diameter, 45° half-angle entry protection shields attached throughout their descent.

The probes all transmitted directly to Earth using antennas with approximately hemispherical coverage[15]. The dispersion of the probes over the surface of Venus was such that the Earth (where the signals were received) was about 30° above the horizon over each landing site (except, significantly, for the day probe, where the Earth elevation was about 40°).

The probes impacted the surface at velocities of approximately 9–10 m/s, impact being indicated by a sudden change in the Doppler shift of the received radio frequency. Signals from two of them (the large probe and the north probe) were lost at impact. Signals were received from the night probe for 2 s after impact, but the day probe continued to transmit for 67 min, at which time its internal temperature reached 126° C. Telemetry suggests that the signal was lost at this point not due to battery exhaustion, but due to thermal failure of a power-amplifier component[14].

Table 1. Previous missions to planetary surfaces

Year	Mission	Nation	Target	Mass (kg)	Dimensions
1966	Luna 9	USSR	Moon	~100	Sphere 58 cm diam.
1966	Surveyor 1	US	Moon	293	Tripod, 3 m high, 4 m across Footpads 30 cm diam.
1966	Luna 13	USSR	Moon	116	As Luna 9
1967	Surveyor 3	US	Moon	293	As Surveyor 1
1967	Surveyor 4	US	Moon	293	As Surveyor 1
1967	Surveyor 5	US	Moon	305	As Surveyor 1
1967	Surveyor 6	US	Moon	300	As Surveyor 1
1968	Surveyor 7	US	Moon	306	As Surveyor 1
1969	Luna 15	USSR	Moon	As Luna 16?	
1970	Venera 7	USSR	Venus	~500	Sphere 1 m diam.?
1970	Luna 16	USSR	Moon	1880	4 m-square platform 4 footpads 30 cm diam.?
1970	Luna 17	USSR	Moon	As Luna 16?	
1971	Mars 2	USSR	Mars	450	1.2 m diam.
1971	Mars 3	USSR	Mars	450	1.2 m diam.
1971	Luna 18	USSR	Mon	As Luna 16	
1972	Luna 20	USSR	Moon	As Luna 16	
1972	Venera 8	USSR	Venus	495	As Venera 7
1973	Luna 21	USSR	Moon	As Luna 17	
1973	Mars 6	USSR	Mars		
1974	Luna 23	USSR	Moon	As Luna 16	
1975	Venera 9	USSR	Venus	660	2.1 m disc + 1 m sphere
1975	Venera 10	USSR	Venus	660	As Venera 9
1975	Viking 1	US	Mars	612	2.1 m tall, 3 m wide 3 footpads, 31 cm diam.
1975	Viking 2	US	Mars	612	As Viking 1
1976	Luna 24	USSR	Moon	As Luna 16	
1978	PV Large	US	Venus	316	Sphere 73 cm diam.
1978	PV Day	US	Venus	93	50 cm-diam. sphere, with 76 cm diam. conical nose
1978	PV Night	US	Venus	93	As PV Day Probe
1978	PV North	US	Venus	93	As PV Day Probe
1978	Venera 11	USSR	Venus	700?	As Venera 9?
1978	Venera 12	USSR	Venus	700?	As Venera 9?
1981	Venera 13	USSR	Venus	760	As Venera 9?
1981	Venera 14	USSR	Venus	760	As Venera 9?
1984	Vega 1	USSR	Venus	760	As Venera 9?
1984	Vega 2	USSR	Venus	760	As Venera 9?

On the one hand, the Pioneer Venus probes were more robustly built than Huygens, the small probes having to endure entry accelerations of the order of 560 g. Also, the probes were built as spherical pressure vessels (the shells were of titanium, several millimetres thick), able to withstand the 200 bar surface pressure at Venus. Huygens has much more modest entry loads (of order 20 g) and has a thin outer aluminium shell which is not sealed.

On the other hand, the Huygens impact velocity will be lower by a factor of almost 2. Secondly, pictures from the Soviet Venera spacecraft (which had broadly similar impact velocities but were equipped with impact-attenuation systems) indicate a very unpleasant surface on which to land, strewn with boulders and large slabs of volcanic rock (see Ref. 8, Fig. 12). Hopefully Titan's surface may be more forgiving!

The two failures that occurred at impact are probably a result either of impact damage directly, or the tipping-over of the probes at impact such that the Earth was no longer in the main antenna lobe. The failure of the night probe 2 s after impact may have been due to tipping over, or perhaps to thermal failure following inrush of the hot (600 K) atmosphere if the pressure vessel was ruptured by the impact.

Thus a major contributing factor to the loss-of-signal of the Pioneer Venus probes

Speed (m/s)	Comments
Less than 3	8 h of contact over 3 d
3	True soft-landing. Operated for 6 months
8.3	Impact accelerometry recorded soil structure to depth of 20–30 cm
Less than 2	Bounced 30 cm at landing (engines on): OK after engines turned off by ground command
Unknown	Contact lost 2.5 min before landing, although automatic landing may have been successful
4.2	Pressurant leak forced late retro sequence
3.8	
130	Crashed
10?	Telemetry multiplexer failure — only temperature data (23 min) from surface. Bad attitude caused 20 dB signal loss (rolled in wind?)
2.5	Sample-return mission
2.5?	Rover mission
?	Crashed (dust storm?)
21	Transmissions discontinued after 20 s: high winds, or failure of relay orbiter?
	Crashed 'due to rugged terrain'
10?	Operated for 50 min
2	
	Contact lost before landing
?	Rough landing damaged drill
8	First pictures from Venus: lasted 53 min
8	Operated for at least 65 min (relay passed out of sight)
2.4	Operated until 1982
2.5	Shut down 1980
9	Failed at impact
10	Operated for 67 min on surface: thermal failure?
10	Operated for 2 s
10	Failed at impact
8?	Instrument failures on landing; operated 95 min
8?	Instrument failures on landing; operated 110 min
8?	Operated for 127 min
8?	Operated for 57 min
8?	Drill sequence started prematurely; no surface science
8?	Operated for 57 min

may well have been the presence of the entry shields on the small probes causing antenna depointing at impact. Indeed, Venus surface data was recovered from what was originally thought [11] to be noise, when the Venera 7 lander's telemetry signal fell to 1 % of its nominal value at impact. Because Huygens is a relatively flat and soft-bottomed spacecraft, we might expect that (except in the case of extremely steep or rocky surfaces) such antenna depointing is unlikely. Further, since the cold Titan atmosphere is much less harsh than the dense, scorching atmosphere on Venus, thermal failure should be at least slower, and perhaps less likely, to occur on Huygens.

4. Spacecraft impact dynamics

A substantial amount of work has been performed on impact dynamics for military applications. Most civil work is in connection with safety engineering, for aircraft[16,17] and automotive crashes[18-20], and the accidental dropping of flasks used to transport radioactive waste[21]. Comparatively little work is reported in the open literature in the West on the impact dynamics of spacecraft (Ref. 22 gives some general information; see references hereafter for particular cases).

The bulk of the available work was performed in connection with the US Mercury, Apollo and Surveyor programmmes, although some recent ESA-sponsored studies have been performed on Mars penetrator/landers[23]. For the Mercury and later Apollo programmes, the work was focussed on estimating impact loads to ensure crew survival, both for the nominal sea landing and for possible impact on land in the event of a launch abort.

As part of the Apollo Programme, models of the mechanical properties of the lunar surface had to be developed (there were initial fears that the surface might be so soft that a spacecraft, or astronauts not equipped with snowshoes, might sink into it[24]) and the Surveyor series of soft-lander missions was designed to assess the lunar surface in preparation for the manned Apollo landings. Some instrumentation (strain gauges on the landing legs and accelerometers on the main body) was devoted to measuring landing loads to assess the bearing strength of the surface[25]. Further indications of soil physical properties were obtained by photographing the 'feet' of the landing legs to measure foot penetration and ejecta throwout, and by measuring motor currents on the sampling arm.

Most of the Apollo and Mercury work was devoted to liquid landings (which were, of course, the nominal mode of ending their missions). Analytic simulation of such landings became well-developed and predictions for Huygens are made in a following section.

Simulation of landings on solid surfaces is rather more difficult and available data is more scarce. First, since the 'hardness' of the surface is comparable with that of the spacecraft, the partitioning of energy and momentum dissipation between the vehicle and the surface becomes complex, so analytical treatment is extremely difficult (although Ref. 26 provides an instructive analysis of a simple case). Secondly, the higher impact loads generally cause damage to the spacecraft, such that even for small-scale models, large series of tests are prohibitively expensive, so there is relatively little available experimental data. Modern finite-element techniques allow the detailed investigation of impact dynamics and structural response, but are also expensive.

In the following sections, relatively simple methods of estimating the loads and response of an impacting spacecraft are presented, with Huygens as the example. While relatively simple, these methods offer useful insight into what may occur at the climax of the Huygens mission.

5. Impact conditions

The Huygens Probe (Figs. 2–4), during most of its descent, is suspended beneath a stabilising drogue parachute (a polyester/kevlar disk-gap-band chute with a reference diameter of 2.45 m)[27]. The terminal velocity of the Probe with parachute at the surface of Titan, with a surface gravity of 1.35 ms^{-2} and an atmospheric density of 5.3 kgm^{-3}, is 5.2 ms^{-1} (approximately the velocity attained on Earth by an object dropped from a height of 130 cm, which is convenient for impact testing!). This is about half of the impact velocity of the Apollo capsules and the Pioneer Venus spacecraft.

There is some uncertainty in the radio-occultation data from the Voyager encounter, and a consequent uncertainty in the knowledge of the atmospheric density[28], which could be 4.57–6.01 kgm^{-3}. Similarly, there is a 10% uncertainty in the drag performance of the parachute, and so combining these uncertainties gives the terminal velocity of the Probe at the surface between 4.6 and 5.8 ms^{-1}.

The horizontal velocity of the Probe is unlikely to be exactly zero as parachutes tend to have a slight 'gliding' action, but certainly the sideways component will be small (say < 1 ms^{-1}). The Probe will be moving along with any winds at the surface, but these (e.g. Ref. 29) are likely to be very small (again < 1 ms^{-1}). The specification on the stabiliser requires it to have pendulum-type oscillations of less than 10° amplitude. Should a wind gust cause a swing greater than this, it should return to within 10° of vertical within about 10 s. Wind gusts near the surface are unlikely anyhow, so for the purposes of this study it is assumed that the impact attitude is vertical, and the corresponding horizontal velocity component is zero.

The Probe mass at impact is expected to be about 207 kg, and its transverse moment of inertia is about 20 kgm^2.

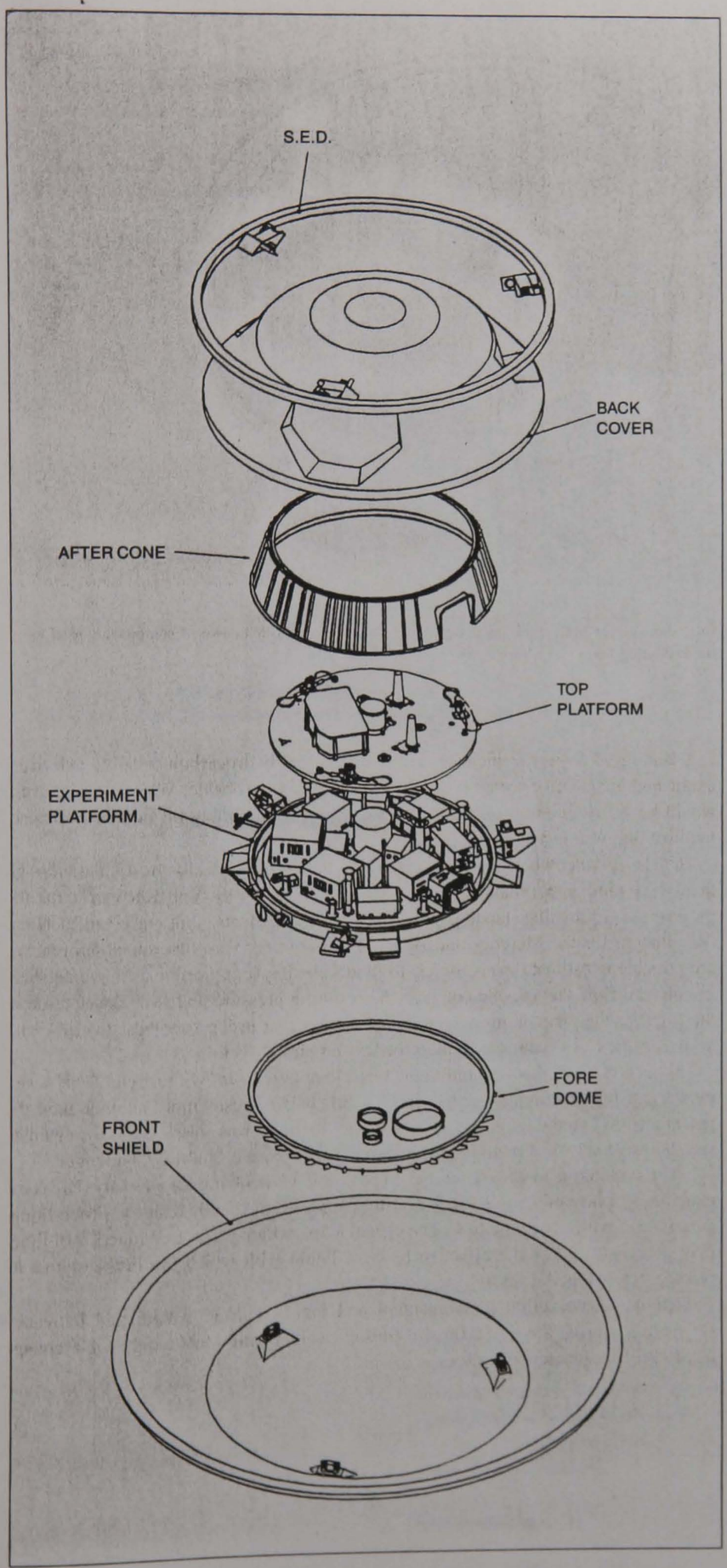

Figure 2. Exploded view of the Huygens Probe. The 2.7 m diameter front shield and an aft cover protect the Probe during entry. The Probe's descent module comprises a round fore-dome and a conical aft section: a top platform carries the two antennas and the parachute box, while the payload and subsystems are mounted on the experiment platform at the centre

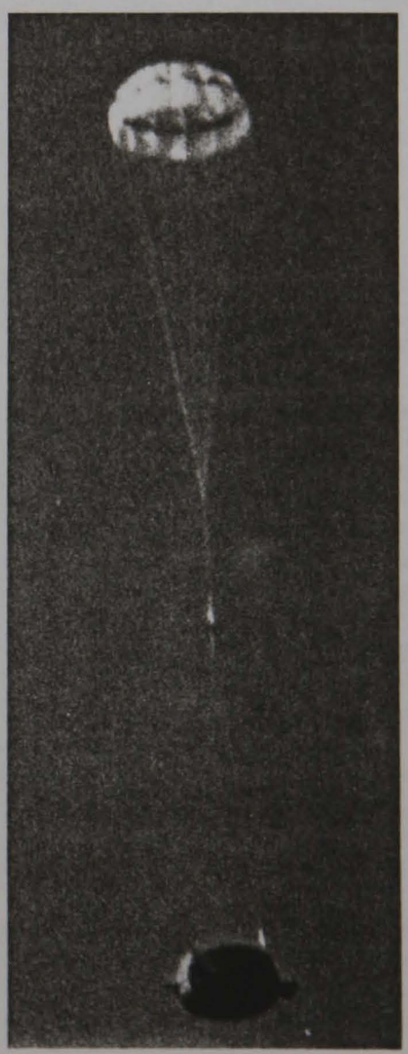

Figure 3. Drop test of Probe in descent configuration, with drogue parachute (photo courtesy of Martin-Baker Aircraft Co.)

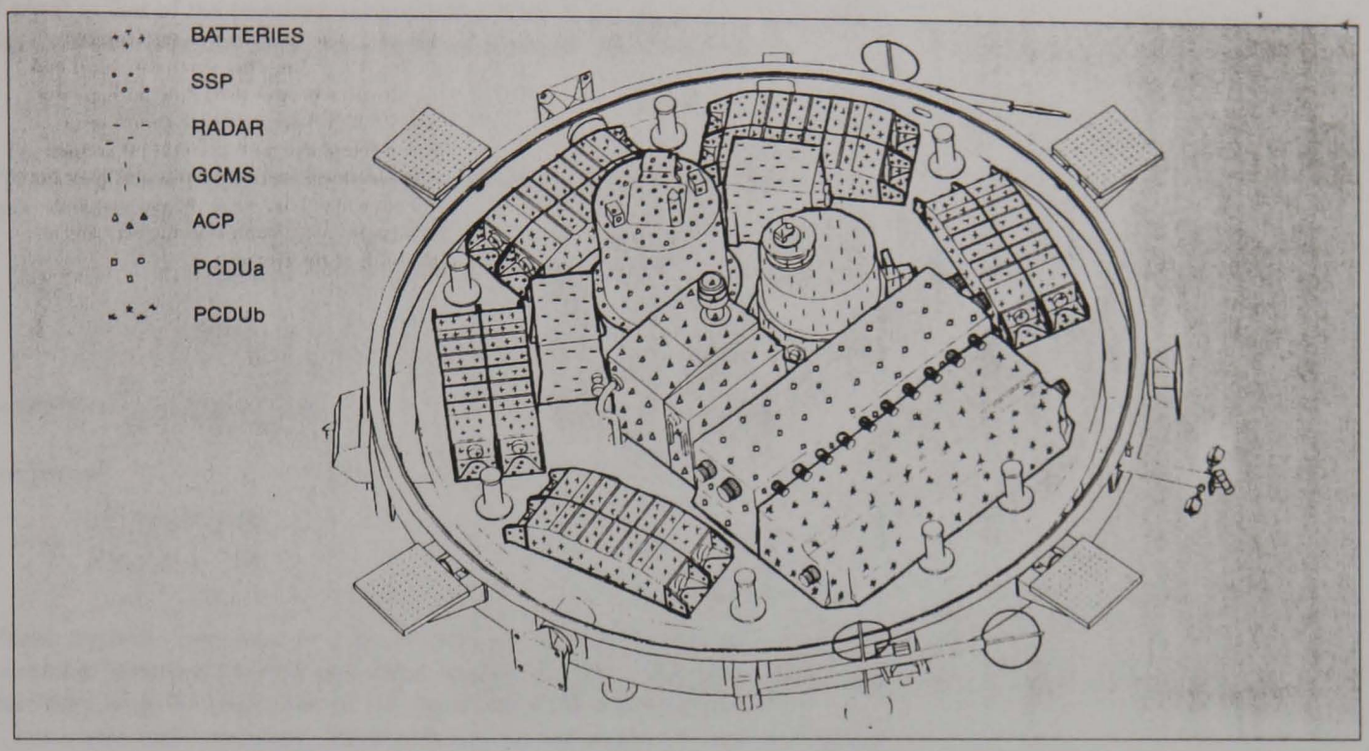

Figure 4. View of the experiment platform's underside, showing the individual units. Colour coding shows the breakdown of components used in the impact model. The aluminium fore-dome, and the insulating foam layer have been removed for clarity

6. Ocean impact

A landing of a space vehicle on an extraterrestrial hydrocarbon ocean is indeed an exotic and imaginative scenario, but is by no means improbable. While such an event would be a first in space exploration, the problem of landing on liquids is a fairly familiar one in a terrestrial context.

Vehicle splashdown loads were first considered theoretically in 1929 (although there was some experimental work in the UK in 1919) by Von Karman[30], for the purpose of estimating landing loads on seaplane floats, but received detailed examination for the Mercury and Apollo Programmes. Two theoretical approaches are possible to estimate loads: one is to model the impacting probe as a source sheet in potential-flow theory, and compute the resulting pressure and flow distribution in the liquid[31]; the other is to assume that the impacting probe becomes 'loaded' with a virtual mass of ocean, using more-or-less empirical factors.

The second method was found to give excellent agreement with results from scale-model and full-size impact experiments[32] and, being considerably simpler than the potential-flow method, is used here. The method was also used to evaluate splashdown loads on the crew compartment of the Space Shuttle 'Challenger'[33].

Let us assume a mass M_0 for the Probe, and vertical impact velocity V_0. As it penetrates, it becomes loaded with a virtual mass M_v of liquid, with the Probe/liquid ensemble moving at a velocity V. The virtual mass, which varies as a function of time, may be considered as the effective mass of liquid with which the Probe shares its momentum at a given instant.

Applying conservation of momentum and ignoring drag, weight and buoyancy forces (e.g. during the first 0.05 s of impact, weight would make only a 1% change in the Probe's momentum) gives

$$(M_o+M_v)V = M_oV_o \tag{1}$$

Differentiating,

$$(M_o+M_v)\frac{dV}{dt} + V\frac{dM_v}{dt} = 0 \tag{2}$$

The virtual mass M_v is usually taken as a fraction k (0.75 in Ref. 32 and $2/\pi$ (=0.64) in Ref. 34: here k=0.75 is used) of the mass of a hemisphere of liquid with a radius R equal to that of the (assumed axisymmetric) body at the plane of the undisturbed liquid surface (Fig. 5). Thus, for a liquid of density ρ, the virtual mass is

$$M_v = 2k\pi\rho R^3/3 \tag{3}$$

For a general axisymmetric shape $R=f(h)$, where h is the penetration distance, it is easy to show that

$$\frac{dM_v}{dh} = 2k\pi\rho R^2 \frac{dR}{dh} \tag{4}$$

noting that $\frac{dh}{dt} = V$ and $\frac{dV}{dt} = a$

we obtain

$$a = \frac{-V^2(2\pi k\rho R^2)}{(M_0+M_v)} \frac{dR}{dh} \tag{5}$$

These equations are easy to solve numerically (indeed in the early days[32] the numerical computation was performed manually). Terms for drag, weight and buoyancy could be added, but do not significantly affect the peak loads.

For a spherically-bottomed vehicle with a radius of curvature R_N and a penetration distance h (Fig. 5), this 'waterline' radius is given simply as

$$R = (2R_N h - h^2)^{1/2} \tag{6}$$

and the equations can be solved analytically to derive (for example) the peak loads (see, for example Ref. 34).

The above method can also be used to estimate the loads on a 75 kg human diving into a swimming pool. If the nose radius corresponds to the size of the head, the peak load is a little under 1 g: if, on the other hand, the nose radius is increased to, say, 30 cm (i.e. a 'bellyflop'), the loads increase to ~6 g. This order-of-magnitude change in load is painfully apparent to those unfortunate enough to verify the nose-radius dependence experimentally!

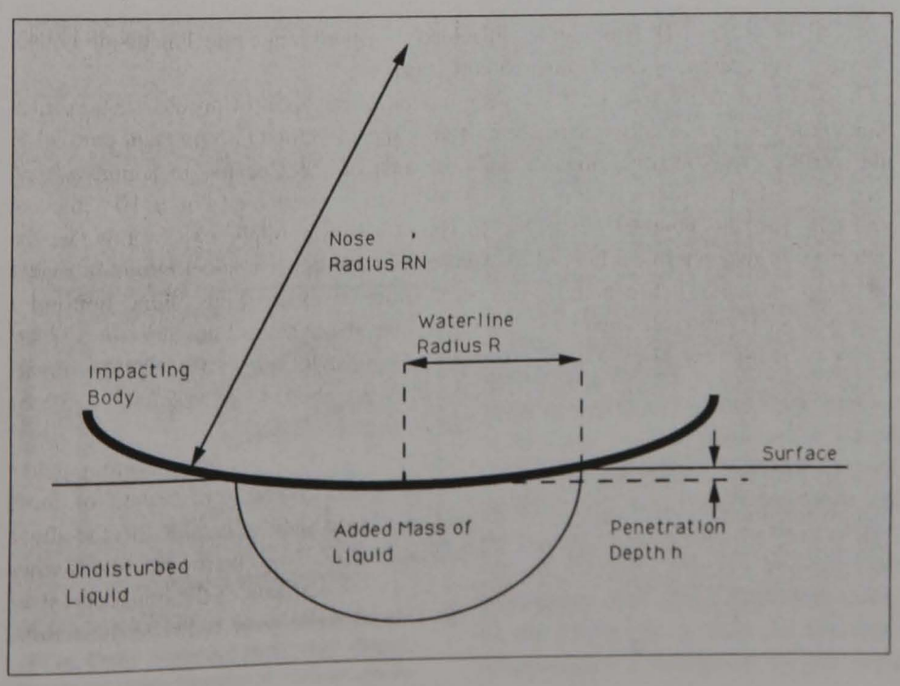

Figure 5. Idealised geometry for a vertical impact of a sphere-nosed body into a liquid

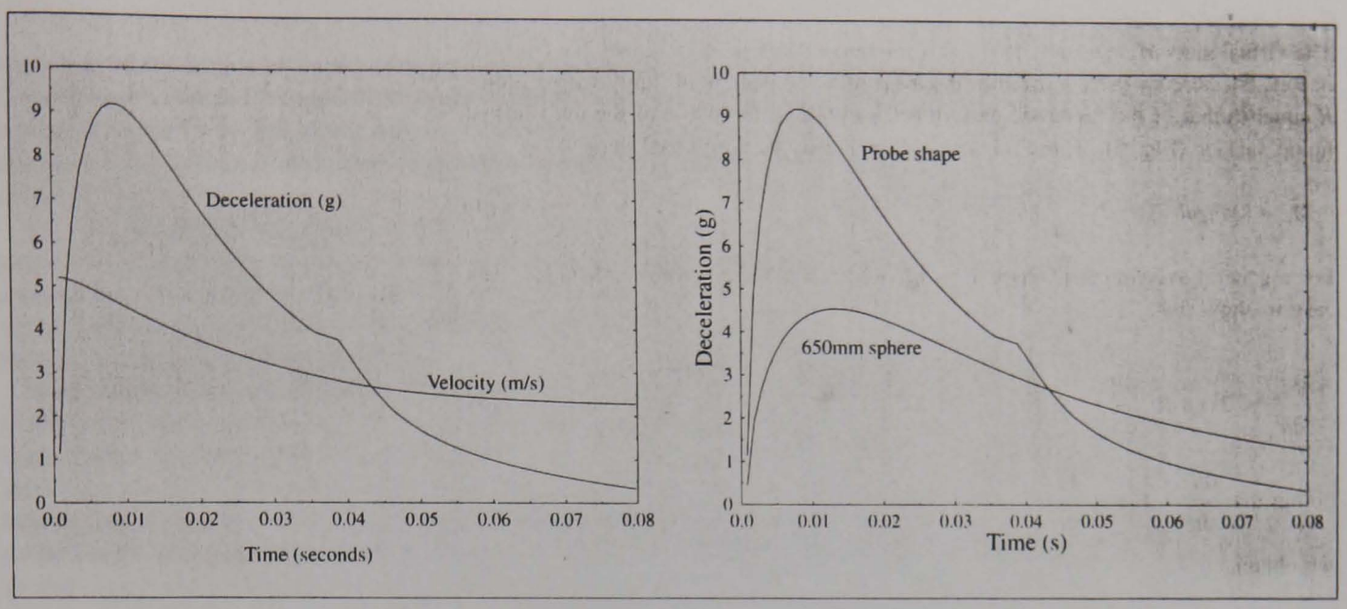

Figure 6a. Deceleration and velocity profile for the nominal impact case, assuming the Probe shape as described in the Appendix to be perfectly rigid (drag and buoyancy not modelled)

Figure 6b. Deceleration profile for the same impact case, but also showing the profile for a spherical nose radius of 650 mm for comparison (drag and buoyancy not modelled)

It is tempting to approximate the shape of the Probe with a sphere of 650 mm but, due to the sensitivity to nose radius, this might lead to underestimation of the peak loads. Figure 6 shows the acceleration versus time and speed versus time profiles for a 207 kg Probe splashing into liquid of density 600 kgm^{-3} for the actual Huygens Probe shape (see Appendix). A corresponding profile assuming a sphere of 650 mm radius is shown for comparison. It is apparent that the peak load is reached after about 0.01 s, after the Probe has penetrated to a depth of about 5 cm. After the peak, the loads decay away; after this, drag, buoyancy and weight begin to significantly modify the Probe's motion, but this is not evaluated here.

(Note that there should be a slight jump in the acceleration level at about $t=0.1$ s as the bulky attachment mechanisms used to hold the front shield during entry hit the liquid, but this has not been modelled here).

The peak impact loads are shown in Figure 7 for the actual Huygens Probe shape with mass 207 kg for various impact velocities and ocean densities (pure liquid methane has a density of about 450 kgm^{-3}, ethane about 600 kgm^{-3} and liquid nitrogen about 800 kgm^{-3}). The ocean compositions suggested in Reference 35 indicate the most likely density range as 600–650 kgm^{-3}.

A method similar to that above can be used to estimate the loads on appendages, such as the booms of the Huygens Atmospheric Structure Instrument (HASI). First estimates suggest that the splash loads should generate bending moments at the boom roots of the order of 10 Nm, and so, provided the boom hinge attachments do not act as stress concentrators, the booms should survive.

It was found during tests on a 1/4-scale model of the Apollo Capsule[36] that vertical landing loads are virtually independent of any impact-velocity component parallel to the surface. Additionally, impacts with the axis of the Capsule in a non-vertical orientation had lower accelerations (e.g. 60% of normal load for a 10° pitch at impact) than the nominal vertical case (intuitively we might expect this, as the interface of the spheroidal bottom of Apollo with the upper conical structure makes a 'sharp' corner which penetrates the ocean more easily than the 'blunt' bottom).

Thus, loads along the main axis of the Probe at impact are highest for vertical impact (the nominal case). The worst-case loads occur for a light Probe, high impact velocity, and dense ocean. These worst-case loads are about 13 g, assuming the Probe to be rigid; nominal loads are of the order of 9 g.

Tests on the Apollo Module[37] showed that vehicles with non-rigid bottoms (such as Huygens) may experience peak loads approximately 50% in excess of those encountered with a rigid bottom, so perhaps a margin should be added to the above figures (in Ref. 36, for example, accelerations of 38 g were measured when calculations indicated a rigid-body value of 22 g). An estimate of the impact pressure on the Probe can be made by dividing the impact force (equals Probe mass times instantaneous acceleration) by the wetted surface area of the Probe. Ignoring the

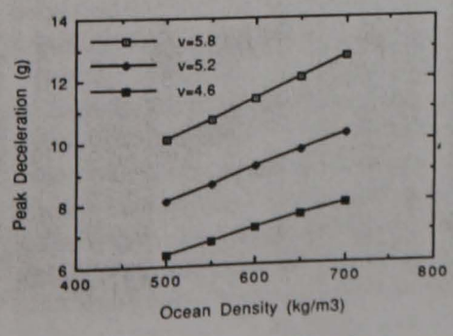

Figure 7. Peak impact decelerations for a 207 kg Probe (assuming rigid 'real' shape) in various ocean densities at various speeds

singularity at the instant of impact, this pressure is of the order of 10−20 N/cm^2. Comparing this with the strengths of Probe elements (see Section 9 and the Appendix) indicates that the Probe will indeed deform, modifying the deceleration history given in Figure 6. No attempt is made here, however, to model the coupled flow/structural effects.

Since the Huygens Probe is designed for (axial) entry loads of the order of 20 g in any case, the axial loads for liquid impact should be perfectly survivable, even with a margin for non-rigid effects imposed on the splash load predictions. Note, however, that the entry loads are conducted to the experiment platform via a different load path, leading to compressive stress on underside units.

Should there be a sideways velocity component at impact, there will naturally be a sideways (radial) acceleration. This will be small, however, compared with the axial loads (in Ref. 36, for example, an impact with an 11° pitch angle, a 7 ms^{-1} vertical velocity, and a 3 ms^{-1} horizontal velocity had an axial load of 30 g, with a sideways load of only 2.9 g). The radial loads on the Probe are in effect in the same direction as the launch loads (the Probe is attached sideways to the Cassini Orbiter at launch), so that, given the anticipated impact conditions, sideways loads should not cause damage to the Probe. A sideways impact will also produce an angular acceleration pulse, but this is not considered further here.

After the initial acceleration pulse, the acceleration decays until the Probe's entire lower surface is immersed. There will be a slight pulse due to liquid inertia loads on the radar altimeter antennae and the appendages used to attach the Probe to its entry shield. After this, however, the inertia loads are minimal and the forces of hydrodynamic drag and buoyancy are the most important. For the nominal (5.2 ms^{-1}) vertical impact with an ethane ocean (600 kgm^{-3}), the Probe will have been decelerated to about 2.5 ms^{-1} by the time its lower surface is completely immersed. Rough estimates suggest that the Probe will continue moving for another 1 s to a depth of about 1 m, with the top platform a few tens of centimetres below the depth of the ocean (the antennas should be submerged only momentarily, if at all). Buoyancy brings the Probe bobbing back up to the surface about 1.5 s after first contact. Note that the slightly lower impact loads and deeper penetration reported in Reference 7 were computed for a somewhat narrower Probe shape, before the current design had evolved.

7. Post-impact dynamics for liquid landing

In the event of a landing in a lake or sea, the subsequent dynamics and flotation characteristics of the Probe are of interest, since these will affect the post-impact scientific measurements.

A key question is naturally whether the Probe will float at all. Since the bulk density of the Probe is of the order of 200−300 kgm^{-3}, while that of the ocean (assuming it is free of bubbles) is about 600 kgm^{-3}, the answer is that it will. However, the level at which it floats is also of interest, to determine whether the Descent Imager and Spectral Radiometer (DISR) is above the 'waterline', and to verify that the measurement cavity of the Surface Science Package (SSP) is below it, so that its transducers are in contact with the liquid.

In order to determine the flotation level, a simple model (Fig. 8) has been set up to calculate the force and moment due to buoyancy for the Probe at any immersion depth and orientation. This is done simply by assuming that the Probe is axisymmetric, and breaking it down into small elements. Simple geometry determines whether each element is submerged or not; if submerged, it has a buoyant force equal to the weight of the displaced liquid. This force also has a moment arm associated with it. Summing these forces and moments allows the overall upthrust and torque to be determined. These quantities are given in Figures 9 and 10 for a nominal ocean density of 600 kgm^{-3}; the forces and moments scale directly with ocean density.

It is seen, by comparing the upthrusts with the Probe weight (Fig. 9), that the Probe should float with the 'waterline' almost at the level of the Probe centre-of-gravity. Thus, happily, the DISR is above the surface, and the SSP cavity is filled.

Figure 8. Geometry of floating Probe. Upthrust acts at centroid of the submerged portion of the Probe: weight acts at centre-of-gravity

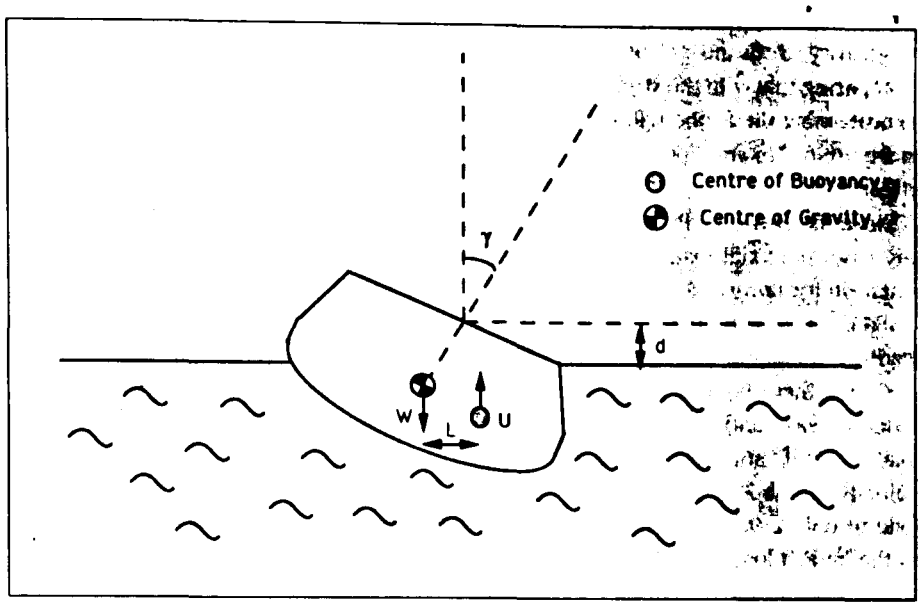

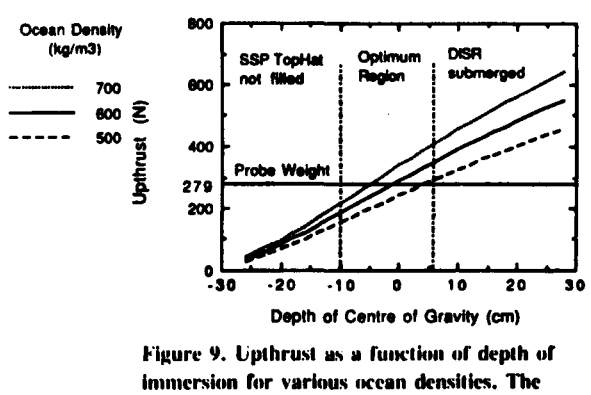

Figure 9. Upthrust as a function of depth of immersion for various ocean densities. The 'waterline' exists where the upthrust equals the weight. The waterline for the expected cases lies, reassuringly, in the most suitable region, around the 'equator' of the Probe

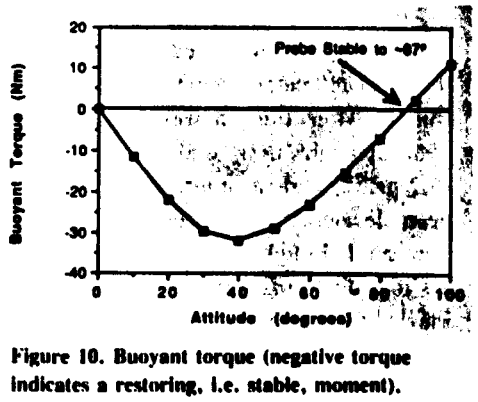

Figure 10. Buoyant torque (negative torque indicates a restoring, i.e. stable, moment). Note the linear dependence for small angles, and the onset of capsizing instability at large tilt

As all the moments are negative, the Probe is stable in its nominal vertical attitude (assuming that it is not significantly deformed during the impact). It would need to be tilted to about 87° before capsizing, which is presumably only possible in the event of improbably high (>impact speed) surface winds.

These negative moments are, for small angles, approximately proportional to the angle of the Probe (Fig. 10). A 'rocking' period can thus be determined by assuming that the rocking is a simple harmonic motion. If the buoyant torque $J = UD = k\gamma$, where γ is the angle of the Probe (Fig. 8), then the period of the motion is simply $2\pi\sqrt{(I/k)}$ where I is the Probe's transverse moment of inertia. Further, since the constant of proportionality (~ 68 Nm/rad for $P = 600$ kgm^{-3}) is itself proportional to the ocean density, and the Probe's orientation can be measured with tilt sensors (part of the SSP experiment), this leads to a crude method of determining ocean density. For a density of 600 kgm^{-3}, the rocking period is 3.4 s; for a 650 kgm^{-3} ocean, the period is 3.26 s. Bobbing periods for vertical oscillations (since the upthrust is proportional to displacement) can also be established, and can be measured with Probe accelerometers to derive another, albeit coarse, density measurement.

In the event of landing in a lake or sea, the payload will be able to measure currents and wave properties, ocean composition, physical properties (e.g. dielectric constant, useful in interpreting radar data), turbidity, and depth. The DISR camera will be above the 'waterline' and will be able to image the surface and lower atmosphere. The detailed science plans for the surface are still under discussion (see later).

8. Impact with solid surface

Impacts with solid surfaces are much harder to evaluate, due both to the paucity of experimental data and the difficult analytical treatment. A handful of drop tests onto sandy surfaces were performed in connection with the Mercury[38] and Apollo[36] programmes. In addition, a large series of experiments were conducted in connection with using penetrators to evaluate the lunar surface (before the Surveyor series of missions was performed). In these experiments[39], small dense ball-nosed vehicles were dropped or shot into a variety of materials including sand, earth, lead, balsa wood and concrete.

If the rock/ice at the landing site is finely-divided and non-cohesive (since it is so cold), we may perhaps treat it as sand (although it will have a lower density than sand, so predictions here will perhaps be slightly pessimistic). A formula developed in Reference 39 gives peak deceleration for nose diameter D (m), mass M (kg) and impact velocity V (ms^{-1}) as proportional to $D^{1.6}V^{1.6}M^{-1}$. However, this empirical formula does not appear to scale well to the Apollo and Mercury results (see Table 2).

Reference 39 also gives some theoretical expressions for the impact of spheres into elastic ('The Hertz Law') and plastic ('The Meyer Law') materials which appear to scale with much more success to the other results. Since the Mercury and Apollo models are more similar in size to Huygens, and their speeds and masses are comparable, these results are the most pertinent to validating the estimation methods. Expressions (7) and (8) below predict peak decelerations (assuming Huygens has a diameter of 1.3 m, and mass and velocity as in the previous sections) of 32 g and 26 g, respectively, for landing on sand surfaces.

The expressions as given in Reference 39 depend explicitly on given material properties: in the expressions below, however, I have simply made an empirical fit to the data in Table 2. Thus the peak impact accelerations are given (in Earth g) as

$$a_{max} = 35\ D^{0.2}V^{1.2}M^{-0.4} \quad (7)$$

or

$$a_{max} = 60\ D^{0.5}V^{1.6}M^{-1} \quad (8)$$

Since the bearing stress in sand increases with depth (see later), Expression (7) is probably preferable on theoretical grounds. Additionally, it appears to give a marginally better fit to the (limited) dataset in Table 2.

Thus if Huygens can be considered as a rigid sphere of radius 650 mm, its peak impact deceleration on landing on sand (i.e. a moderately dense, non-cohesive fine particulate material, or regolith) should be in the range 26−32 g. The presence of larger lumps of material like boulders will, of course, modify this prediction (see, for example, Ref. 40).

This impact deceleration is rather larger than the entry deceleration, but perhaps is within engineering margins. Consider, for example, the power distribution relays (Deutsch EL415). Sudden deceleration at impact could cause these to 'chatter', causing momentary interruption to the power supply. The 'all axes' acceleration specification is 15 g, but the shock (6 ms) tolerance is 200 g. For the Probe to stop with 30 g from 5.2 ms^{-1} takes about 16 ms, and so one would cautiously expect that the specification should not be exceeded. However, the situation is marginal.

Table 2. Comparison of theoretical predictions of peak impact loads for sand impact with experimental data. Huygens model data are from unpublished work by A. Seiff of NASA Ames, using 1/3 and 1/9 scale models of the Phase-A Huygens Probe design

Model	Ref	Peak load measured	Hertz law $35D^{0.2}V^{1.2}M^{-0.4}$	Meyer law $60D^{0.5}V^{1.6}M^{-1}$	Empirical (Ref. 39) $80D^{1.6}V^{1.6}M^{-1}$
1/3-scale Phase-A Huygens	-	26	27.1	27.4	10.72
1/9-scale Phase-A Huygens	-	20	17.4	15.67	2.2
1/6-scale Mercury Capsule	38	74	102	103	106
1/4-scale Apollo Capsule	36	49	49.6	52	54.77
3-inch hemisphere	39	50	249	149	51.8
Huygens	-	??	31.6	24.7	8.2

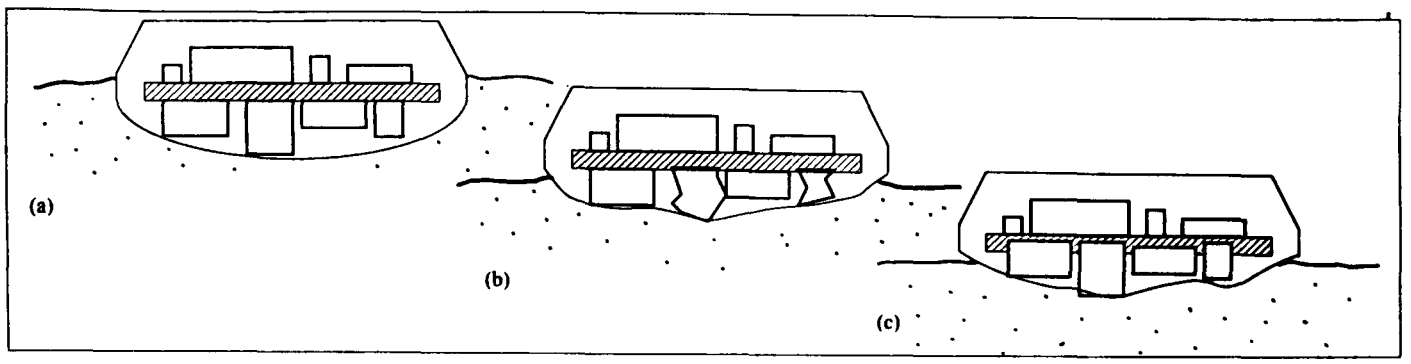

Figure 11. Consequences of impact depend on relative strengths of landing-site material, subsystems boxes and experiment platform:
(a) soft material: becomes compressed
(b) hard material: loads applied to boxes, causing failure
(c) hard material: loads applied to boxes, punching them into honeycomb of experiment platform

All the above considerations assume the Probe does not deform. However, since the impact process leads to the application of structural loads directly onto units on the Probe's underside, these units may be deformed, leading to failure. Figure 11 indicates how the impact energy may be dissipated in the soil, the units, or the experiment platform. To examine in detail the structural effects of the impact on the Probe, and the sensitivity of the Probe deceleration history to surface mechanical properties, a more detailed approach is required.

9. Impact-dynamics model

The model considers the Probe essentially as a point mass, mounted atop several (seven in the nominal model) 'stacks', each of four elements (Fig. 12). Each element is defined with an undistorted length, and a stress vs. compression characteristic described by linear interpolation between four given points (Fig. 13). Each stack is allocated a cross-sectional area.

For example, one 'stack' represents the spacecraft batteries, and comprises the following elements: the experiment platform (a honeycomb sandwich), the batteries themselves (modelled as essentially rigid boxes), an airgap, and a layer of thermal-insulation foam. Note that although there are actually five batteries on the Probe, they are modelled (for speed) as one stack with an area equal to that of the sum of the actual battery boxes. The 0.8 mm aluminium fore-dome is treated separately in these calculations (see Appendix). It is assumed that the dome does not interact (i.e. exchange loads) with the stacks.

The impact simulation works as follows: starting from a given height above the surface (assumed flat), the program steps down in height increments of 1 mm (the height is defined from the upper side of the experiment platform to the undisturbed surface). The penetration of a given stack into the surface material is computed by subtracting the sum of the lengths of its elements (each multiplied by its own compression factor) from the height. The penetration yields a certain bearing strength (see Section 10). The program considers each element in turn, to determine which element is the 'softest' (i.e. yields the lowest compressive stress for the next height decrement), whether one of the stack elements or the soil itself, and allows this selected element to deform.

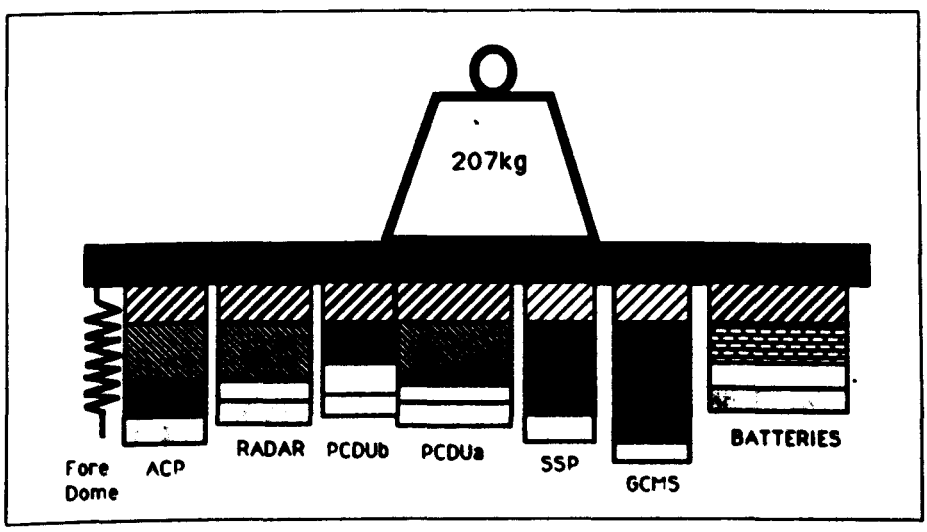

Figure 12. Schematic of crash model used in this study. Different box shadings indicate different element strengths

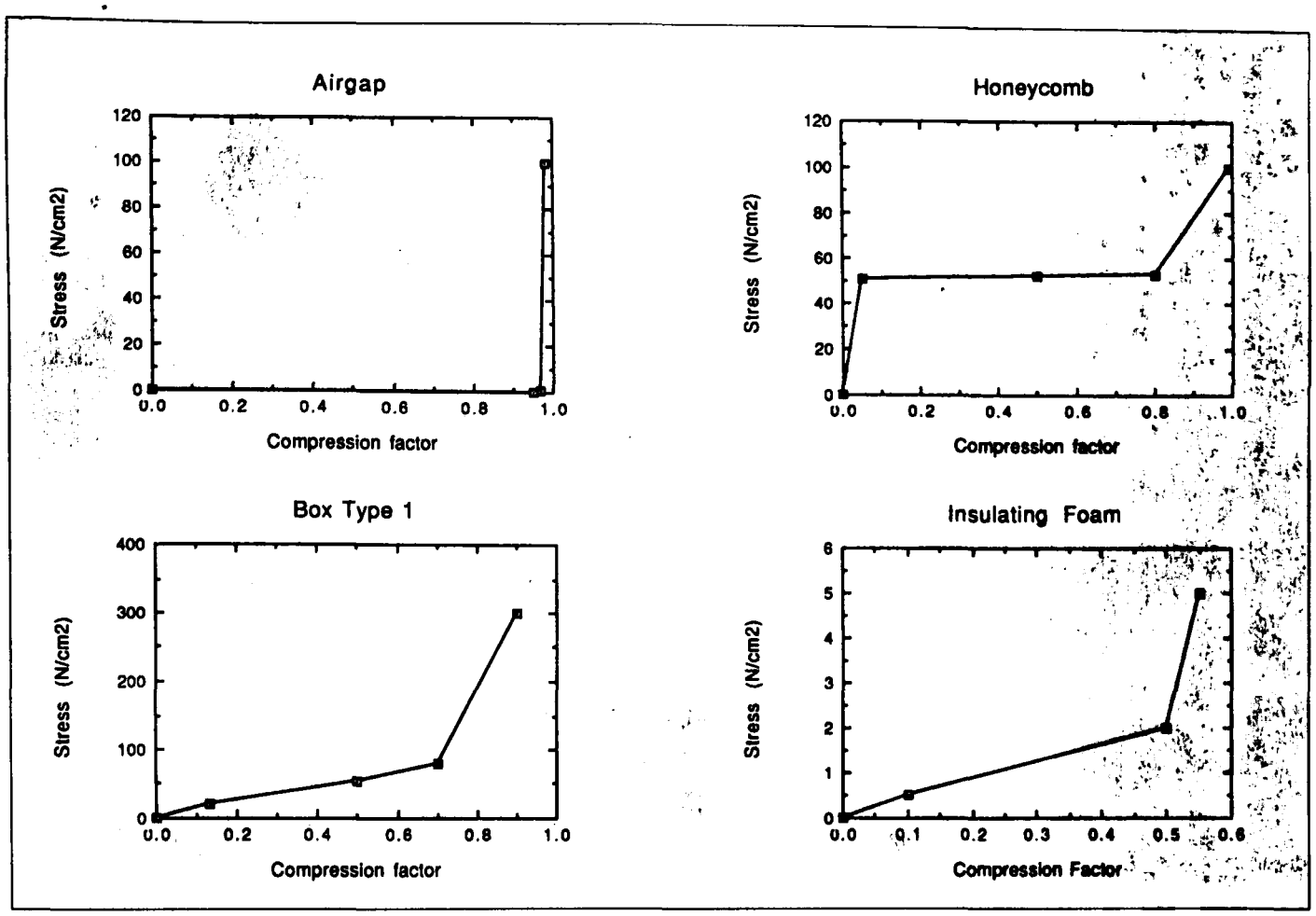

Figure 13. Stress-compression characteristics for four example elements from Table 4

As an element deforms, it resists more stress (typically), and thus is less likely to deform first, while stronger elements do not begin to deform until the loading on the stack becomes quite high (e.g. due to deeper soil penetration). The deceleration of the Probe platform is derived by summing the various loads and dividing by the Probe mass. Note that depth is the independent variable, not time. The simulation is stopped when the velocity falls to zero, giving the peak loads and depth of penetration.

The element lengths and stack areas are taken from Probe engineering drawings, and (for ACP, GCMS and SSP) from payload engineering drawings, and are summarised in Table 3. The methods used to estimate the stress-compression characteristics of the various elements, listed in Table 4, are described in the Appendix.

The program runs in a couple of minutes on a standard 386 PC: sample screen dumps are shown in Figure 14. The (quite primitive) numerical methods used in the program yield results accurate to about 10%. More accurate methods are not justified, given the overall simplicity of the model and the uncertainty of model parameters (such as buckling stresses, etc.). Thus, while the model's results are useful in gaining a qualitative idea of what is happening (i.e. discriminating between the cases in

Table 3. Elements of Probe impact model: lengths are in millimetres, while stress/compression characteristics are given in Table 4

Unit	Area (cm^2)	Element 1 length/type		Element 2 length/type		Element 3 length/type		Element 4 length/type	
SSP	250	80	4	50	9	150	8	30	2
ACP	506	80	3	165	11	40	12	50	2
GC-MS	302	80	4	150	7	50	6	50	2
BATTS	2625	80	3	80	5	40	1	50	2
PCDUa	1044	80	3	150	10	40	1	50	2
RADAR	295	80	3	150	11	40	1	50	2
PDCUb	1140	80	3	110	10	50	1	50	2

Table 4. Characteristics of element types used in the model. C denotes compression factor (i.e. strain), while S is the stress in N/cm^2

No	Type		1	2	3	4
1	Air gap	C	0.95	0.97	0.98	1.00
		S	0.01	1.00	100.00	1000.00
2	Basotect foam	C	0.10	0.50	0.55	0.90
		S	0.50	2.00	5.00	1000.00
3	100% honeycomb	C	0.05	0.50	0.80	0.99
		S	51.00	52.00	53.00	1000.00
4	50% honeycomb	C	0.05	0.50	0.80	0.99
		S	25.00	26.00	27.00	1000.00
5	Hard box	C	0.01	0.10	0.20	0.99
		S	10.00	100.00	1000.00	2000.00
6	GCMS top dome	C	0.25	0.50	0.70	0.90
		S	4.60	10.00	20.00	200.00
7	GCMS cylinder	C	0.10	0.20	0.30	0.90
		S	80.00	100.00	400.00	600.00
8	SSP top-hat body	C	0.10	0.20	0.50	0.90
		S	80.00	60.00	30.00	200.00
9	SSP top-hat cone	C	0.10	0.20	0.80	0.90
		S	200.00	400.00	500.00	600.00
10	Box type 1	C	0.13	0.50	0.70	0.90
		S	20.00	55.00	80.00	2000.00
11	Box type 2	C	0.13	0.55	0.90	0.95
		S	40.00	50.00	200.00	300.00
12	Box type 3	C	0.20	0.55	0.90	0.95
		S	13.00	50.00	200.00	300.00

Fig. 11) and estimating deceleration histories for the Probe, not too much attention should be paid to the deformation of individual units until the model has been refined with as-built structural parameters or validated with finite-element simulations.

10. Surface models

Having established the structural properties of the Probe, it remains to obtain plausible, but usable, surface models to interact with it. A review of current understanding of Titan's surface can be found in Reference 8. In principle, any surface type is possible, but only three principal types are examined, namely regolith, sludge, and hard ice/rock.

Since surface heat flow on Titan is sufficiently high that the crust may be convective, mountain-building and tectonics cannot be ruled out, and so the possibility of sloping terrain cannot be excluded. Similarly, aeolian transport[8,29] of surface particulates could form dunes[41]. However, for the purposes of this work, I assume that the impact occurs on flat, horizontal terrain.

Fresh, hard ice might exist where there has been recent cryo-volcanic activity, at the base of young impact craters, or where fluvial or aeolian activity has scoured the surface free of loose particulates. This may be modelled by setting the surface hardness to an arbitrarily large value.

Particulate material is likely to cover some, if not all, of Titan's surface. This material would include solid photochemical aerosols (acetylene and higher organics) and icy impact ejecta. However, the mechanical properties of these deposits are not well-constrained. Dry deposits of aerosol particles (which appear to have a fractal

```
  HUYGENS IMPACT SIMULATION   R D Lorenz 93/94  a:\res\s1

Soil Parameters: k1= 1  k2= .1  k3= 0   Mprobe= 207 kg      Vimpact= 5.2 m/s
Shell Model  1000  N/m        GC-MS fails at 8000 N


Time : 50 ms       Height  150 mm        Speed 0.000m/s       Accel(g)23.383

                .SSP.  .ACP.  GC-MS  BATTS  PCDUa  RADAR  PCDUb
crush( 1 )      0.03   0.01   0.01   0.00   0.00   0.00   0.00  Shell Load (N)
crush( 2 )      0.00   0.04   0.01   0.00   0.07   0.03   0.05       175.0
crush( 3 )      0.01   0.20   0.52   0.97   0.99   0.99   0.98
crush( 4 )      0.53   0.90   0.90   0.54   0.56   0.56   0.56

Stress:        15.00  13.40  11.60   4.40  10.24  10.74   6.90
Force (N)       3750   6780   3503  11550  10691   3168   7866
Pen (cm)       14.00  12.40  10.60   3.40   9.24   9.74   5.90

          AngleZ (deg) -1.3     AngleY (deg)  1.9   DISR clearance (mm) 211.6
(a)  maximum g 23.38315  at  48.09193  msecs



  HUYGENS IMPACT SIMULATION   R D Lorenz 93/94  a:\res\s1

Soil Parameters: k1= 1  k2= .1  k3= 0   Mprobe= 207 kg      Vimpact= 5.2 m/s
Shell Model  1000  N/m        GC-MS fails at 8000 N


Time : 9 ms        Height  289 mm        Speed 5.102m/s       Accel(g) 2.244

                .SSP.  .ACP.  GC-MS  BATTS  PCDUa  RADAR  PCDUb
crush( 1 )      0.00   0.00   0.00   0.00   0.00   0.00   0.00  Shell Load (N)
crush( 2 )      0.00   0.01   0.01   0.00   0.01   0.01   0.01        36.0
crush( 3 )      0.01   0.03   0.10   0.00   0.77   0.77   0.02
crush( 4 )      0.43   0.70   0.52   0.00   0.00   0.00   0.00

Stress:         1.70   2.00   2.00   0.00   1.00   1.00   1.00
Force (N)        425   1012    604      0   1044    295   1140
Pen (cm)        0.70   1.00   1.00   0.00   0.00   0.00   0.00

(b)          AngleZ (deg) -0.0     AngleY (deg)  0.0   DISR clearance (mm) 329.1
```

Figure 14. Example screen dumps from the program. Rows of figures marked 'Crush(X)' denote the current compression of each element; X = 1 are topmost elements (honeycomb). Also shown are the stress, total force and penetration depth of each stack. Figure 14a shows status early in impact event, with large crushing of airgaps (PCDU, RADAR 3) and deformation of foam on SSP, GCMS, ACP 4. Figure 14b shows status at end of impact, with more extensive crushing

structure, judging from Pioneer 11 polarimetry and Voyager I infrared results, and theoretical modelling) could be very soft, like fluffy snow. On the other hand, rainfall or other processes could compact these deposits into much harder soils.

A comprehensive soil-mechanics[42] treatment would be impractical and so a simple soil model is given here. Following Sperling & Galba[25], I use a soil stress p of the form

$$p = k_1 + k_2 x + k_3 v^2 \tag{9}$$

where p is the force per unit area on the spacecraft, x is the penetration depth into the soil, and v is the instantaneous impact velocity of the spacecraft. For all the cases I examine here, k_3 is set to zero (as in Ref. 25). Note that in Reference 26, $k_1 = 0$, and k_2 is called the 'subgrade modulus'.

In order to obtain realistic figures for k_1 and k_2, data for a variety of terrestrial and planetary surfaces have been collected in Table 5. These values, and their corresponding soil stresses from Equation (9), are used to select appropriate values for use in the model. It is instructive to compare the soil stress at various depths with, for example, the pressure on the sole of a shoe (say $1-2$ Ncm^{-2})

From a review of the data in Table 5, the nominal 'regolith' model assumed in this work is essentially that of the lunar soil as measured by Surveyor, namely $k_1 = 1$ N/cm^2, $k_2 = 0.1$ N/cm^2/mm. A 'soft, fluffy aerosol' deposit would have parameters $k_1 \sim 0$, $k_2 \sim 0.01$ N/cm^2/mm.

As for wet mixes of aerosols/ejecta with liquid ethane/methane, i.e. 'sludge', a useful terrestrial analogue may be clay, at one extreme. The other extreme, naturally, is thin sludge, which should be treated similar to a 'pure' liquid impact. Penetration tests on clay typically yield a constant 'flow presure': i.e. $k_2 \sim 0$. Tests on sod (Ref. 39 found that a value of 37 psi, or $k_1 = 25$ N/cm^2 gave a good fit to data, so sludge models in this study have k_1 values around, or lower than, this.

Table 5. Soil parameters from field measurements, and data from planetary landers

Type	Density kg m^{-3}	'Bearing strength' N cm^{-2}	Modulus N cm^{-2} mm^{-1}	Conditions	References
Very soft snow	200	0.6		5 kg load on fist will penetrate	43
Soft snow		4		5 kg load on fingers will penetrate	43
Medium snow	400	16		5 kg load on one finger will penetrate	43
Hard snow	600	150		5 kg load on pencil will penetrate	43
Very hard snow		300		5 kg load on knife will penetrate	43
Compacted snow	500	10	0.5	Collins Glacier. 30 cm diam. load plate	44
	720	15	1.3	Collins Glacier. 30 cm diam. load plate	44
Lunar dust	300	0.16		For 1 m support, based on pre-Surveyor photographs of crater slopes	24
Lunar soil		1.3	0.08	Surveyor landing dynamics	25
	1100–1600	0	0.1	Surveyor footpad penetration, etc.	45
Compressed lunar soil	1800	100		Yield strength	46
Mars soil 'Sandy Flats'	1000–1600		.03	Viking 1 landing dynamics - footpad penetration	47
Mars soil 'Rocky Flats'	1800		0.6	Viking 1 landing dynamics - footpad penetration	47
Venus soil (Venera 13)	1400–1500	4–5		Shock absorber loads on landing	12
(Venera 13)		2.5–10		Penetrometer	48
(Venera 14)	1150–1200	2		Shock absorber loads on landing	12
Venus rock		65–250		Venera 14 penetrometer	48
White Sands Missile Range 'Coarse-grained sandy silt'			2.7–10		26
0.18 mm glass beads	2230	0.7	.11	Penetration by flat-ended 2 cm-diam. rod	49
0.36 mm resin beads	1050	0.7	.05	Penetration by flat-ended 2 cm-diam. rod	49

11. Model results

Some useful comparisons with the rough estimations in Section 8 can be made by setting the stiffness of all Probe elements to large values (i.e. forcing the Probe to act like a 'rigid body'). For the nominal regolith model (k_1=0.1 Ncm^{-2}, k_2=0.1 $Ncm^{-2}mm^{-1}$) the peak acceleration obtained is 28 g, reassuringly in the estimate range of Section 8.

With the Probe structural strengths set as in the Appendix, and Tables 3 and 4, the peak acceleration is 23.4 g. Varying the impact velocity from 4.6 to 5.8 ms^{-1} yields peak accelerations of 19.6–27.4 g.

The deceleration history for the nominal Probe strengths, but various soil properties, is given in Figure 15; Figure 16 shows the dependence of the peak load on soil hardness.

If the ground is made very stiff (i.e. generates extremely large bearing strength for minimal penetration, by setting k_2 to very large values), the peak load is determined by the stiffness of the Probe elements alone. It was found that loads were >100 g, and significant crushing of most of the Probe elements occurred. Thus, impact on an arbitrarily hard surface would lead to failure of the Probe.

Table 6. Peak accelerations, and loads on individual Probe units, for various soil strengths

Soil stiffness k_2 (N/cm^3/mm)	Peak deceleration (g)	Load on GCMS (kN)	Load on SSP (kN)	Load on ACP (kN)	Load on PCDU box (kN)	Load on radar boxes (kN)
0.01	11.6	.95	.83	1.6	5	0.8
0.1	25	3.6	3.6	7.0	19	3.4
1	35	7.6	6.5	21	28	8.6
10	40 (41)	7.6 (7.6)	8.3 (8.3)	23 (23)	31 (32)	13 (13)
100	79 (75)	8 (45)	32 (32)	75 (75)	42 (0.2)	12 (0.1)

Figures in parentheses refer to the case where the GCMS mounting is deformed 'normally', without the GCMS being removed from the model when its load exceeds 8 kN

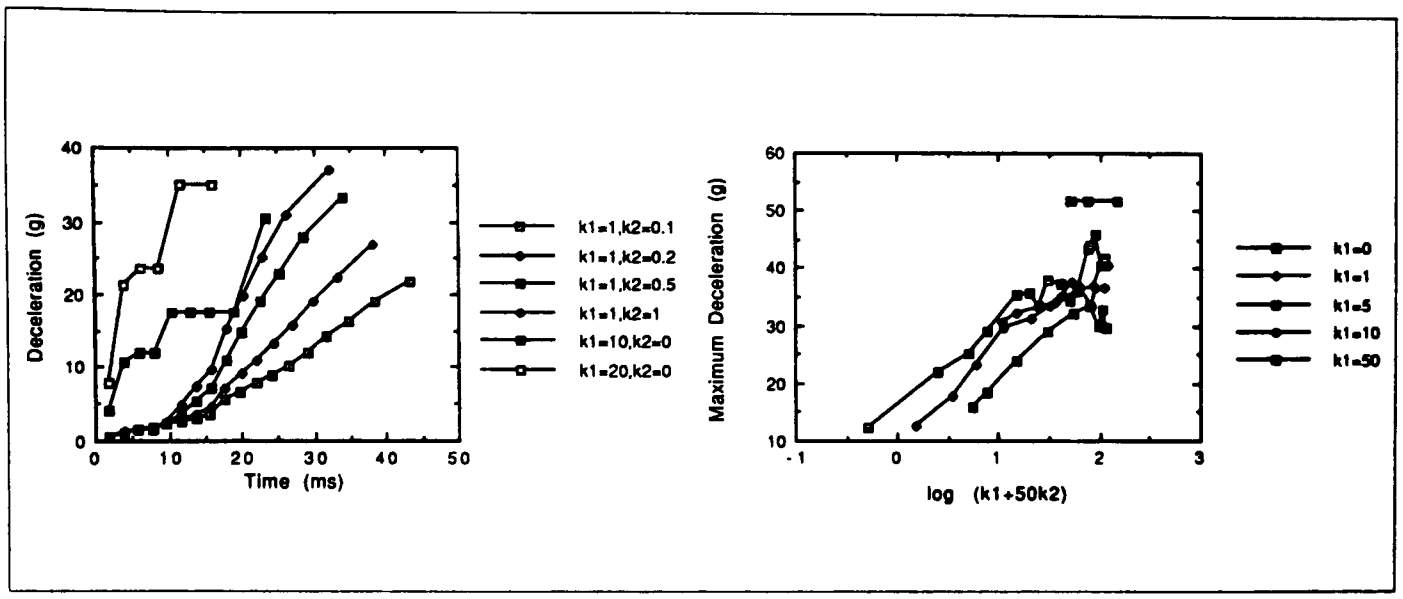

Figure 15. Deceleration profiles for various soil parameters

Figure 16. Correlation of peak g-load with average strength of top 10 cm of soil

For the nominal Probe model, landing onto regolith, the peak deceleration is marginally above the entry g-load. Some slight deformation of the GCMS and PCDU occurs, and the experiment platform above the SSP and GCMS is somewhat deformed. Nevertheless, at least partial Probe operation after such an impact seems likely.

For heavy sludge impact, the partitioning of loads is less effective than for regolith and so the GMCS and its attachment to the experiment platform would be damaged, with the ACP and SSP also receiving large loads. However, the Probe stops sufficiently quickly that loads are not applied to the PCDU box, so that survival of the Probe (and topside experiments such as the DISR) is still probable.

Landing on fluffy aerosols ($k_1=0$, $k_2=0.01$) leads to modest g-loads, and very little deformation of the Probe. However, the Probe does penetrate deep enough for the sensor head of the DISR to be buried, compromising post-impact imaging.

The caveat mentioned in Section 9 is repeated: while the depth of penetration and deceleration histories predicted by the model are probably representative, the structural results for individual units should be trusted only qualitatively.

12. Probe survival and post-impact science

For a scientific data return post-impact, one or more of the experiments must survive the impact, the power system must remain operational, and at least one of the redundant data-handling and transmission chains must function. An additional aspect is that the attitude of the Probe must be such as to keep the orbiter spacecraft within the antenna lobe to keep the radio link open. As the Huygens Probe is relatively flat-bottomed, this is quite probable. Furthermore, the link is guaranteed for Probe attitudes up to 10° from normal, so for shallow slopes at least (and surfaces with 'boulders' of the order of 20 cm) the attitude of the Probe should not be sufficiently perturbed to break the link: without knowledge of Titan's topography, it is impossible to assign probabilities to this (see Ref. 50 for an approach where topography is known). Should there be a significant horizontal velocity component at impact, the Probe could also roll[51].

Other aspects vital to Probe survival (e.g. thermal environment) are unlikely to be dramatically altered at impact (although the performance of the insulating foam will be degraded by crushing). The mission energy and link budgets are guaranteed for a minimum of 3 min after impact but, depending on the exact descent location (which affects the time-above-horizon and link margin of the radio link to the Cassini Saturn Orbiter) and spacecraft performance in terms of energy utilisation, could permit a somewhat longer surface mission, of perhaps 30 min or more. Thus impact damage is probably the main constraint on surface operation.

As for the experiment payload, the Ultra-Stable Oscillator for the Doppler Wind Experiment, the Huygens Atmospheric Structure Instrument, and the Descent

Imager/Spectral Radiometer are all on the upper side of the experiment platform, as are the electronics for the Surface Science Package. These elements (including the accelerometers which will measure the impact accelerations, and may subsequently search for seismic activity) should be safe from impact damage by crush loading.

The Aerosol Collector/Pyrolyser (ACP) is mounted on the lower surface, but has completed its mission well before impact. The 'TopHat' sensor accommodation structure of the Surface Science Package is made of glass-fibre panels and insulating foam. In the event of an impact with a hard surface, the TopHat will probably break, although the individual sensor subsystems may still function (in any case, most of these sensors are optimised for liquid surfaces, so the science loss in this scenario is small). The Gas Chromatograph/Mass Spectrometer is a long cylindrical instrument and projects from the base of the Probe through the experiment platform. A hard impact will probably crush the inlets of the instrument, although some instrument operation may still be possible (the inlets are heated to volatilise surface material for analysis); extreme loading would punch the GCMS through the experiment platform.

Thus a reasonable portion of the payload should remain operational after impact on a solid surface, in particular the Descent Imager/Spectral Radiometer, on the upper part of the spacecraft, which will be able to return images (using its side-looking imager) and spectra from the surface. Additionally, upward-looking photometric sensors on this instrument will be able to measure any impact-generated dust cloud (see later). A group has been set up within the Huygens Science Working Team (HSWT) to consider the measurements that are expected (or should be aimed for) post-impact.

13. Impact-dynamics measurements

The impact decelerations of Huygens will be recorded by the accelerometers of the HASI experiment (three-axis piezoresistive, with a force-balance ('servo') accelerometer along the vertical axis, all mounted near the Probe centre of gravity, and by a piezoelectric accelerometer in the SSP electronics box, about 20 cm from the Probe axis. Since both the SSP and HASI are on the upper side of the experiment platform, they should measure accelerations similar to those predicted by the model (i.e. they are in the same location as the 207 kg mass in Figure 12). Combining the data from both sensors should allow the elimination of structural oscillations generated by the impact.

As seen from Figure 7, the peak deceleration is a possible way of measuring ocean density. However, given the uncertainty in Probe structural effects and the presence of various appendages, etc., on the fore-dome, it should probably not be relied upon. The bobbing/rocking periods described in Section 7 may be better in this respect. In any case, ocean composition will be measured directly by the GCMS, and by inference from physical-properties measurements (refractive index, speed of sound, density, etc.) on the SSP.

The impact deceleration for landing on solid surfaces is strongly dependent on soil hardness. From the peak load alone it is not possible to discriminate between high-k_1 and high-k_2 materials, although the combination of the two (e.g. $k_1+50\ k_2$ is a measure of the average bearing strength in the top 10 cm of soil) does show a broad correlation with peak load (Fig. 16) for weaker soils. However, examining the acceleration-time profiles (Fig. 15) shows that high-k_1 materials (sludge) have a much faster rise-time than high-k_2 materials. It is possible to discriminate sludge from liquids because, although their rise times are similar, the peak load for sludge is higher. Further investigations with the model will explore the sensitivity of acceleration profiles to surface properties, and variation of the stiffness of Probe structural elements.

It is probably impossible to discriminate from accelerometry between coarse and fine-grained soil deposits and, for that matter, determine soil stiffness for hard soils. However, there is a small impact sensor or 'penetrometer'[32] that forms part of the University of Kent's Surface Science Package (SSP), comprising a small (14 mm diameter) force transducer mounted on a short mast projecting from the bottom of the Probe. The force profile measured by this instrument (over a much shorter time scale,

and thus corresponding to a much smaller spatial scale) should give an indication of particle size in the range 4–25 mm, discriminate between cohesive and non-cohesive surface materials, and give a better indication of soil stiffness for regolith and harder soils.

Identification of particle size would provide an indication as to whether the surface materials at the landing site had been sorted by aeolian or fluvial processes. For example, pyroclastic fall deposits (tephra) from terrestrial volcanoes often display a strong central peak in a grain-size histogram[53] due to 'winnowing' by wind as the erupted material falls back to Earth.

14. Impact-induced dust clouds

Following the landing of spacecraft on Venus and Mars, optical measurements have indicated the generation of dust clouds. These have been thrown up owing to the interaction of the aerodynamic wakes of the Venera and Pioneer Venus probes and the retro-rockets on the Viking spacecraft[54]. Calculations of the mass and momentum in the aerodynamic wake of Huygens, and a comparison of the terminal descent velocity of dust particles on Mars, Venus and Titan[61], suggests that a similar phenomenon may occur at the Huygens impact.

Generation of a dust cloud implies that material at the landing site is fine and non-cohesive. Efforts[56,57] to measure the particle size on the basis of the opacity history (i.e. decay time) of the dust cloud have been relatively unsatisfactory, as the interaction of the wake with the ground is complex. However, recent theoretical and experimental investigations[58,59] of the associated fluid-dynamics processes (e.g. the wake of a decelerating disk is of interest for the sometimes catastrophic 'wake recontact' problem in parachute dynamics where the wake catches up with a decelerating parachute and causes it to deflate) show promise that, by the time Huygens reaches Titan, interpretation of dust-cloud data should yield better results.

A significant complication for Huygens is the fact that the parachute is still attached: it may be difficult to discriminate a drop in ambient light due to a dust cloud from that due to the parachute[60].

15. Conclusions

Simple analytical expressions have been presented for estimating the impact decelerations when landing space probes onto liquid and solid (particulate) surfaces. While necessarily limited in utility, these expressions are convenient 'rules of thumb'.

A modest numerical model has been presented to make more accurate predictions of the Huygens impact-deceleration history for impacts onto solid surfaces. This model has enabled the investigation of the sensitivity of impact deceleration to surface mechanical properties, and the estimation of the Probe's deformation during the impact.

These studies, and analogy with the Pioneer Venus and other missions, lead us to be cautiously optimistic about the prospects for a productive scientific return from the surface of Titan. Additionally, measurements of the impact deceleration and any impact-induced dust cloud will make modest, but useful, contributions to our knowledge of the physical state of Titan's surface.

Acknowledgements

The author acknowledges the support of the ESA Huygens Project, and a postgraduate research grant from the UK SERC/PPARC. Some early parts of the work reported here were conducted while the author was a Young Graduate Trainee in the Huygens Project Team (PYP) at ESTEC in 1990/91.

Useful insights into crash-dynamics analysis techniques for aerospace vehicles were gained by a visit to the Cranfield Impact Centre Ltd., and fruitful discussions there with Dr Sadeghi and his colleagues. B. Steckemetz, of OHB System (Germany) helpfully provided details of the ESA Mars Lander study.

A. Seiff of San Jose State University (USA) is thanked for providing unpublished model impact data. J. Underwood of Martin Baker Aircraft (UK) is thanked for providing Figure 3.

The review of an early version of the paper by J-P. Lebreton of ESA Space Science Department is gratefully acknowledged, as are useful discussions with members of the Huygens Science Working Team, in particular T. Owen and J. Lunine.

The author thanks the following individuals for their cooperation in providing information on the Huygens Probe, payload and components: D. Wyn-Roberts (ESTEC, NL), M. Bannister (RAL, UK), J-F. Brun and M. Tintignac (CNRS, France), A. Nairn (ETCA, Belgium), C. Lewis and S. Way (GSFC, USA) and J. Underwood (Martin Baker, UK).

References

1. Kohhase C. 1993, Meeting with a Majestic Giant: The Cassini Mission to Saturn, *The Planetary Report*, Vol. 13, No. 4, pp. 5–10.
2. Lebreton J-P. & Matson D. 1992, An Overview of the Cassini Mission, *Il Nuovo Cimento*, Vol. 15C, pp. 1137–1147.
3. Lebreton J-P. & Matson D. 1990, Cassini – A Mission to Saturn and Titan, Proc. 24th ESLAB Symposium on the Formation of Stars and Planets and the Evolution of the Solar System, Freidrichshafen, September 1990, ESA SP-315, November 1990, pp. 7–12.
4. Lebreton J-P. 1992, The Huygens Probe, Proc. Symposium on Titan, Toulouse, 9–12 September 1991, ESA SP-338, April 1992, pp. 287–292.
5. Mooij E. 1992, De Cassini-missie, *Ruimtevaart*, June 1992, pp. 2–8.
6. NASA/ESA Cassini Phase-A Study, ESA/SCI 88(5).
7. Lorenz R. 1992, Huygens Probe – The Surface Mission, Proc. Symposium on Titan, Toulouse, 9–12 September 1991, ESA SP-338, April 1992, pp. 359–364.
8. Lorenz R. 1993, The Surface of Titan in the Context of ESA's Huygens Probe, *ESA Journal*, Vol. 17, pp. 275–292.
9. Lebreton J-P., Verdant M. & Wills R. 1994, Huygens: The Science, Payload and Mission Profile, *ESA Bulletin No.77*, February 1994, pp. 31–41.
10. Hassan H., McCarthy C. & Wyn-Roberts D., Huygens – A Technical and Programmatic Overview, *ESA Bulletin No. 77*, February 1994, pp. 21–30.
11. Wilson A. 1987, Solar System Log, Janes Publishing Company 1987.
12. Arduevsky V.S. et al. 1983, Physico-Mechanical Characteristics of the Venusian Surface by Measuring Shock-Worker at Landing of Automatic Stations Venera 13 and Venera 14 (in Russian). *Kosmicheski Issledovania*, Vol. 21, pp. 331–339.
13. Fimmel R.O., Colin L. & Burgess E. 1983, Pioneer Venus, NASA SP-461.
14. Brodsky R.F. (Ed.) 1985, Pioneer Venus Case Study in Spacecraft Design, AIAA Professional Study Series.
15. Hanson A.H. 1978, Antenna Design for Pioneer Venus Probes, IEEE International Symposium Digest — Antennas and Propagation, 15–19 May 1978, Washington DC.
16. Melosh R.J. & Karat M.F. 1977, Computer Simulation of Light-Aircraft Crash, *J. Aircraft*, Vol. 14, No. 10, pp. 1009–1014.
17. Fasanella E.L., Widmeyer E. & Robinson M.P. 1986, Structural Analysis of the Controlled Impact Demonstration of a Jet Transport Plane, AIAA-86-0939, 27th Structures, Structural Dynamics and Materials Conference, San Antonio, Texas, May 1986.
18. Argyris J., Balmer H.A., Doltsinis I.S. & Kurz A. 1986, Computer Simulations of Crash Phenomena, *Int. J. Numerical Methods in Engineering*, Vol. 22, pp. 497–519.
19. Argyris J., Balmer H. & Doltsinis I.S. 1988, Some Thoughts on Shell Modelling for Crash Analysis, *Computer Methods in Applied Mechanics and Engineering*, Vol. 71, pp. 341–365.
20. Hagiwara I., Satoh Y. & Tsuda M. 1990, Study of an analytical technique and system for conducting vehicle crash simulations, *Int. J. Vehicle Design*, Vol. 11, pp. 564–577.
21. Miller G.K. 1993, Calculation of Impact Loads for High-Energy Drops of Cylindrical Containers, *Int. J. Impact Engineering*, Vol. 13, pp. 511–526.

22. Thomson R.P. 1966, The Practical Problem of Landing on Mars, *Aeronautics & Astronautics*, July 1966, pp. 66–73.
23. Steckemetz B., Wienss W., Bradbury B., Pickett A., Natenbruck P. & Roumeas R. 1993, Flight and Impact Dynamics of Landers for Mars Exploration, IAF-93-Q.1.379, Presented at the 44th International Astronautical Federation, Graz, Austria, October 1993.
24. Jaffe L.D. 1965, Strength of the Lunar Dust, *J. Geophys. Res.*, Vol. 70, pp. 6139–6146.
25. Sperling F. & Garba J. 1967, Treatise on the Surveyor Lunar Landing Dynamics and an Evaluation of Pertinent Telemetry Data Returned by Surveyor 1, Technical Report 32-1035, Jet Propulsion Laboratory, Pasadena, USA.
26. Mironet A., Urquhart R. & Walters R. 1983, Limiting Payload Deceleration during Ground Impact, *J. Spacecraft & Rockets*, Vol. 20, pp. 193–194.
27. Neal M.F. & Wellings P.J. 1993, Descent Control System for the Huygens Probe, AIAA 93-1221 RAeS/AIAA 12th Aerodynamic Decelerator Systems Technology Conference, London, 10–13 May 1993.
28. Lellouch E. & Hunten D.M. 1989, Titan Atmosphere Engineering Model, ESLAB 87/199 (see also Lellouch et al. 1989, Titan's Atmosphere and Ocean: A re-analysis of the Voyager 1 IRIS 7.7 micron data, *Icarus*, Vol. 79, pp. 328–349).
29. Allison M. 1992, An Assessment of Titan's Boundary Layer, Symposium on Titan, Toulouse, September 1991, ESA SP-338, pp. 113–118.
30. Von Karman T. 1929, The Impact of Seaplane Floats during Landing, NACA TN-321, October 1929.
31. Parr W.E. 1966, Water Entry, Proc. Seminar on Theoretical Inviscid Fluid Mechanics NOLTR 66-191, US Naval Ordnance Laboratory, September 1966.
32. McGehee R., Hathaway M.E. & Vaughan V.L. Jr. 1959, Water-Landing Characteristics of a Reentry Capsule, NASA Memorandum 5-23-59L.
33. Wierzbicki T. & Yue D.Y. 1986, Impact Damage of the Challenger Crew Compartment, *J. Spacecraft & Rockets*, Vol. 32, pp. 646–654.
34. Hirano Y. & Miura K. 1970, Water Impact Accelerations of Axially Symmetric Bodies, *J. Spacecraft & Rockets*, Vol. 7, pp. 762–764.
35. Dubouloz N., Raulin F., Lellouch E. & Gautier D. 1989, Titan's Hypothesized Ocean Properties: The influence of Surface Temperature and Atmospheric Composition Uncertainties, *Icarus* , Vol. 82, pp. 81–96.
36. Stubbs S.M. 1967, Dynamic Model Investigation of Water Pressures and Accelerations Encountered during Landings of the Apollo Spacecraft, NASA TN D-3980.
37. Stubbs S.M. & Hathaway M.E. 1967, Effects of Bottom-Structure Flexibility on Water Landing Loads of Apollo Spacecraft Models, NASA TN D-5108.
38. Vaughan V.L. 1961, Landing Characteristics and Flotation Properties of a Reentry Capsule, NASA TN D-655.
39. McCarty J.L. & Carden H.D. 1962, Impact Characteristics of Various Materials Obtained by an Acceleration-Time-History Technique Applicable to Evaluating Remote Targets, NASA TN D-1269.
40. McCarty J.L. & Howlett J.T. 1969, Protuberance Effects on Limiter-Equipped Hard Landing Payloads, *Shock & Vibration Bulletin 40*, pp. 183–191.
41. Grier J.A. & Lunine J.I. 1993, Speculation into Possible Aeolian and Fluvial Dune Deposits on Titan, *Bull. Amer. Astron. Soc.*, Vol. 25, p. 1105.
42. Scott R.F. 1963, Principles of Soil Mechanics, Addison-Wesley, Reading, Massachusetts.
43. Perla R.I. & Martinelli M. 1976, Avalanche Handbook, Agriculture Handbook 489, US Department of Agriculture, Forestry Service.
44. Retamal E. 1983, Some Experimental Results on Snow Compaction, Proc. 5th International Conference on Permafrost, Fairbanks, Alaska, pp. 1054–1059.
45. Jaffe L.D. 1969, Lunar Surface Material: Spacecraft Measurements of Density and Strength, *Science*, Vol. 164, pp. 1514–1516.
46. Jaffe L.D. 1971, Bearing Strength of Lunar Soil, *The Moon*, Vol. 3, pp. 337–345.

47. Shorthill R.W., Moore H.J., Scott R.F., Hutton R.E., Liebes S. & Spitzer C.R. 1976. The 'Soil' of Mars (Viking 1) *Science*, Vol. 194, pp. 91–97.
48. Kemurdzan A.L. et al. 1983. Preliminary Results of the Determination of Physico-Mechanical Properties of Venusian Ground by Soviet Automatic Stations Venera-13 and Venera-14 (in Russian), *Kosmicheski Issledovania*, Vol. 21, pp. 323–330.
49. Yamashiro M. & Yuasa M. 1983. A Penetration Test for Granular Materials using Various Tip Angles and Penetrometer Shapes, *Powder Technology*, Vol. 34, pp. 99–103.
50. Chenoweth H.B. 1971. Monte Carlo Simulation of the Apollo Command Module Land Landing, *J. Spacecraft & Rockets*, Vol. 8, pp. 1074–1078.
51. Perminov V.G. 1990. Dynamics of Soft Landing of Spherically-Shaped Probes, *Cosmic Research*, Vol. 28, pp. 960–965 (translated from *Kosmicheskie Issledovaniya*, Vol. 28, pp. 539–544, 1990).
52. Lorenz R. et al. 1994. An Impact Penetrometer for a Landing Spacecraft, to be published in *Measurement Science & Technology*.
53. Francis P. 1993. Volcanoes: A Planetary Perspective, Oxford University Press.
54. Garvin J.B. 1981. Landing Induced Dust Clouds on Venus and Mars, Proc. Lunar and Planetary Science Conference 12B, pp. 1493–1505.
55. Lorenz R. 1993. Wake-Induced Dust Cloud Formation following Impact of Planetary Landers, *Icarus*, Vol. 101, pp. 165–167.
56. Moshkin B.E., Ekonomov A.P. & Golovin Yu.M. 1979. Dust on the Surface of Venus, *Cosmic Research*, Vol. 17, pp. 232–237 (translated from *Kosmicheskii Issledovania*, Vol. 17, pp. 280–285, 1979).
57. Ragent B. & Blamont J. 1979. Preliminary Results of the Pioneer Venus Nephelometer Experiment, *Science*, Vol. 203, pp. 790–792.
58. Balligand H. A. & Higuchi H. 1993. Wake of a Decelerating Disk, AIAA-93-1218, Proc. 12th RAeS/AIAA Aerodynamic Decelerator Systems Technology Conference, London, May 1993.
59. Walker J.D.A., Smith C.R., Cerra A.W. & Doligalski T.L. 1987. The Impact of a Vortex Ring on a Wall, *J. Fluid Mechanics*, Vol. 181, pp. 99–140.
60. Lorenz R.D. 1993. Scientific Implications of the Huygens Parachute System, AIAA-93-1215, Proc. 12th RAeS/AIAA Aerodynamic Decelerator Systems Technology Conference, London, May 1993.
61. Timoshenko S. 1940. Theory of Plates and Shells, McGraw-Hill, New York.
62. Weber H. & Krueckau F. 1985. New M[illegible]mine-based Elastic Foam, translated from *Kunstoffe*, Vol. 75, pp. 843–848.

Appendix

Shape and Strength of Probe Shell

The Probe shape used in this study for the liquid-impact and post-impact dynamics is that of the outer aluminium shell, and is taken from Aerospatiale drawings. Essentially it is a dome with radius of curvature 1.25 m, until 15 cm along the Probe's central axis, when it becomes 15 cm, to meet a short cylindrical section (height ~7 cm, diameter 1.3 m) which corresponds to the location of the experiment platform. For about 30 cm above this, the shell is conical, meeting the flat top platform of 1.1 m diameter.

The various appendages (attach mechanisms, HASI booms, radar-altimeter antennae and the DISR) are not considered.

For the impacts with a solid surface, the contact area with the soil is computed by assuming the fore dome is an ellipsoid of revolution, with major and minor axes equal to the diameter and height of the actual shell.

Calculation of the force/deformation characteristics of even a simple shell is difficult (see, for example, Ref. 61) and so it has been assumed here that the shell obeys a linear force/deformation law. Thus, the force on the shell is directly proportional to the distance between the surface and where the shell's apex would be had it not been deformed, except where this force is more than the surface bearing strength multiplied by the contact area, in which case the shell force is set to be the latter.

In the nominal model, a shell force constant of 1000 N/m has been used. Investigation of various impact cases suggests that the impact deceleration history is relatively insensitive to variations of one order of magnitude in this parameter. In this case, the work done in deforming the shell is only about 2% of the impact kinetic energy.

Estimation of Structural Characteristics of Probe Underside Units

Detailed study of each individual unit could yield accurate stress/compression relations. However, this would be impractably labour-intensive, and difficult to justify given the uncertainties elsewhere (e.g. in the soil models, impact orientation, etc.). Thus what follows is a set of engineering estimates, using rules-of-thumb, to derive first-order guesses for the response of individual elements. The loads and accelerations calculated by the model are only modestly sensitive to variations in individual element properties; the aggregate validity of the 28 elements should be adequate. Consequently, it is hoped that the results of the model are believable.

Only the aluminium fore-dome, parts of the insulating foam, and exposed experiment components will be chilled to ambient temperature (94 K), and so the engineering properties assumed here are the room-temperature values, obtained from standard data books, except where indicated otherwise.

Air gaps have essentially zero bearing strength until their compression exceeds 95%, when the strength is increased to transfer loads to other elements.

Foam layers have a modest initial stiffness, readily deforming to about 50% compression, and then bearing strength rises sharply. The points used to define the stress-compression characteristic (Fig. 13) were taken from Figure 8 in Reference 62.

The honeycomb sandwich of the experiment platform takes a fairly large loading, until the 'punch-through' threshold of 51 N/cm^2 is exceeded. This value was supplied by CASA, contractor for the Probe's inner structure susbsystem, via Aerospatiale and the ESA Project Team. The overall response shape (Fig. 13) was set to resemble that of the aluminium footpads of the Surveyor spacecraft[25].

Note that for some units (SSP and GCMS) the platform area that supports the unit is smaller than the area used to compute the soil loads: e.g. the GCMS is a 9-inch diameter cylinder, with an effective soil penetration area of 300 cm^2 (its end is domed and has a circular inlet flange), but is only held by a support ring of area ~ 160 cm^2 bolted to inserts in the platform. Consequently, the failure stress used in the model for the honeycomb element in these stacks is modified by the ratio of the two areas.

Unit boxes are assumed to be relatively rigid, with a slight deformation due to the inward bending of the loaded face (using relations from Ref. 61), until a fail stress is reached, estimated by multiplying the yield stress of the box material (assumed glass-fibre-reinforced plastic for SSP, magnesium alloy for the PCDU box, and aluminium elsewhere) by the cross-sectional area of the box walls (and any reinforcement pillars). Note that all the box units are sufficiently squat that yield failure occurs before an Euler buckling stress is reached. Additional justification for this approach is the equivalence of experimental loads measured during the collisional crushing of a box-beam section, finite-element analysis of the same case[20], and the yield load computed as above. Since the boxes are not empty, however, a change of stress is assumed to occur as compression continues and the internal components are crushed together.

Some elements (e.g. the batteries) are considered rigid (i.e. their stiffness is considerably larger than that of the other elements).

Manuscript received 22 April 1994

Pergamon

Planet. Space Sci., Vol. 42, No. 1, pp. 1–4, 1994

0032-0633/94 $7.00+0.00

0032-0633(93)E0032-8

Crater lakes on Titan: rings, horseshoes and bullseyes

Ralph D. Lorenz

Unit for Space Sciences, University of Kent, Canterbury, Kent CT2 7NR, U.K.

Received for publication 3 December 1993

Abstract. Recent observations indicate that Titan has a predominantly icy surface, although photochemical models suggest that substantial amounts of liquid hydrocarbons may exist near or on the surface: the most plausible model of Titan's surface therefore is an icy one, with lakes or small seas of hydrocarbons (principally ethane), many in impact craters. Medium-sized craters will have central peaks, while large craters may undergo viscous relaxation, their centres doming upwards, to push the liquids into an annulus, thereby forming a ring lake. Additionally, craters with central pits may form "bullseye" lakes. The large tidal effects of Saturn on such lakes will affect their shape, distorting rings into horseshoes, and may also cause erosive migration.

Introduction: the surface of Titan

The nature of Titan's surface is largely unknown (Lunine, 1993; Lorenz, 1993), due to the optically opaque haze in its thick atmosphere, but by analogy with other outer planet satellites, it should be predominantly composed of ice. The high observed abundance (a few percent) of methane (which should have been depleted photolytically within $\sim 10^7$ years), and the proximity of the surface conditions to its triple point, suggested that reservoirs of liquid methane could exist on the surface (Eshleman *et al.*, 1983; Flasar, 1983). Further, photochemical models (Yung *et al.*, 1984) predicted that over the age of the Solar System (4.5 Gyears), a global ocean of some 600 m depth of ethane (also a liquid at Titan surface conditions) should have been produced by methane photolysis: a global ethane–methane–nitrogen ocean (Lunine *et al.*, 1983), of depth 0.7–10 km, depending on the methane content (Dubouloz *et al.*, 1989) was a favoured model of Titan's surface. However, observations by radar (Muhleman *et al.*, 1990, 1992), microwave radiometry (Grossman and Muhleman, 1992), and measurements of albedo in atmospheric "windows" in the near-infrared (Griffith *et al.*, 1991; Lemmon *et al.*, 1993; Noll and Knacke, 1993; Griffith, 1993) are incompatible with a pure hydrocarbon surface, and indicate that the surface is composed predominately of "dirty ice", although lakes and seas of hydrocarbons are possible. A recent photochemical model (Lara *et al.*, 1994), with improved treatment of transport and condensation processes and updated reaction coefficients, gives excellent agreement with observations of atmospheric composition, and suggests that the ethane production is of the order of 100–400 m. This ethane inventory is rather easier to reconcile with observations (Stevenson, 1992; Lunine, 1993), since much of it may be stored in the 0.3–8 km thick ice regolith (Lara *et al.*, 1994) near the surface. However, since the ethane is deposited (by sedimentation or rainout) from above, it may accumulate in impact craters or basins on the surface. The observational data are perfectly compatible with the existence of such lakes.

Formation and evolution of crater lakes

If Titan's surface is old (4 Gyears), then interpolating between Hyperion and Rhea (the satellites adjacent to Titan) suggests that there should be about 100–200 craters of diameter 20 km or greater in every 10^6 km^2 of surface (Plescia and Boyce, 1985; Neukum, 1985), or about 10,000 over Titan's entire surface. Most of these will have been generated in the initial heavy bombardment following the formation of the Saturnian system. The "steady-state" production rate of >20 km craters is 4×10^{-15} km^{-2} year^{-1} (Thompson and Sagan, 1992).

Observed crater densities may be much lower if resurfacing has occurred recently on Titan, although the crater density may be rather higher than indicated above, since Titan may have suffered an intense bombardment episode following the fragmentation of Hyperion (Lorenz, 1993; Lara *et al.*, 1994; Farinella *et al.*, 1990; McKinnon, 1990).

Correspondence to: R. D. Lorenz

Studies of crater morphology on Ganymede and other icy satellites suggests some differences from craters on the terrestrial planets (Schenk, 1989, 1993). Assuming crater morphology on Titan is similar to that on Callisto and Ganymede, small craters (less than 5–10 km diameter) will have simple, bowl-shapes. Above about 10 km, central peaks tend to be prominent, while above about 40 km diameter, craters tend to have a central pit, sometimes occupied by a small dome. Note that impactors that would generate craters smaller than 200 m diameter will be screened out by atmospheric shielding (Thompson and Sagan, 1992).

Photochemical models suggest that ethane will be deposited in a crater at the rate of about 1 m depth every 20 Myears: depending on the atmospheric conditions at the surface (about which there is still some ambiguity), atmospheric methane may dissolve in the ethane to form an equilibrium mixture up to 16 times deeper (Dubouloz *et al.*, 1989). In the same interval, about 1.5 m of water-ice impact ejecta [deposited on average at a rate of about 8×10^{-6} g cm^{-2} year^{-1} (Thompson and Sagan, 1992)], and about 0.25 m of (solid) photochemical aerosol will have been deposited in the lake. Due to viscous relaxation (Parmentier and Head, 1981), the centre of a crater 100 km in diameter, however, will have domed upwards on this timescale, such that the liquid will be forced into an annulus. If the crater has a central pit, some liquid will probably accumulate here, so a "bullseye" appearance will result (centre liquid, then ice, then a liquid annulus, then the crater rim; if a central dome exists in the pit, then the sequence may be ice, liquid, ice, liquid, ice, although such a configuration would probably be short-lived).

The relaxation timescale cited above applies for ice rheology at the 120K surface temperature of the Galilean satellites: for water ice at Titan's 94K surface temperature, the timescale will be orders of magnitude longer. However, ices on Titan may incorporate a significant fraction of ammonia and other volatiles, which tend to reduce viscosity. Thus, using Galilean relaxation rates is perhaps as good an estimate as any. Since, in any case, the liquid deposition rate (bearing in mind the current uncertainty in the methane/ethane mix that can be in equilibrium with the atmosphere) is also poorly constrained with present data, the timescale for doming of the crater may be small or large compared with its filling time. Thus, if doming is fast (see Fig. 1), the ring lake configuration will be common, while if doming is slow compared with liquid deposition, craters will tend to fill completely forming simple circular lakes (with a slightly shallow region in the centre).

Note that lake appearance will be modified by subsequent impact events: a large, old crater may have several smaller craters superimposed on it. By studying the crater morphology, it may be possible to determine whether the impact sites of these smaller craters were deeply submerged or not when the impact occurred, giving an indication of the liquid depth history of the larger crater.

The appearance of large crater lakes may also be modified because Saturn induces a strong near-stationary tide in fluids on Titan (Sagan and Dermott, 1982; Lorenz, 1992), yielding a tangential acceleration $f = 3/2GM_S R_t r^{-3} \sin 2\phi$, where G is the gravitational constant, M_S the mass of Saturn, r is the Saturn–Titan distance and R_t Titan's radius. ϕ is the Titanocentric angle between the sub-Saturn point and the point under consideration. This acceleration tilts the local vertical by an angle $\delta = f/g$, where g is the local gravitational acceleration (1.35 m s^{-2}). This angle varies with location and time between zero and a maximum of about 6×10^{-5} rad (for $\phi = 45°$). This may be compared with the 10^{-6}–10^{-7} tilt in the level of a lake on Earth due to wind friction (Leeder, 1982), and the 10^{-7} tilt due to tides.

Thus, for a 100 km diameter lake, the difference in level between shores is up to 6 m, comparable with the depth after an age of 6–300 Myears, so that the low-tide region may "dry up" completely—causing the lake to be horseshoe shaped. Lakes in smaller craters, which relax much more slowly (Parmentier and Head, 1981) are likely to remain circular, although should they fill up, are more likely to burst their banks at the "high-tide" end.

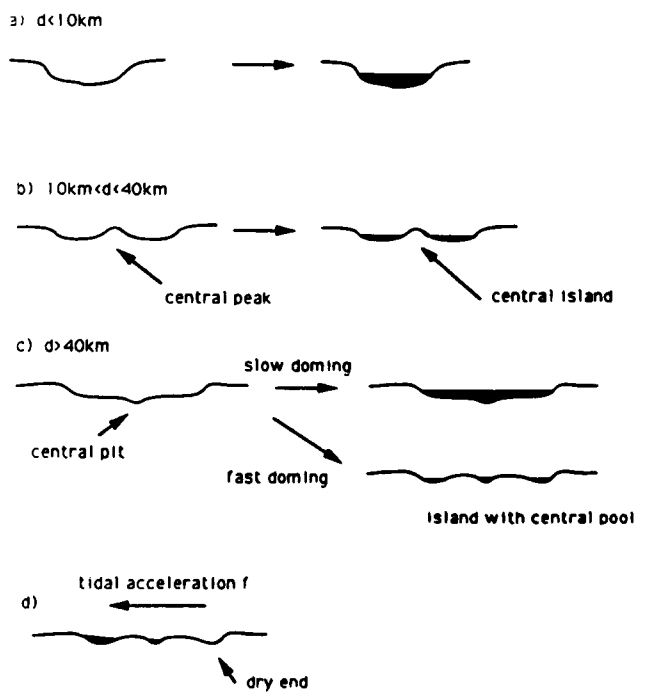

Fig. 1. Comparative evolution of crater lakes: (a) small, simple craters fill up; (b) larger craters, with central peaks, form ring lakes; (c) large craters may have central pits: fast doming leads to a ring lake, with a small lake in the middle of the island, while slow doming leads simply to a large circular lake; and (d) if the local vertical is tilted appreciably by tidal acceleration f, one end of a ring lake may dry up, forming a horseshoe

Tide dynamics in crater lakes

Because the orbit of Titan is non-circular (eccentricity 0.029), the Saturnocentric angular rate of Titan varies with orbital position, while the angular velocity of Titan about its own axis is constant. Thus, there is an oscillation of the Titanocentric longitude of the sub-Saturn point of amplitude ~3°, corresponding to about ±130 km along

the equator. In addition there is a once-per-orbit variation of $3e = 9\%$ in the magnitude of the tide (Sagan and Dermott, 1982).

These variations in tidal strength and direction, coupled with Coriolis forces, may lead to strong currents, causing erosion (Sagan and Dermott, 1982; Lunine and Stevenson, 1985) at the edge of the lake nearest the sub- or anti-Saturnward points [even though water-ice is relatively insoluble in cryogens (Rest *et al.*, 1990), a significant pathway for erosion may be by abrasion due to suspended particles (Lunine, 1990) although this is difficult to quantify. The solubility of solid organic compounds is low enough (Raulin, 1987) that these will appear as suspended particles rather than dissolve in the lakes]. If Titan rotates non-synchronously (Muhleman *et al.*, 1992)—not unlikely since the orbit is non-circular (Greenberg and Wiedenschilling, 1984; see also Sears *et al.*, 1993) with a period of 15.911 days (its orbit period is 15.945 days)—then there is superimposed on the oscillation in the longitude of the sub-Saturn point a secular drift (0.05° day^{-1}), which will "smear out" lakeside erosion to become anti-poleward, all over Titan.

The above arguments apply for a perfectly spherical "billiard ball" Titan. However, it is likely that Titan's crust may have responded to the tidal potential induced by Saturn: if this is the case, and Titan rotates synchronously, tidal effects in lakes will be quite small. If Titan rotates non-synchronously, then the crust will respond to the tidal potential (a rotating prolate spheroid averaged over the crust relaxation timescale, thus an oblate spheroid) and the tidal effects will manifest themselves according to the difference between the instantaneous tidal potential (a prolate spheroid with the long axis pointing toward Saturn, to which liquids will quickly respond to attain equilibrium) and the crustal shape. In general, this may mean that high (but more modest than suggested above) tides may occur on the edges of lakes closest to and furthest from the sub-Saturn point, although on the equator, the tide will be unidirectional and horseshoe lakes may indeed appear.

Especially since the tides on Titan are relatively large in any case, it is worthwhile examining whether resonant tides are likely on Titan. A good terrestrial example is the Bay of Fundy in Nova Scotia where the natural period of oscillation is half that of the semidiurnal tide, leading to large tidal amplitude and strong tidal currents (Bearman, 1989). The speed of a shallow ocean wave, where depth is much smaller than wavelength, is $(gD)^{0.5}$ or 1.2–11.6 m s^{-1} for a depth of 1–100 m on Titan. For seas of diameter 100 km ($\sim$ the displacement of the tidal bulge due to eccentricity) the resonant period is $2 \times 10^5/1.2 \approx 1.7 \times 10^5$ s, much shorter than the orbital period of 5.4×10^6 s, so resonant tides are unlikely to occur, even in improbably wide, shallow seas.

Even without resonant effects, however, the tidal amplitude is significant. In terrestrial seas, for those regions ("tidal flats") where wave effects are minimal and mass transport is dominated by tidal action, gradients are comparatively shallow (Bearman, 1989), of order 0.001. Thus the intertidal distance of a 100 km diameter lake may be up to $100\ \text{km} \times (6 \times 10^{-4}) \times 0.09/0.001 \approx 540$ m.

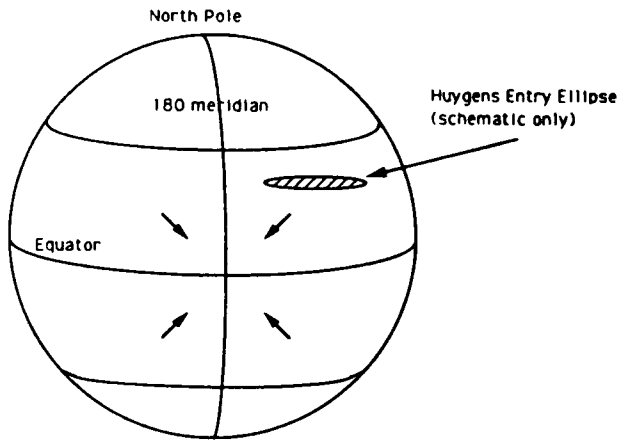

Fig. 2. Orientation of tide. Arrows show direction of tidal acceleration, pointing towards anti-Saturnward point (0 N, 180 E): from the *Huygens* landing site, the accelerations point SW. If Titan's crust has relaxed, however, the direction becomes ambiguous

Conclusions

We will only be confident about our understanding of Titan's surface after the arrival of the ESA *Huygens* probe, which will descend through Titan's atmosphere in late 2004/early 2005. Its camera will give high-resolution images of the area around the landing site [probably about 20° N, 200 E for mission planning reasons (Ott, 1992)], complemented by more extensive radar, visual and infrared mapping from orbit. The arguments I have presented here suggest that we may find small circular lakes, and larger ring-, bullseye- or horseshoe-shaped lakes, with tides of high amplitude (around the *Huygens* landing site, the tides may be "high" on the SW margin of lakes: see Fig. 2). Study of the lake morphology, and any cratering in lakes, may give indications as to the softness of Titan's crust.

It may be noted that the dynamics of tidal currents, and the consequent erosive processes, are likely to be complex and will be an interesting topic of further study. Further work is also required in quantifying the likely response of Titan's crust as a whole to tidal effects.

Acknowledgements. The author acknowledges the support of a postgraduate research grant from the U.K. Science and Engineering Research Council. Jonathan Lunine made a helpful review of the paper and Mark Lemmon made useful comments. Productive discussions with William Sears are also acknowledged.

References

Bearman, G. (Ed.), *Waves, Tides and Shallow-water Processes*. Open University/Pergamon Press, Milton Keynes/Oxford, 1989.

Dubouloz, N., Raulin, F., Lellouch, E. and Gautier, D., Titans hypothesized ocean properties: the influence of surface temperature and atmospheric composition uncertainties. *Icarus* **82**, 81–106, 1989.

Eshleman, V. R., Lindal, G. F. and Tyler, G. L., Is Titan wet or dry? *Science* **221**, 53–55, 1983.

Farinella, P., Paolicchi, P., Strom, R. G., Kargel, J. S. and Zappala, V., The fate of Hyperion's fragments. *Icarus* **83**, 186–204, 1990.

Flasar, F. M., Oceans on Titan. *Science* **221**, 55–57, 1983.

Greenberg, R. and Wiedenschilling, S. J., How fast do the Galilean satellites spin? *Icarus* **58**, 186–196, 1984.

Griffith, C. A., Evidence for surface heterogeneity on Titan. *Nature, Lond.* **364**, 511–513, 1993.

Griffith, C. A., Owen, T. and Wagener, R., Titans surface and troposphere, investigated with ground-based, near-infrared observations. *Icarus* **93**, 362–378, 1991.

Grossman, A. W. and Muhleman, D. O., Observations of Titan's radio light-curve at 3.5 cm. *Bull. Am. Astron. Soc.* **24**, 954, 1992.

Lara, L. M., Lorenz, R. D. and Rodrigo, R., Liquids and solids on the surface of Titan: results of a new photochemical model. *Planet. Space Sci.*, in press, 1994.

Leeder, M. R., *Sedimentology*. George Allen & Unwin, London, 1982.

Lemmon, M. T., Karkoshka, E. and Tomasko, M., Titan's rotation: surface feature observed. *Icarus* **103**, 329–332, 1993.

Lorenz, R., Gravitational tide in the atmosphere of Titan. *Proc. Symp. on Titan*, ESA SP-338, pp. 119–123. ESA, Noordwijk, 1992.

Lorenz, R., The surface of Titan in the context of ESA's *Huygens* probe. *ESA J.* **17**, 275–292, 1993.

Lunine, J. I., Evolution of the atmosphere and surface of Titan. *Proc. Symp. on Formation of Stars and Planets, and the Evolution of the Solar System*, ESA SP-315, pp. 159–165. ESA, Noordwijk, 1990.

Lunine, J. I., Does Titan have an ocean? A review of current understanding of Titan's surface. *Rev. Geophys.* **31**, 133–149, 1993.

Lunine, J. I. and Stevenson, D. J., Coupled evolution of Titan's ocean–atmosphere system and interaction of ocean with bedrock, in *Ices in the Solar System* (edited by J. Klinger, *et al.*), pp. 741–747. Reidel, Dordrecht, 1985.

Lunine, J. I., Stevenson, D. J. and Yung, Y. L., Ethane ocean on Titan. *Science* **222**, 1229–1230, 1983.

McKinnon, W. B., The Hyperion hypothesis. *Nature, Lond.* **346**, 414–415, 1990.

Muhleman, D. O., Grossman, A. W., Butler, B. J. and Slade, M. A., Radar reflectivity of Titan. *Science* **248**, 975–980, 1990.

Muhleman, D. O., Grossman, A. W., Slade, M. A. and Butler, B. J., The surface of Titan and Titan's rotation: what is radar telling us? *Bull. Am. Astron. Soc.* **24**, 954, 1992.

Neukum, G., Cratering records of the satellites of Jupiter and Saturn. *Adv. Space Res.* **5**(8), 107–116, 1985.

Noll, K. S. and Knacke, R. F., Titan: 1–5 μm photometry and spectrophotometry and a search for variability. *Icarus* **101**, 272–281, 1993.

Ott, S., *Cassini* mission: the targetting of the *Huygens* probe. Paper *IAF*-92-0067, presented at the World Space Congress, Washington DC, 1992.

Parmentier, E. M. and Head, J. W., Viscous relaxation of impact craters on icy planetary surfaces: determination of viscosity variation with depth. *Icarus* **47**, 100–111, 1981.

Plescia, J. B. and Boyce, J. M., Impact cratering history of the Saturnian satellites. *J. Geophys. Res.* **90**, 2029–2037, 1985.

Raulin, F., Organic chemistry in the oceans of Titan. *Adv. Space Res.* **7**, (5)71–(5)81, 1987.

Rest, A. J., Scurlock, R. G. and Wu, M. F., The solubilities of nitrous oxide, carbon dioxide, aliphatic ethers and alcohols, and water in cryogenic liquids. *Chem. Engng J.* **43**, 25–31, 1990.

Sagan, C. and Dermott, S. F., The tide in the seas of Titan. *Nature, Lond.* **300**, 731–733, 1982.

Schenk, P. M., Crater formation and modification on the icy satellites of Uranus and Saturn: depth/diameter and central peak occurrence. *J. geophys. Res.* **94**, 3813–3832, 1989.

Schenk, P. M., Central pit and dome craters: exposing the interiors of Ganymede and Callisto. *J. geophys. Res.* **98**, 7475–7498, 1993.

Sears, W., Lunine, J. I. and Greenberg, R., Equilibrium non-synchronous rotation of Titan. *Icarus* **105**, 259–262, 1993.

Stevenson, D. J., Interior of Titan. *Proc. Symp. on Titan*, ESA SP-338, pp. 29–33. ESA, Noordwijk, 1992.

Thompson, W. R. and Sagan, C., Organic chemistry on Titan–surface interactions. *Proc. Symp. on Titan*, ESA SP-338, pp. 167–176. ESA, Noordwijk, 1992.

Yung, Y. L., Allen, M. and Pinto, J. P., Photochemistry of the atmosphere of Titan: comparison between model and observations. *Astrophys. J. (Suppl. Ser.)* **55**, 465–506, 1984.

ABLATION AND CHEMISTRY OF METEORIC MATERIALS IN THE ATMOSPHERE OF TITAN

Mark English§, Luisa Lara¶+, Ralph Lorenz§, Paul Ratcliff§, R Rodrigo¶

§ *Unit for Space Sciences, University of Kent at Canterbury UK.*
¶ *Instituto de Astrofisica de Andalucia, CSIC, Granada, Spain.*
+*currently at DESPA, Observatoire de Meudon, Paris, France*

ABSTRACT

We compute the input of meteoric materials expected on Titan, and integrate this dust model with an ablation model and a comprehensive chemical model, investigating the effects on the atmosphere and surface. We find a water deposition of ~10-100 times the expected interplanetary dust flux, or a recent large impact, is required to produce the observed CO_2 abundance. Ionisation due to meteoric activity is not likely to be higher than that due to other sources.

INTRODUCTION

Previous workers/1,2,3/ have considered the effects of meteoric materials in Titan's atmosphere on ion density and oxygen chemistry. Typically, the meteoric input has been assumed to be similar to that of the Earth, with a passing mention of Saturn's rings. We take a more rigourous approach to generating a meteoric input, and investigate its implications for oxygen chemistry, surface composition, ionisation and stratospheric condensates.

DUST MODEL

In order to calculate the interplanetary dust flux into Titan's atmosphere two parameters were needed: the spatial number density of particles at 10 AU and their speed distribution. The number density at 10 AU was generated from an expression for the dust flux at 1 AU/4/, and the Pioneer 11 observation that the spatial density remained constant from 1AU to 18 AU/5/. In order to assess the speed of the meteoroid population the Erickson meteor speed distribution/6/ was scaled from 1 AU to 10 AU. The gravitational enhancement by Saturn, and then by Titan was applied, along with compensation for the motion of Titan around Saturn. The flux onto Titan was binned into 72 angular bins, and twenty speed and size bins. This allowed the flux to be evaluated at different points on Titan, taking account of motional effects. The model shows that the leading face flux is enhanced by a factor of ~20 from that on the trailing face. The globally-averaged mass flux onto Titan is 9.93E-16 $kgm^{-2}s^{-1}$, and the total accretion rate is 5700 tonnes/yr /7/, compared with 40,000 tonnes/yr (~2.5E-15 $kgm^{-2}s^{-1}$) for Earth/8/.

Work is continuing on estimating the contribution of Saturnocentric particles. Contrary to previous suggestions /2,3/ we assert that ring particles make no contribution, since there are no mechanisms adequate to increase their orbital energy, and (D. Hamilton, personal communication) the inner satellites shield Titan from the rings. Ejecta from impacts of interplanetary material on the outer satellites Hyperion, Iapetus and Phoebe may enhance the flux on Titan by a factor of a few, however.

ABLATION MODEL

Explicit numerical integration of the equation of motion using a 7th order Gear Method (favoured in previous work/9/) is used to calculate the flight paths of particles entering the atmosphere. The thermal histories of particles during aerobraking are calculated using a standard energy balance equation for an isothermal particle /eg 10/, namely

warming = energy input by drag + solar insolation - radiated energy - ablation

and is expressed:

$$\frac{4}{3}\pi r^3 \rho_m c \frac{dT_m}{dt} = \frac{\Lambda}{2}\pi r^2 \rho_a v^3 + \pi r^2 S(1-A) - 4\pi r^2 \varepsilon_{rad} \sigma T_m^4 + L\frac{dm}{dt}$$

where: r, ρ_m, c, T_m, A, ε_{rad}, L, m are the meteroid's radius, density, specific heat capacity, temperature, albedo, emissivity, latent heat of vapourisation and mass respectively. ρ_a is the atmospheric density, v is the particle velocity relative to the atmosphere, S is the solar constant, σ is the Stephan-Boltzmann coefficient. Λ is a measure of the efficiency of energy transfer and has been calculated using the method of

Hood and Horanyi /11/ for the hyperthermal regime.

The ablation profiles for each particle are computed by relating the mass loss rate to the vapour pressure of the particle material at temperature T_m. These profiles are summed over the mass, velocity and trajectory distributions to produce the deposition profiles for the leading and trailing faces of Titan.

Figure 1 shows the calculated profiles for 100% water-ice particles. The fine structure in the profiles results from coarseness in the trajectory and velocity binning: the important features are that the peak ablation (and hence water deposition) occurs at an altitude of ~700 km, over an altitude range equal to a few scale heights, and that an order of magnitude more water is deposited on the leading face than the trailing face. Fluxes on polar regions (where CO_2 abundance is lower than near the equator) are only slightly higher than the trailing-edge flux.

Figure 2 shows the temperature profiles for silicate grains of 3 sizes on the leading face of Titan: the particles are heated to a high temperature, then mass loss by ablation holds the temperature constant. Similar effects occur for ice meteoroids, but at a lower temperature (~240K).

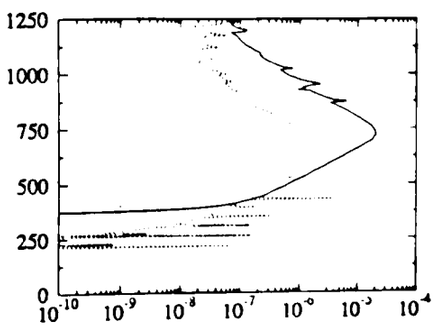

Figure 1. Leading and trailing face deposition profiles for interplanetary meteoroids made of 100% water ice. Ordinate is altitude in km, abscissa is deposition in $kgm^{-2}s^{-1}$ per 6km altitude bin. Solid line is for leading face, dotted curve for trailing face.

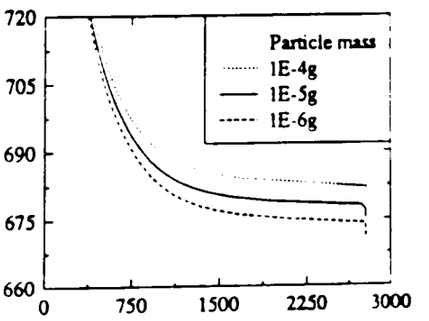

Figure 2. Temperature profiles for 100% silicate interplanetary meteorids. Ordinate is altitude in km, abscissa temperature in K.

CHEMICAL MODEL

The vertical distribution of 43 compounds in Titan's atmosphere has been calculated using a 1-D numerical model/12/ covering the altitude range 40-1432 km. The model features a comprehensive treatment of photochemical, eddy diffusion and condensation processes.

The low temperatures in Titan's atmosphere lead to a strong condensation sink for most compounds. While the hydrocarbon and nitrogen compounds' mixing ratios observed by Voyager 2 can be explained by the CH_4 and N_2 chemistry prevailing in this atmosphere, the CO_2 would be removed by condensation in under 5E4 years /2/ unless it could be replenished.

CO_2 can be formed by the reaction $CO + OH \rightarrow CO_2 + H$. Production of OH by a cyclé involving CO_2 dissociation, forming $O(^1D)$, which in turn reacts with methane to generate OH, is largely inhibited by hydrocarbon shielding of UV light. Thus, to explain the observed /14/ CO_2 stratospheric mixing ratio of 1.3E-9, it is necessary to invoke an external source rich in oxygen bearing material /2,13/, typically meteoric water vapour which is photolysed into OH in the mesosphere and thermosphere.

Without an oxygen input, the chemical model suggests a CO_2 abundance of 1E-12, the saturation limit at the tropopause. If we deposit H_2O vapour in the atmosphere assuming the model leading-face interplanetary flux (2.23E-15$kgm^{-2}s^{-1}$) only, we find (figure 3) that the CO_2 abundance is still too small. If we enhance the H_2O mass flux by a factor of 200, the required CO_2 abundance is met, but the water vapour concentration in the atmosphere would be higher than its non-detection would suggest, and the CO abundance begins to push against observational limits/15/ (figures 4,5). However, since outer solar system material is likely to contain ices other than water ice, we also investigated a comet-like composition

of 90% H_2O, 7% CO and 3% CO_2: the input of only ~20 times the leading edge interplanetary mass flux of this material agrees well with the observed abundances of all three compounds. We note that the oxygen chemistry produces other compounds (HCO, H_2CO, CH_2CO)at rates of 1E5~1E7 $cm^{-2}s^{-1}$, about ~100 times higher than suggested earlier/13/: if abundances are similarly higher, these compounds may be detectable by current groundbased techniques.

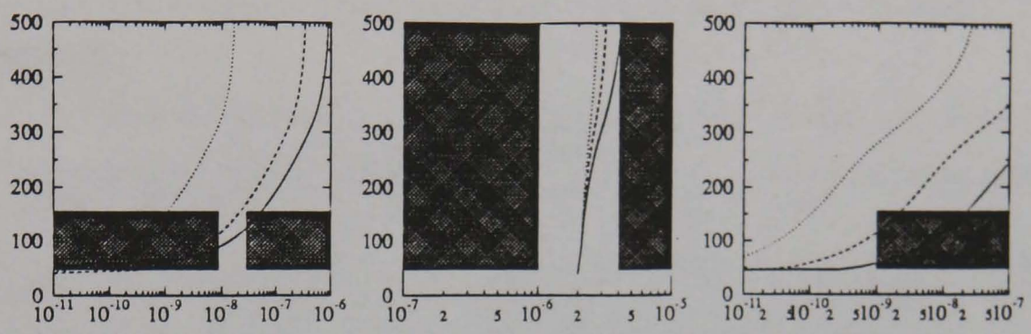

Figures 3,4,5. Mixing ratio (abscissa) profiles versus altitude (ordinate) for CO_2, CO and H_2O respectively, as predicted by the model for interplanetary-only leading-face flux H_2O(dotted), 200x H_2O flux (solid) and 20x Halley composition (dashed). Shaded regions denote mixing ratios not permitted by observations, although note that the H_2O limit is uncertain.

The models with CO_2 mixing ratio in the observed range suggest the CO_2 condensation flux to the surface should be 2~5E6 $cm^{-2}s^{-1}$. This CO_2 flux is about an order of magnitude higher than that found earlier /2,13/, presumably due to different treatment of condensation and eddy diffusion processes in the models, and the lower CO mixing ratio /15/ used in our model /12/. Our required meteoric water supply is correspondingly higher, although since back reactions of H_2CO, CH_2CO etc. into CO_2 are not modelled in the current model, the actual required water fluxes are probably lower than we state above by a factor 2~5.

The above considerations assume a steady state. We note, however, that a large, recent impact could project large amounts of crustal (presumably water-bearing) material high into Titan's atmosphere, leading to a temporarily high CO_2 abundance. An enhanced water flux into the atmosphere (or the residue from a recent impact plume) perhaps make the recent identification/17/ of water ice in the stratosphere easier to understand.

SILICATES AND IONS

One (controversial) interpretation of near-IR spectra of Titan, which appear to sense the surface, is that the dominant surface materials are anhydrous silicates /18 /. As cryovolcanic eruption of anhydrous materials seems unlikely, we suggest meteoric deposition is the most plausible source. As seen in figure 2, meteoric particles attain high enough temperatures to be dehydrated during entry, although we note that the meteoric flux required to exceed the deposition of photochemical organics (~2E9$cm^{-2}s^{-1}$ flux of liquid ethane, and ~7E8 $cm^{-2}s^{-1}$ for solid acetylene/16/) seems improbably high.

Following work by Ip /1/, Grard /3/ has suggested that meteors could cause an ionised layer on Titan at ~500km, with an electron density of ~1E5 cm^{-3}. This could have prevented detection of lightning spherics by Voyager 1, although Voyager placed upper limits on electron densities at two points at 3~5E3 cm^{-3}. Grard's estimate was based on an electron production of 0.1cm^{-3}, an *upper limit* for Earth. Although the oxygen chemistry considerations suggest that the mass flux on Titan may be 4~100x that of Earth, we find Grard's (entirely hypothetical) layer unlikely - the larger scale height on Titan (50km vs. 6km on Earth) means meteoric ions are distributed over a larger volume (by a factor ~10). Also, our velocity distribution suggests a mean speed of ~9.5kms^{-1} for interplanetary meteors on Titan (only ~3kms^{-1} for Saturnocentric material), whereas terrestrial meteors have a mean speed of ~16kms^{-1}. Ionisation efficiency (the number of free electrons yielded by each ablated meteor atom) scales/19/ as $v^{3.5}$, or 10~1000 times less efficient on Titan. Thus we find no reason to suspect an electron density as high as that suggested by Grard/3/, nor, by implication 'hidden' lightning.

CONCLUSIONS

We find that a model of interplanetary dust is insufficient to supply the observed CO_2 abundance in Titan's atmosphere. A composition-dependent enhancement of 4–100, perhaps from Saturn's outer satellites, is required. We suggest that a search for additional oxygen compounds in Titan's atmosphere may be fruitful, especially on the leading face. Solid surface material on Titan should contain a small fraction of meteoric dust (silicates) and condensed oxygen species (mostly CO_2) of meteoric origin. Silicate meteoric material is probably dehydrated, and meteoric ionisation is not as high as previously suggested.

REFERENCES

1. W. H. Ip, Meteoroid Ablation Processes in Titans Atmosphere,*Nature*, 345 pp.511-512 (1990)

2. R. E. Samuelson, W. C. Maguire, R. A. Hanel, V. G. Kunde, D. E. Jennings, Y. L. Yung and R. C. Aiken, CO_2 on Titan, *Journal of Geophysical Research*, 88 pp.87090-8715 (1983)

3. R. J. L. Grard, The significance of meteoric ionisation for the Propagation of Lightning Spherics in the Atmosphere of Titan, *Proceedings Symposium on Titan*, Toulouse 1991, ESA SP-338 pp.125-128 (1992)

4. E. Grun, H. A. Zook, H. Fechtig and R. H. Giese, Collisional Balance of the Meteoric Complex, *Icarus*, 62 pp.244-272 (1985)

5. D. H. Humes, Results of Pioneer 10 and 11 Meteoroid Experiments : Interplanetary and Near-Saturn, *Journal of Geophysical Research*, 85 No.A11 pp.5841-5852 (1980)

6. J. E. Erickson, Velocity Distribution of Sporadic Photographic Meteors, *Journal of Geophysical Research*, 7 No.12 pp.3721-3726 (1968)

7. M.A.English, J.C. Zarnecki, A proposed dust model for Titan, considering both Interplanetary and Saturnocentric sources (abstract), *Annales Geophysicae*, 12 (Suppl. III), pC677 (1994)

8. S.G.Love, D.E. Brownlee, A Direct Measurement of the Terrestrial Mass Accretion Rate of Cosmic Dust, *Science*, 262 pp.550-553 (1993)

9. P.R. Ratcliff, A.D. Taylor and J.A.M. McDonnell, The Relative Efficiency of Aerocapture for Interplanetary Dust by the Planets, *Planetary and Space Science*,.41 No.8, 603-608 (1993).

10. J. I. Moses, Meteoroid Ablation in Neptune's Atmosphere, *Icarus*, 99 pp.368-383 (1992)

11. L.L. Hood and M. Horanyi, Gas Dynamic Heating of Chondrule Precursor Grains in the Solar Nebula, *Icarus*, 93, 259-269 (1991).

12. L. M. Lara, Estudio fotquimico de los componentes neutros de la atmosfera de Titan, Ph.D. Thesis, University of Granada, Spain (1993)

13. Y. L. Yung, M. Allen and J. P. Pinto, Photochemistry of the Atmosphere of Titan : Comparison between model and Observations, *Astrophysical Journal*, 55 pp.465-506 (1984)

14. A. Coustenis, B. Bezard and D. Gautier, Titans atmosphere from Voyager Infrared observations. I. The gas composition of Titans equatorial region, *Icarus*, 80 pp. 54-76, (1989)

15. A. Marten, D Gautier, L Tanguy, A. Lecacheaux, C. Rosolen and G. Paubert, Abundance of Carbon Monoxide in the Stratosphere of Titan from millimeter Observations, *Icarus*, 76 pp.562-588 (1988)

16. Lara, R D Lorenz and Rodrigo, R, Liquids and Solids on the Surface of Titan: Results of a New Photochemical Model, *Planetary and Space Science*, in press (1994)

17. A. Coustenis, B. Schmitt, R. E. Samuelson and R.K.Khanna, Water Ice and Other Condensates in Titan's Stratosphere, submitted (1994)

18. A. Coustenis, E Lellouch, J P Maillard and C P McKay, Titan's Surface: Composition and Variability from the Near Infrared Albedo, *Icarus*, (submitted), 1994

19. V. N. Lebedinec and V. B. Suskova, Evaporation and Deceleration of Small Meteoroids, pp.193-204 in Kresak and Millman (eds), *Physics and Dynamics of Meteors*, D. Reidel, Dordrecht (1968)